UNIVERSITY OF COPENHAGEN
NIELS BOHR INSTITUTE

DOCTORAL THESIS

Synchronisation, shocks and contagion in a connected world

Author:
Jonas Søgaard Juul

Supervisors:
Mogens H. Jensen
Joachim Mathiesen

This thesis has been submitted to the PhD School of The Faculty of Science, University of Copenhagen

Department of Biocomplexity
Niels Bohr Institute

December 25, 2019

Resumé

af Jonas Søgaard Juul

Mange biologiske, sociale og kunstigt fremstillede systemer består af flere interagerende dele. Nogle gange er interaktionerne mellem de mindre dele årsag til makroskopiske fænomener. Fra stamceller som sammen skaber et levedygtigt foster, til sociale interaktioner som muliggør spredningen af sygdomme, udviser grupper af interagerende enkeltdele opførsel, som er vigtig at forstå. I denne afhandling bruges analytiske, numeriske og statistiske metoder til at studere opførslen af systemer som består af mange forbundne elementer. Afhandlingen er delt op i tre dele.

I første del studeres grupper af koblede, oscillerende stamceller i musefostre. Stamcellepopulationen skaber det komplekse mønster af forstadier til rygradsknogler, somitter, i mus. Vi udvikler en matematisk teori for en mekanisme, som for nyligt blev foreslået at stå bag timingen og skaleringen af somitter. Ved hjælp af teorien finder vi hidtil ukendte forbindelser mellem vigtige variable i det biologiske system. Vi viser endvidere, at de observerede værdier for disse variable er konsistente med den foreslåede mekanisme. Herefter gør vi brug af teorien til at foreslå en række eksperimenter, som muliggør falsificering af somitskaleringsmekanismen. Vi viser også hvordan eksperimentelt observerede fasebølger kan kontrolleres. Denne kontrol vil kunne bruges til at teste, om bølgerne er nødvendige for timingen af somitskabelse, hvilket er en udbredt hypotese i forskningsfeltet.

I anden del af afhandlingen studeres spredningsprocesser i netværk. I den første artikel studerer vi en model af kompleks smitte med synergieffekter. Ved at kombinere analytiske og numeriske analyser opdager vi, at synergieffekterne kan muliggøre eller umuliggøre smitte af netværksenheder med bestemte egenskaber. I et andet projekt undersøger vi hvordan antiestablishmentindivider kan påvirke udbredelsen af to produkter i befolkninger. Modellen er inspireret af nylige antiestablishmentudfald af valg og folkeafstemninger. I modellen kan en lille gruppe med antiestablishmentholdninger forårsage, at et ellers upopulært produkt ender med at blive det mest udbredte i befolkningen. Vi argumenterer desuden for, hvorfor dette er muligt i modellen. Endelig undersøger vi udbredelsen af muterede sygdomme i befolkninger. Den Spanske Syge er et eksempel på en muteret sygdom. Vi udleder en skaleringslov for alvorligheden af muterede sygdomme og finder evidens for dens rigtighed i simuleringer og data fra memespredning på Facebook.

I den sidste del af afhandlingen studeres mønstre i telekommunikation mellem mennesker. Først undersøger vi korrelationer mellem narcissistiske personlighedstræk og social opførsel. Vi finder korrelationer mellem narcissistisk personlighedsscore og antallet af forskellige mennesker, forsøgsdeltagere er i kontakt med. Vi finder også, at personers interaktionsfrekvens korrelerer med deres score i narcissistisk beundring. Observationerne er konsistente med nogle eksisterende psykologiske hypoteser vedrørende folk med narcissistisk grandiositets adfærd. Til sidst undersøger vi kommunikationsmønstre efter terrorangreb i adskillige Vesteuropæiske lande. Selvom både mandlige og kvindelige forsøgsdeltagere ændrer adfærd efter angrebene finder vi signifikante forskelle i graden af adfærdsændringer for mænd og kvinder.

Abstract

Synchronisation, shocks and contagion in a connected world

by Jonas Søgaard Juul

Biological, engineered and social systems often consist of many interacting parts. Sometimes the interactions between these smaller components give rise to macroscopic behavior. From stem cells joining their efforts to create a fetus capable of living, to social interactions allowing diseases to spread, interacting populations on many different scales exhibit dynamics that are important to study and understand. In this dissertation, numerical, analytical, and statistical methods are used to study the dynamics of systems consisting of interacting components. The thesis contains three parts.

In Part I, a system of coupled oscillating stem cells in mouse embryos is studied. The stem cells create the complex spatial pattern of vertebrae precursors – somites – in mice. We develop a theoretical framework for a recently proposed mechanism for the size and timing of somite creation. We use the theory to establish previously unknown relations between key variables in the biological system, and show that the experimental values of these variables are consistent with the proposed mechanism. We also suggest experiments capable of falsifying the proposed mechanism. In another study, we show how to control experimentally observed phase waves. This method could be used as a means of testing whether these waves are critical to the timing of somites, which is a widespread hypothesis in the field.

In Part II, we study the impact of contagion in networked populations. Firstly, we consider a model of complex contagion with synergy. Combining analytical and numerical analyses, we find that the synergistic effects determine which nodes can be infected and which cannot. Secondly, in another study, we examine the impact of anti-establishment nodes in a model of complex contagion describing the spread of two competing products. The model is inspired by recent anti-establishment outcomes in elections and referendums. We find that a very small number of anti-establishment nodes can cause an otherwise insignificant product to become the most adopted at equilibrium. We also argue why a few nodes can have such a considerable influence. Finally, we study what impact mutant contagion, such as the 1918 Spanish flu, has in structured populations. We analytically derive a scaling law for this impact in infinite-dimensional networks. We find that numerical analyses and existing empirical results for meme-spreading on Facebook support this law.

In Part III of this dissertation, telecommunication in human populations is studied. In one paper, we examine correlations between narcissistic personality traits and social behaviour. We find correlations between the number of social contacts nodes have and their narcissistic scores. We also find evidence of homophily in so-called narcissistic admiration. The observations are in agreement with some existing hypotheses regarding the psychology of grandiose narcissists. In the final paper, we examine telecommunication patterns following terror attacks in several Western European cities. We find that, although both females and males change behaviour following terror attacks, there are significant gender differences between the changes of behaviour.

Acknowledgements

I am indebted to several people without whom I could not have written this dissertation. First of all, I wish to thank my supervisors, Mogens H. Jensen and Joachim Mathiesen, for giving me the opportunity to carry out this work. I am grateful for your friendship and the freedom you have given me over the course of the last three years. I am also immensely thankful for the opportunities you have given me. Your support in establishing scientific collaborations has been second to none. I can think of no more invaluable gifts to receive from academic advisors than the experiences and friends I have made with your help.

I also wish to express my great gratitude to the scientific mentors who have supported me during my scientific career so far. Christopher H. Joyner, Uzy Smilansky, and Mason A. Porter for being incredibly patient and for taking me as a student before I had much research experience. I have learned much from your mentorship, and I am incredibly grateful for your continued advice and support. I also wish to thank Sandeep Krishna, for valuable advice on working in the intersection of biology and physics and for working hard on our joint projects. Finally, my gratitude goes to Steven H. Strogatz for taking me as a student just before publishing your latest book. The semester I spent at the Center for Applied Mathematics at Cornell University was amazing. It taught me a lot about myself as a researcher and gave me so many great experiences.

In addition to my mentors and advisors, I would like to thank Bente Markussen, Erika Fowler-Decatur, and Søren Granat. In addition to your help and your advice on administrative matters, I have thoroughly enjoyed your company. I admire each of you immensely on many different levels.

I could not have finished the dissertation without the generous support of my friends. Honorable mention goes to Vartovkollegiet for five incredible years, during one of which I was a Ph.D. student. Also, I wish to thank Mateo, Stephen, Kath, David, Lindsay, and the other grad students at the Center for Applied Mathematics for making my visit so enjoyable.

I wish to thank my family for your endless support and for encouraging me in both good and bad times. Lastly, my endless gratitude goes to Mette Lybker Juul, min livsfordobler. For your patience, support, unconditional love, and for being the best life companion anyone could wish for. Thank you for being my rock all the way through this adventure. Here's to the next adventure, and the ones after that – I cannot wait to get started!

Jonas Søgaard Juul
Copenhagen, December 2019

List of Publications

The following publications are the constituting parts of this dissertation. The publications are ordered chronologically in this list but will appear in a different order in the dissertation text.

1. **Juul, Jonas S**. and Porter, Mason A., Synergistic Effects in Threshold Models on Networks, Chaos **28** 013115 (2018)
2. **Juul, Jonas S.**, Krishna, Sandeep, and Jensen, Mogens H., Entrainment of oscillations as a means of controlling somite patterning in a model of coupled presomitic mesoderm cells, Phys. Rev. E **98** 062412 (2018)
3. **Juul, Jonas S.** and Porter, Mason A., Hipsters on Networks: How a Small Group of Individuals Can Lead to an Anti-Establishment Majority, Phys. Rev. E **99** 022313 (2019)
4. **Juul, Jonas S.**, Jensen, Mogens H., and Krishna, Sandeep, Constraints on somite formation in developing embryos, J. R. Soc. Interface **16** (2019)
5. **Juul, Jonas S.** and Strogatz, Steven H., Scaling law for the impact of mutant contagion, arXiv:1910.00655, submitted
6. **Juul, Jonas S.**, Alessandretti, Laura, Dammeyer, Jesper, Zettler, Ingo, Lehmann, Sune, and Mathiesen, Joachim, Gender-specific behavior change following terror attacks, submitted
7. Zettler, Ingo, **Juul, Jonas S.**, Back, Mitja D., Gebauer, Jochen E., Küfner, Albrecht C. P., Dammeyer, Jesper, Lehmann, Sune, and Mathiesen, Joachim, Investigating Homophily, Network Centrality, and Social-Connection Duration of Grandiose Narcissists: Narcissistic Admiration and Rivalry in Big Data Social Networks, in preparation

The following research article was published during the course of the Ph.D. period but is not included as part of the dissertation.

- **Juul, Jonas S.** and Joyner, Christopher H., Isospectral discrete and quantum graphs with the same flip counts and nodal counts, J. Phys. A.: Math. Theor. **39** 13999 (2018)

Contents

Dedicated to my parents. For every second spent reading me books about dinosaurs.

Dedikeret til mine forældre. For hvert sekund brugt på at læse bøger om dinosaurer højt for mig.

Chapter 1

Introduction

1.1 Foreword

Nothing in our universe is completely isolated; everything is connected. For the past three years, I have had the great privilege of exploring many wonders of our connected world. The projects I have worked on deal with interacting systems of very different nature: From particular processes carried out by stem cells in developmental biology, to idealised contagion in abstract models of connected individuals. The projects also make use of very different methods. In some cases, I seek to answer questions using calculations and simulations. Other projects are entirely data-driven.

The diversity in projects is partially due to this work being funded by three different grants. The grants had very different scopes, and each provided one-third of the funding of this doctoral work. But the heterogeneity in topics also illustrates the fantastic importance of understanding how interactions of individual agents shape the world around us. Interactions are simply present in systems of all scales; big or small; biological, engineered, or social. Some interactions are of great importance, while others are nothing but noise.

I have enjoyed spending three years of my life exploring this connected world. I hope that this dissertation will succeed in conveying both the scientific importance of studying connected systems and my own fascination with the topic.

1.2 The purpose and content of this dissertation

Seven research articles constitute the backbone of this dissertation. These manuscripts were written during my Ph.D., and for each of the articles, I made important contributions to the presented research. I elaborate on these contributions in the coauthorship statements submitted with this dissertation.

The publications contain all of my most important academic achievements and are good representations of what I have spent my time on as a doctoral student. For this reason, I have written this dissertation as a synopsis of manuscripts and publications that are integrated parts of this dissertation. I present the papers as they were published or submitted.

The dissertation consists of 3 parts. Each part contains a number of chapters. Each chapter presents one of the manuscripts I have written during my Ph.D. The most important content of each chapter is the publication (and its corresponding Supplementary Information). In addition to a copy of the publication, each chapter contains: 1) an introductory section which motivates why the topic is interesting; 2) an introduction to the state-of-the-art, scientific context, and the objective of the manuscript; 3) a recap of the results of the manuscript. In addition to these sections,

some chapters contain a section commenting on work published after the publication came out.

The final chapter in each of the three parts ends with a section containing conclusions and perspectives for further research.

1.3 The structure of this dissertation

Each of the three parts consists of two or three articles that are related to each other in that they study the same system or data, concern related phenomena, or use similar methods.

Part I of the dissertation contains two papers that both concern the mechanism behind the timing and scaling of vertebrae precursors in mice. Chapter 2 gives an introduction to the biological system and presents my theoretical work on the somite-formation mechanism and how recent experimental results motivate this work. Chapter 3 introduces fundamentals in the theory of coupled oscillators. After this, I present my work on controlling phase waves in somite formation using external periodic forcing. Chapter 3 wraps up Part I with conclusions for both papers and perspectives for further research.

Part II of the dissertation contains three papers on contagion in networks. Chapter 4 introduces the concept of networks and three common ways of creating synthetic networks. The chapter also introduces simple contagion and complex contagion. These concepts are all necessary to present to understand the three papers in Part II. The rest of the chapter concerns models of contagion with synergistic effects. The publication at the end of Chapter 4 studies a deterministic model of synergistic complex contagion. Chapter 5 studies the formation of anti-establishment majorities in the light of complex contagion. Chapter 4 covers most of the prerequisites for understanding this piece of work. For this reason, the Chapter 5 primarily motivates why anti-establishment majorities are essential to study. Chapter 5 also introduces recent work on anti-establishment majorities. The final paper in Part II concerns the impact of mutant contagion. First, Chapter 6 presents some examples of mutant contagion and why such contagions are important. Then, existing work on diffusion paths and a simple model of mutations are introduced. The last thing to be presented before proceeding to the paper is recent experimental results that support the theoretical results derived in the article. A section with conclusions and scientific outlook completes Part II.

Part III of the dissertation presents two publications focusing on patterns in telecommunication data. Chapter 7 studies correlations between telecommunication patterns and scores on the Narcissistic Admiration and Rivalry Questionnaire. First, the chapter motivates why telecommunication data can be used as a means of studying human behavior. Following this, I briefly introduce the modern perception of narcissism and the concept of homophily. The chapter concludes with a summary of our results and a copy of the most recent manuscript version. (The manuscript is still in preparation). Chapter 8 presents a study of gender differences in behavior change following terror attacks. The chapter starts with a motivation for understanding how terror attacks impact the general population. Following this, the literature on the topic is introduced. In doing this, I mention the objectives of the presented publication. The chapter ends with a section containing conclusions and perspectives for further research concerning our projects on patterns in telecommunication.

Part I

Somite formation in mice

Chapter 2

Phase-gradient encoding in somite formation: Theory and predictions

The moment of conception sparks an intricate process of biological self-organization. In ever-increasing numbers, cells coordinate efforts to make an inanimate collection of biological building blocks into a living organism. At the same time as the fetus is growing, the complexity of the organism is developed. From the vulnerable organs to the protecting structure of the skeleton; from the global network of nerves to the delicateness of the heart valve, a living organism is created from the interplay of mindless biological entities.

That the complexity of living organisms arise from microscopic interacting ingredients is a fascinating fact of nature. With nobody overseeing the whole process, the collection of cells smoothly go about their business. Each cell can only sense and affect a tiny fraction of its cocreators but nonetheless the development runs on time like a clockwork. Not only are inevitable errors efficiently mitigated or corrected. The sequence at which each feature of the fetus is created is predictable and regular.

Considering the predictability of the result of seemingly tumultuous microscopic interactions of inanimate cells, the metaphor for biological development running like a clockwork is appealing. Could it be that such a clockwork exists, responsible for cueing stem cells to differentiate at exactly the right time? Or could it be that different subprocesses were controlled by clocks of their own, and interactions of these clocks were responsible for the predictable order of developmental events?

Clocks have been discovered in practically every corner of living organisms (Strogatz, 2004). Interactions between clocks are common too. From long oscillations of female menstrual cycles (McClintock, 1971), to daily variations in body temperature (Aschoff, 1965), and fast oscillations of protein regulatory circuits (Bar-Or et al., 2000; Geva-Zatorsky et al., 2006), the oscillations have diverse functions and characteristics. Many of these oscillatory behaviors are due to clocks residing in the organism itself, possibly being kept on a tight schedule through interactions with its immediate environment (Woller et al., 2016; Aschoff, 1965; Strogatz, 2004; Hardin, Hall, and Rosbash, 1990; Dibner, Schibler, and Albrecht, 2010). The *zeitgeber* which provides a signal the clock can synchronise to could be in the form of periodic environmental cues such as the day-night cycle (Weitzman et al., 1982; Aschoff, 1965; Hardin, Hall, and Rosbash, 1990), or other oscillating inputs such as feeding and fasting (Woller et al., 2016). Instead of asking "*Do clocks exist in biological development*?", one should rather ask "*How many clocks exist in biological development?*"; "*How is the timing of clocks translated into timely formation of patterns and organs?*"; "*How do different clocks keep in lockstep with each other?*", and "*Can we control the developmental clocks, and, thereby, developmental processes*?"

Enter physicists. Many of the above questions have to do with the dynamics of interacting oscillators. As we shall see in Chapter 3, such interactions can give

rise to fascinating behavior even in the simplest of settings. Exploring the link between biological interactions and observed behavior constitutes an overwhelming landscape of open questions. One strategy to explore this landscape is reductionism. By making simplifying assumptions on the system of interest, one can hope to find minimal requirements for specific dynamic behavior to occur. Simplification also has the added benefit of making numerical and analytical treatment simpler.

A stunning example of interplay between timing and pattern formation takes place in the *presomitic mesoderm* (PSM) in developing embryos. Across species, hundreds of stem cells act like clocks ticking at different speeds. The joint oscillations of these stem cells give rise to waves running across the PSM. Although the stem cells all beat with different frequencies, new waves occur with a fixed period. Rhythmically travelling across the stem cell population, the waves appear to control the formation of the vertebrae themselves.

How does a group of oscillators with diverse frequencies give rise to travelling waves with a fixed period, and how can such waves facilitate the creation of the complex pattern of vertebrae? These questions are still open, and they are at the core of my work on somitogenesis. In this and the following chapter, I present my results concerning these coupled oscillations, waves, and patterns. The end goal of this research is to understand and manipulate the travelling waves and the spatial pattern of segments created in the PSM.

2.1 Somite formation in developing embryos

2.1.1 A quick introduction to somite formation

In all vertebrates, the developmental machinery must cause the creation of a specified number of vertebrae. The precursors of vertebrae are called *somites*, and the creation of somites is called *somitogenesis*. Different vertebrates have different numbers of vertebrae. For example, humans have 33, mice have 65, and for snakes the number can exceed 300 (Gomez et al., 2008; Tam, 1981; Theiler et al., 1972). While the biological details can vary between different species (Soroldoni et al., 2014), somites are formed in the developing embryo, while the embryo is growing.

Figure 2.1 shows where the PSM is located in developing mouse and zebrafish embryos. It lies between the tailbud of the embryo and the created somite segments, which will later constitute the backbone of the animal. The tailbud region of the PSM is called the *posterior* PSM, while the part near the somite front is called the *anterior* PSM (Soroldoni et al., 2014). The PSM consists of stem cells, huddled together in a 3-dimensional elongated configuration. While the embryo is growing, the PSM length changes. It is shortened from the anterior, as groups of stem cells form new somites, differentiating with a fixed species-dependent period. It also gets longer as new stem cells get added in the posterior PSM. Whether the shortening or elongation is happening faster depends on the stage of development. The growth rate eventually comes to a halt. Hence, by the end of somitogenesis, the PSM only shortens.

The systematic differentiation of stem cells create the intricate pattern of vertebrae in vertebrates. But how do the right number of stem cells differentiate at the right time? What signals to individual stem cells that the time is right? And is this signal external and global, or internal to the cells and communicated between neighbours? Or some third option? Several frameworks accounting for this signalling and decision making have been put forward in the last half-century. I will touch upon the most important ones later in this chapter. Before proceeding to these frameworks, however, it is worth dwelling at one stunning experimental observation.

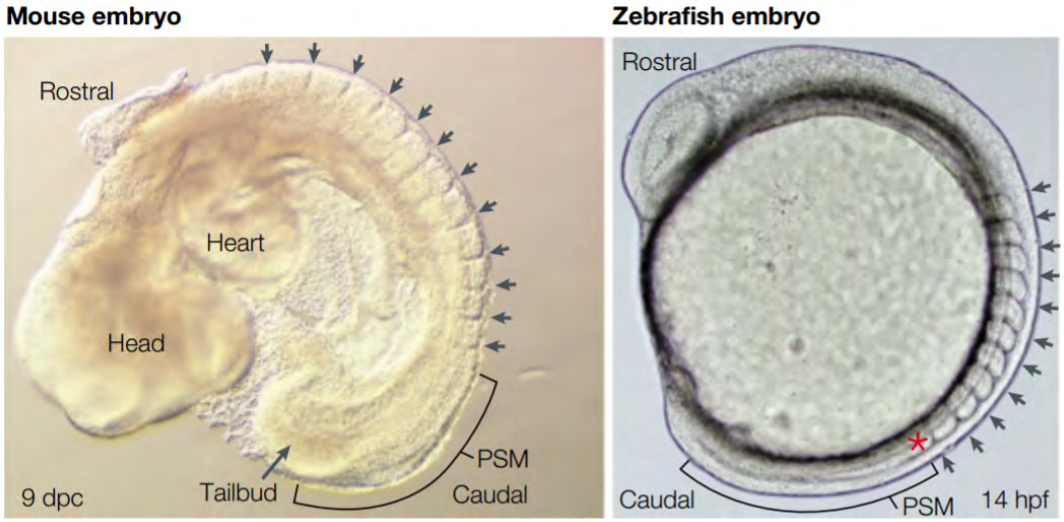

FIGURE 2.1: Illustration of the presomitic mesoderm (PSM) in two different vertebrate embryos. The PSM is an elongated, 3-dimensional population of stem cells. The PSM closest to the tailbud is called the posterior PSM. The opposite end is the anterior PSM. The arrows show borders between somites that have already been formed by PSM cells differentiating in a coordinated manner. Figure from (Saga and Takeda, 2001).

Across species, from chicks to mice and zebrafish, waves of gene expression have been found to travel the presomitic mesoderm from posterior to anterior (Oates, Morelli, and Ares, 2012; Palmeirim et al., 1997; Soroldoni et al., 2014; Lauschke et al., 2013; Cotterell, Robert-Moreno, and Sharpe, 2015). The waves are created by the timing of gene-expression oscillations in hundreds of cells. In each of these single stem cells, several genes oscillate – in mice, oscillations have been found in several different pathways (Tsiairis and Aulehla, 2016), e.g. Notch, Wnt and FGF (Özbudak and Pourquié, 2008). Somehow, cells coordinate their oscillations to form waves. Moreover, the arrest of the waves in the anterior PSM consistently correlates with somite formation – across species!

The correlation between the arrival of waves and somite formation, of course, does not imply a causal relation. The waves could be nothing but a byproduct of the real mechanism leading to somite formation. Nonetheless, the waves could provide the signal needed for the stem cells to differentiate at the right time and in the correct numbers. As we shall see, some experimental studies have reported evidence that the waves do have central roles to play in some species. The picture gets complicated by a number of experimental results showing how the machinery responsible for the timely somite formation depends on the species in question. The following section introduces these complications, a classical model for the somite-formation mechanism, and comments on some of the most recently reported experimental results contradicting the clock-and-wavefront model.

2.1.2 Mechanisms for somite formation

How the stem cells in the presomitic mesoderm successfully differentiate into somites at the right time and in the correct numbers is an intriguing question. In this section, I introduce the classical clock-and-wavefront model. This model has been extremely

influential, and only recently have experimental observations made it clear that alternative models are needed. Following the introduction of this classical model, I will mention recent experimental results on zebrafish and chicks, indicating that the real picture is more complicated than the model suggests.

The clock-and-wavefront model

The clock-and-wavefront model was proposed by Cooke and Zeeman in 1976 to account for the mechanism controlling the number of repeated segments during animal morphogensis (Cooke and Zeeman, 1976). Somitogenesis was one of the systems they wanted the model to describe. Somites are formed in the anterior PSM and are discrete segments formed by groups of cells. Any theory describing somite formation therefore must address 2 points: 1) *the when*; 2) *the where*. How do groups of stem cells differentiate together? How does this only happen in the anterior part of the PSM?

Cooke and Zeeman solved the two points using a clock and a wavefront, respectively. The central idea is that all cells can monitor time using some internal clock. At the same time, they can be advised of their spatial position by a "wavefront", meaning environmental cues.

Cells get added in the posterior PSM. They then gradually move towards the anterior following the addition of more cells in the posterior, and tissue shortening in the anterior. Eventually, cells enter a region of the PSM where they receive a signal. Once they have received this signal, they differentiate at a specified time – in synchrony with surrounding cells. In the original paper, Cooke and Zeeman only described this mechanism qualitatively. They did not suggest what would constitute the clocks, nor did they provide information about the nature of the wavefront providing spatial cues.

Since Cooke and Zeeman proposed the model, many studies have focused on uncovering the nature of the clock and wavefront. Oscillations have been found in several pathways, and models for the molecular clocks have been constructed (Özbudak and Pourquié, 2008; Aulehla and Herrmann, 2004; Horikawa et al., 2006; Lewis, 2003; Jensen et al., 2010; Mengel et al., 2010; Monk, 2003; Pedersen, Jensen, and Krishna, 2011). Moreover, morphogen gradients have been found to span the PSM, constituting plausible candidates for the wavefront mechanism (Dubrulle, McGrew, and Pourquié, 2001; Aulehla et al., 2003; Aulehla and Herrmann, 2004; Aulehla et al., 2008; Dunty et al., 2008). In other words, as cells move toward the anterior PSM, some surrounding chemicals change their concentration gradually. The concentration of these chemicals can consequently inform cells about their spatial position.

Although the existence of morphogen gradients and cellular clocks seem encouraging, experiments have repeatedly reported results that seem to be in contradiction with the clock-and-wavefront model (Packard Jr and Jacobson, 1976; Aoyama and Asamoto, 1988; Stern et al., 1988; Lauschke et al., 2013; Soroldoni et al., 2014; Cotterell, Robert-Moreno, and Sharpe, 2015). This has caused the model to be reformulated and reanalysed several times, bearing witness to the popularity of the model (Schnell and Maini, 2000; Baker, Schnell, and Maini, 2006b; Baker, Schnell, and Maini, 2006a; Murray, Maini, and Baker, 2011; Baker, Schnell, and Maini, 2008; Dubrulle and Pourquié, 2002; Pourquié, 2004).

Two of the most prominent examples of observations contradicting the clock-and-wavefront model were published very recently. The two cases concern the somite formation mechanism in zebrafish and chicks, respectively. In zebrafish, a study reported the time-scale of genetic oscillations to be insufficient to account for

the periodicity of segmentation (Soroldoni et al., 2014). The rate of tissue shortening and a gradual change in the PSM phase profile contribute to the period of segmentation too. This is much more complicated than the process being controlled by just a single clock in combination with spatial cues.

In chicks, a thorough theoretical and experimental analysis recently concluded that a range of experiments supported a model based on a local reaction-diffusion mechanism over the clock-and-wavefront model (Cotterell, Robert-Moreno, and Sharpe, 2015). The authors did not rule out that global morphogen gradients could be necessary in somitogenesis. Nonetheless, the study suggested that a clock-and-wavefront mechanism was insufficient to account for the outcomes of several experiments.

These recent results illustrate the striking diversity in observations for different species. Recent observations in mice add to this diversity. For mice, however, no theoretical framework accompanied the experimental observations. A simple theoretical framework describing the empirical results is what I have sought to formulate and explore. The following section introduces the recent empirical observations regarding the somite-formation mechanism in mice.

2.1.3 Evidence of phase-gradient encoding in mice

Above, I mentioned recent experimental and theoretical results regarding the somite-formation mechanisms in chicks and zebrafish. The research I have conducted on this topic concerns the somite-formation mechanism in mice. My interest in this topic was sparked by fascinating observations reported in the paper "Scaling of embryonic patterning based on phase-gradient encoding" published *Nature* in 2013 by Lauschke et al (Lauschke et al., 2013).

In a captivating study, Lauschke et al. examined how somite size is regulated during PSM growth. Previous studies had found that number and proportions of somites remained constant even under experimental manipulations of embryo size (Pourquié, 2004; Gregor et al., 2005; Tam, 1981; Brown et al., 2006). In other words, if the embryo was reduced in size, the segments became proportionally smaller, but otherwise resembled what observations in embryos of normal size. This ability to scale somite size during different growth conditions is intimately connected to one of the major questions presented earlier in this chapter: How is the number of cells that choose to differentiate and form a somite controlled?

To illuminate this scaling mechanism, the authors designed a novel experimental model. They made ex-vivo (quasi) single-layer cultures of stem cells consisting of stem-cells from the tailbud of mouse PSMs. These monolayer cultures they called mPSMs (monolayer PSMs). After an initial growth phase, they found that these mPSMs formed segments similar to the somites developed in the mouse PSM. The experimental model allowed them to study the scaling in detail, including how variations in external conditions affected the segment size.

Using a fluorescence to highlight oscillatory gene expression, Lauschke et al. found that waves of gene expression travelled the mPSMs. The cellular oscillators giving rise to these waves oscillated with frequencies similar to what is observed in real embryos. In the posterior, the oscillation period was similar to the segmentation period: approximately $T_0 = 130$ min. The period then increased linearly toward the anterior, the anteriormost cells oscillating with a period around 25%-30% longer than in the posterior.

At the arrest of the travelling waves at the segmentation front, new segments formed. This observation was even stable as the mPSM changed in size, and as external temperature was varied. Observing the travelling waves allowed the authors

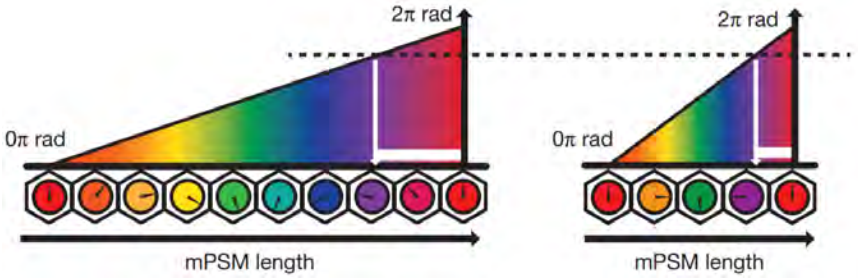

FIGURE 2.2: Illustration of the phase-gradient encoding reported by Lauschke et al. At somite formation, the total phase difference across the PSM is 2π. The cells containing the anterior-most 21% of this phase will constitute the newly formed somite. This mechanism persists for different PSM lengths. Figure from (Lauschke et al., 2013).

to make an extraordinary finding. For different temperatures, and unaffected by mPSM length, *exactly one wave spanned the mPSM when a new somite formed*. In other words, as one wave hit the anterior mPSM and a new somite formed, a new wave was always setting out from the posterior part of the mPSM.

Furthermore, the cells differentiating into the somite consistently accounted for the 21% anterior-most phase in the PSM. The authors concluded that these two key numbers, the 2π of phase difference spanning the PSM (equivalent of 1 wave) and the 21% of phase deciding the width of the somite, could be how somites scale across the growth of the PSM in mice. Figure 2.2 illustrates this proposed scaling mechanism. The reported phase-gradient encoding as a means of somite scaling is different from what mechanisms reported in connection to somite formation in both chicks and zebrafish (Soroldoni et al., 2014; Cotterell, Robert-Moreno, and Sharpe, 2015). Several details about the proposed mechanism remained unanswered after the publication of this paper. 4 of such questions are

1. Why 21% and 2π? What is the connection between these numbers?

2. If a new somite forms when 2π of phase spans the PSM, will the resulting somite always consist of cells accounting for the 21% anterior-most phase? Or can this "phase width" be altered?

3. Are there other observable consequences of the proposed scaling mechanism by phase-gradient encoding?

4. If the global phase differences are causing somites to form, cells must have access to this global information. What mediates this information?

The first 3 of these questions are the topic of my research presented in this chapter. The results are published in the paper "Constraints on somite formation in developing embryos", published in Journal of the Royal Society Interface (Juul, Jensen, and Krishna, 2019). They constitute a demystification of fundamental figures in the proposed mechanism of phase-encoded scaling and a set of predictions that follow from the proposed mechanism. Question 4 is better answered experimentally. Nonetheless, we comment on this question toward the end of the paper. In Section 2.3, I shall recapitulate recent work related to this question and repeat the argument from the article in this context. In the following section, I convey the main results of our paper.

2.2 Our results: Connecting key figures in phase-gradient encoding and providing predictions

In the paper "Constraints on somite formation in developing embryos", published in Journal of the Royal Society Interface (Juul, Jensen, and Krishna, 2019), Sandeep Krishna, Mogens H. Jensen and I study a simple model of the mPSM. We ignore spatial dimensions orthogonal to the anteroposterior axis, thereby reducing the mathematical system to a single dimension. We suppose that cells lie along this axis and that their periods and oscillation phases resemble what observations in experiments in PSMs and mPSMs. Specifically, we make oscillation periods increase linearly from posterior ($x = 0$) to anterior ($x = 1$), $T(x) = T_0(1 + x\lambda)$. The PSM also changes in size; new cells are added in the posterior end, and cells are removed in chunks in the anterior end (mimicking somite formation). We assume that somite formation happens with period T_s, and pay special interest to the case $T_s = T_0$, as this captures experimental observations.

Using the simple model, we provide a mathematical argument that the assumptions above (all following from experimental observations) lead to a connection between period gradient, phase width, which we denote $\tilde{\phi}$, and phase difference across the PSM at somite formation. This connection is summarised in the formula,

$$\tilde{\phi} = 2\pi k \frac{\lambda}{1+\lambda}. \tag{2.1}$$

If $T_s = T_0$, $k = 1$. We show that experimental observations are in agreement with this relation even if we assume only 5% error on the measurements. This connection answers the 1st of the questions posed in the previous section.

Because phase-gradient encoding connects physical somite size to the phases of cellular oscillators, we make an effort to calculate expressions for the stable "phase profile" of the PSM under different growth conditions. The phase profile is the distribution of phases from posterior to anterior. We manage to do this for two essential cases: 1) When the PSM grows as quickly as it is shortened ("constant length"); 2) When the PSM does not grow at all. The latter case corresponds to the experiments of Lauschke et al. We find that any monotonously increasing period gradient leads to a concave phase profile in the former case. We find that with the parameters reported by Lauschke et al., the phase profile in the latter case is almost linear (slightly convex). We argue that this, too, is in agreement with experimental observations. Seeking to understand the biological impact of phase-profile shape, we argue that concavity of the phase profile can reduce the impact of erroneous phase decoding on the physical pattern of somites.

We also use our insight on phase profiles for PSMs with "constant length" to derive relations between the period gradient, physical somite size, and maximal phase difference over the PSM. In particular, we find that if exactly 2π spans the PSM at somite formation, the fraction of cells that constitute the next somite is approximately described by $\lambda/2$. These claims can all be tested explicitly, and answer the 3rd question of the previous section.

Lastly, having found the connection between phase width and period gradient, Eq. (2.1), we propose changing the phase width by perturbing the period gradient. Specifically, we suggest perturbing the periods of all cells by a constant amount of ξT_0, $\xi \in \mathbb{R}$. We provide explicit formulas for the phase width as a function of perturbation size, $\tilde{\phi}(\xi)$, and convert this relation into physical somite size for the particular cases of constant length and no growth. We find that increasing the period of all cells

causes both phase width and spatial somite width to decrease. These results answer the 2nd of the questions posed in the previous section.

2.3 Recent work and how this relates to our results

Our results are part of an ongoing effort to understand the mechanism behind somite formation and scaling. After having derived our results, we were made aware of experiments that had possibly already tested some of our predicitions. Recent studies have also illuminated how the differentiation mechanism might work in the mouse PSM. In this paragraph I comment on these related studies.

Possible contradiction between experiments

One of our main results is that the proposed phase-encoding mechanism couples the somite width to the oscillation periods in the PSM. We showed that increasing all oscillation periods by a constant amount of ξT_0 would decrease phase width. In the cases of constant length and no growth, we concluded that this perturbation would also reduce physical somite width. In a striking coincidence, similar experiments have been carried out and published in (Harima et al., 2013).

Harima et al. reduced the oscillation period of *Hes7*, a cyclic gene that has been studied meticulously in relation to somitogenesis in mice. They sped up these oscillations by modifying the *Hes7* gene; specifically they reduced the number of intron, thereby affecting the amount of delay in the oscillation. The experiments were carried out in mice, and they found that the modification made segments smaller in size and larger in number. This finding is exciting because we concluded that the proposed phase-encoding mechanism should cause segments to become *larger* if the oscillation period were reduced.

It thus seems that the experimental results of Harima et al. could contradict the findings of Lauschke et al. Before this can be concluded with certainty, however, we must be positive that the assumptions of our calculations are not broken in the experiment carried out by Harima et al. The experiment did not quantify differences across space in the PSM. Hence, we do not know whether a phase difference of 2π occupied the PSM at somite formation or whether 21% of this turned into the next somite. We also do not know the growth rate of the PSM, or whether the period was changed uniformly over the whole PSM. It could be that the period gradient changed shape as a consequence of the experimental procedure. The only period that is quantified is the average period in the PSM. In addition to these reservations, it is not clear that results in *in vitro* mPSMs translate directly to *in vivo* results from actual mouse embryos. Thus, it is not clear that we can falsify the proposed phase-encoding mechanism from the results presented by Harima et al. On a brighter note, the results indicate that it might be possible to carry out the experiments we propose and directly test the phase-encoding mechanism in vivo.

Interacting clocks: Experiments and models

If the global phase distribution in part controls somite formation, cells must have access to system-level information about the phase distribution. The exact nature of such information mediation remains unknown, but recent experiments have indicated that this mediation could come down to interacting cellular clocks. In this section, I briefly introduce these latest results, a theoretical study supporting the possibility of such a mechanism. I will end the section by commenting on how these

new findings relate to our results and the phase-encoding mechanism proposed by Lauschke et al.

As mentioned previously in this chapter, oscillations exist in several pathways in mouse-PSM cells. Among these, the most prominent pathways are the FGF, Wnt, and Notch pathways (Özbudak and Pourquié, 2008). Lauschke et al. (Lauschke et al., 2013) and other related studies have mostly studied waves produced by oscillations in the Notch pathway (Aulehla et al., 2008; Tsiairis and Aulehla, 2016; Bulusu et al., 2017; Delaune et al., 2012; Masamizu et al., 2006). In an innovative study, Sonnen et al. studied the interaction between the Wnt and Notch signalling by visualising and manipulating oscillations in these two pathways (Sonnen et al., 2018; Sonnen and Aulehla, 2014). Their findings were striking. While the oscillations in the two pathways were out of phase in the posterior PSM, oscillations beat in synchrony in the anterior PSM. If the authors manipulated oscillation phases such that the two pathways oscillated out of phase in the whole PSM, segmentation was impaired! In other words, the phase difference between two clocks seemed to control the timing of somite formation.

The finding of Sonnen et al. that the phase difference between two biological clocks could control somite patterning raises the following question. What kinds of coupled clocks significantly change their oscillatory behavior depending on their phase difference? Given some "output variable" in one of two coupled gene networks, what kinds of networks make the magnitude of this output depend on the phase difference between the two gene networks? Beauxpeux & François identified several classes of coupled, oscillating gene networks that could cause such variation in output variables depending on phase differences (Beaupeux and François, 2016). These networks show "shocks" for certain phase-differences and their existence demonstrates that coupled-clocks phase encoding is a plausible mechanism for somite formation in mice.

One might also ask: How do these recent result directly relate to the theoretical framework we developed? For the phase-encoding mechanism proposed by Lauschke et al. to work, every oscillator must be able to compare their Notch-oscillation phase to the posteriormost oscillator. If this is not the case, somite formation happening when the total phase difference over the PSM is 2π cannot be guaranteed. The mechanism of phase encoding by interacting clocks provides a way for single cells to gain information about the global phase distribution in this way.

Suppose the Wnt oscillations were synchronised or nearly synchronised for all cells. Also, suppose that the phase differences between Notch and Wnt oscillations in the posteriormost cell were fixed (as reported by Sonnen et al.). A cell comparing its Notch-oscillation phase to its Wnt-oscillation phase would effectively be comparing its Notch-oscillation phase to the Notch-oscillation of the posteriormost PSM cell. Interestingly, such nearly-synchronised Wnt oscillations are exactly what the experiments by Sonnen et al. uncovered in the Wnt pathways. While waves of Notch oscillations travelled across the PSM, the Wnt oscillations came in nearly-synchronised pulses. Hence, the coupling between oscillators in the Notch and Wnt pathways provide not only a mechanism for initiation of somite formation. It also provides a way for somites to scale according to the 21% rule put forward by Lauschke et al.

2.4 Paper: Constraints on somite formation in developing embryos

INTERFACE

royalsocietypublishing.org/journal/rsif

Research

Cite this article: Juul JS, Jensen MH, Krishna S. 2019 Constraints on somite formation in developing embryos. *J. R. Soc. Interface* **16**: 20190451.
http://dx.doi.org/10.1098/rsif.2019.0451

Received: 27 June 2019
Accepted: 29 August 2019

Subject Category:
Life Sciences–Physics interface

Subject Areas:
biocomplexity, biophysics, systems biology

Keywords:
somites, oscillators, phase waves, scaling, dynamical scaling

Authors for correspondence:
Jonas S. Juul
e-mail: jonas.juul@nbi.ku.dk
Sandeep Krishna
e-mail: sandeep@ncbs.res.in

Electronic supplementary material is available online at https://doi.org/10.6084/m9.figshare.c.4656155.

THE ROYAL SOCIETY PUBLISHING

Constraints on somite formation in developing embryos

Jonas S. Juul[1], Mogens H. Jensen[1] and Sandeep Krishna[2]

[1]Niels Bohr Institute, University of Copenhagen, Blegdamsvej 17, Copenhagen 2100, Denmark
[2]Simons Centre for the Study of Living Machines, National Centre for Biological Sciences, Tata Institute of Fundamental Research, Bangalore, India

JSJ, 0000-0002-5728-9269; SK, 0000-0002-0581-173X

Segment formation in vertebrate embryos is a stunning example of biological self-organization. Here, we present an idealized framework, in which we treat the presomitic mesoderm (PSM) as a one-dimensional line of oscillators. We use the framework to derive constraints that connect the size of somites, and the timing of their formation, to the growth of the PSM and the gradient of the somitogenesis clock period across the PSM. Our analysis recapitulates the observations made recently in *ex vivo* cultures of mouse PSM cells, and makes predictions for how perturbations, such as increased Wnt levels, would alter somite widths. Finally, our analysis makes testable predictions for the shape of the phase profile and somite widths at different stages of PSM growth. In particular, we show that the phase profile is robustly concave when the PSM length is steady and slightly convex in an important special case when it is decreasing exponentially. In both cases, the phase profile scales with the PSM length; in the latter case, it scales dynamically. This has important consequences for the velocity of the waves that traverse the PSM and trigger somite formation, as well as the effect of errors in phase measurement on somite widths.

1. Introduction

A particularly striking example of biological self-organization is that of segmental patterning in vertebrate embryos. During somitogenesis in vertebrate species, somite segments, the precursors of vertebrae, form periodically as the embryo elongates. In mice, chick and zebrafish embryos, cells in the presomitic mesoderm (PSM) behave like a population of coupled oscillators. Expression of many genes oscillate in each cell, and cells coordinate their oscillations such that kinematic waves of gene expression travel from the posterior end of the PSM to the anterior. The arrival of each wave at the anterior end is correlated with the formation of a new somite [1–4]. In this paper, we investigate the constraints that connect these waves to the somite width and the gradient of oscillation periods across the PSM.

Several genes are known to oscillate in the PSM of vertebrates, most importantly those in the Notch, Wnt and FGF pathways [5]. The period of oscillations often depends on the position of the cell along the antero-posterior axis. There is a region in the tail bud where all cells oscillate synchronously with a time period characteristic of the species, which can range from ≈30 min for zebrafish to ≈2 h in mice. The oscillations slow down as one moves from the posterior end of the PSM (right after the tail bud) to the anterior end [1,4,6]. In mice, this 'period gradient' is linear—see [4], who find that the posterior-most cells oscillate with a period ≈130 min, linearly increasing to 25–30% higher for the anterior-most cells.

As mentioned earlier, examining how the oscillations develop over time revealed travelling kinematic waves of gene expression that move from posterior to anterior. For instance, Lauschke *et al*. [4] report that the position of

peak levels of LuVeLu, a Notch signalling reporter, moves from posterior to anterior in *ex vivo* cultures of mouse PSM cells (so-called mPSMs), with a velocity that depends on the length of the mPSM [4]. Similar waves are observed in a reporter for the oscillating gene *her1* in zebrafish [3]. An important difference between these species is that in zebrafish, several waves can simultaneously co-habit the PSM [3], whereas experiments on mPSMs have found maximally one wave existing at a time [4]. However, in both cases, as well as in other species, the formation of the next somite is coincident with the arrival of a wave at the anterior end, in the vicinity of the previous somite. The mechanism that triggers the formation of a new somite is still a matter for debate. It was thought for years to be the classic clock and wavefront model [7], but this theory has recently been challenged. Cotterell *et al.* [8] combine theory and experiments to suggest that, in chick embryos, formation of new somites might be caused by a reaction–diffusion mechanism in the anterior PSM that interacts with the oncoming wave, while Sonnen *et al.* [9] suggest that interactions between two different oscillating pathways may be what triggers somite formation in mice.

Regardless of the mechanism, some interesting observations have been made about the periodicity of somite formation and scaling of the somite widths. In mPSMs, the formation of a new somite was found to occur when 2π of phase (i.e. one full wave) was spanning the PSM. That is, when a wave reached the anterior end, and a new somite formed, the next wave was just setting out from the posterior end. Furthermore, each new somite consisted of the anterior-most cells that contained 21% of the total phase difference across the PSM, irrespective of the length of the PSM at that time [4]. Although many different aspects of the coupled oscillating cells in the PSM have been investigated theoretically, ranging from models of global wave patterns and morphogen gradients, to models of the underlying biological clocks and the effect of couplings on defect-free patterning [8,10–20], nothing is known about the measurable consequences of such phenomenological observations about the phase of the cells in the PSM. In the present paper, this is what we seek to illuminate. A second goal of our work is to understand the interplay between such oscillations (and travelling waves) and the growth of the PSM. Across species, the PSM is known to elongate at the posterior end as the tail bud extends. The length of the PSM is determined by a combination of this growth at the posterior end, and shrinkage at the anterior end as new somites are formed. During somitogenesis, the PSM length typically initially increases, then may remain steady for a duration and finally decreases (indicating an eventual decrease in the growth rate at the posterior end). We examine how the period gradient, growth of the PSM and shrinkage due to somite formation combine to affect the phases of oscillating cells, and what quantitative constraints this places on the somite widths and the timing of their formation.

The rest of the paper is structured as follows. In §2, we introduce our model and key assumptions. In §3.1, we show that the period gradient, the total phase difference across the PSM at somite formation, the growth rate of the PSM and the width of the new somite cannot be independent of each other. We explicitly derive the mathematical constraint that connects these quantities and, in §3.1.1, show that experimental measurements from mPSMs match this constraint. Section 3.2 calculates the phase profile across the PSM in the specific situation where the PSM length is in steady state, i.e. it is shortened by somite formation at the same rate as it grows at the posterior end, and §3.3 calculates the constraints on somite widths that exist in a PSM with steady-state length. Our analysis provides explicit predictions for how the phase of a cell should depend on the antero-posterior location of that cell in wild-type embryos that abide by these constraints (§3.2), and for the expected change in somite widths in an experiment that would perturb the period gradient (§3.4). Finally, we examine the case where PSM growth is arrested, similar to the end of somitogenesis, and make predictions for how somite widths and the PSM length change with time in this case (§3.5). Section 4 discusses the experimental predictions stemming from our analysis and speculates on the implications for somitogenesis.

2. Theoretical framework for analysing the phase of the oscillating cells in the presomitic mesoderm

We focus on the phase of the oscillation in cells rather than the full waveform of gene expression levels. That is, we associate with each cell a single dynamical variable taking values between 0 and 2π representing the phase of the somitogenesis clock in that cell, and a time period that sets the rate of change of the phase. In doing so, we make the implicit assumption that varying the time period simply scales the oscillation waveform without changing its shape otherwise. This seems to be consistent with experimental data (e.g. see fig. 2 in [3]) and is what allows us to characterize each cell by a single variable, its phase, and a single parameter, its time period, that controls how quickly the phase changes. Furthermore, we simplify the PSM into a one-dimensional line of cells since the spatial periodicity in somite formation is along the posterior–anterior axis.

Thus, the system we consider (figure 1) consists of a one-dimensional line of cells, each associated with a phase and a time period, pictorially represented by a clock face with the clock hand showing the current value of the phase. As observed in embryos, new oscillators are frequently added at the posterior end of the PSM and, when a new somite is formed, oscillators are removed from the anterior end of the PSM. Thus, we allow cells to be added to the posterior end periodically every T_g time units ($1/T_g$ is thus the PSM growth rate),[1] and removed from the anterior end whenever a somite is formed. The evolution of the phase of each cell depends only on the time period of that cell, which in turn depends only on the location of the cell on the line. Thus, the period of a cell may change as addition or removal of cells changes the relative distance of the cell from the posterior end of the line. Travelling waves can occur in this set-up. For instance, if the periods of all cells were identical, but the phases initially decreased progressively from 2π at the posterior (left) end to 0 at the anterior (right) end, then over time one would observe that the location of phase 2π (or 0) would move from left to right, corresponding to a travelling wave moving from posterior to anterior (figure 1). In this purely illustrative scenario, the speed of the wave would depend only on the initial phase differences between adjacent cells but, in general, the periods may be different for different cells, in which case the speed of the wave would depend on the period gradient as well as the phase differences.

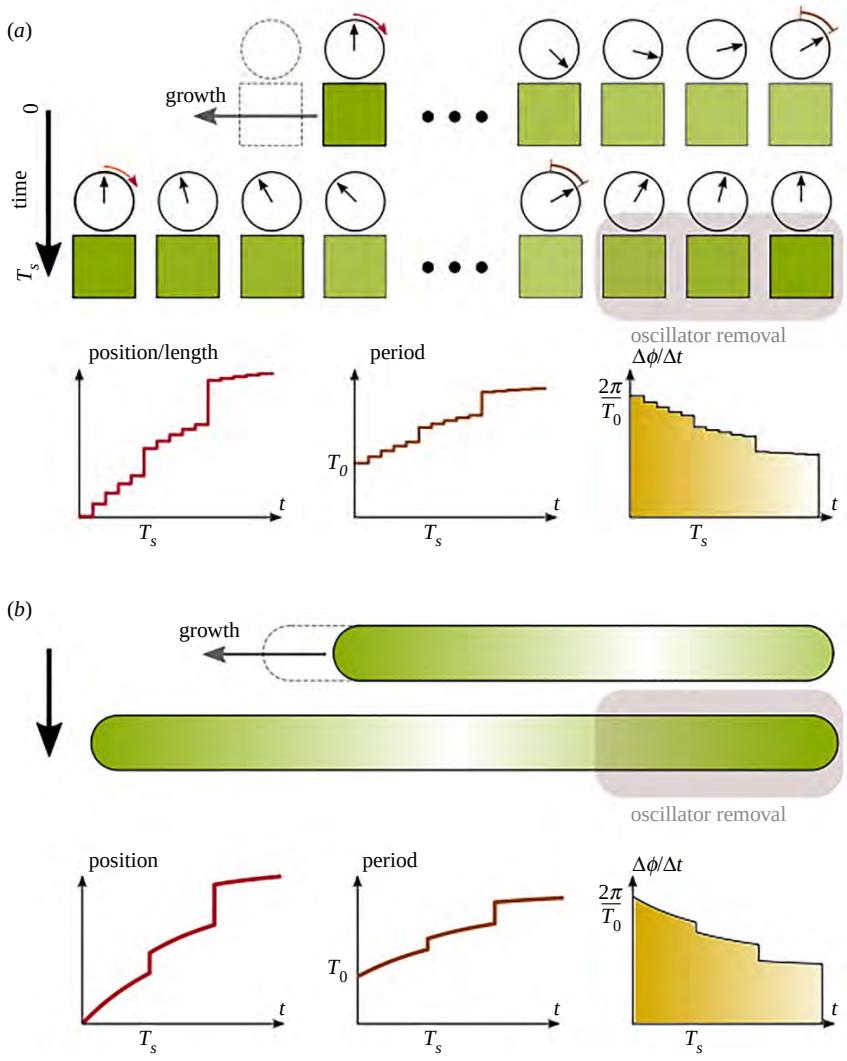

Figure 1. Illustration of the idealized PSM. (*a*) Discrete system. The PSM is approximated as a finite number of oscillators on a line. The phase of each oscillator changes according to a position-dependent oscillation period $T(x)$. The posterior-most cell is located at $x = 0$, while the anterior-most cell is at $x = 1$. The relative position of an oscillator changes as cells are gradually added to the posterior (with period T_g), and removed (with period T_s) in chunks from the anterior end. As time progresses, each cell effectively moves toward the anterior; the three insets show, as a function of time, the relative position, oscillation period and change of phase per time of a cell which is initially located at the posterior-most position. (*b*) The same as in (*a*), but in a PSM where the relative position x does not take a finite number of discrete values, but is taken to be continuous $x \in [0, 1]$. This approximation is justified when the number of cells in the PSM is large. (Online version in colour.)

2.1. Key assumptions

We make the following assumptions regarding the phases and periods that characterize the oscillations of each cell:

(A) Cells oscillate with a time period $T_0(1 + x\lambda)$, where x is the location of the cell relative to the posterior end, normalized to the total length of the PSM (thus $x \in [0, 1]$), and T_0 is a species-dependent base time period.
(B) A new cell that is added to the posterior end, whenever the PSM grows, is assigned a phase identical to its immediate neighbour, the cell that was until then the posterior-most PSM cell. Subsequently, of course, the phases may start to differ as the two cells will have different time periods.

Assumption (A) posits a linearly increasing period gradient, similar to observations in mPSMs [4], as discussed earlier. In §3.2, we show that our key results hold for any increasing period gradient, but for now we assume that the period gradient is linearly increasing. Assumption (A) also implicitly assumes that as new cells are added and removed, due to growth and somite formation, the morphogen gradient determining the periods is quickly reset in such a way that the new posterior and anterior ends retain their periods, T_0 and $(1 + \lambda)T_0$, respectively. This is justified by observations in real embryos and *ex vivo* cell cultures in mice: in embryos, the time period of somite formation, which also coincides with the time period of the posterior-most cell, is found to be stable at ≈2 h between days 8 and 13.5, during which time more than 60 somites are formed [21]. In *ex vivo* experiments, the posterior period has been found to be stable at ≈130 min while the tissue was shortening periodically, and other cells slowed down their oscillations as they moved towards the anterior of the

colony, ending up with periods of length ≈170 min [6] when they were located at the anterior end of the PSM. Note that, when a new somite is formed, this implies that the period gradient (in real length units) becomes steeper. If the phase differences between oscillators in such a resetting were not altered too much, then such a steepening of the gradient should result in slower travelling waves in the smaller PSM. This matches experimental observations [4]. Assumption (B) seems reasonable given that cells in the tailbud and the posterior end of the PSM show stable synchronized oscillations.

Note that we do not explicitly include inter-cellular coupling between the phases of the adjacent cells. However, we do implicitly take into account the effects that coupling would have on the time periods of cells because we use the empirically observed time period gradient. For a line of coupled oscillators, the time period of each oscillator will be determined both by external factors (e.g. morphogen gradients) that affect the natural (uncoupled) time period, as well as the coupling to adjacent oscillators. A sufficiently strong coupling between adjacent oscillators in a one-dimensional line can lead to complete synchronization of all the oscillators even if they had substantially different uncoupled time periods. Since the oscillators do not synchronize their oscillations, the coupling must be relatively weak to allow the time period to vary across the PSM. Nevertheless, even a weak coupling might modify the observed time period gradient from that produced by the morphogen gradient alone. We therefore proceed with the assumption that such a weak coupling would have little effect on the dynamics of the phases of the cells beyond modifying the period gradient from that produced by the morphogen gradients alone, and perhaps also mitigating the effects of noise on the phases. Hence, for our purpose it is sufficient to include the coupling only implicitly by using the empirically observed period gradient.

With the assumptions mentioned above, we will attempt to obtain and study phase profiles $\phi(x)$ that are in steady state. By steady state, we do not mean that $\phi(x)$ is time independent, but rather that $\phi(x)$ is the same, modulo 2π, at corresponding times between somite formation (for example, right before, or right after, a somite forms). This means that the phase profile exhibits what has been termed 'dynamical scaling' in the literature [22], i.e. as the PSM changes in length the pattern of oscillations across it scales correspondingly. We will impose the constraint that new somites are formed from the cells that contain the anterior-most $\tilde{\phi}$ of phase. We shall refer to $\tilde{\phi}$ as the phase width of the somite. This constraint, and the scaling of $\phi(x)$ with PSM length, are the key observations of recent experiments [4], the consequences of which we set out to explore.

3. Results

3.1. The period gradient constrains the somite width and vice versa

Let $\phi(t, x)$ denote the phase of a cell at time t and location x, where $x \in [0, 1]$ is the distance from the posterior end, normalized by the PSM length. Let $\Delta\phi(t) \equiv \phi(t, x = 1) - \phi(t, x = 0)$ denote the total phase difference across the PSM at time t. Assumptions (A) and (B) imply that between somite formations $\Delta\phi(t)$ increases linearly in time:

$$\Delta\phi(t) = \Phi_{\text{before}} - \tilde{\phi} + \frac{2\pi\lambda}{T_0(1+\lambda)}t, \tag{3.1}$$

where we assume the previous somite formed at time $t = 0$ and left a total phase difference of $\Phi_{\text{before}} - \tilde{\phi}$ across the PSM just after somite formation ($\tilde{\phi}$ is the phase width of the somite, described previously, and Φ_{before} is the total phase difference across the PSM before the somite is formed). If the phase profile is in steady state just before every somite formation event, it follows that $\Delta\phi(nT_s)$ is equal to the same constant, Φ_{before}, for any integer value of n. Therefore, it must be that the total increase in $\Delta\phi$ between somite formations must exactly match $\tilde{\phi}$, i.e.:

$$\tilde{\phi} = \frac{2\pi T_s}{T_0}\frac{\lambda}{1+\lambda}, \tag{3.2}$$

where T_s is the time at which the next somite forms. Because we are considering a steady state, the phase of the anterior-most cell of the PSM must also be the same (modulo 2π) before each somite formation. Therefore, T_s must be a multiple of T_0, and we obtain

$$\tilde{\phi} = 2\pi k\frac{\lambda}{1+\lambda}, \tag{3.3}$$

where k is a positive integer. Thus, assuming steady state implies that the slope of the period gradient, λ, and the phase-width of the somite, $\tilde{\phi}$, cannot be independent. Note that here we only assume that $\Delta\phi$ is in 'steady state'—this does not necessarily imply that the PSM length is a constant before each somite formation. Assuming that the length is a constant imposes additional constraints. Note also that the PSM growth rate does not appear in equation (3.3). Its role emerges in determining the width (as opposed to the phase width) of somites. Both these issues will be explored in §3.2.

3.1.1. Comparison with data

In the mouse PSM, the period gradient has been measured in [6] along with the phase width of the newly formed somites [4]. They find that $\lambda \approx 0.275$, $\tilde{\phi} = 0.21 \cdot 2\pi$ and $T_s = T_0 = 130$ min. All numbers are not provided with experimental error bars in [4], but even with as low as 5% error, using $\lambda = 0.275$ in equation (3.3) gives $\tilde{\phi}_{\text{predicted}} = 0.216 \cdot 2\pi \pm 0.008\pi$, while using $\tilde{\phi} = 0.21 \cdot 2\pi$ in equation (3.3) gives $\lambda_{\text{predicted}} = 0.266 \pm 0.017$. Either way, the experimental observations are consistent with equation (3.3).

3.2. When presomitic mesoderm length is constant steady-state phase profile is concave in shape

As mentioned, equation (3.3) does not assume that the length of the PSM right before (or after) each somite formation is a constant. Adding the assumption that the PSM length is also in steady state allows us to calculate not just $\Delta\phi$ but also the entire steady-state phase profile, which we will denote $\phi_{ss}(x)$. Electronic supplementary material, sections 1 and 2 show this calculation both for the continuum limit, where the number of cells in the PSM is assumed to be infinite, and for the discrete case where the number of cells is finite.

Figure 2 shows the steady-state phase profile obtained from our calculations when $T_s = T_0$, $\lambda = 0.266$, $\tilde{\phi} = 0.21 \cdot 2\pi$,

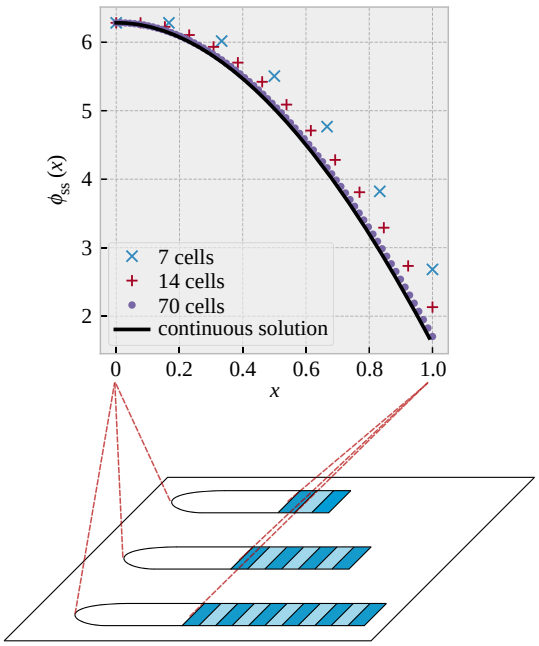

Figure 2. Steady-state phase profile of a PSM of constant length, $\phi_{ss}(x)$. The black curve shows the steady-state phase profile in the continuum limit (calculated from equation (16) in electronic supplementary material, section S2), when we choose $T_s = T_0$, $\lambda = 0.266$, $\Phi_{\text{before}} = 2\pi$ and $\tilde{\phi}$ and T_g are chosen such that the length of the PSM varies in a sawtooth manner as follows: $\mathcal{L}(t) = L_0(1 + (t \bmod T_0)/(7T_0))$. Note that due to the freedom to choose units of time and length, $\phi_{ss}(x)$ will not depend on what specific values we choose for T_0 and L_0. Also plotted are the steady-state phase profiles calculated for PSMs consisting of a finite number of cells; symbols correspond to PSM lengths after somite formation, $N = 7$ (cross symbols), 14 (plus symbols) and 70 cells (filled circles). These profiles are calculated for the case where $T_s = T_0$, $\lambda = 0.266$ and T_g and $\tilde{\phi}$ are chosen such that the PSM length varies in a sawtooth manner as $N(t) = N + \lfloor t/T_g \rfloor \bmod N/7$. We numerically approximate the phase profiles the discrete calculation of electronic supplementary material, section 1 would produce for these parameters, by simulating a discrete PSM with length varying as above and updating the phases of each oscillator in time according to equation (7) in electronic supplementary material, section S1, until steady-state is achieved. Here, Φ_{before} is determined by the remaining parameters, and as seen in the plots, converges to the value obtained in the continuum calculation when N becomes large. Note the concave shape of all the phase profiles plotted. In section B1 and electronic supplementary material, section 6, we show analytically that this concave shape is robust to changes in parameter values and holds for all increasing period gradients, linear or nonlinear. (Online version in colour.)

PSM lengths just after somite formation are $N = 7$ (cross symbols), 14 (plus symbols) and 70 cells (filled circles), and T_g is chosen such that we obtain maximum PSM lengths of $N(1 + 1/7)$. These parameters, based on the observations of [4] result in a phase profile with a *concave* shape. The curve is concave both immediately before and after somite formation, since somite formation amounts to removing the anterior-most part of the pre somite-formation curve, and 'stretching' the remaining part to cover the full interval [0, 1], neither of which changes the concavity.

When N is large enough, the phase profile is indistinguishable for different N, which means that the PSM exhibits scaling—the entire somitogenesis pattern scales with the real length of the embryo but does not change in structure otherwise. The calculation for large N also matches our continuum calculation for a PSM with infinitely many oscillators, which is shown by the continuous line in figure 2 (see figure 1*b* for a schematic for the continuous approximation of the PSM).

A testable prediction from our model is that the steady-state phase profile is not linear, but concave in shape. This has consequences for the speed of the travelling waves and reduces the influence of errors in differentiation decisions on somite size, which we will return to in the Discussion. The concave shape is in fact a robust feature of the steady-state phase profile whenever the PSM length is in steady state, the growth rate is constant and the time period of cells $T(x)$ is an increasing (linear or nonlinear) function of x. We demonstrate this in the next section.

3.2.1. Concavity is a robust property of the steady-state phase profile for any increasing period gradient

That the steady-state phase profile must be concave in shape for any increasing $T(x)$, can be seen from the following general argument.

Suppose that the PSM consists of a very large number of cells, so we can use the continuous variable $x \in [0, 1]$ to describe a cell's position relative to the posterior (at $x = 0$) and the anterior end (at $x = 1$). Let $T(x)$ be the period gradient of the PSM, and let this be increasing from posterior to anterior. Suppose that one cell has initial position $x_{0,\text{first}} = x^*$, and another has initial position $x_{0,\text{second}} = x^* + \epsilon$, where $0 \leq x^* < 1$, and $0 < \epsilon \ll 1$. Let us assume $t = 0$ to be immediately after somite formation, and let the phase difference between the two cells at this time be $\delta\phi_\epsilon = \phi(x) - \phi(x + \epsilon) > 0$. We now examine how the phase difference between these cells changes between $t = 0$, and the time following the next somite formation at $t = T_s$. The change in phase difference between the two cells in this time period is

$$\Delta\phi_\epsilon(t = T_s) = \int_0^{T_s} \frac{2\pi}{T(t, x^*)}\,\mathrm{d}t - \int_0^{T_s} \frac{2\pi}{T(t, x^* + \epsilon)}\,\mathrm{d}t. \tag{3.4}$$

Now, since $\epsilon \ll 1$, we expand the fraction in the final integral[2]

$$\frac{1}{T(t, x^* + \epsilon)} \approx \frac{1}{T(t, x^*)} - \epsilon \frac{1}{(T(t, x^*))^2}\left(\frac{\partial T(t, x^*)}{\partial x(t)}\right)\frac{L_0}{\mathcal{L}(t)}, \tag{3.5}$$

where L_0 is the length of the PSM at $t = 0$, and $\mathcal{L}(t)$ is the length of the PSM at time $t \geq 0$. Inserting this expression in equation (3.4) yields

$$\Delta\phi_\epsilon(t = T_s) = \epsilon \int_0^{T_s} \frac{1}{(T(t, x^*))^2}\left(\frac{\partial T(t, x^*)}{\partial x(t)}\right)\frac{L_0}{\mathcal{L}(t)}\,\mathrm{d}t. \tag{3.6}$$

Since $T(x)$ is increasing and positive, and since $\mathcal{L}(t)$ is positive and increasing between successive somite formations, $\Delta\phi_\epsilon > 0$. This means that the phase difference between the two cells increases between the two successive somite formations. The phase difference is the same after the somite formation at $t = T_s$, and because the PSM length is in steady state, the difference in position between the two cells is still ε after the somite formation at $t = T_s$. The convexity or concavity of the phase profile is determined by the second derivative—a decreasing, concave function has a negative second derivative, while the second derivative is positive for a decreasing, convex function. An alternative formulation of this is that a decreasing, concave function decreases faster at larger values of the variable it is plotted against, while a decreasing, convex function decreases slower for larger

values of the variable. We shall use this formulation to show generality of the phase profile concavity.

The phase profile gradient between the cells at their initial position is $\delta\phi_\epsilon/\epsilon$, and the phase profile gradient between the cells at their final position is $(\delta\phi + \Delta\phi_\epsilon)/\epsilon$. Calculating the ratio yields

$$\frac{(\delta\phi_\epsilon + \Delta\phi_\epsilon)/\epsilon}{\delta\phi_\epsilon/\epsilon} = 1 + \frac{\Delta\phi_\epsilon}{\delta\phi_\epsilon} > 1. \tag{3.7}$$

From this, we conclude that the steady-state phase profile decreases faster as x is increased; or equivalently, the steady-state phase profile is concave.

3.3. Constraint on phase differences when presomitic mesoderm length is constant

Now that we have calculated $\phi_{ss}(x)$ we can ask what is the phase difference across the PSM in this state. Following exactly the same argument as in §3.1, it must be true that $\tilde{\phi} = 2\pi k\lambda/(1+\lambda)$. However, in this case, we can also derive the actual width of the somite, i.e. the number of cells removed from the anterior end, which must equal the number of cells added between somite formations, T_s/T_g. Since the steady-state phase profile scales with respect to the PSM length right after somite formation, N, it is of interest to calculate the fractional width of the somites $\beta \equiv T_s/(NT_g)$ (i.e. β is defined as the width of the somite divided by the length of the PSM just *after* somite formation). Just before somite formation, this fractional width must satisfy:

$$\phi_{ss}\left(1 - \frac{\beta}{1+\beta}\right) - \phi_{ss}(1) = \tilde{\phi} = 2\pi k\frac{\lambda}{1+\lambda}. \tag{3.8}$$

Similar to equation (3.3), this is a constraint between the fractional somite width β, the period gradient and the parameters that determine $\phi_{ss}(x)$, namely, T_s, T_0, Φ_{before} and $\tilde{\phi}$. See electronic supplementary material, section 5 for more details on how the phase width, $\tilde{\phi}$, can be converted to the fractional width of the somite, β, using this constraint.

Figure 3 shows a heat map of this constraint, derived from our continuum calculation, when $T_s = T_0$ and $\tilde{\phi} = 0.21 \cdot 2\pi$. The colours show the value of Φ_{before} that satisfy the constraint equation (3.8) for different values of β and λ. This heat map is another prediction of our analysis. Qualitative features that should be experimentally observable include the following: the phase difference between posterior and anterior right before somite formation, Φ_{before}, (i) decreases with somite size β (for fixed λ), (ii) increases with λ (for fixed β) and (iii) the line $\beta \approx \lambda/2$ corresponds to the special case $\Phi_{\text{before}} = 2\pi$. Prediction (iii) suggests that any change in the period gradient in the mPSM *ex vivo* cultures should result in exactly the same change in the fractional width of the somites. Moreover, our calculations predict that this linear relationship depends on there being exactly one wave spanning the PSM at a time. If the system exhibited multiple waves, say $\Phi_{\text{before}} = 4\pi$ corresponding to two waves, then the relationship between β and λ would be nonlinear.

3.4. Variation of somite width caused by perturbing the period gradient

Assuming that the general constraint of equation (3.3) holds in embryos that are perturbed in various ways, our framework makes specific predictions for the effect of such perturbations. A perturbation that could be feasible to implement experimentally, for instance, by affecting the Wnt or FGF gradient in the PSM, would be to change the period of *all* cells by the same additive amount ξT_0. Equation (3.3) would then become

$$\tilde{\phi}(\xi) = 2\pi k\frac{\lambda}{1+\lambda+\xi}. \tag{3.9}$$

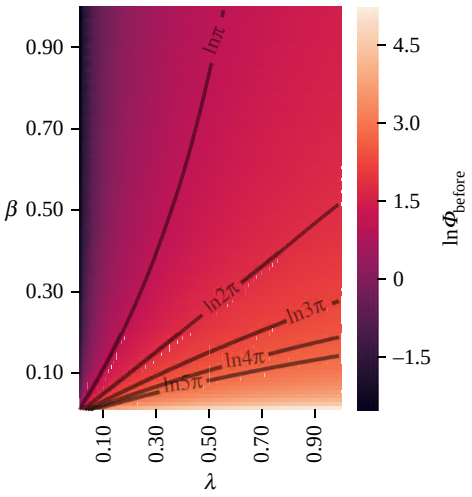

Figure 3. Heat map of logarithm of the total phase difference across the PSM just before somite formation, Φ_{before}, in steady-state phase profiles when the PSM length is constant, as given by the analytical continuum calculation of the constraint equation (3.8). The phase difference is 2π on a line $\beta \approx \lambda/2$. (Online version in colour.)

In figure 4*a*, we show how the somite phase width varies with ξ, assuming all other parameters remain the same. Using our analytical calculation in the continuum limit of a PSM of constant length, we can convert the predicted phase width of somites to an actual fractional width (as described above and in electronic supplementary material, section S5). The result is shown in figure 4*b*. Thus, we predict that increasing (decreasing) the period of the cells in this manner would decrease (increase) both the phase width and actual width of the somites. Generally, the fractional width of somites, β, will be a non-increasing function of ξ whenever the steady-state phase of cells decreases from posterior to anterior.

3.5. Physical somite size and convexity of phase profile in presomitic mesoderms with no growth

Finally, we consider a case where after the system has reached the steady-state described above, new cells stop being added to the posterior part of the PSM but cells continue to be cut off from the anterior end when new somites are formed. This approximates the very end of somitogenesis (although there the rate of addition of new cells decreases continuously over time rather than falling abruptly to zero). When no new cells are added to the PSM, but the phase across the PSM is in steady-state, we find (see electronic supplementary material, section S3) that the length of the PSM of course decreases with time, shrinking by a constant multiplicative factor after each somite formation, which results in an exponential decrease of PSM length with time.[3] Nevertheless, our calculations (see electronic supplementary material, section S3) show that the phase profile can attain a steady state. This

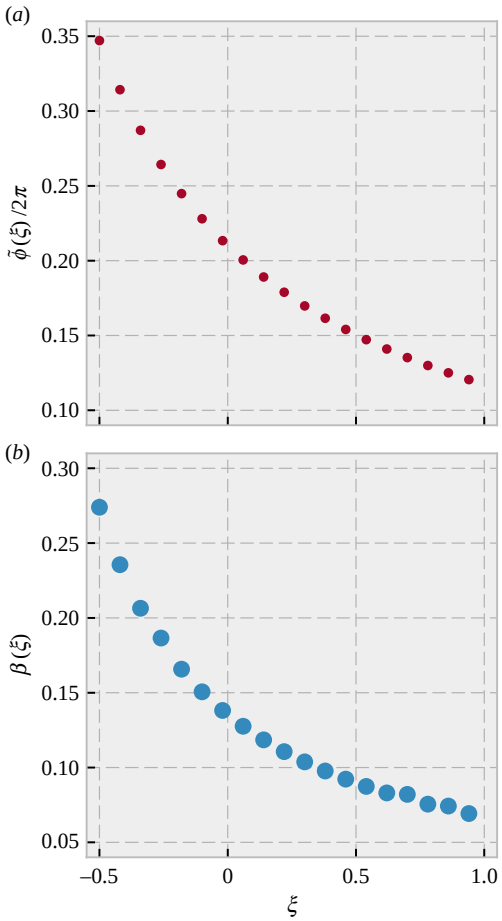

Figure 4. Effect of perturbations on somite widths. Assuming $T_s = T_0$, and that the constraint expressed in equation (3.3) holds under perturbation of periods in the PSM, we predict that perturbing all periods by an additive amount ξT_0 will alter somite width. (*a*) The phase width of somites (small dots) will decrease with ξ, and is described by equation (3.9). (*b*) In a PSM of constant length, phase width can be mapped to the actual spatial width of the somite using the continuum solution plotted in figure 2. We find that this spatial width also decreases with ξ as shown by the big dots. (Online version in colour.)

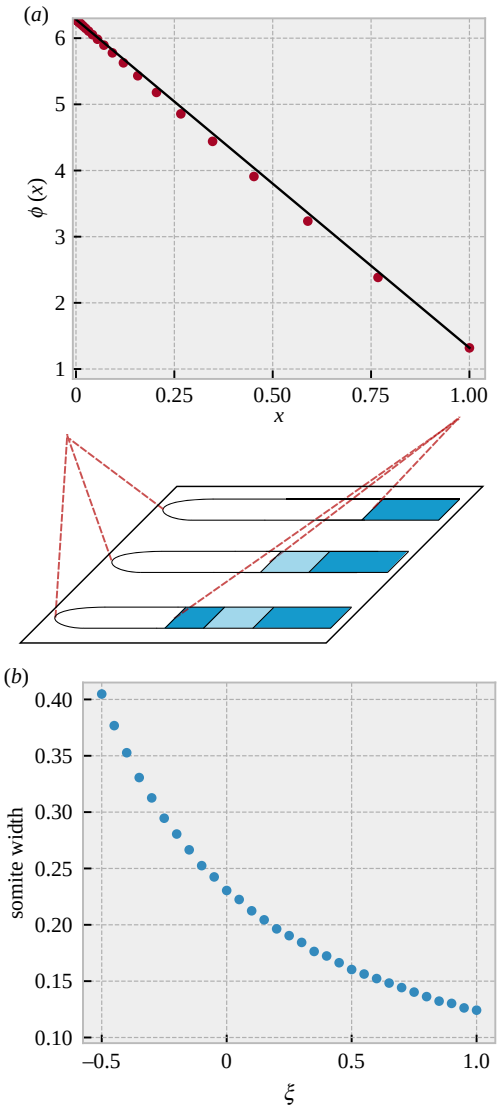

Figure 5. Steady-state phase profile for a PSM that does not grow, but is shortened periodically by removing the anterior-most $0.21 \cdot 2\pi$ of phase when the total phase difference between anterior and posterior is 2π. The period gradient is linear with $\lambda = 0.266$. (*a*) The points show the steady state phase profile just after somite formation, and a straight line between the end points is shown for comparison. The profile is close to linear and is convex rather than concave in shape. (*b*) Assuming a perturbation of all periods by an additive amount ξT_0, we plot the actual somite width as a function of perturbation size. The physical size decreases as periods get longer. (Online version in colour.)

analytically calculated steady-state profile is plotted in figure 5*a* (dots), and is much closer to linear, as opposed to the concave shape obtained in the case of a steady-state PSM length. In fact, it is very slightly *convex*.[4] This almost-linear phase profile also scales with the PSM length in the continuum limit.

Also in this case, we can examine the consequence of perturbing all periods in the PSM by a fixed amount ξT_0. Electronic supplementary material, section S4 shows the calculation of the new somite widths caused by this perturbation, and figure 5*b* plots these as a function of ξ. We find that the width decreases as the periods get longer, similar to what we found in the case of constant PSM length. The exponential decrease of PSM length with time and the shift to an almost-linear phase profile are both testable predictions of our model.

4. Discussion

The experimental observation in [4] that the total phase difference across *ex vivo* mPSMs is 2π and that 21% of this phase constitutes the next somite, independent of PSM size, is a curious one. It is not obvious what the consequences of this may be for somites, and even more unclear why it would be necessary or useful (if indeed it is either) for mice embryos to develop in this way. Our work here shows that this observation directly results in a constraint that connects the width of somites and the period gradient across the PSM during somitogenesis. The constraint applies to what we term the phase-width of the somite, while in the particular case where we assume a steady-state PSM length an additional constraint applies to the actual width of the somite. This constraint influences the shape of the phase

profile. For a PSM with steady-state length, we predict that the phase profile will be concave, while a PSM with no growth would have an almost linear (slightly convex) phase profile.

The shape of the phase profile is important for at least two reasons. The first is that it affects how travelling waves develop over time—for a concave profile, the waves slow down as they approach the anterior end, while for a convex profile they speed up. The experiments of Lauschke *et al.* are in *ex vivo* cultures where there is no growth. Our calculations for the no-growth scenario predict an almost linear phase profile, which would predict that the waves propagate with close to constant velocity. This is in fact what [4] observe. By contrast, slowing down of waves, corresponding to a concave profile, is visible in kymographs from zebrafish experiments [3]. The shape of the phase profile thus has a significant effect on the timing of somite formation, and would therefore be worth measuring in more quantitative detail in future experiments.

The second reason is reducing the effect of errors in somite formation. Recent experiments have found that gene-expression noise increases from posterior to anterior [19] in zebrafish. If some error were present in the phase width of formed somites (suppose that the phase width in one instance was $0.23 \cdot 2\pi$ instead of $0.21 \cdot 2\pi$), then the steepness of the phase profile would determine the effect of such errors on the spatial pattern. If the phase profile were steep in the anterior, phase width would change quickly with spatial location, and forming a somite with this slightly increased phase width would alter the physical size of the formed somite very little. Hence, a steep phase profile in the anterior PSM diminishes errors in the physical size of somites. A concave phase profile gets steeper towards the anterior end of the PSM, i.e. the phase difference between neighbouring cells increases from posterior towards the anterior. The opposite is true for a convex phase profile which flattens out toward the anterior end. These considerations suggest that if somite formation depends on a measurement of phases of the cells, and if, as is likely, these measurements are error-prone, then one should observe smaller errors in the somite widths when the PSM length is steady, compared to later in somitogenesis when it is decreasing.

The constraint of equation (3.3) also has predictable consequences for perturbation experiments, which might be experimentally tractable. One study reduced the number of introns in the Hes7 gene, resulting in more rapid oscillations [24]. They observed shorter segments, i.e. the opposite behaviour of what we expect from our calculations in §3.4 based on the experiments in mouse *ex vivo* cultures [4]. So it seems that the two experiments contradict each other. The experiment of [24] did not, however, measure the phase difference across the PSM. So, it would be useful to determine whether the assumption of constant phase difference is violated in this case. It would be interesting to study when perturbations of this sort break the assumption of constant difference and when they do not. If perturbations that do not break the assumption can be found, they would provide a very useful tool to control somite width in a precise and predictable manner.

Another type of perturbation that may be feasible experimentally is to alter the steepness of the period gradient by suitably altering the expression of the morphogen that controls the time period of the somitogenesis clock. In mPSMs, if such a perturbation still results in a steady state with a single wave spanning the PSM at any time, then we predict the change in fractional somite width should be close to half the fractional change in the slope of the period gradient (figure 3). Conversely, if the number of waves spanning the PSM increases under this perturbation, then we predict the relationship between the change in the fractional somite width and the change in the slope of the period gradient would become nonlinear.

Our analysis begs the question of how the embryo maintains the constant phase difference across the entire PSM just before each somite formation. Does the embryo 'know' that the peak of a travelling wave has reached the anterior end, and send a 'signal' to the posterior end to start a new wave? Or is the information transmitted in the other direction, such that the onset of a new peak at the posterior end 'causes' the travelling wave to reach the other end at the same time? A third possibility is that this is simply a non-causative correlation caused by some other constraint in the system. We speculate that inter-cellular coupling between the phases of the oscillating cells could be responsible for this behaviour. However, as mentioned before, inter-cellular coupling cannot be too strong or else the cells would start to synchronize despite their intrinsically different time periods, and this has not been observed. It would be interesting to study what kinds of weak coupling in a one-dimensional line of oscillators with varying time periods could produce travelling waves that are constrained in such a manner. The framework we have introduced here (or the approach of Ares *et al.* [25], whose model includes coupling which produces synchronized oscillations across the PSM) could be easily extended for this purpose.

These lines of thought also have implications for the mechanisms of somite formation. The well-known clock and wavefront model assumes that somites form when an oscillating cell moves into a sub-threshold region of an existing morphogen gradient that is tied to the growing posterior end of the PSM. Such a model does not necessarily need travelling waves of gene expression, but one could postulate that somites form when the peak of the travelling wave hits some low threshold of the morphogen gradient. Cotterell *et al.* [8] suggest instead that the somite forms due to reaction–diffusion events in the vicinity of the previous somite when the oncoming travelling wave interacts with a gradient of molecules whose source is the previous somite. It is not clear if there is a simple way to connect such events with the formation of a new wave peak at the posterior end. In both cases, somite formation would be triggered by events at the anterior end and would need some additional mechanism to constrain the total phase difference across the PSM. Recently, a third mechanism has been proposed in mice: Sonnen *et al.* [9] reported that Wnt and Notch pathways oscillate out-of-phase in cells in the posterior PSM, and in-phase in cells at the segmentation front. They found that the Wnt pathway does not have slow waves travelling periodically from posterior to anterior like the Notch pathway does. Instead, fast-travelling, pulse-like waves were reported [9], which indicates that the Wnt clocks are (nearly) synchronized across the PSM. Thus, with one clock oscillating with frequency dependent on the spatial position of the cell, while the other clock is synchronized (or nearly synchronized) for all cells across the PSM, measuring the phase difference between the two clocks of a single cell would be equivalent to measuring the phase difference between the Notch clock of the posterior-most cell, and the Notch clock of the cell in question, somewhere else in the PSM. This could serve as a signal to trigger somite formation directly dependent on a measurement of the total phase difference across the PSM, a

mechanism similar to what was reported by Lauschke *et al.* [4] and whose consequences we have studied in this paper.

Data accessibility. No data were collected. All calculations are elaborated in the electronic supplementary material.

Authors' contributions. J.S.J., M.H.J. and S.K. designed the study. J.S.J. developed the theoretical formalism and carried out the calculations. J.S.J. and S.K. wrote the manuscript, and M.H.J. contributed significantly to this process.

Competing interests. We declare we have no competing interests.

Funding. S.K. thanks the Simons Foundation and the National Centre for Biological Sciences for funding. J.S.J. and M.H.J. acknowledge support from the Danish Council for Independent Research and Danish National Research Foundation through StemPhys Center of Excellence, grant no. DNRF116.

Acknowledgements. We are grateful to Alexander Aulehla, Andy Oates and Raj Ladher for discussions.

Endnotes

[1]Our framework allows T_g to vary in time, as it often does during somitogenesis. However, in this paper, we will examine cases where T_g is assumed to be constant.
[2]See electronic supplementary material, section S6.1 for more details.
[3]This is consistent with observations in [23] which show that the rate of decrease of PSM length slows down over time in the latter part of somitogenesis, although the data are not precise enough to determine whether the slow down is exponential or not. We note that this predicted exponential decrease could also be inferred directly from scaling arguments, if one assumes that even in this decreasing phase of somitogenesis the embryo pattern scales with embryo size. However, our calculation provides additional information on exactly how the exponential rate depends on the period gradient (or equivalently the phase width). For $\lambda = 0.266$, $\Phi_{\text{before}} = 2\pi$ and $\tilde{\phi} = 0.21 \cdot 2\pi$, we find the multiplicative factor to be ≈ 0.77.
[4]See electronic supplementary material, section S6.2 for more on this convexity.

References

1. Oates AC, Morelli LG, Ares S. 2012 Patterning embryos with oscillations: structure, function and dynamics of the vertebrate segmentation clock. *Development* **139**, 625–639. (doi:10.1242/dev.063735)
2. Palmeirim I, Henrique D, Ish-Horowicz D, Pourquié O. 1997 Avian hairy gene expression identifies a molecular clock linked to vertebrate segmentation and somitogenesis. *Cell* **91**, 639–648. (doi:10.1016/S0092-8674(00)80451-1)
3. Soroldoni D, Jorg DJ, Morelli LG, Richmond DL, Schindelin J, Julicher F, Oates AC. 2014 A doppler effect in embryonic pattern formation. *Science* **345**, 222–225. (doi:10.1126/science.1253089)
4. Lauschke VM, Tsiairis CD, François P, Aulehla A. 2013 Scaling of embryonic patterning based on phase-gradient encoding. *Nature* **493**, 101–105. (doi:10.1038/nature11804)
5. Özbudak EM, Pourquié O. 2008 The vertebrate segmentation clock: the tip of the iceberg. *Curr. Opin. Genet. Dev.* **18**, 317–323. (doi:10.1016/j.gde.2008.06.007)
6. Tsiairis CD, Aulehla A. 2016 Self-organization of embryonic genetic oscillators into spatiotemporal wave patterns. *Cell* **164**, 656–667. (doi:10.1016/j.cell.2016.01.028)
7. Cooke J, Zeeman E. 1976 A clock and wavefront model for control of the number of repeated structures during animal morphogenesis. *J. Theor. Biol.* **58**, 455–476. (doi:10.1016/S0022-5193(76)80131-2)
8. Cotterell J, Robert-Moreno A, Sharpe J. 2015 A local, self-organizing reaction–diffusion model can explain somite patterning in embryos. *Cell Syst.* **1**, 257–269. (doi:10.1016/j.cels.2015.10.002)
9. Sonnen KF *et al.*2018 Modulation of phase shift between Wnt and notch signaling oscillations controls mesoderm segmentation. *Cell* **172**, 1079–1090.e1. (doi:10.1016/j.cell.2018.01.026)
10. Baker R, Schnell S, Maini P. 2006 A clock and wavefront mechanism for somite formation. *Dev. Biol.* **293**, 116–126. (doi:10.1016/j.ydbio.2006.01.018)
11. Jörg DJ, Morelli LG, Soroldoni D, Oates AC, Jülicher F. 2015 Continuum theory of gene expression waves during vertebrate segmentation. *New J. Phys.* **17**, 093042. (doi:10.1088/1367-2630/17/9/093042)
12. McHale P, Rappel W-J, Levine H. 2006 Embryonic pattern scaling achieved by oppositely directed morphogen gradients. *Phys. Biol.* **3**, 107–120. (doi:10.1088/1478-3975/3/2/003)
13. Jörg DJ. 2015 Nonlinear transient waves in coupled phase oscillators with inertia. *Chaos* **25**, 053106. (doi:10.1063/1.4919831)
14. Goldbeter A, Pourquié O. 2008 Modeling the segmentation clock as a network of coupled oscillations in the Notch, Wnt and FGF signaling pathways. *J. Theor. Biol.* **252**, 574–585. (doi:10.1016/j.jtbi.2008.01.006)
15. Jensen PB, Pedersen L, Krishna S, Jensen MH. 2010 A Wnt oscillator model for somitogenesis. *Biophys. J.* **98**, 943–950. (doi:10.1016/j.bpj.2009.11.039)
16. Mengel B, Hunziker A, Pedersen L, Trusina A, Jensen MH, Krishna S. 2010 Modeling oscillatory control in NF-κB, p53 and Wnt signaling. *Curr. Opin. Genet. Dev.* **20**, 656–664. (doi:10.1016/j.gde.2010.08.008)
17. Juul JS, Krishna S, Jensen MH. 2018 Entrainment as a means of controlling phase waves in populations of coupled oscillators. *Phys. Rev. E* **98**, 062412. (doi:10.1103/PhysRevE.98.062412)
18. Vroomans RM, ten Tusscher KH. 2017 Modelling asymmetric somitogenesis: deciphering the mechanisms behind species differences. *Dev. Biol.* **427**, 21–34. (doi:10.1016/j.ydbio.2017.05.010)
19. Keskin S *et al.* 2018 Noise in the vertebrate segmentation clock is boosted by time delays but tamed by notch signaling. *Cell Rep.* **23**, 2175–2185.e4. (doi:10.1016/j.celrep.2018.04.069)
20. Glass DS, Jin X, Riedel-Kruse IH. 2016 Signaling delays preclude defects in lateral inhibition patterning. *Phys. Rev. Lett.* **116**, 128102. (doi:10.1103/PhysRevLett.116.128102)
21. Saga Y. 2012 The synchrony and cyclicity of developmental events. *Cold Spring Harbor Perspect. Biol.* **4**, a008201. (doi:10.1101/cshperspect.a008201)
22. Ishimatsu K, Hiscock TW, Collins ZM, Sari DWK, Lischer K, Richmond DL, Bessho Y, Matsui T, Megason SG. 2018 Size-reduced embryos reveal a gradient scaling-based mechanism for zebrafish somite formation. *Development* **145**, dev161257. (doi:10.1242/dev.161257)
23. Tam P. 1981 The control of somitogenesis in mouse embryos. *Development* **65**, 103.
24. Harima Y, Takashima Y, Ueda Y, Ohtsuka T, Kageyama R. 2013 Accelerating the tempo of the segmentation clock by reducing the number of introns in the Hes7 gene. *Cell Rep.* **3**, 1–7. (doi:10.1016/j.celrep.2012.11.012)
25. Ares S, Morelli LG, Jörg DJ, Oates AC, Jülicher F. 2012 Collective modes of coupled phase oscillators with delayed coupling. *Phys. Rev. Lett.* **108**, 204101. (doi:10.1103/PhysRevLett.108.204101)

Supplementary Information: Constraints on somite formation in developing embryos

Published in Journal of the Royal Society Interface

Jonas S. Juul *[1], Mogens H. Jensen[1], and Sandeep Krishna†[2]

[1]Niels Bohr Institute, University of Copenhagen, Blegdamsvej 17, Copenhagen 2100-DK, Denmark
[2]Simons Centre for the Study of Living Machines, National Centre for Biological Sciences, Tata Institute of Fundamental Research, Bangalore, India

August 21, 2019

1 Phase profile in a PSM consisting of a finite number of cells

In this section, we will calculate phase profiles for a system, in which a finite number of oscillators are placed on line. We assume that new oscillators are added at the left end of the line with time intervals $T_g = m_L/T_0$, with $m_L \in \mathbb{N}$, $T_0 > 0$, and that the rightmost $m_R \in \mathbb{N}$ oscillators are removed with time intervals $T_s = T_0$ (it is straight forward to substitute another value of T_s in our analysis). Here, T_0 is the time period of the oscillator at the left end of the line, corresponding to the posterior end of the PSM. For simplicity, we furthermore consider the case $m_L = m_R = m$, corresponding to a line in steady state: In a time interval T_0, it grows as much as it is shortened. The system is illustrated in Fig. 1 in the main text. If we choose $t = 0$ to coincide with the addition of an oscillator at the left end of the line, and removal of m oscillators at the rightmost part of the line, and assume that the line consists of N oscillators at $t = 0$, the number of oscillators on the line is given by

$$\mathcal{L}(t) = N + \left(\left\lfloor \frac{t}{T_g} \right\rfloor \mod m \right). \tag{1}$$

Because the line of oscillators changes its length with time, each oscillator will also change its position on the line, relative to the left end (the time dependent position of an oscillator starting on the leftmost position on the line is shown on the leftmost plot, Fig. 1 A in the main text. Because new oscillators are added on the left end of the line, an oscillator effectively moves one position to the right each time a new oscillator is added. Likewise, every time m oscillators are removed from the right end of the line, each oscillator, remaining on the line, effectively moves to the right relative to the length of the line. To formulate an expression for the relative position of an oscillator on the line, let us first consider the case where no oscillators are removed on the right hand side. The line only grows, and it does this by the addition of oscillators on the leftmost end of the line. In this case, no matter the length of the line, the number of oscillators to the right of oscillator i is constant. Assuming that the line initially had length $\mathcal{L}(0) = N$, and that the initial position of the oscillator was $0 \leq i_0 \leq N - 1$, we can exploit this fixed distance to the rightmost end of the line in writing

*jonas.juul@nbi.ku.dk
†sandeep@ncbs.res.in

down an expression for the relative position of the oscillator at time t,

$$x_{\text{only\_growth}}(t) = \frac{\mathcal{L}(t) - (N - i_0)}{\mathcal{L}(t) - 1}. \tag{2}$$

In the above expression, the numerator is an integer, which is $N - i_0$ smaller than the total number of oscillator on the line. Dividing by the total length (minus 1) yields a number in the interval $[0, 1]$, the relative position of the oscillator. When including periodic removal of oscillator from the right, the expression for the relative position of an oscillator becomes

$$x_i(t) = \frac{\mathcal{L}(t) - \left[N - \left(i_0 + \left\lfloor \frac{t}{T_0} \right\rfloor m\right)\right]}{\mathcal{L}(t) - 1}. \tag{3}$$

This expression is similar to Eq. (2), except for the term that is added to i_0 in the numerator. This term, $\left\lfloor \frac{t}{T_0} \right\rfloor m$ accounts for the removal of m oscillators in time intervals of length T_0. This is taken into account because every time oscillators are removed to the right of oscillator i, its distance to the rightmost end of the line changes, and this is what we use to calculate $x_i(t)$.

With the above definitions, we are almost ready to calculate steady state phase profiles. First, however, we must define how oscillation periods change as a function of position on the line of oscillators.

We will assume that oscillation period increases linearly from $T(x = 0) = T_0$ at the posterior end (leftmost end of the line, where new oscillators are added) to $T(x = 1) = (1 + \lambda)T_0$ at the anterior end (rightmost end of the line, where oscillators are removed from). This assumption is based on experimental observations in mouse mPSMs, as discussed in the main text. λ has been determined to be between 0.25 and 0.30 experimentally. Furthermore, we assume that newly added oscillators have initial phase identical to that of the oscillator which occupied the leftmost point on the line until the moment when this new oscillator was added. We implement this assumption by defining the period of oscillators having *negative* spatial positions to have a period and initial phase identical to that of the oscillator on the position $x = 0$ (still referred to as the leftmost oscillator, even though oscillators can now take negative spatial positions, corresponding to oscillators that have not been added to the line yet). Thus, the period distribution is,

$$T(x) = \begin{cases} T_0(1 + \lambda x) & , \text{ if } x \geq 0, \\ T_0 & , \text{ if } x < 0. \end{cases} \tag{4}$$

This allows us to write down the phase of oscillator i at time t,

$$\phi_i(t) = \phi_i(t = 0) + \int_0^t \frac{2\pi}{T(t')} dt' \tag{5}$$

$$= \phi_i(t = 0) + \int_0^{t_{\text{intro}}} \frac{2\pi}{T_0} dt' + \int_{t_{\text{intro}}}^t \frac{2\pi}{T(t')} dt' \tag{6}$$

$$= 2\pi(1 + \frac{t_{\text{intro}}}{T_0}) + \int_{t_{\text{intro}}}^t \frac{2\pi}{T(t')} dt', \tag{7}$$

where t_{intro} is the time at which the oscillator is introduced at the leftmost end of the line. We can calculate the steady state phase distribution of a line of minimum length N, given $T_g = m/T_0$. We can do this, by identifying N oscillators that will take positions $0, 1, \ldots, N - 1$ at some point, right after oscillators are removed from the rightmost end of the line. First, we notice that all oscillators that end up at the rightmost position, $N - 1$ immediately after removal of oscillators, must previously have taken positions $N - 1 - mn$, $n \in \mathbb{N}$, at corresponding times. One oscillator, which has negative position, but satisfies this, is an oscillator with position $N - 1 - \lceil N/m \rceil m$. If this oscillator starts at position $N - 1 - \lceil N/m \rceil m$ at time $t = 0$, it will arrive at position $N - 1$ at time $\lceil N/m \rceil T_0$ immediately after oscillator removal. Another oscillator with initial position $N - 1$ to the left of the initial position stated above will occupy position 0 at the time the

oscillator mentioned above occupies position N. Hence, by calculating the phase at time $\lceil N/m \rceil T_0$ for all oscillators with initial positions $x_0 \in \{-\lceil N/m \rceil m - 1, -\lceil N/m \rceil m, \ldots, N - 1 - \lceil N/m \rceil m\}$, we can calculate the steady state phase distribution of the line of N oscillators. Without loss of generality, we assume that the leftmost oscillator of the line has phase 2π at time $t = 0$, and denote the time at which an oscillator is introduced at the line, $t_{\text{intro}} = -x_0 T_g = |x_0| T_g$. Using Eq. (7),

$$\phi(\left\lceil \frac{N}{m} \right\rceil T_0) = 2\pi(1 + \frac{t_{\text{intro}}}{T_0}) + \int_{t_{\text{intro}}}^{\lceil N/m \rceil T_0} \frac{2\pi}{T(t')} dt' \tag{8}$$

$$= 2\pi(1 + \frac{t_{\text{intro}}}{T_0}) + \int_{t_{\text{intro}}}^{\lceil t_{\text{intro}}/T_0 \rceil T_0} \frac{2\pi}{T(t')} dt' + \int_{\lceil t_{\text{intro}}/T_0 \rceil T_0}^{\lceil N/m \rceil T_0} \frac{2\pi}{T(t')} dt'. \tag{9}$$

Here we split the last two integrals to make all upper boundaries coincide with oscillator removal. We now convert all integrals to sums over the positions the oscillator takes in each time interval, and insert $t_{\text{intro}} = |x_0| T_g$. The formula for the phase then becomes

$$\phi(\left\lceil \frac{N}{m} \right\rceil T_0) = 2\pi(1 + \frac{|x_0| T_g}{T_0}) + \sum_{p=0}^{p_{\max}-1} \frac{2\pi T_g}{T\left(\frac{p}{N + (|x_0| \mod m) + p - 1}\right)} + \sum_{c=1}^{c_{\max}-1} \sum_{p=0}^{m-1} \frac{2\pi T_g}{T\left(\frac{p_{\max} + p + m(c-1)}{N + p - 1}\right)}, \tag{10}$$

where we have defined $p_{\max} = m - (|x_0| \mod m)$, which is the position an oscillator with initial condition x_0 takes on the line, immediately after oscillators are removed for the first time following its addition to the line, and $c_{\max} = \lceil N/m \rceil - \lceil t_{\text{intro}}/T_0 \rceil$, which is the number of oscillator removals that an oscillator with initial condition x_0 experiences after being added to the line before $t = \lceil N/m \rceil T_0$ is reached. In the last term, the first sum takes oscillator removals into account, while the second sum ensures that all m positions an oscillator takes between oscillator removals are counted.

2 Phase profile in a continuous PSM

In this section, we extend our methods from the previous section to lines of infinitely many oscillators. We will use this method to solve two different example problems. We consider a line of infinitely many oscillators. Oscillators are constantly added on the left end of the line, and a fraction of the line length is removed from the rightmost end of the line in time intervals of T_0. For simplicity, we assume that the length of the line grows linearly between removal of oscillators, and hence, between removals, the length of the oscillator line we define $\mathcal{L}(t) = L_0(1 + \beta t/T_0)$, where βL_0 is the difference between the maximum and minimum lengths of the PSM. If we now assume that oscillators are removed at times $t = nT_0$ (this amounts to assuming $T_s = T_0$; once again, it is straight forward to replace this value of T_s with another), $n \in \mathbb{N}$, and that this removal restores the length of the oscillator line to the length it had at $t = 0$, the length is described by

$$\mathcal{L}(t) = L_0 \left(1 + \frac{\beta}{T_0} (t \mod T_0)\right). \tag{11}$$

As was the case in our discrete description of the line of oscillators, the position of each oscillator relative to the length of the line, effectively moves right as new oscillators are added at the left end of the line. To express the position of an oscillator as a function of time, we again exploit the fact that the distance between

the rightmost point of the line, and an oscillator is constant between removals of oscillators. We write down the relative position of an oscillator as a function of time in the same way as we did in the previous section. First, if no oscillators are removed from the right end of the line, the relative position of an oscillator which had position $x_0 L_0$ ($0 \leq x_0 \leq 1$) at $t = 0$, is

$$x_{\text{only\_growth}}(t) = \frac{\mathcal{L}(t) - (1 - x_0)L_0}{\mathcal{L}(t)}. \tag{12}$$

Taking removal of oscillators into account means that $x_0 \to x_0 + \beta \lfloor t/T_0 \rfloor$, since each point moves βL_0 right every time βL_0 is removed from the line from the rightmost end. Therefore,

$$x(t) = \frac{1 + \frac{\beta}{T_0}(t \mod T_0) - (1 - x_0 - \beta \left\lfloor \frac{t}{T_0} \right\rfloor)}{1 + \frac{\beta}{T_0}(t \mod T_0)}. \tag{13}$$

Positions on the line have values $x \in [0, 1]$. With the same reasoning as in the previous section, for a steady state phase profile, if an oscillator ends up in position $x = 1$ at time $t = nT_0$, $n \in \mathbb{N}$, it has occupied the same positions as all oscillators that ended up at $x = 1$ at $t = n_- T_0$, $n_- \leq n - 1$. From this follows that these oscillators were added to the line of oscillators at corresponding times between two removals of oscillators. We can characterise such oscillators by the negative position they held at the final oscillator removal before they were added to the line. If the oscillator is added to the line at time $0 \leq t_{\text{intro}} \leq T_0$, this negative position is $x_{\text{start}} = -\beta t_{\text{intro}}/T_0$.

If an oscillator ends up at position $x = 1$ at a time $t = nT_0$, this negative position is

$$x_{\text{start}} = 1 - \left\lceil \frac{1}{\beta} \right\rceil \beta. \tag{14}$$

That is, given the period gradient in Eq. (4), and that a newly added oscillator has the same phase as the oscillator to its immediate right, all oscillators that end up at $x = 1$ at a time $t = nT_0$ were added to the leftmost end of the line at time $t_{\text{intro}} = -x_{\text{start}} T_0/\beta$, with phase $\phi_{\text{intro}} = \phi_0 + t_{\text{intro}} 2\pi/T_0$, where ϕ_0 is the phase of the leftmost oscillator of the line right after a removal of oscillators at the right hand end of the line.

We can write down the phase of an oscillator, starting at any position x_0, at any time after it is added to the line,

$$\phi(t) = \phi_{\text{intro}} + \int_{t_{\text{intro}}}^{t} \frac{2\pi}{T(x(t'))} dt'. \tag{15}$$

With this formula we can calculate the phase at time t, for specific initial conditions $x(t = 0) = x_0$. Using this, we can get the steady state phase profile as it looks immediately after oscillator removal, if we calculate $\phi(t)$ for a set of initial condition that occupies $x \in [0, 1]$ at a time $t = nT_0$. An interval of initial conditions that satisfies this is $x_0 \in [-\lceil 1/\beta \rceil \beta, 1 - \lceil 1/\beta \rceil \beta]$. The right boundary of this interval, we already concluded will end up at position $x = 1$. It will arrive at position $x = 1$ at time $t = \lceil 1/\beta \rceil T_0$, and will eventually be removed from the position at $t = (\lceil 1/\beta \rceil + 1)T_0$. The lower boundary of the interval is exactly L_0 to the left of this point, and hence will be at position $x = 0$, when the rightmost oscillator of the interval arrives at $x = 1$. This reasoning is similar to the one we used in the discrete case. For this reason, we calculate $\phi(t = \lceil 1/\beta \rceil T_0)$ for all initial conditions in the mentioned interval, which gives us the phase profile as a function of initial conditions, x_0, right after oscillator removal at time $t = \lceil 1/\beta \rceil T_0$, $\phi(x_0, t = \lceil 1/\beta \rceil T_0)$. From this, we obtain the steady state phase profile after oscillator removal $\phi(x)$ by replacing $x_0 \to x - \lceil 1/\beta \rceil \beta$.

For our convenience, we will split the contribution to the phase of the oscillator in question into four parts: 1) The initial phase; 2) Phase acquired before the oscillator is added to the line; 3) Phase that the oscillator acquires after being added to the line, but before the first oscillator removal happens after this; 4) Phase that is acquired at later times. Assuming that all oscillators with negative initial position have initial

phase 2π, the phase of an oscillator with position $x(t=0) = x_0 \leq 0$ can then be expressed,

$$\phi(\lceil 1/\beta \rceil T_0) = 2\pi + \int_0^{t_{\text{intro}}} \frac{2\pi}{T_0} dt' + \int_{t_{\text{intro}}}^{\lceil t_{\text{intro}}/T_0 \rceil T_0} \frac{2\pi}{T(t')} dt' + \int_{\lceil t_{\text{intro}}/T_0 \rceil T_0}^{\lceil 1/\beta \rceil T_0} \frac{2\pi}{T(t')} dt'. \tag{16}$$

In this expression, the i^{th} term corresponds to the i^{th} contribution stated above. We will solve the three integrals one by one. The first integral has no explicit time dependence and the solutions is

$$\int_0^{t_{\text{intro}}} \frac{2\pi}{T_0} dt' = \frac{2\pi}{T_0} t_{\text{intro}}. \tag{17}$$

To solve the second integral, we must know $T(t')$. To know this, we need to know the position of the oscillator as a function of time. We can use the rescaling arguments given above, and write the position for $t_{\text{intro}} \leq t' \leq \lceil t_{\text{intro}}/T_0 \rceil T_0$ as

$$x(t') = \frac{\mathcal{L}(t') - \left(\frac{\mathcal{L}(t_{\text{intro}})}{L_0} - 0 \right)}{\mathcal{L}(t')}. \tag{18}$$

The last oscillator removal prior to t_{intro} happens at $\lfloor t_{\text{intro}}/T_0 \rfloor T_0$, and the first oscillator removal following t_{intro} happens at $\lceil t_{\text{intro}}/T_0 \rceil T_0$. For this reason, $\mathcal{L}(t_{\text{intro}}) = L_0(1 + (t_{\text{intro}} - \lfloor t_{\text{intro}}/T_0 \rfloor T_0)\beta/T_0)$, and $\mathcal{L}(t') = L_0(1 + (t' - \lfloor t_{\text{intro}}/T_0 \rfloor T_0)\beta/T_0)$. Inserting this in the expression above, we get

$$x(t') = \frac{\frac{\beta}{T_0}(t' - t_{\text{intro}})}{1 + \frac{\beta}{T_0}\left(t' - \left\lfloor \frac{t_{\text{intro}}}{T_0} \right\rfloor T_0 \right)}. \tag{19}$$

We can insert this in the expression for the period as a function of position in Eq. (4), and insert in the second integral above. We get

$$\int_{t_{\text{intro}}}^{\lceil t_{\text{intro}}/T_0 \rceil T_0} \frac{2\pi}{T(t')} dt' = \int_{t_{\text{intro}}}^{\lceil t_{\text{intro}}/T_0 \rceil T_0} \frac{2\pi}{T_0 \left(1 + \lambda \frac{\frac{\beta}{T_0}(t' - t_{\text{intro}})}{1 + \frac{\beta}{T_0}\left(t' - \left\lfloor \frac{t_{\text{intro}}}{T_0} \right\rfloor T_0 \right)} \right)} dt' \tag{20}$$

$$= \frac{2\pi}{\beta(1+\lambda)} \left\{ \frac{\beta}{T_0} \left(\left\lceil \frac{t_{\text{intro}}}{T_0} \right\rceil T_0 - t_{\text{intro}} \right) + \left(1 + \beta \left\lfloor \frac{t_{\text{intro}}}{T_0} \right\rfloor - \frac{\beta}{T_0} C \right) \ln \left(\frac{C + \left\lceil \frac{t_{\text{intro}}}{T_0} \right\rceil T_0}{C + t_{\text{intro}}} \right) \right\} \tag{21}$$

with

$$C = T_0 \left(\frac{1 - \beta \left\lfloor \frac{t_{\text{intro}}}{T_0} \right\rfloor - \frac{\lambda\beta}{T_0} t_{\text{intro}}}{\beta(1+\lambda)} \right). \tag{22}$$

Having solved this integral, we now turn to the last integral in the expression of the phase at time $\lceil 1/\beta \rceil T_0$. The final integral represents the phase that the oscillator acquires after the first oscillator removal. This time interval is an integer number of periods of the leftmost oscillator. The number of periods that the leftmost oscillator goes through before the time $t = \lceil 1/\beta \rceil T_0$ is reached, we denote $c_{\max} = \lceil 1/\beta \rceil - \lceil t_{\text{intro}}/T_0 \rceil$. From this insight, we can write the integral as a sum $c_{\max}$ integrals over time intervals of length T_0. This is expressed as follows,

$$\int_{\lceil t_{\text{intro}}/T_0 \rceil T_0}^{\lceil 1/\beta \rceil T_0} \frac{2\pi}{T(t')} dt' = \sum_{c=0}^{c_{\max}-1} \int_0^{T_0} \frac{2\pi}{T(t' + \left\lceil \frac{t_{\text{intro}}}{T_0} \right\rceil T_0 + cT_0)} dt' \tag{23}$$

To solve this we once again need to know the length of the line at the time at which the integrand is evaluated. In $t' + \left\lceil \frac{t_{\text{intro}}}{T_0} \right\rceil T_0 + cT_0$ the final two terms are both integer powers of T_0. Since $\mathcal{L}(t) = \mathcal{L}(t + jT_0)$, $j \in \mathbb{N}$, we know that $\mathcal{L}(t' + \left\lceil \frac{t_{\text{intro}}}{T_0} \right\rceil T_0 + cT_0) = \mathcal{L}(t')$. To write down the position of the oscillator at time $t' + \left\lceil \frac{t_{\text{intro}}}{T_0} \right\rceil T_0 + cT_0$, we need to know the position of the oscillator at time $\left\lceil \frac{t_{\text{intro}}}{T_0} \right\rceil T_0 + cT_0$. After each full time interval T_0, the line is restored to length L_0, and all oscillators have moved βL_0 to the right. For this reason, at time $\left\lceil \frac{t_{\text{intro}}}{T_0} \right\rceil T_0 + cT_0$, an oscillator with initial condition x_0 has position $x(\left\lceil \frac{t_{\text{intro}}}{T_0} \right\rceil T_0 + cT_0) = x_0 + \lceil t_{\text{intro}}/T_0 \rceil \beta + c\beta$. We can use these pieces of information to express the position of the oscillator at time $t' + \left\lceil \frac{t_{\text{intro}}}{T_0} \right\rceil T_0 + cT_0$ as follows

$$x\left(t' + \left\lceil \frac{t_{\text{intro}}}{T_0} \right\rceil T_0 + cT_0\right) = \frac{\mathcal{L}(t' + \left\lceil \frac{t_{\text{intro}}}{T_0} \right\rceil T_0 + cT_0) - L_0\left(1 - x\left(\left\lceil \frac{t_{\text{intro}}}{T_0} \right\rceil T_0 + cT_0\right)\right)}{\mathcal{L}\left(t' + \left\lceil \frac{t_{\text{intro}}}{T_0} \right\rceil T_0 + cT_0\right)} \tag{24}$$

$$= \frac{\frac{\beta}{T_0}t' + x_0 + \left\lceil \frac{t_{\text{intro}}}{T_0} \right\rceil \beta + c\beta}{1 + \frac{\beta}{T_0}t'}. \tag{25}$$

This, we can insert into Eq. (4) to get the oscillator period at the time in question. The final integral then becomes

$$\int_{\lceil t_{\text{intro}}/T_0 \rceil T_0}^{\lceil 1/\beta \rceil T_0} \frac{2\pi}{T(t')} dt' = \sum_{c=0}^{c_{\max}-1} \int_0^{T_0} \frac{2\pi}{T_0\left(1 + \lambda \frac{\frac{\beta}{T_0}t' + x_0 + \left\lceil \frac{t_{\text{intro}}}{T_0} \right\rceil \beta + c\beta}{1 + \frac{\beta}{T_0}t'}\right)} dt' \tag{26}$$

$$= \frac{2\pi}{\beta(1+\lambda)} \sum_{c=0}^{c_{\max}-1} \left\{ \beta + (1 - K\beta) \ln\left(\frac{K+1}{K}\right) \right\}, \tag{27}$$

where

$$K = \frac{1 + \lambda\left(x_0 + \left\lceil \frac{t_{\text{intro}}}{T_0} \right\rceil \beta + c\beta\right)}{\beta(1+\lambda)}. \tag{28}$$

The steady-state phase profile is obtained by adding all 4 contributions, and this is the black curved plotted in Fig. 2 in the main text.

3 Phase profile in a PSM that does not grow

In the previous sections we analyzed a line of oscillators that grows as much as it is shortened in one posterior period. We now turn to another important special case: A line in which there is no growth, only oscillator removal. In this case, the length of the line is conserved between oscillator removals, and an oscillator does not change its position relative to line length between oscillator removals. We will assume that 1) the phase difference between the two ends of the line is Φ_{before} at oscillator removal (Inserting $\Phi_{\text{before}} = 2\pi$ is the special case of mouse mPSMs with no growth); 2) That a phase profile is rescaled to line length but otherwise identical (mod 2π) at oscillator removal; 3) That oscillation period increases linearly along the line like above; 4) That $T_s = T_0$ (once again, it is straight forward to substitute this assumption with another value of T_s; 5) That the $\tilde{\phi}$ rightmost phase is removed at oscillator removal – this means that a certain fraction of the line length $1 - x_c$ is removed from the right end of the line at oscillator removal (that is, the oscillator with position $x_c \in (0, 1)$ before oscillator removal has position $x = 1$ after oscillator removal). In assumption 5), the value of $\tilde{\phi}$ is intimately connected to the period-profile on the line; we will be using the experimentally observed value $\tilde{\phi} = 0.21 \cdot 2\pi$. With these assumption we will estimate the phase profile over

the line and determine x_c, or equivalently the fraction of the oscillator population that is removed at each oscillator removal $1 - x_c$.

Assumption 5) above means that an oscillator which has position xx_c just before oscillator removal will have position x until next time oscillators are removed. The oscillator changes its phase $\delta\phi(x) = 2\pi T_0/T(x)$ between these two consecutive oscillator removals. But because the leftmost oscillator acquires 2π of phase between consecutive oscillator removals, and the phase profile is in steady state, $\phi(x, t = nT_0) = 2\pi + \phi(x, t = (n+1)T_0)$, $n \in \mathbb{N}$. These insights make us capable of writing down the following equation for the phase of the oscillator on position x just before oscillator removal

$$2\pi + \phi(x) = \phi(xx_c) + \delta\phi(x). \tag{29}$$

In accordance with the assumptions above, we, without loss of generality, take the phase in the line endpoints to be $\phi(x = 0) = \Phi_{\text{before}}$ and $\phi(x = 1) = 0$ just before oscillator removal. We now work towards an expressions that will allow us to determine the phase in infinitely many different points, and determine x_c under our above assumptions. Evaluating Eq. (29) in $x = x_c^n$ yields

$$2\pi + \phi(x_c^n) = \phi(x_c^{n+1}) + \delta\phi(x_c^n) \tag{30}$$

$$\Rightarrow \phi(x_c^{n+1}) = 2\pi + \phi(x_c^n) - \delta\phi(x_c^n) \tag{31}$$

This is a recursive relation. Given a period distribution, which in this case is $T(x) = T_0(1 + \lambda x)$, we can use this to determine x_c such that Φ_{before} and 0 are the phases of the endpoints of the line (these are specific to our example biological system and could be chosen differently if wanted). We can now insert $\delta\phi(x) = 2\pi T_0/(1 + \lambda x)$, and reduce the expression in Eq. (31) to obtain the recursive relation

$$\phi(x_c^{n+1}) = \phi(x_c^n) + 2\pi \frac{\lambda x_c^n}{1 + \lambda x_c^n}. \tag{32}$$

Using $\phi(x_c^0) = \phi(1) = 0$, and the recursive relation above, the phase at any point x_c^m can be calculated

$$\phi(x_c^m) = \sum_{n=0}^{m-1} 2\pi \frac{\lambda x_c^n}{1 + \lambda x_c^n}. \tag{33}$$

Taking the limit $m \to \infty$, we know $\lim_{m\to\infty} \phi(x_c^m) = \phi(0) = \Phi_{\text{before}}$, and this gives us

$$\lim_{m\to\infty} \phi(x_c^m) = \lim_{m\to\infty} \sum_{n=0}^{m-1} 2\pi \frac{\lambda x_c^n}{1 + \lambda x_c^n} = \Phi_{\text{before}} \tag{34}$$

This is an equation in x_c, which is nontrivial to solve analytically. Numerically, we evaluate the sum to e.g. $n = 550$ for different values of x_c. For $\Phi = 2\pi$, we find that $x_c = 0.767622$ solves the equation. A bound for the error on this evaluation can be found by the following estimation

$$\sum_{i=550}^{\infty} \frac{x_c^i}{\frac{1}{\lambda} + x_c^i} < \sum_{i=0}^{\infty} x_c^i - \sum_{i=0}^{550-1} x_c^i \tag{35}$$

$$= \frac{1}{1 - x_c} - \sum_{i=0}^{550-1} x_c^i, \tag{36}$$

where we used that $x_c^i + 1/\lambda > 1$, and $\sum_{i=0}^{\infty} x_c^i = 1/(1 - x_c)$. This yields an error on the evaluation smaller than 10^{-15}.

Having estimated $x_c = 0.767622$, we now know the fraction of oscillators that are removed periodically, $1 - x_c = 0.232378$, and can plug $x_c = 0.767622$ into Eq. (33) to obtain the steady state phase in any point x_c^m, $m \in \mathbb{N}$. In the previous sections, we plotted phase profiles *after* oscillator removal, and not *before* oscillator removal like here. The steady state phase profile after oscillator removal is obtained by replacing $x \to x/x_c$ for the evaluated points, and removing the point $x = 1$. This is plotted in Fig. 5A in the main text.

4 Changing somite width in a PSM that does not grow

In the previous section, we determined the somite width in a PSM that does not grow. This we did for a specific value of λ. In this section, we imagine perturbing the period gradient such that every oscillator has its period altered by an additive amount ξT_0. So the new period distribution is $T(x,\xi) = T_0(1+x\lambda+\xi)$. We assume that a somite is formed once every posterior period, and we assume that the phase width of the somite is equal to the phase difference that occurs between posterior and anterior in one posterior period. Lastly, we assume that the phase difference between anterior and posterior is 2π at the time of somite formation, and that somites form with period $T_s = T_0$. It is straight forward to substitute the assumed values of Φ_{before} and T_s with other values.

Eq. (29) is still valid, except that we now have an additional variable,

$$2\pi + \phi(x) = \phi(xx_c) + \delta\phi(x,\xi). \tag{37}$$

$\delta\phi(x,\xi)$ is equal to the difference that occurs between posterior and anterior in one posterior period, and is given by

$$\delta\phi(x,\xi) = \left(1 - \frac{T_0(1+\xi)}{T_0(1+\lambda x+\xi)}\right)2\pi \tag{38}$$

$$= 2\pi\frac{\lambda x}{1+\lambda x+\xi}. \tag{39}$$

We now proceed as we did in the previous section. Inserting $\phi(x_c^n)$ recursively gives us the equation

$$\phi(x_c^{n+1}) = \phi(x_c^n) + 2\pi\frac{\lambda x_c^n}{1+\lambda x_c^n+\xi}. \tag{40}$$

If we use $\phi(x_c^0) = 0$, we can calculate

$$\phi(x_c^m) = \sum_{n=0}^{m-1} 2\pi\frac{\lambda x_c^n}{1+\lambda x_c^n+\xi}, \tag{41}$$

and with this, we can demand that the posteriormost oscillator has phase Φ_{before} at somite formation,

$$\lim_{m\to\infty}\phi(x_c^m) = \lim_{m\to\infty}\sum_{n=0}^{m-1} 2\pi\frac{\lambda x_c^n}{1+\lambda x_c^n+\xi} = \Phi_{\text{before}}. \tag{42}$$

So for a given ξ, the corresponding x_c satisfies the equation

$$\sum_{n=0}^{\infty} 2\pi\frac{\lambda x_c^n}{1+\lambda x_c^n+\xi} = \Phi_{\text{before}}. \tag{43}$$

We evaluate the first 550 terms of this sum, for $\Phi_{\text{before}} = 2\pi$, and use this to find the x_c that satisfies Eq. (43). The error on this evaluation is estimated as we did in the previous section,

$$\sum_{i=550}^{\infty}\frac{x_c^i}{\frac{1+\xi}{\lambda}+x_c^i} < \sum_{i=0}^{\infty}x_c^i - \sum_{i=0}^{550-1}x_c^i \tag{44}$$

$$= \frac{1}{1-x_c} - \sum_{i=0}^{550-1}x_c^i. \tag{45}$$

This holds if $(1+\xi)/\lambda > 1$. This is definitely true for $\xi \in [-0.5, 1]$, which is the range that we plot $x_c(\xi)$ for in Fig.5B in the main text. In the main text we refer to $x_c(\xi)$ as the physical somite width.

5 Physical somite width as a function of period perturbation size

The calculation in Supplementary Section 2 gave us the phase profile in a steady-state PSM whose maximal length is βL_0 longer than its minimal length L_0. In this calculation, we have not assumed a specific Φ_{before}. For different choices of β and λ, we get different values for the phase difference Φ_{before}, and phase width $\tilde{\phi}$. This lets us examine how perturbing the period for all cells in the PSM by an amount ξT_0 changes the physical somite width. We will do this with the following approach

1. Choose a parameter β,
2. Try different input values of λ, and find the value that corresponds to the wanted Φ_{before}, e.g. $\Phi_{\text{before}} = 2\pi$,
3. Calculate what value of ξ, corresponds to the determined value of λ.

The first two steps in this approach are straight forward to carry out, using the analytical expression for the phase profile in a steady-state PSM in the continuum limit. We only need to figure out how to convert a chosen λ-parameter to a ξ-value. First, we note that if oscillators are removed once every posterior period (assuming $T_s = T_0$, other values for T_s are easy to plug in to the calculations), the phase width of a somite in a PSM with posterior period $T_{\min}$ and anterior period $T_{\max}$ is given by,

$$\tilde{\phi} = \int_0^{T_{\min}} \frac{2\pi}{T_{\min}} dt - \int_0^{T_{\min}} \frac{2\pi}{T_{\max}} dt \tag{46}$$

$$= 2\pi \left(1 - \frac{T_{\min}}{T_{\max}}\right). \tag{47}$$

So the phase width is not determined by the *difference* between the posterior and anterior periods, but by the *ratio* between the posterior and anterior periods. We will now take advantage of our theoretical framework from Section 2 of this supplementary file. In our framework, we can choose any value for the difference in periods over the PSM, λ, we like. However, suppose that we know that only a single value $\lambda = \lambda_0 := 0.21/0.79$ corresponds to the period gradient in the PSMs observed in an *unperturbed* experiment. Suppose all other values of λ correspond to the period gradient in experiments where an additive perturbation ξT_0 affects all cells in the PSM. In the rest of this section, this is what we will assume. By assuming this, we will provide a formula for matching the chosen λ to a unique value of the perturbation size, ξ, given λ_0.

For a chosen parameter λ, the ratio between periods in the simulation is

$$\frac{T_{\min}}{T_{\max}} = \frac{1}{1+\lambda} =: f_{\text{sim}}. \tag{48}$$

As described above, we now assume that any $T_{\min}$ from our simulations can be written $T_{\min} = T_0(1+\xi)$, and likewise for $T_{\max} = T_0(1+\lambda_0+\xi)$. If we demand that the observed ratio between periods f_{sim} is equal to the ratio between these perturbed periods, we get

$$\frac{1+\xi}{1+\lambda_0+\xi} = f_{\text{sim}} = \frac{1}{1+\lambda}. \tag{49}$$

Solving for ξ gives us

$$\xi = \frac{\lambda_0 - \lambda}{\lambda}. \tag{50}$$

This formula lets us match the λ-value, which ensures the wanted Φ_{before} for a chosen β, with a ξ-value. We plot matching β and ξ-values for $\Phi_{\text{before}} = 2\pi$ in Fig. 4B in the main text.

6 Phase profile shape and somite size for different growth conditions

In the previous sections, we have examined somite size, and phase profiles in the absence of growth in PSMs, and in PSMs with steady-state length. We found that while the phase profile was convex in the absence of growth, it was concave in PSMs with steady-state lengths. We also found that the physical somite size was larger in PSMs that do not grow. In this section, we will use perturbation theory to argue

- For any $T(x)$, $x \in [0,1]$, which is an increasing function of x, and PSM that has steady-state length, the corresponding steady-state phase distribution is concave.
- How the steady-state phase distribution could become convex, if the PSM does not have steady-state length.

6.1 Concave phase profiles if PSM length is in steady state

First, we examine the phase profile in a PSM in steady state. Suppose that the PSM consists of a larger number of cells. We use the continuous variable $x \in [0,1]$ to describe the position of each cell relative to the posterior end (at $x = 0$) and the anterior end (at $x = 1$). Let $T(x)$ be the period gradient of the PSM, and let this be increasing from posterior to anterior. Suppose that two cells have initial positions $x(t=0)_{\text{first}} := x_{0,\text{first}}$ equal to $x_0 = x^*$, and $x_{0,\text{second}} = x^* + \epsilon$, where $0 \leq x^* < 1$, and $0 < \epsilon \ll 1$. Let us assume $t = 0$ to be immediately after somite formation, and let the phase difference between the two cells be $\delta\phi_\epsilon = \phi(x) - \phi(x+\epsilon) > 0$. We now examine how the phase difference between these cells changes between $t = 0$, and just after the following somite formation at $t = T_s$. The change in phase difference between the two cells in this time period is

$$\Delta\phi_\epsilon(t = T_s) = \int_0^{T_s} \frac{2\pi}{T(t, x^*)} dt - \int_0^{T_s} \frac{2\pi}{T(t, x^* + \epsilon)} dt. \tag{51}$$

Now, since $\epsilon \ll 1$, we expand the fraction

$$\frac{1}{T(t, x^* + \epsilon)} = \frac{1}{T(t, x^*)} - \epsilon \frac{1}{(T(t, x^*))^2} \frac{\partial T(t, x_0)}{\partial x_0}\bigg|_{x_0 = x^*} + O(\epsilon^2), \tag{52}$$

$$\approx \frac{1}{T(t, x^*)} - \epsilon \frac{1}{(T(t, x^*))^2} \left(\frac{\partial T(t, x_0)}{\partial x(t)} \frac{\partial x(t)}{\partial x_0} \right) \bigg|_{x_0 = x^*}, \tag{53}$$

$$= \frac{1}{T(t, x^*)} - \epsilon \frac{1}{(T(t, x^*))^2} \left(\frac{\partial T(t, x_0)}{\partial x(t)} \right) \bigg|_{x_0 = x^*} \frac{L_0}{\mathcal{L}(t)}. \tag{54}$$

$$\tag{55}$$

Here we used Eq. (12) to calculate $\partial x(t)/\partial x_0$. Inserting this expression in Eq. (51) yields,

$$\Delta\phi_\epsilon(t = T_s) = \epsilon \int_0^{T_s} \frac{1}{(T(t, x^*))^2} \left(\frac{\partial T(t, x_0)}{\partial x(t)} \right) \bigg|_{x_0 = x^*} \frac{L_0}{\mathcal{L}(t)} dt \tag{56}$$

Since $T(x)$ is increasing and positive, and since $\mathcal{L}(t)$ is positive and increasing between somite formation, $\Delta\phi_\epsilon > 0$. This means that the phase difference between the two cells increases between the two somite formations. The phase difference is the same after the somite formation at $t = T_0$, and because the PSM length is in steady state, the difference in position between the two cells is still ϵ at $t = T_0$. We can determine whether the phase profile is convex or concave by comparing whether the phase profile is decreasing more quickly at positions that are more posterior or more anterior . This tells us whether the phase profile is convex or concave because a decreasing, concave function has a negative second derivative, while the second derivative is positive for a decreasing, convex function (See Fig. 1S in this Supplementary file). The phase

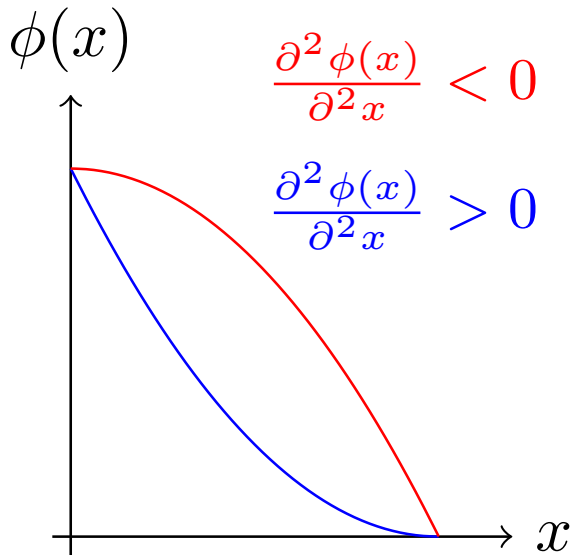

Figure 1S: Illustration of decreasing functions that are concave (red), and convex (blue). The concave function has a negative second derivative, while the convex function has a positive second derivative.

profile gradient between the cells at their initial position is $\delta\phi_\epsilon/\epsilon$, and the phase profile gradient between the cells at their final position is $(\delta\phi + \Delta\phi_\epsilon)/\epsilon$. Calculating the ratio yields

$$\frac{\frac{\delta\phi_\epsilon+\Delta\phi_\epsilon}{\epsilon}}{\frac{\delta\phi_\epsilon}{\epsilon}} = 1 + \frac{\Delta\phi_\epsilon}{\delta\phi_\epsilon} > 1. \tag{57}$$

From this we conclude that the steady-state phase profile decreases faster as x is increased. Or equivalently: *the steady-state phase profile is concave.*

6.2 Convex phase profile with $T(x)$ linear, increasing

In the previous subsection we found that the phase difference between two cells increases between somite formation if $T(x)$ is an increasing function. This was expressed in Eq. (51). With this in mind, one may wonder how one can obtain a convex phase profile with an increasing period profile $T(x)$, as we found in the case of no growth. The answer lies in the shortening of the PSM: Even though the phase difference between two cells increases between somite formations, the somite formation itself causes the difference in position of the cells to grow relative to the length of the PSM. This may influence the ratio between the phase profile gradients greatly.

Let us return to the case of a PSM with period-profile $T(x) = T_0(1 + x\lambda)$, that does not grow. We can evaluate Eq. (51) in this case,

$$\Delta\phi_\epsilon(t = T_0) = \epsilon\frac{2\pi\lambda}{(1 + \lambda x_0)^2}. \tag{58}$$

If two cells were a distance ϵ apart from each other before somite formation, and if x_c is the length of the PSM after somite formation, the distance between the same cells after the somite formation will be ϵ/x_c relative to the new PSM length. Taking this into account, we can now calculate the ratio between the phase profile gradient between two cells at two consecutive somite formation events, as we did in the previous subsection,

$$\frac{\frac{\delta\phi_\epsilon+\Delta\phi_\epsilon}{\epsilon/x_c}}{\frac{\delta\phi_\epsilon}{\epsilon}} = x_c\left(1 + \epsilon\frac{2\pi\lambda}{\delta\phi_\epsilon(1 + \lambda x_0)^2}\right) \tag{59}$$

if x_c, and $\epsilon/\delta\phi_\epsilon$ are sufficiently small, this may be less than 1, resulting in a convex phase profile. This is the case for the phase profile plotted in Fig. 5A in the main text.

Chapter 3

Controlling phase waves in developing embryos using entrainment

In diverse species of vertebrates such as chicks, zebrafish, and mice, the arrest of phase waves of gene expression has been found to coincide with somite formation (Oates, Morelli, and Ares, 2012; Palmeirim et al., 1997; Soroldoni et al., 2014; Lauschke et al., 2013; Cotterell, Robert-Moreno, and Sharpe, 2015). The generality of this correlation is striking, but it is still not clear whether there is a causal relationship between the travelling phase waves and somite formation. If scholars could control phase waves from the lab, such causality might be studied systematically. In collaboration with Professors Sandeep Krishna and Mogens H. Jensen, I examined how to achieve control of phase waves by entraining the cellular oscillators to a single external periodic signal. In addition to the proof-of-concept of phase-wave control, we examined how recent observations in space-less entrainment studies could be extended to spatial systems of coupled oscillators such as the PSM.

The proposed method of phase-wave control builds on the theory of *Arnol'd tongues*. I will introduce Arnol'd tongues in the following section. In Section 3.2, I summarise our findings. Following this, the research article is presented. The final section of the chapter concludes Part I of the dissertation and suggests possible directions for further research.

3.1 Entrainment of oscillators

In February 1665, more than 350 years ago, the inventor of the pendulum clock, Christiaan Huygens, wrote a letter to his father (Bennett et al., 2002; Strogatz, 2004). In this letter, Huygens beautifully describes a new dynamical phenomenon he has observed. Strogatz quotes the letter as follows (Strogatz, 2004),

> *"Being obliged to stay in my room for several days and also occupied in making observations on my two newly made clocks, I have noticed an admirable effect which no one could have ever thought of. It is that these two clocks hanging next to one another separated by one or two feet keep an agreement so exact that the pendulums always oscillate together without variation. After admiring this for a while, I finally figured out that it occurs through a kind of sympathy: mixing up the swings of the pendulums, I have found that within a half hour they always return to consonance and remain so constantly afterwards for as long as I let them go. I then separated them, hanging one at the end of the room and the other fifteen feet away, and noticed that in a day there was five seconds difference between them. Consequently their earlier agreement must in my opinion have*

> *been caused by an imperceptible agitation of the air produced by the motion of the pendulums. The clocks are always shut in their boxes, weighing a total of less than 100 pounds. When in consonance, the pendulums do not oscillate parallel to one another, but instead they approach and separate in opposite directions."*

The scientific discovery described in this beautiful tale will be at the center of this chapter.

Huygens observed that two pendulum clocks synchronise their oscillations if they hang close enough to each other. While he attributed this synchronisation to "imperceptible agitation of the air produced by the motion of the pendulums", experiments later found that the material from which the clocks hung mediated it (Czolczynski et al., 2011). In the letter, Huygens interestingly recounts that increasing the separation between the clocks would hinder the synchronisation. If we imagine describing this separation as a parameter of Huygens's experiments, this is an important observation of the mathematical properties of synchronising clocks. Only for certain choices of parameters do the clocks synchronise.

In this chapter, I will be interested in such synchronisation between clocks. I shall always be in complete control of one of the clocks; this clock affects the other clock, and sometimes this makes the second clock synchronise to the oscillations of the controlled clock. In cases where one of the clocks is controlled externally, I will refer to the synchronisation as *entrainment* of the uncontrolled clock, and the set of parameters leading to entrainment are referred to as *Arnol'd tongues* (Pikovsky, Rosenblum, and Kurths, 2003). The point of the chapter is not to understand *why* synchronisation occurs but rather understand the properties of the phenomenon of synchronisation. The first step down this road is introducing Arnol'd tongues.

3.1.1 Entrainment and Arnol'd tongues

Entrainment is a fascinating topic, and many wonderful mathematical phenomena occur when oscillators interact. Many of these phenomena can be understood in the light of Arnol'd tongues. In this section, I introduce some of the mathematical properties that are tied to these parameter regions of synchronisation.

Suppose we are interested in entraining some clock to a beat under our control. I will call the clock we do not control the "internal oscillator", as this clock will be ticking inside PSM cells in the specific setting of the following paper. The clock we do control I shall refer to as the "external oscillator". External indicates that it is not an integrated part of the system in question. If the internal oscillator has a natural frequency ω, how can we entrain the oscillation to an external beat with frequency Ω instead?

As Huygens described to his father, only some parameters will result in the clocks beating in sync. Huygens found that the separation of the clocks mattered. This separation I shall refer to as the *coupling strength*, $K \geq 0$. If $K = 0$, the two oscillators are entirely independent of each other. Increasing K increases the coupling, similar to hanging the pendulum clocks closer and closer to each other in Huygens's experiment. Another important parameter in the struggle to entrain the internal clock is the similarity in frequencies of the two clocks, Ω, and ω. The intuition is as follows: if ω and Ω are nearly identical, a small coupling between the oscillators will suffice to entrain the internal clock successfully. If ω and Ω are very different from each other, the coupling must be sizable for synchronicity to occur. In a diagram with the external-frequency parameter on the horizontal axis and the coupling strength on the vertical axis, this makes the region of entrainment widen with increasing K.

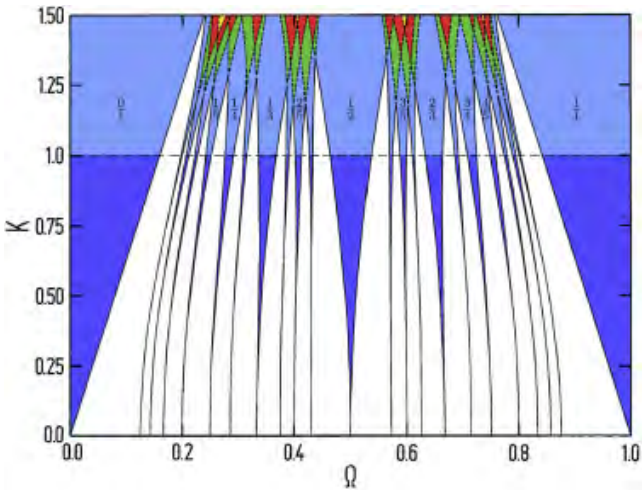

FIGURE 3.1: A finite number of Arnol'd tongues (coloured) plotted for the circle map. In the $p : q$ Arnol'd tongue, the external oscillator makes p revolutions in the same time as the internal makes q revolutions. An Arnol'd tongue exists for any two integers p, q. At $K = 1$, tongues start to overlap. Red and green colors show examples of such overlapping regions. The figure was originally published in (Jensen, Bak, and Bohr, 1984); this colored version appeared in (Heltberg et al., 2016).

Figure 3.1 illustrates this widening. From a single point at $K = 0$, because only identical frequencies $\omega = \Omega$ will allow the two oscillators to beat in synchrony if there is no coupling between the oscillators, to wider regions for increasing K. This widening looks similar to that of a tongue from tip to anchor. Therefore this region of entrainment is affectionately known as an Arnol'd tongue.

In the above example, the external frequency was close to the internal frequency, $\Omega \approx \omega$, which caused the internal oscillator to locksteps with the external forcing. Interestingly, the frequencies do not need to be almost identical for such lockstep to occur. If the external frequency is approximately half that of the internal, $2\Omega \approx \omega$, the internal oscillator can be entrained to the external signal too. In this case, the external oscillator would make two revolutions in the same amount of time as the internal oscillator makes one. Similar to above, for $K = 0$ only if $2\Omega = \omega$ exactly, will the two oscillators be oscillating together. Increasing the coupling K makes the region of entrainment expand, giving the region its tongue-like shape.

In fact, the internal oscillator can get entrained to perform q oscillations in the same time span as the external oscillator makes p, for any integers p, q. The corresponding Arnol'd tongues vary in shape and width, but they all exist side-by-side in the parameter plane. Figure 3.1 illustrates this for a classic oscillator model called the "circle map" (Jensen, Bak, and Bohr, 1983; Bak et al., 1984; Bohr, Bak, and Jensen, 1984; Martin and Martienssen, 1986; Cvitanovic, Shraiman, and Söderberg, 1985; Feigenbaum, Kadanoff, and Shenker, 1982).

Arnol'd tongues are parameter regions of entrainment, but there is more to them than that. The properties of Arnol'd tongues are integral to the work I present in this chapter, and thus I will dedicate two subsections to these. The first subsection introduces phenomena that arise when one explores an Arnol'd tongue vertically by gradually increasing the coupling strength, K. The second subsection introduces Arnol'd-tongue properties characteristic of the horizontal axis inside a tongue.

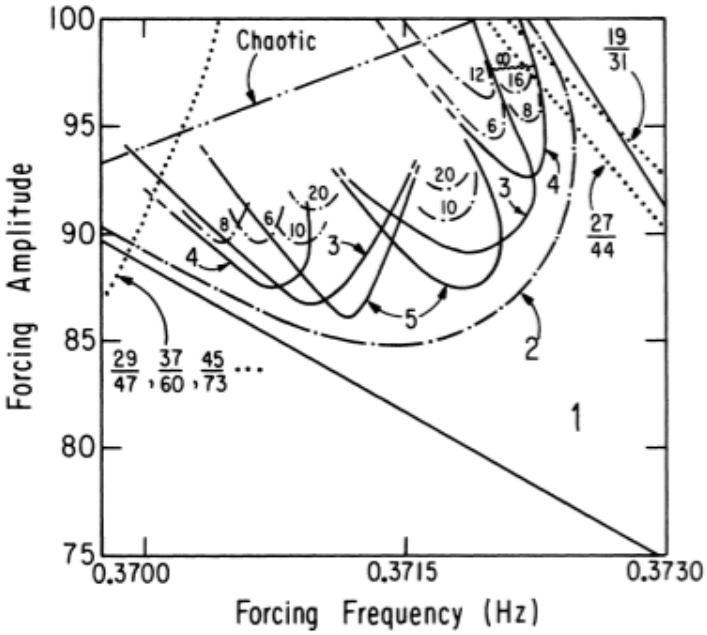

FIGURE 3.2: Illustration of the anatomy of the region of an 8 : 13 Arnol'd tongue at high external forcing. The Arnol'd tongue bends left in this case. Starting from the bottom right corner and proceeding left and upwards, lines labeled by integers, say n, are encountered. After crossing such a line, it takes n times as long for the system to return to its initial configuration. That is, instead of the system repeating itself every time one oscillator makes 8 revolutions and the other makes 13, it now takes $8n$ and $13n$ oscillations for it to do so. Dotted lines show neighbouring tongues intruding on the 8 : 13 tongue. For high enough forcing, chaos becomes possible. This is visible in the top left corner of the figure. The figure was originally published in (Glazier et al., 1986).

"Vertical" properties of Arnol'd tongues

Suppose we affect an oscillator with an external beat with parameters (Ω, K). Suppose the set of parameters (Ω, K) are located in the bottom of the $p : q$ Arnol'd tongue and therefore causes $p : q$ entrainment. We now gradually increase K and change the Ω in such a way that we move upwards in the Arnol'd tongue. What would we find? For a while, $p : q$ entrainment would be the only stable solution for the internal oscillator under our external influence. Eventually, this solution transitions into more complicated periodic states. One such transition is period-doubling, after which the internal oscillator goes on for twice as long before it repeats itself (Strogatz, 2018). More complicated transitions could result in the internal oscillator taking other multiples of its original period before repeating itself. Eventually, as K is increased, chaotic dynamics can occur. Figure 3.2 illustrates these transitions.

The many transitions mentioned in the previous paragraph are present inside a single Arnol'd tongue. Increasing K further, makes other exciting parameter regions come to exist: Regions of overlapping Arnol'd tongues. When Arnol'd tongues meet, the corresponding stable solutions may coexist, or one may turn unstable. These regions of overlapping tongues have recently generated significant interest in another oscillating biological system, namely the nF-κB system (nuclear factor

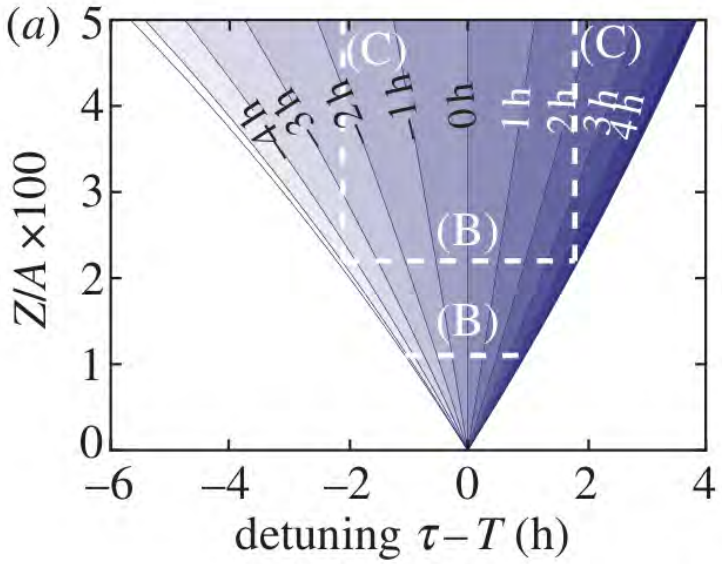

FIGURE 3.3: Anatomy of an Arnol'd tongue for low external forcing. T is the period of the zeitgeber, and τ is the period of the affected oscillator. From left to right in the tongue, the phase between the synchronised external and internal oscillations changes. At the leftmost border, the oscillation of the internal oscillator precedes that of the external oscillator by 6 hours. At the opposite edge, the converse is true. The figure was originally published in (Bordyugov et al., 2015).

κB) (Heltberg et al., 2016). Oscillations in the nF-κB system are associated with inflammatory responses (Jensen and Krishna, 2012). In this system, coexisting periodic solutions were reported. The study suggested that noise could kick the system between these stable solutions, thereby varying protein levels in the cells. This suggested mechanism has since been extended to the chaotic regime (Heltberg, Krishna, and Jensen, 2019). The authors proposed that control of genes downstream of the nF-κB system could be achieved by forcing the oscillating system into Arnold-tongue regions containing chaos or multiple stable solutions.

"Horizontal" properties of Arnol'd tongues

If an Arnol'd tongue is explored "horizontally", by varying the external frequency Ω and keeping K sufficiently low, rather than vertically, bifurcations do not take place. In the letter to his father, Huygens mentions that his synchronised pendulum clocks oscillate out-of-phase with each other. As one fixes K and varies Ω, one finds that the phase difference between the internal and external oscillator changes. Such changes in phase difference happen even as synchrony between the oscillators persists. This detuning is illustrated in Figure 3.3. The figure shows an Arnol'd tongue for a system of "Kuramoto" oscillators with an internal period of 24 hours (Bordyugov et al., 2015; Kuramoto, 2003; Acebrón et al., 2005). On one boundary of the tongue, the oscillation of the external signal precedes that of the internal by 6 hours. On the other boundary of the tongue, the internal oscillation precedes that of the external oscillation by 6 hours. In total, the phase difference between oscillators varies with phase π across the tongue.

3.2 Our results: Entraining phase waves

In the paper "Entrainment as a means of controlling phase waves in populations of coupled oscillators", published in Physical Review E, (Juul, Krishna, and Jensen, 2018), we simulate various entrainment experiments applied to coupled cells on a line. The cells on a line mimick cellular oscillators in the presomitic mesoderm. In each cell, we keep track of the concentrations of 4 different proteins. For this reason, the whole system is described by $4n$ ordinary, coupled differential equations (n being the number of cells on the line). For the particular choice of parameters, the protein concentrations oscillate with a linear period gradient similar to that seen in the mouse. The oscillations of neighbouring cells are coupled, and this coupling can cause cells with identical parameters to synchronise.

We first affect all cells on the line with a single, external periodic forcing. We show that the forcing parameters can be chosen such that all cells entrain to the external signal in a $1:1$ manner. Thus, all $1:1$ Arnol'd tongues overlap for some (Ω, K) despite all oscillators having different natural frequencies. The key point of this simulation is as follows. Because all cells have slightly different frequencies than their neighbours do, all the $1:1$ Arnold tongues are slightly displaced compared to each other. The parameters that entrain all oscillators correspond to the rightmost part of the $1:1$ Arnold tongue for the fastest oscillator and the leftmost for the slowest. Hence the phase difference between the external signal and the oscillators will change systematically from left to right on the line – phase waves! In other words, by applying an external periodic signal, we create phase waves that are under our control.

Having shown that we can control phase waves using entrainment, we move on to investigate the region of overlapping Arnol'd tongues for cells on a line. We simulate a system of cells – all with the same internal frequency – and apply the same external periodic signal to all cells. Choosing parameters (K, T_{force}) that lie in the overlapping region between the $3:1$ and $2:1$, we show that multiple stable oscillatory solutions can coexist. This is true even when the coupling between neighbouring cells would make pairs of cells synchronise their oscillations if no external force were applied. The observed coexistence of oscillatory solutions persists for as long as we run our simulations.

3.3 Paper: Entrainment as a means of controlling phase waves in populations of coupled oscillators

PHYSICAL REVIEW E **98**, 062412 (2018)

Entrainment as a means of controlling phase waves in populations of coupled oscillators

Jonas S. Juul,[1] Sandeep Krishna,[2,*] and Mogens H. Jensen[1,†]

[1]*Niels Bohr Institute, University of Copenhagen, Blegdamsvej 17, Copenhagen 2100-DK, Denmark*

[2]*Simons Centre for the Study of Living Machines, National Centre for Biological Sciences, GKVK Campus, Bellary Road, Bangalore 560065, India*

(Received 22 May 2018; published 21 December 2018)

We explore waves and entrainment in a model of coupled oscillators, inspired from the cellular oscillators in the presomitic mesoderm (PSM) of mice. The internal clock in each cell is based on a negative feedback loop which couples to the clocks of neighboring cells through a Notch mechanism. We investigate how a morphogen gradient in the mesoderm, which affects the period of oscillating cells, gives rise to phase waves traveling from the posterior to the anterior part of the PSM. We show that the phase waves can be entrained by an external periodic variation in this morphogen and also observe that multiple oscillatory solutions can coexist in the cell population. Together, these provide a way to potentially control phase waves and thereby manipulate somite patterning in embryos, based on entrainment properties of coupled nonlinear oscillators.

DOI: 10.1103/PhysRevE.98.062412

I. INTRODUCTION

Biological oscillators are ubiquitous in a wide range of systems from the molecular level up to macroscopic scales and play a fundamental role in how living systems function. These include ultradian biological clocks (period less than 24 h) that affect tumor growth [1–5] or vertebrae precursors in the vertebrate embryo [6–15] and the circadian clocks (period of approximately 24 h) that coordinate rhythms in mammalian physiology to the day-night cycle [16–18].

A natural task is to investigate ways to control the oscillations. Dynamical systems theory tells us that an oscillator can be entrained if it is driven by an external, periodic signal [19–23]. If the external periodic signal is characterized by a period T_{force} and a "strength" K_{force}, then certain combinations of the parameters (T_{force}, K_{force}) will successfully entrain the oscillator to have the period T_{force} or a rational multiple of this: $T_{\text{force}}P/Q$ with P and Q being positive integers. The region of this parameter space in which the oscillator is entrained and oscillates with period $T_{\text{force}}P/Q$ is referred to in the dynamical systems literature as a $P{:}Q$ Arnold tongue [24].

Entrainment of biological oscillators has been studied in several biological cases [25–34], with well-known, crucial functions such as the coordination of various rhythms to the day-night cycle. One biological process where oscillators are of fundamental importance is *somitogenesis*, the formation of vertebrae precursors in vertebrate embryos. In the vertebrate embryo, somites, the precursors of vertebrae, are periodically formed in the presomitic mesoderm (PSM) [35]. The PSM consists of a population of interacting stem cells [36], which we will refer to as PSM cells. Geometrically, the PSM can be described by an anteroposterior axis, where somites form in the anterior PSM and new PSM cells are continuously added in the posterior PSM [37]. Each PSM cell is an ultradian oscillator [38], exhibiting rhythmic pulsations in several pathways until it arrives at the anterior end of the PSM where it eventually becomes part of a newly formed somite.

Somitogenesis has been studied in great detail in particular in zebrafish, chicks, and mice. The exact mechanism behind somite formation is not known. Cooke and Zeeman [8] developed a famous framework, the "Clock and Wavefront Model," in which oscillating cells ("clocks") encounter a wavefront which moves from the anterior to the posterior PSM, thereby causing the cells to form somites. This mechanism depends on global morphogen gradients and has recently been challenged in theoretical and experimental studies which suggest, instead, mechanisms based on local reaction-diffusion behavior [39] or on interactions between several intracellular clocks [40]. Although the somite formation mechanism remains elusive, waves of protein expression have been observed to travel through the population of somite precursor cells from the posterior to the anterior PSM, and in all three species, the arrest of these waves in the anteriormost PSM has been found to coincide with the formation of a new somite [41–43]. Hence, we hypothesize that controlling the wave pattern, which is intimately linked to the individual cellular oscillators, may lead to controlling the spatial pattern of somites.

Recently, experiments have concluded that presomitic mesoderm cells in mice can be entrained [44] by external periodic variations in pathway modulators, and for this reason, theoretical studies of observable phenomena related to the entrainment of coupled, oscillating cells are important. Especially, studies focusing on the control of phase waves should be encouraged. In this paper, we take a previously proposed minimal model for the internal clock in PSM cells and add a coupling to achieve a limit cycle oscillator that is coupled to the oscillators in neighboring cells. We show that imposing a linear morphogen gradient gives rise to period and amplitude gradients across the PSM that are similar to what is observed experimentally. We then simulate an experiment in

*sandeep@ncbs.res.in
†mhjensen@nbi.dk

which the morphogen concentration is varied periodically in each cell in the PSM and find that this can entrain the traveling phase waves, thereby providing control over the wave pattern. Finally, we study entrainment of cell populations consisting of cells with similar natural frequencies. This corresponds to populations of cells that originate from the same position in the PSM. We find that when the external entraining signal forces the cellular oscillators into a region of overlapping Arnold tongues, multiple oscillatory solutions coexist. This generalizes a recent observation of coexisting oscillatory solutions in the NF-κB system [45]. In our case unlike the NF-κB case, cells are coupled in space, and thus coupled cells may be entrained to different limit cycles, which might manifest in the spatial pattern of somites.

The remainder of this paper is structured as follows: In Sec. II we describe our model of coupled PSM cells and their oscillatory behavior. In Sec. III we present our results in three subsections: in Sec. III A we show that a gradient of Wnt3a in this model leads to period and amplitude gradients in the PSM, resulting in traveling phase waves; in Sec. III B we vary the Wnt3a level in each PSM cell periodically and thereby entrain the traveling phase waves; Sec. III C deals with entrained populations of similar cells leading to coexisting oscillatory solutions. In Sec. IV we discuss the validity and implications of our results.

II. MODEL OF COUPLED, OSCILLATING CELLS

We aim to obtain a limit cycle oscillator with a parameter corresponding to the level of a morphogen gradient across the PSM, which we can use to study the possible effects of entrainment of oscillating cell populations. The internal clock in each cell is modeled by a negative feedback loop involving Axin2, β-catenin, and Axin2 messenger RNA, as was suggested in Refs. [14,46,47]. Several experiments have concluded that PSM cells coordinate their oscillations with their neighbors, and that Notch is the key in the coupling mechanism between cells in the PSM [11,13,48,49]. For this reason, we couple cells through the concentration of Notch in neighboring cells. It is unknown what mediates the cross talk between the Wnt pathway (the internal clock in our model) and the Notch pathway. We choose glycogen synthase kinase-3beta (GSK3β) in this model because experiments have indicated that GSK3β can bind to, and phosphorylate, Notch in other biological systems [50,51] and is involved in a destruction complex [52,53] along with β-catenin and Axin1 (which is functionally equivalent to Axin2 [54]). Thus, a coupling of cells via Notch interaction with GSK3β is biologically plausible.

Our model of interacting cells [Fig. 1(a)] is formulated in terms of a set of delay differential equations. For each cell, we keep track of the concentration of β-catenin, Axin2 mRNA, Axin2, and Notch, abbreviated B, A_m, A, and N, respectively. GSK3β enters effectively into our description via a parameter G_{tot} that sets the total amount of GSK3β, summing its concentration in free form and as part of the destruction complex. We assume that the Notch level which affects a given cell is dependent on the combined level of the Notch concentrations of the neighboring cells, $\sum_j N_j$. Recently it was found that a time delay in the coupling between cells can ensure defect-free patterning [55]. We incorporate such a delay in the production terms of Notch. The model then takes the form

$$\frac{dB_i}{dt} = S - \frac{\lambda G_t}{K_{BAG}} \frac{B_i A_i}{1 + \frac{N_i}{K_{NG}} + \frac{A_i}{K_{AG}}}, \tag{1}$$

$$\frac{dA_{m,i}}{dt} = c_{tsA} B_i^2 - \frac{A_{m,i}}{\tau_{Am}}, \tag{2}$$

$$\frac{dA_i}{dt} = c_{tlA} A_{m,i} - \nu L_{tot} \frac{A_i}{\frac{c_{b[AL]}+\nu}{c_{f[AL]}} + A_i}, \tag{3}$$

$$\frac{dN_i}{dt} = p_0 + \frac{\alpha k^n}{k^n + I_i(t-\tau)^n} - \frac{\epsilon G_{tot}}{K_{NG}} \frac{N_i}{1 + \frac{A_i}{K_{AG}} + \frac{N_i}{K_{NG}}}, \tag{4}$$

where i is an index that labels the cells. In the Notch equation, $I_i(x)$ is a coupling function given by

$$I_i(x) = \begin{cases} N_{i-1}(x) + N_{i+1}(x) & \text{if } 1 < i < N, \\ 2N_{i+1}(x) & \text{if } i = 1, \\ 2N_{i-1}(x) & \text{if } i = N. \end{cases} \tag{5}$$

τ is the delay in cell-to-cell signaling, p_0 a basic production rate, and $p_0 + \alpha$ is the maximal production rate.

All values of the parameters are listed in Table I. ν is the parameter which is proportional to the Wnt3a level of the cell [47]. In Fig. 1(b) the period of two coupled cells is plotted as a function of ν. This is the only parameter which we allow to vary from cell to cell. In each simulation, we will state the ν distribution for the particular study of interest. In Fig. 1(c) we show the time to synchronization of two cells with identical parameters and random initial conditions, as a function of the delay τ. The cells synchronize only for an interval of large τ values. For the remaining τ values, the cells tend to oscillate completely out of phase with each other. We choose $\tau = 25$ min for all cells in all simulations since experiments have shown that Notch helps synchronize the oscillations of cells [11,13,48,49].

Geometrically, we will approximate the PSM to be a line of cells, each connected only to two neighbors on either side of it. It has been observed that there is a gradient of Wnt3a over the PSM [14,42]. This correlates with the gradient of the oscillation period in the PSM. In our model, the ν parameter is proportional to the Wnt3a level in the cell [47]. Hence, we will simulate a presomitic mesoderm using a gradient in ν, going from high ν in the posterior PSM to low ν in the anterior PSM [Fig. 1(d)].

Experimentally, the period has been found to increase linearly from posterior (with period around 130 min) to anterior [42], the period being approximately 25%–30% longer in the anterior than in the posterior. The period in our model (1)–(4) is shorter [Fig. 1(b)], but since this model is derived from a larger model [47], which did have the correct period length, this seems to be a result of losing delay when simplifying from eight to three differential equations for the core clock. Hence, we do not consider this to be of importance. From our simulations, we find that a ν gradient decreasing linearly from

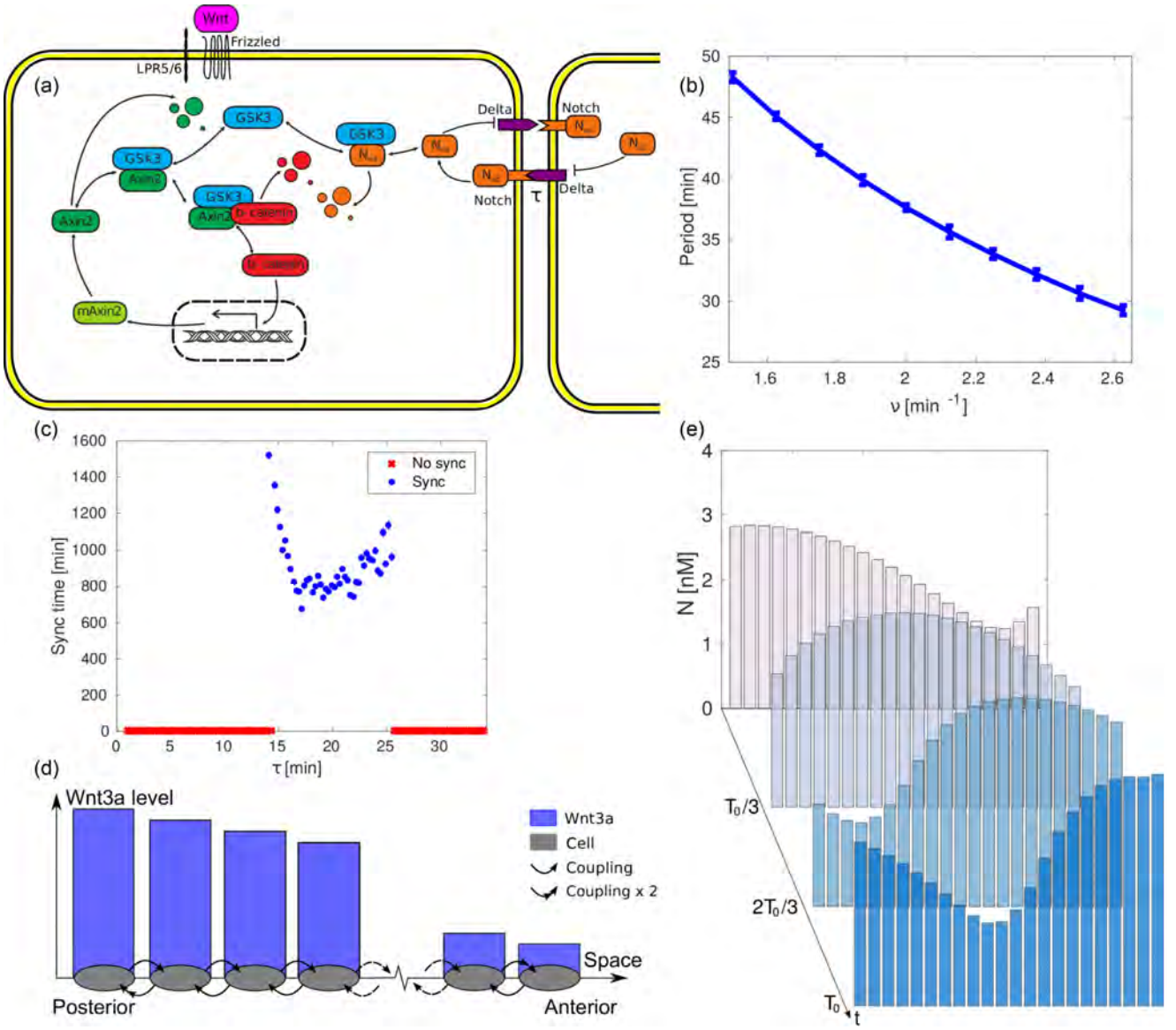

FIG. 1. *Basic characteristics of our model of interacting PSM cells.* (a) Schematic of the components and interactions in our model. The internal clock is based on the Axin2-β-catenin negative feedback loop, and neighboring cells are coupled with a delay τ through their Notch levels. Notch is phosphorylated by GSK3β internally in the cell. (b) The period of two coupled cells as a function of the parameter ν in Eqs. (1)–(5) [with $N = 2$, making $I_1(t-\tau) = 2N_2(t-\tau)$ and $I_2(t-\tau) = 2N_1(t-\tau)$], which is proportional to the Wnt3a level in the cells. (c) The time before synchronization of two coupled cells with identical parameters and initial conditions drawn uniformly at random from the interval $[0, 10]$ nM for all variables. Each data point is averaged over 20 simulations. If cells failed to synchronize in any one of these simulations, the data point was defined as 0 ("No sync"). The plot shows that the delay needs to be in a specific range for the cells to synchronize. (d) Implementation of the model when simulating a PSM. Cells are placed on a line and couple to their nearest neighbors. Outermost cells have only a single spatial neighbor. As a boundary condition, we let the outermost cells couple to two copies of this neighbor. A linear Wnt3a gradient is placed over the line: posterior cells have a higher Wnt3a level than anterior cells. (e) Phase wave resulting from simulation of the model implemented as shown in (d), with the anterior period being $\approx$30% longer than the posterior period. Waves travel from posterior to anterior, with the amplitude of the Notch expression growing towards the anterior. This is in agreement with experimental observations [42].

posterior to anterior,

$$\nu_i = \nu_{\text{posterior}} + (\nu_{\text{anterior}} - \nu_{\text{posterior}})\frac{i-1}{N-1}, \qquad (6)$$

with $\nu_{\text{posterior}} = 2.500$ min^{-1} to $\nu_{\text{anterior}} = 2.125$ min^{-1} creates a gradient in the period with the correct fractional difference between posterior and anterior. A simulation with this type of ν gradient, and all initial protein concentrations equal to 2 nM, yields phase waves going from posterior to anterior [Fig. 1(e)]. In the following section, we will examine these waves in more detail.

TABLE I. *Parameters for the model of coupled PSM cells.* The first two parameters, K_{AG} and S, were chosen to be realistic values, from Jensen *et al.* [47,56]. The next three, c_{tsA}, c_{tlA}, and τ_{Am}, were chosen to be the estimated values of Jensen *et al.* [47]. K_{NG} was chosen to be one third of the size of K_{AG}, and λG_{tot} and ϵG_{tot} to have the same magnitude as K_{NG}. p_0 and α were chosen to be 0.5 nM min^{-1} each such that the maximal production rate of Notch is 1 nM min^{-1}. The three parameters $c_{f[AL]}$, $c_{b[AL]}$, and L_{tot} were chosen such that terms in Eqs. (1)–(4) had the same values as in the original model [47]. The next three parameters were chosen from parameter scans: ν (which is proportional to the Wnt3a level in the simulated cell) such that the period difference between posterior and anterior is ∼30% [Fig. 1(b)], and k and τ such that two coupled cells with the same parameters synchronize. When reducing the single-cell model from eight variables [47] to three variables [38], the final parameter, K_{BAG}, was given in terms of several parameters from the larger model. The value of the parameter was chosen such that the known realistic values of its constituents were used. The value of one of its constituents (called $c_{b,C}$) was determined such that two coupled cells with the same parameters synchronized their oscillations.

Parameter	Process	Default value
K_{AG}	Dissociation constant of G and A into the complex $[GA]$	6 nM
S	Constant source of β-catenin	0.4 nM min^{-1}
c_{tsA}	Transcription of Axin2 gene	0.7 nM^{-1} min^{-1}
c_{tlA}	Translation of Axin2 mRNA	0.7 min^{-1}
τ_{Am}	Average lifetime of Axin2 mRNA	40 min
K_{NG}	Dissociation constant of $[NG]$ and N, G	2 nM
$G_{tot}\epsilon$	Total G level times constant	2 nM min^{-1}
$G_{tot}\lambda$	Total G level times constant	2 nM min^{-1}
α	Constant in numerator of coupling term	0.5 nM min^{-1}
p_0	Constant production rate of Notch	0.5 nM min^{-1}
n	Hill coefficient	1
$c_{f[AL]}$	Binding of A to L	250 nM^{-1} min^{-1}
$c_{b[AL]}$	Dissociation of $[AL]$ into A and L	2 min^{-1}
L_{tot}	Total L level	2.8 nM
ν	Degradation of Axin2 in $[AL]$ complex (Wnt level included)	2.125–2.500 min^{-1}
τ	Delay in cell-cell coupling	1 nM min^{-1}
k	Constant in denominator of coupling term	2 nM
K_{BAG}	Dissociation constant of $[BAG]$ and B, A, G	2.48 nM^2

III. RESULTS

A. Traveling phase waves along the PSM in the absence of external forcing

We first explore the phase waves that can travel along the PSM in our model. The spatial implementation of the coupling between cells [Eqs. (1)–(4)] is shown in Fig. 1(d) (posterior being the leftmost part of the line). All cells are assigned the same parameter values except that the ν parameter is varied as described above. All cells are given the same initial conditions by setting all initial concentrations to 2 nM. In Fig. 1(e) we show that phase waves appear in the system after an initial transient period. Similar traveling waves have also been observed previously in Ref. [57], which differs from our model in two ways: it implements the PSM as a continuous line rather than a discrete set of cells as in our model and focuses on phase oscillators rather than limit-cycle oscillators.

In our model, after a transient period, cell trajectories lie on limit cycles. These are shown in Figs. 2(a) and 2(b). We see that the amplitude of oscillations in the variables N and A becomes larger the more anterior a cell is located. Experimentally, Notch oscillations have been reported to increase in amplitude in a similar way [42].

In Fig. 2(c) the oscillations in Notch concentrations of all cells are plotted as a function of time. A phase wave travels from posterior to anterior and grows in amplitude as it travels in this direction. In Fig. 2(d) the periods of the cells are shown. The estimated periods are average values for each cell over 200 min of simulation. The period grows approximately linearly from posterior to anterior. The anteriormost period is approximately 30% longer than the posteriormost period. Because period depends on position, the phases of the cellular oscillators drift apart, resulting in the number of waves traveling the PSM increasing with time. The number of waves can be adjusted by either "cutting off" cells in the anterior (somite formation) or adding new cells in the posterior (PSM growth). This we examine in a forthcoming publication. Here we focus on the possibility of entraining these waves.

B. Entraining wave patterns in a simulated PSM by external periodic forcing

As mentioned in Sec. I, the arrest of phase waves in the presomitic mesoderm has been found to coincide with somite formation. Controlling the phase waves might thus provide a way to control the somite patterning. In this section, we investigate one way of obtaining such control, namely, by entrainment of all PSM oscillators to an external, periodic signal. The external, periodic signal we imagine to be imposed, not by something in the biological system itself, but by an outside observer, who actively wants to affect the oscillating population.

The cells are perturbed by an external periodic variation of the ν parameter (Wnt3a concentration)

$$\nu \to \nu\left[1 + K_{\text{force}} \sin\left(\frac{2\pi}{T_{\text{force}}} t\right)\right]. \tag{7}$$

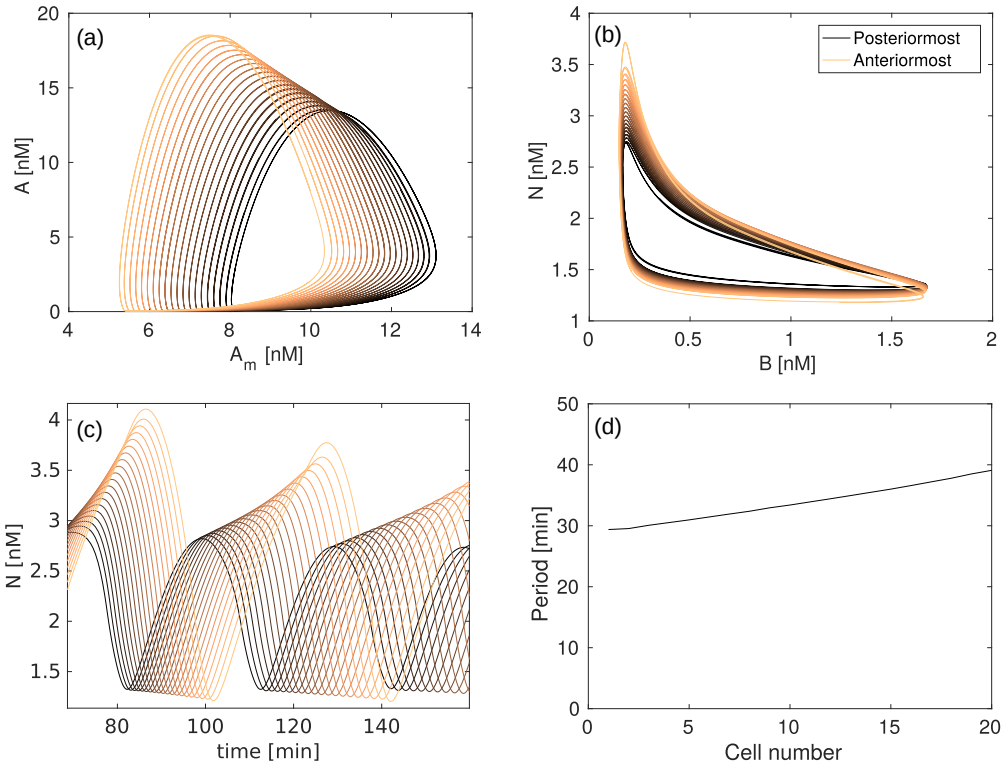

FIG. 2. *Oscillations and traveling phase waves in a PSM with a Wnt3a gradient in the absence of external periodic forcing.* Simulations of 20 cells on a line with a linear gradient in ν as described in Fig. 1 and all concentrations equal to 2 nM as initial conditions. (a, b) Plot of limit cycles for all cells. Cells located closer to the posterior end are plotted with a darker color, and those closer to the anterior end with a lighter color. The amplitude in oscillations in variables N and A increase the closer a cell is to the anterior PSM. Experimentally, the amplitude of Notch oscillations is reported to increase from posterior to anterior [42]. (c) Visualization of phase wave traveling from posterior to anterior. The amplitude in N increases from posterior to anterior. (d) Periods of PSM cells. Anterior cells have approximately 30% longer periods than posterior cells. The difference in period means that the wave pattern is not stable: the phase of the oscillators *drifts apart*.

Depending on the period (T_{force}) and the amplitude (K_{force}), the oscillations of a cell may synchronize to those of the external signal. As described above, the interval of external periods T_{force} that can entrain an oscillator to a period identical to that of an external signal is named the 1:1 Arnold tongue. We obtain 1:1 Arnold tongues in Fig. 3 for cells at three different positions, characterized by different values for the ν parameter. The leftmost Arnold tongue is for cells from the posterior PSM ($\nu = 2.500$ min^{-1}), the middle Arnold tongue is for cells from the middle of the PSM ($\nu = 2.3125$ min^{-1}), and the rightmost Arnold tongue is for cells from the anterior PSM ($\nu = 2.125$ min^{-1}). We obtained the Arnold tongues by simulating five cells on a line under the influence of each parameter pair (T_{force}, K_{force}) for 9000 min of simulations. If the oscillations of the cells were synchronized at the end of the simulation (if no neighboring cells had average periods, over the last 6000 min, which deviated more than 1 min), and if their period were identical to that of the external signal (defined as a period T_{cells} for which $|T_{\text{force}} - T_{\text{cells}}| < 0.02$ min and $T_{\text{cells}}/T_{\text{force}} < 1.01$), a 1:1 Arnold tongue was associated with the parameter pair.

The phase difference with which the cell oscillator will be entrained to the external signal depends on the position of parameters (T_{force}, K_{force}) within the Arnold tongue [23]. For an entrained cell oscillation, we measure the minimal distance between peaks of N (from any cell of the PSM) and peaks of ν, $(t_{\text{peak}\nu} - t_{\text{peak}N})/T_{\text{force}}$, and plot the results as a colormap in Fig. 3(a), overlaid on top of the previously obtained Arnold tongues. Positive values correspond to the external force peaking first.

In Fig. 3 the three Arnold tongues overlap at (T_{force}, K_{force}) = (34 min, 0.035). Hence, an external Wnt3a oscillation with these parameter values may entrain all cells in the PSM. Furthermore, with this choice of parameters, the Notch level N in posterior cells peaks before the external signal, and peaks after the external signal in anterior cells. Hence, a phase wave will travel the PSM from posterior to anterior. In Figs. 3(b) and 3(c) the limit cycles of the entrained PSM cells are shown. In this case, the amplitude of N, A, and B decrease in amplitude from posterior to anterior. In Fig. 3(d) the Notch oscillations are shown as a function of time. Phase waves travel from posterior to anterior with decreasing amplitude. In Fig. 3(e) the periods of the cells (averaged over 1000 min of simulation) are plotted. All cells have similar periods, and hence the phases of the oscillators do not drift apart. Through an external periodic variation of Wnt3a we have thus shown it is possible to obtain "external" control of the phase waves in the PSM.

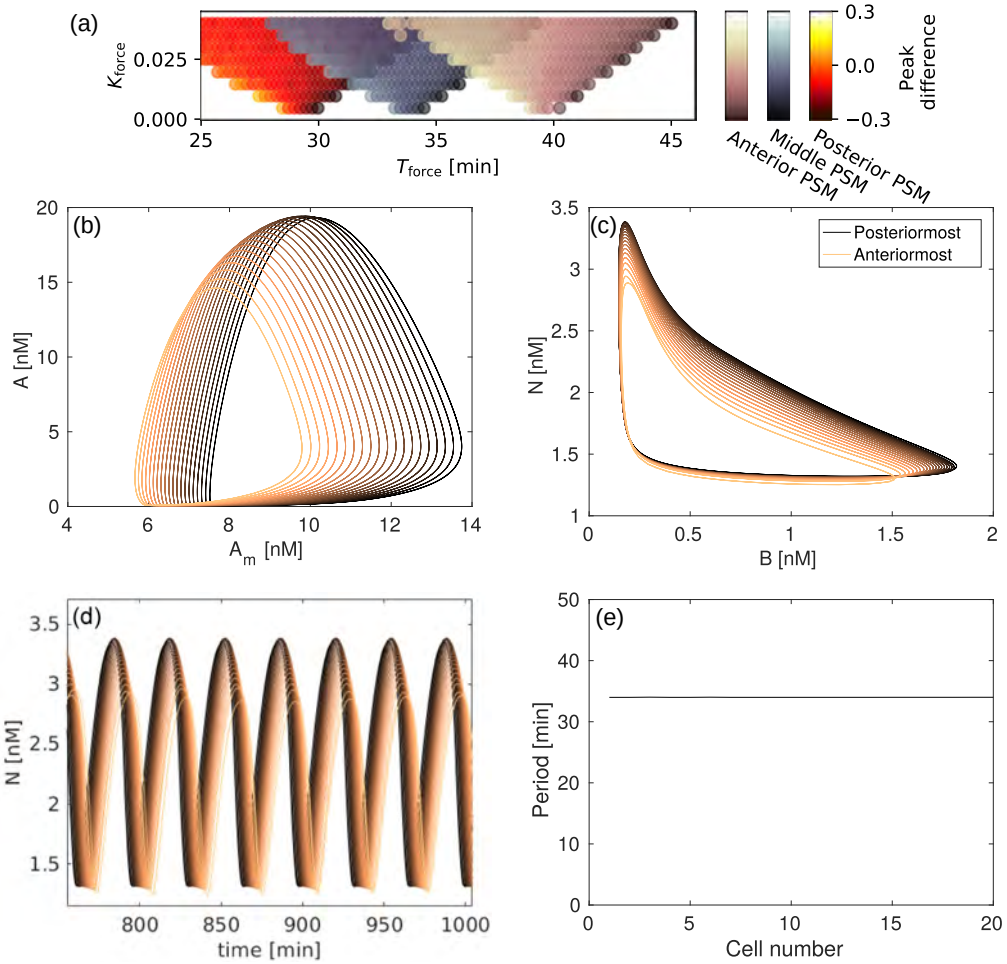

FIG. 3. *Entrainment of traveling phase waves in the presence of external periodic forcing.* (a) 1:1 Arnold tongues for cells originating from three different positions in the PSM: posterior, halfway between posterior and anterior, and anterior. The colormap indicates the value of $(t_{\text{peak}\nu} - t_{\text{peak}N})/T_{\text{force}}$. Positive values indicate that the Notch levels of cells peak after the external forcing signal. In the overlap between the three tongues, posterior cells peak before the external signal and the anterior cells peak after the external signal. Hence, a wave of maxima may travel the PSM from posterior to anterior. (b–e) A PSM, with a linear ν gradient as given by Eq. (6), under the additional influence of an external periodic forcing, as given by Eq. (7), with $(T_{\text{force}}, K_{\text{force}}) = (34\text{ min}, 0.035)$. This parameter pair lies in the overlap between the three tongues in panel (a). (b, c) Limit cycles for each cell in the PSM under influence of the external periodic forcing. Compared to Fig. 2, the amplitude of oscillations now varies with cell position for both A and B and N. Interestingly, the amplitude is now greatest in all variables for posterior cells, not anterior cells as in Fig. 2. (d) Notch expression N of all cells as a function of time. Phase waves travel from posterior to anterior, with oscillations decreasing in amplitude with distance from the posterior end. (e) Period of cell oscillations in the phase wave of inset (d). All cells oscillate with, on average, identical period.

C. Coexisting limit cycles in PSM cells perturbed by a single external periodic signal

Properties of oscillating cells originating from similar parts of the PSM have been studied experimentally [42,49]. In these studies it was reported that the phase gradient in monolayer PSMs (an *ex vivo* culture of PSM cells that recapitulates patterning and segment scaling in the mouse PSM) decides the width of formed somites, and that mixed cells are capable of synchronizing their oscillations. In this section, we investigate the effects of a wide range of forcing parameters on cells originating from identical parts of the PSM.

We position cells on a line with the same ν parameter (i.e., we no longer have a gradient), corresponding to positions in the central part of the PSM, and vary ν periodically according to Eq. (7). To quantify whether the cell population is entrained to this external signal or not, we measure the difference between the period of the stable oscillations of the Notch concentration of the cell populations and the period of the external signal. We do this for different values of the parameters $(T_{\text{force}}, K_{\text{force}})$. The results are plotted in Fig. 4(a); colored areas in the parameter space indicate the entrainment of the oscillations of the cell population in Arnold tongues corresponding to the fraction P/Q equal to 4, 3, 2, 3/2, 1, 2/3, and 1/2. In Fig. 4(b) the oscillations of all cells are plotted along with the external forcing. All cells are entrained to the external signal.

In Fig. 4(c) the external period is approximately twice the period of the cells, which shows that the cell population has

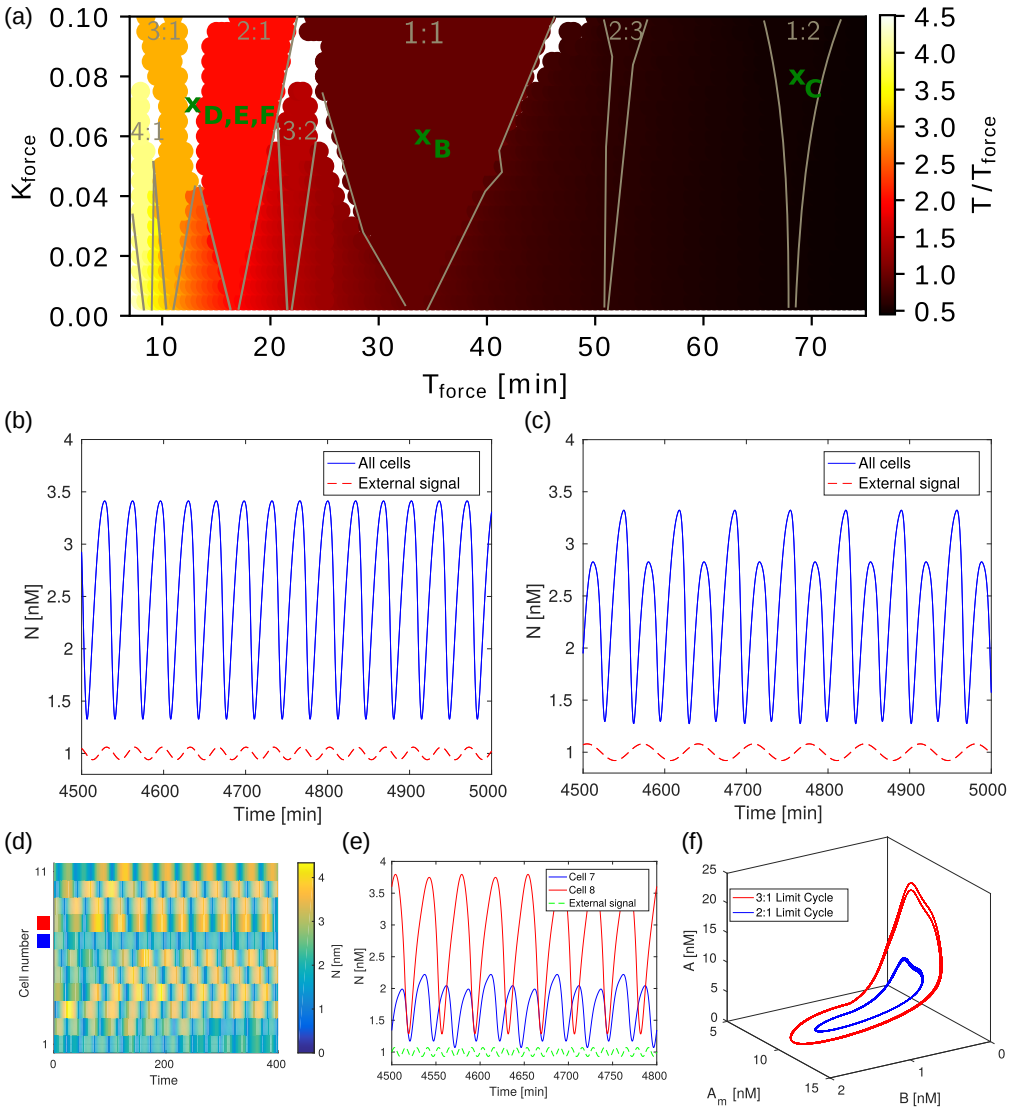

FIG. 4. *Coexistence of limit cycles induced by an external periodic forcing in the absence of a period gradient.* (a) Colormap showing the ratio of the period of a population of synchronized cells (originating from the central part of the PSM) to T_{force}, the period by which the ν level of the cells is varied. Distinct Arnold tongue structures of entrainment are clearly visible. White areas correspond to sets of parameters in which cells in the population were not synchronized after a very long time (9000 min). These areas are visible at the overlap of tongues where complex phenomena such as chaos can exist, and at the edge of the tongues where the convergence to entrainment is very slow. (b) Under the influence of an external periodic variation of the ν parameter (Wnt3a level) according to Eq. (7) with $(T_{\text{force}}, K_{\text{force}}) = (35\ \text{min}, 0.06)$ (parameter pair lies in the 1:1 tongue), 11 cells on a line synchronized their oscillations. In the simulation, all cells had $\nu = 2.3125\ \text{min}^{-1}$. The external forcing with which we multiply ν is plotted by a dashed red line. (c) Oscillations of all 11 synchronized cells with forcing parameters $(T_{\text{force}}, K_{\text{force}}) = (68\ \text{min},\ 0.08)$. The forcing is shown in dashed red. Interestingly, the cells have undergone a period doubling: the maxima of the peaks alternate with double period. (d–f) Cell population under identical periodic forcing with parameters that lie between the 3:1 and 2:1 tongues, $(T_{\text{force}}, K_{\text{force}}) = (12.5\ \text{min},\ 0.07)$. (d) Kymograph showing three cells entrained to one frequency or amplitude corresponding to the 2:1 tongue (blue square), and eight cells with another corresponding to the 3:1 tongue (red square). (e) Plot of Notch time series for two cells marked with squares in panel (d). Cells are entrained to different frequencies. (f) Three-dimensional projection of limit cycles that the cells can be entrained to.

undergone what is termed in the nonlinear dynamics literature as a "period doubling" [58]. Interestingly, this seems to be a general feature of the oscillations in the 1:2 tongue in our model.

Next, we investigate the behavior for parameters in the white spaces of the overlapping Arnold tongue regions in Fig. 4(a). Coexisting limit cycles in such overlapping Arnold tongues are known to exist in spin-torque oscillators affected by an injected alternating current [59] and were recently found in a system of NF-κB cells [45]. In Figs. 4(d)–4(f) we plot results obtained by performing simulations identical to the ones we performed above but with the parameters $(T_{\text{force}}, K_{\text{force}}) = (12.5\ \text{min}, 0.07)$, lying between the 2:1 and 3:1 Arnold tongues. We find that two limit cycles coexist and predict that

an experiment examining the response of a PSM cell population, taken from a single PSM location, to periodic external driving may find part of the population oscillating with one frequency while other parts oscillate with the other frequency.

From a dynamical systems perspective, the coexistence of limit cycles in certain areas in parameter space means that some bifurcation takes place on the boundary of such areas. In the sine circle map, it has previously been determined that such bifurcations are heteroclinic [60]. In the present system, however, we find that when crossing from the region in which only the 2:1-limit cycle exists, into the region in which the 2:1-limit cycle coexists with the 3:1-limit cycle, the latter limit cycle appears "out of the blue," with a finite period and amplitude. Together with the fact that we did not find any fixed points appearing or disappearing or changing in stability, this suggests that the bifurcation is a saddle-node bifurcation of cycles [58]. This is similar to what was observed in Ref. [59]. We observed coexisting limit cycles in the overlapping region between the 4:1 and 3:1 Arnold tongues as well.

IV. DISCUSSION

Locally interacting oscillating cells is a topic of fundamental interest and has been widely studied from biological, physical, and mathematical viewpoints both with and without time delays in the coupling [57,61,62]. In this paper, we use a simple limit cycle oscillator model to investigate the consequences of an external periodic variation of a morphogen gradient on a population of coupled oscillating presomitic mesoderm cells. While traveling phase waves on a line of coupled nonlinear oscillators have been well studied, to our knowledge our result that these waves can be entrained by an external periodic forcing has not been reported before. We also showed that in the context of the presomitic mesoderm such external forcing can lead to the coexistence of different limit cycles in coupled cell populations. This is to be expected due to the existence of overlapping Arnold tongues in our coupled oscillator model but is a feature that has not been observed experimentally during somitogenesis. Together, our results suggest powerful ways of controlling the spatial and temporal patterning process during somitogenesis by the relatively simple means of controlling the morphogen gradients that determine the frequency of the cellular oscillators. Such means to control the oscillations would be useful both for understanding the nonlinearities of the somitogenesis "clock" as well as the properties of the inter-cellular coupling between PSM cells.

The model we use is based on a core, negative feedback loop in the canonical Wnt pathway, and a Notch coupling between neighboring cells. The cross talk between these pathways occurs in our model via GSK3β. This remains an assumption, albeit a plausible one because experimentally GSK3β has been found to bind and phosphorylate Notch in other systems [50,51].

The Wnt oscillator is known to interact with the Notch pathway, which is known to be instrumental in coupling of cells, and this provided us a concrete way to model both the intracellular clock as well as the intercellular coupling. However, while the Wnt pathway does show oscillations, it has not been proven to be the driving clock of the PSM cells. Several other negative feedback loops exist in various somitogenesis-related pathways. It is quite possible that one of these is the main clock driving somitogenesis, as well as the oscillations in other pathways. Despite this we believe our results still provide strong "proof of principle" that external periodic variation can be used to entrain phase waves and thereby provide control of somite patterning, because synchronization, entrainment, and coexistence of multiple oscillatory modes are deep and fundamental properties of coupled oscillators that do not depend much on specific details of the oscillators [24]. Thus, we expect that even if another clock is the one driving somitogenesis, we would obtain qualitiatively similar results.

We believe our results are important for understanding the control of oscillating cell populations. We provided numerical evidence that coupled limit cycle oscillators under the influence of an external periodic force might have multiple coexisting stable limit cycles. This too depends on fundamental properties of limit cycle oscillators, and hence we expect such coexisting oscillating states to be achievable in a broad range of locally coupled, oscillating systems.

Generally, when frequencies of oscillators are proportional to spatial position along some axis, as is the case in the PSM [49], the 1:1 Arnold tongues of the cells will occupy different areas in the parameter space (T_{force}, K_{force}) of an external, periodic change in any parameter which the periods of the cells depend on. This makes control of the phase waves via entrainment possible. In the PSM, it would be very interesting to find a parameter that could be used to control the phase waves *in vivo*, because this would allow a direct and dynamic control of the spatial patterns formed during somitogenesis.

ACKNOWLEDGMENTS

We are very grateful to Alexander Aulehla and his laboratory members for valuable discussions, sharing his knowledge and results on populations of coupled PSM cells during the symposium "Biological Oscillators: Design, Mechanism, Function" at EMBL. We are also grateful to Ala Trusina for valuable discussions about Notch interactions. S.K. thanks the Simons Foundation for funding via the Simons Centre for the Study of Living Machines. M.H.J. and J.S.J. acknowledge support from the Danish Council for Independent Research (Grant No.: 4002-00395B) and StemPhys DNRF Center of Excellence (DNRF116). J.S.J. also acknowledges support from the Lørup Foundation.

[1] D. A. Hamstra, Cancer Res. **66**, 7482 (2006).
[2] M. S. Greenblatt, W. P. Bennett, M. Hollstein, and C. C. Harris, Cancer Res. **54**, 4855 (1994).
[3] D. E. Nelson, Science **306**, 704 (2004).
[4] A. Hoffmann, Science **298**, 1241 (2002).
[5] M. M. Chaturvedi, B. Sung, V. R. Yadav, R. Kannappan, and B. B. Aggarwal, Oncogene **30**, 1615 (2011).
[6] A. Aulehla and O. Pourquié, Curr. Opin. Cell Biol. **20**, 632 (2008).
[7] A. Aulehla and O. Pourquié, Brain Struct. Funct. **211**, 3 (2006).

[8] J. Cooke and E. C. Zeeman, J. Theor. Biol. **58**, 455 (1976).
[9] A. Aulehla, W. Wiegraebe, V. Baubet, M. B. Wahl, C. Deng, M. Taketo, M. Lewandoski, and O. Pourquié, Nat. Cell Biol. **10**, 186 (2008).
[10] H. Forsberg, F. Crozet, and N. A. Brown, Curr. Biol. **8**, 1027 (1998).
[11] C. Soza-Ried, E. Ozturk, D. Ish-Horowicz, and J. Lewis, Development **141**, 1780 (2014).
[12] E. M. Ozbudak and O. Pourquié, Curr. Opin. Genet. Dev. **18**, 317 (2008).
[13] Y. J. Jiang, B. L. Aerne, L. Smithers, C. Haddon, D. Ish-Horowicz, and J. Lewis, Nature (London) **408**, 475 (2000).
[14] A. Aulehla, C. Wehrle, B. Brand-Saberi, R. Kemler, A. Gossler, B. Kanzler, and B. G. Herrmann, Dev. Cell **4**, 395 (2003).
[15] A. Aulehla, Genes Dev. **18**, 2060 (2004).
[16] S. M. Reppert and D. R. Weaver, Annu. Rev. Physiol. **63**, 647 (2001).
[17] B. Pfeuty, Q. Thommen, and M. Lefranc, Biophys. J. **100**, 2557 (2011).
[18] S. Becker-Weimann, J. Wolf, H. Herzel, and A. Kramer, Biophys. J. **87**, 3023 (2004).
[19] A. Pikovsky, M. Rosenblum, and J. Kurths, *Synchronization: A Universal Concept in Nonlinear Sciences*, Cambridge Nonlinear Science Series (Cambridge University Press, Cambridge, 2003), Vol. 12.
[20] L. Glass and J. Sun, Phys. Rev. E **50**, 5077 (1994).
[21] M. H. Jensen, P. Bak, and T. Bohr, Phys. Rev. Lett. **50**, 1637 (1983).
[22] M. H. Jensen, P. Bak, and T. Bohr, Phys. Rev. A **30**, 1960 (1984).
[23] G. Bordyugov, U. Abraham, A. Granada, P. Rose, K. Imkeller, A. Kramer, and H. Herzel, J. R. Soc. Interface **12**, 20150282 (2015).
[24] V. I. Arnol'd and A. Avez, *Ergodic Problems of Classical Mechanics* (W. A. Benjamin, New York, NY, 1968).
[25] R. Kellogg and S. Tay, Cell **160**, 381 (2015).
[26] L. Glass, M. R. Guevara, J. Belair, and A. Shrier, Phys. Rev. A **29**, 1348 (1984).
[27] L. Glass, M. R. Guevara, A. Shrier, and R. Perez, Physica D **7**, 89 (1983).
[28] A. Gupta, B. Hepp, and M. Khammash, Cell Syst. **3**, 521 (2016).
[29] M. Guevara, L. Glass, and A. Shrier, Oecologia (Berlin) **19**, 75 (1975).
[30] M. H. Jensen and S. Krishna, FEBS Lett. **586**, 1664 (2012).
[31] B. M. Friedrich and F. Jülicher, Phys. Rev. Lett. **109**, 138102 (2012).
[32] K.-A. Stokkan, S. Yamazaki, H. Tei, Y. Sakaki, and M. Menaker, Science **291**, 490 (2001).
[33] A. Woller, D. Gonze, and T. Erneux, Phys. Biol. **11**, 045002 (2014).
[34] N. Mitarai, U. Alon, and M. H. Jensen, Chaos **23**, 023125 (2013).
[35] K. Kusumi, W. Sewell, and M. L. O'Brien, in *Somitogenesis*, edited by M. Maroto and N. V. Whittock, Advances in Experimental Medicine and Biology Book Series (Springer, New York, 2009), Vol. 638, pp. 140–163.
[36] K. J. Dale and O. Pourquié, BioEssays **22**, 72 (2000).
[37] J. Dubrulle, Development **131**, 5783 (2004).
[38] B. Mengel, A. Hunziker, L. Pedersen, A. Trusina, M. H. Jensen, and S. Krishna, Curr. Opin. Genet. Dev. **20**, 656 (2010).
[39] J. Cotterell, A. Robert-Moreno, and J. Sharpe, Cell Syst. **1**, 257 (2015).
[40] M. Beaupeux and P. François, Phys. Biol. **13**, 036009 (2016).
[41] I. Palmeirim, D. Henrique, D. Ish-Horowicz, and O. Pourquié, Cell **91**, 639 (1997).
[42] V. M. Lauschke, C. D. Tsiairis, P. François, and A. Aulehla, Nature (London) **493**, 101 (2012).
[43] D. Soroldoni, D. J. Jörg, L. G. Morelli, D. L. Richmond, J. Schindelin, F. Jülicher, and A. C. Oates, Science **345**, 222 (2014).
[44] K. F. Sonnen, V. M. Lauschke, J. Uraji, H. J. Falk, Y. Petersen, M. C. Funk, M. Beaupeux, P. François, C. A. Merten, and A. Aulehla, Cell **172**, 1079 (2018).
[45] M. Heltberg, R. A. Kellogg, S. Krishna, S. Tay, and M. H. Jensen, Cell Syst. **3**, 532 (2016).
[46] A. Goldbeter and O. Pourquié, J. Theor. Biol. **252**, 574 (2008).
[47] P. B. Jensen, L. Pedersen, S. Krishna, and M. H. Jensen, Biophys. J. **98**, 943 (2010).
[48] Y.-J. Jiang, L. Smithers, and J. Lewis, Curr. Biol. **8**, R868 (1998).
[49] C. Tsiairis and A. Aulehla, Cell **164**, 656 (2016).
[50] L. Espinosa, J. Ingles-Esteve, C. Aguilera, and A. Bigas, J. Biol. Chem. **278**, 32227 (2003).
[51] D. R. Foltz, M. C. Santiago, B. E. Berechid, and J. S. Nye, Curr. Biol. **12**, 1006 (2002).
[52] X. He, Dev. Cell **4**, 791 (2003).
[53] C. Y. Logan and R. Nusse, Annu. Rev. Cell Dev. Biol. **20**, 781 (2004).
[54] I. V. Chia and F. Costantini, Mol. Cell. Biol. **25**, 4371 (2005).
[55] D. S. Glass, X. Jin, and I. H. Riedel-Kruse, Phys. Rev. Lett. **116**, 128102 (2016).
[56] E. Lee, A. Salic, R. Krüger, R. Heinrich, and M. W. Kirschner, PLoS Biol. **1**, e10 (2003).
[57] S. Ares, L. G. Morelli, D. J. Jörg, A. C. Oates, and F. Jülicher, Phys. Rev. Lett. **108**, 204101 (2012).
[58] S. H. Strogatz, *Nonlinear Dynamics and Chaos: With Applications to Physics, Biology, Chemistry, and Engineering* (Westview Press, Boulder, 2014).
[59] D. Li, Y. Zhou, C. Zhou, and B. Hu, Phys. Rev. B **83**, 174424 (2011).
[60] T. Bohr and G. Gunaratne, Phys. Lett. A **113**, 55 (1985).
[61] H. Daido, Phys. Rev. Lett. **78**, 1683 (1997).
[62] H. G. Schuster and P. Wagner, Prog. Theor. Phys. **81**, 939 (1989).

3.4 Conclusions of Part I and perspectives for further research

We have derived concrete constraints on somitogenesis in mice, assuming that the formation and scaling happens by phase-gradient encoding. In particular, we proposed experiments that should alter the width of somites. These could be used to falsify the proposed phase-gradient encoding. Recent experiments in mice seem to have qualitatively different outcomes than would be expected, given a mechanism based on phase-gradient encoding. These experiments, however, cannot yet falsify the phase-gradient mechanism; first, system variables such as the exact period-gradient perturbation and the phase profile need to be known for the experiments.

We also showed that phase waves could be entrained by external variation of morphogen levels. Because the phase variation across an Arnol'd tongue is π, such entrainment cannot lead to a full wave occupying the PSM. Hence, we can only hope to use the entrainment to test whether a phase difference of 2π is necessary for somite formation to occur.

There are several interesting possibilities for future research. One obvious direction is the experimental realisation of our proposed experiments. It is already possible to entrain and alter oscillation periods in PSM cells. Detailed tests of the phase-encoding mechanisms, like the ones we suggest in our papers, have the potential to increase our understanding of somite formation in mice considerably. Theoretically, there are open questions too. We provided analytical results for two special cases: a PSM of constant length, and a PSM with no growth. Studying the cases of shrinking PSMs with growth and PSMs of increasing length would be interesting. What happens in these cases? Does the phase profile change gradually? Perhaps the phase width must change as the PSM is shortened? Our calculations found two different steady-state phase profiles for constant length and no growth, so exploring the intermediate cases seems worthwhile. A possible way to approach this would be formulating the problem as an eigenvalue problem. If the growth and somite formation can be expressed as an operator $\mathcal{S}$, and the phase-profile as a function (or vector) $\phi(x)$, demanding that $\phi(x)$ is only rescaled after each somite formation would be looking for solutions to the eigenvalue problem

$$\mathcal{S}\phi = \sigma\phi. \tag{3.1}$$

Here σ is an eigenvalue of $\mathcal{S}$ and the amount the PSM is shortened or elongated following a full iteration of growth and somite formation. Expressing solutions ϕ as a function of growth conditions could be very interesting.

Other interesting future directions are mentioned in the paper presented in Chapter 2. We argued that a concave phase profile would serve as a way to reduce the influence that errors in the phase width have on physical somite width. A detailed numerical investigation of this influence could be exciting. It would also be interesting to investigate in more detail the role of coupling between PSM cells. A coupling is not needed in order for phase waves to travel the PSM, so perhaps the only function this coupling has is limiting the influence that inevitable noise has on oscillation phases. A very strong coupling might make cells synchronise, and a very weak coupling would not provide any protection against noise. So what is the sweet spot of coupling strength, and does this have any implications that can further increase our understanding of the somite-formation mechanism?

Part II

Contagion in networks

Chapter 4

Synergistic effects in threshold models on networks

On a summer day in June, 2010, a mysterious piece of software was discovered (Anderson, 2012; Nakashima and Warrick, 2012; Karnouskos, 2011; Keizer, 2010). The software, "Stuxnet", actively spread indiscriminately between computers via the operating system Microsoft Windows. When the software reached a computer in charge of specific industrial processes, it released a load designed to destroy this industrial hardware. The computer virus is widely believed to be a military cyberweapon developed to exploit the interconnected nature of computers to target Iranian nuclear facilities.

The worst power outage in US history occurred on November 9 1965 (Vassell, 1990). A malfunction in a safety device caused current sent from the Niagara Falls to be momentarily redirected from its planned path. This single malfunction started a cascade of safety switches being turned on in the power network. Each switch disconnected another part of the US Northeast power system, causing the whole system to become fragmented into a collection of isolated islands in a matter of minutes. 30 million people lost power following that single malfunctioning safety device (Strogatz, 2004).

This second part of my dissertation concerns spreading processes in networks. Such spreading processes range from harmful ones, as illustrated by the two examples above, to sought-after contagion such as viral spreading of online content. This chapter introduces different classes of spreading processes in Section 4.2. Before this, however, I introduce the concept of networks and 3 standard models of networks. A key feature of networks is their generality in Section 4.1. From the foodwebs summarising the complex ecological interactions in nature to terrorist networks, professional networks, and social media, the concept of networks is used to describe an astonishingly diverse set of topics. The goal of the following two sections is to illustrate how a general mathematical framework can capture this diversity.

Following these preliminaries, and the introduction of contagion in Section 4.2, three scientific articles are presented in this part of the dissertation. The present chapter introduces a paper concerning synergistic effects in spreading processes. The topic of Chapter 5 is a paper studying how anti-establishment majorities can be created from spreading processes in networks. And finally, Chapter 6 introduces an article examining the impact of mutant contagion in networks.

Before introducing the scientific work I have done on contagion in networks, however, it is instructive to ask the following question.

4.1 Why networks?

Natural, social, and engineered systems often consist of interacting entities. Sometimes, effectively, all of these entities interact with each other, like chemicals in a container that is continuously shaken. In other cases, the possible interactions between constituents are more limited. From Copenhagen Central Station, one can take a direct train to Hamburg while there are no direct trains to Rome. Sometimes the interactions that are effectively possible are even different from those that are possible in principle. A Ph.D. student could send an email to a professor she never met. Alas, she would probably be more likely to get a reply if she asked a mutual acquaintance, her supervisor, to send the email instead.

The topology of connections in systems of interacting parts can impact how efficiently biological systems function, how quickly people travel, and how successfully messages are shared between people. The concept of *Networks* has turned out to be a powerful abstraction to study this impact. Networks have their roots in the mathematical discipline of graph theory, dating back to 1735 when Leonard Euler solved the famous "Seven Bridges of Königsberg" problem (Sachs, Stiebitz, and Wilson, 1988). Graph theory studies the mathematical properties of *graphs*, which are sets of *vertices* pairwisely connected to each other by *edges*. In network theory, graphs are referred to as *Networks*, vertices as *nodes*, and edges as *links*. I shall use these names interchangeably and often refer to linked nodes as *neighbours*.

Although networks have been used in a wide range of disciplines since the 1930s (Moreno, Whitin, and Jennings, 1932; Moreno and Jennings, 1938; Price, 1976; Granovetter, 1977) (especially within sociology), an explosion of papers on networks emerged around the end of the last century. Often, two articles are attributed igniting this interest: One by Duncan J. Watts and Steven H. Strogatz (Watts and Strogatz, 1998) and the other by Albert-László Barabási and Réka Albert (Barabási and Albert, 1999). Both works used network formulations to investigate the structural properties of connected structures. Watts and Strogatz created networks with high "clustering" (tendency for neighbours to link to the same nodes) and low average path length between pairs of nodes. These properties were found to be present in networked systems from biology and technology (Watts and Strogatz, 1998). High clustering and low average path length had also been reported to characterise some social systems. In particular, these properties seemed to be present in the human global social network, which famously has "6 degrees of separation" between strangers (Travers and Milgram, 1977) even though friends tend to share friends.

Barabási and Albert studied which rules for link creation might lead to node connectivities following power laws. Such power laws in the probability distribution of node connectivities seemed to be present in many different natural and engineered systems, and in particular in the world-wide-web (Barabási and Albert, 1999).

And the rest is history. Since the publication of these two seminal articles, a plethora of papers on the structure and dynamics of networks have emerged. From biology (Milo et al., 2002; Shen-Orr et al., 2002; Maslov and Sneppen, 2002; Alon, 2007; Jeong et al., 2000; Barabási and Oltvai, 2004; Bassett et al., 2011; Lynall et al., 2010), to computer science (Liben-Nowell and Kleinberg, 2007; Leskovec, Kleinberg, and Faloutsos, 2007; Kleinberg, 2000; Ugander et al., 2012; Grover and Leskovec, 2016; Leskovec and Faloutsos, 2006), finance (Battiston et al., 2012; Cont, Moussa, and Santos, 2010; Acemoglu, Özdaglar, and Tahbaz-Salehi, 2015; Allen and Babus, 2009; Amini, Cont, and Minca, 2016), and computational social science (Goel et al., 2015; Goel, Watts, and Goldstein, 2012; Stewart et al., 2019; Aral, Muchnik, and Sundararajan, 2009; Vosoughi, Roy, and Aral, 2018; Aral and Walker, 2012;

Leskovec, Adamic, and Huberman, 2007; Sekara, Stopczynski, and Lehmann, 2016); from papers investigating structural properties such as groups of highly interconnected nodes ("communities") (Blondel et al., 2008; Rosvall and Bergstrom, 2008; Ahn, Bagrow, and Lehmann, 2010; Girvan and Newman, 2002; Newman, 2006; Newman and Girvan, 2004; Clauset, Newman, and Moore, 2004; Schaub et al., 2017), to investigating the impact of failures or epidemics on networks (Rosvall et al., 2014; Pastor-Satorras et al., 2015; Pastor-Satorras and Vespignani, 2001b; Newman, 2002b; Callaway et al., 2000; Ash and Newth, 2007; Brummitt, D'Souza, and Leicht, 2012; Buldyrev et al., 2010; Cohen et al., 2000; Lambiotte, Tabourier, and Delvenne, 2013), networks have found applications in many fields and been useful in answering many different kinds of questions.

4.1.1 Basic mathematical formulation of networks

Depending on the attributes of the nodes and links in the system in question, different network representations can be utilized. In the classic representation, nodes and links are static in time. In the very simplest case, all links are weighted equally – either a link is there, or it is not. Together the nodes and links form a network, which can be represented by matrices such as the adjacency matrix, A. For a network consisting of the set of nodes $\mathcal{V}$ and links $\mathcal{E}$, the entries of the adjacency matrix are given by

$$A_{ij} = \begin{cases} 1 & \text{if } (i,j) \in \mathcal{E}, \\ 0 & \text{otherwise.} \end{cases} \tag{4.1}$$

If all edges are bidirectional, that is, if A is symmetric, the network is *undirected*. In this part of my dissertation, networks will always be undirected and of the form described in Eq. (4.1).

The simplicity of network representations, such as the adjacency matrix in Eq. (4.1), is convenient. In many cases, more detailed information about the links and nodes is necessary to include. A simple extension is to allow links to carry different weights, in which case the network is *weighted*. In a social network, the weight of a link could indicate the average weekly number of social interactions between the pair of nodes in question. If one is studying a network consisting of cities connected by modes of transportation, information about which mode of transportation connects each city would probably be useful. One way of including such information is to let the network consist of different "layers". Edges in the first layer could then represent bus routes, edges in the second layer train connections, etc. *Multilayer networks* can be used to include such information (Kivelä et al., 2014; De Domenico et al., 2013). In some cases, *when* nodes interact could be important. In a network depicting sexual contacts, for example, a node getting infected with a sexually transmitted disease can only pass this disease on to future sexual partners. In this case, the sequence of interactions matters and one might represent the system with *Temporal networks* where edges are timestamped (Holme and Saramäki, 2012). One could also be interested in including connections beyond pairwise interactions. Scientific collaborations, for example, do not exclusively happen between pairs of researchers – often several people coauthor papers together. Such higher-order network structures can be represented using *simplicial complexes* or a *hypergraph* formalism, or other future frameworks (Benson, Gleich, and Leskovec, 2016; Chodrow, 2019; Young et al., 2017; Lambiotte, Rosvall, and Scholtes, 2019; Ghoshal et al., 2009). All of these more advanced representations are currently very active areas of research and have found interesting applications (Saumell-Mendiola, Serrano, and Boguná, 2012; Pilosof et

al., 2017; De Domenico et al., 2016; De Domenico et al., 2015a; De Domenico et al., 2015b; Rocha, Liljeros, and Holme, 2011; Kovanen et al., 2011; Bazzi et al., 2016; Lambiotte, Tabourier, and Delvenne, 2013; Masuda and Lambiotte, 2016; Neuhäuser, Mellor, and Lambiotte, 2019; Paranjape, Benson, and Leskovec, 2017; Yin et al., 2017; Benson, Gleich, and Lim, 2017; Iacopini et al., 2019).

4.1.2 Models of networks

In the following three chapters, a recurring theme will be investigations into how network structure affects the severeness of contagion spreading in populations. One network feature which is particularly popular to study is the *degree distribution*. The degree of a node in an undirected network is the number of links the nodes has. Consequently, the degree distribution, $P(k)$, expresses the probability that a node chosen uniformly at random has degree k.

Empirical network structures can be quite complicated, involving degree correlations, community structure, complicated degree distributions, etc. (Ugander et al., 2011; Myers et al., 2014; Traud, Mucha, and Porter, 2012; Jesus, Schwartz, and Lehmann, 2009; Meunier et al., 2009; Osat, Radicchi, and Papadopoulos, 2019; Boccaletti et al., 2006; Newman, 2001; Girvan and Newman, 2002; Eriksen et al., 2003; Mislove et al., 2008). The structure of every empirical network is a result of the rules under which the network was created. To understand which rules can lead to which network structures, one can create *synthetic networks*. This is done by imposing some regulations as to how nodes and links are created in a network. Networks are then created by simulating these rules. Many methods exist for creating such synthetic networks, each with its own merits (Barabási and Albert, 1999; Overgoor, Benson, and Ugander, 2019; Callaway et al., 2001; Ozik, Hunt, and Ott, 2004; Newman, Strogatz, and Watts, 2001; Young et al., 2017; Chodrow, 2019; Fosdick et al., 2018; Caldarelli et al., 2002; Ergün and Rodgers, 2002; Juul and Joyner, 2018; Watts, 1999; Newman, 2009; Catanzaro, Boguná, and Pastor-Satorras, 2005; Watts and Strogatz, 1998; Erdős and Rényi, 1960; Bollobás and Riordan, 2003; Ross, Strandkvist, and Fontana, 2019b; Ross, Strandkvist, and Fontana, 2019a). Synthetic networks can also be useful in investigating how network structure influences dynamical processes in populations. For example, how network structure affects how widespread a particular disease gets in a population. In the research articles I will introduce in the following three chapters, I will make use of 3 kinds of synthetic networks. I will introduce these classes of synthetic networks, and some of their properties below.

Erdős–Rényi networks

One of the simplest kinds of synthetic networks are Erdős–Rényi networks. N-node Erdős–Rényi networks can be created in two different ways. In the first way of creating Erdős–Rényi networks, one defines: 1) the number of nodes the network has, N; 2) the number of links the network has, m. The Erdős–Rényi network is then created by choosing m pairs of nodes uniformly at random. Only these pairs of nodes are linked in the Erdős–Rényi network. This type of Erdős–Rényi network is usually referred to as $\mathcal{G}(N, m)$. When choosing pairs of nodes, one needs to specify whether nodes are allowed to link to themselves or not and whether the same pair of nodes can be chosen twice. A common choice is to prohibit both of these things happening, thereby making a network that is *simple*.

Another way of making an Erdős–Rényi network is to – instead of specifying the number of links, m – choose a probability p with which each possible link exists.

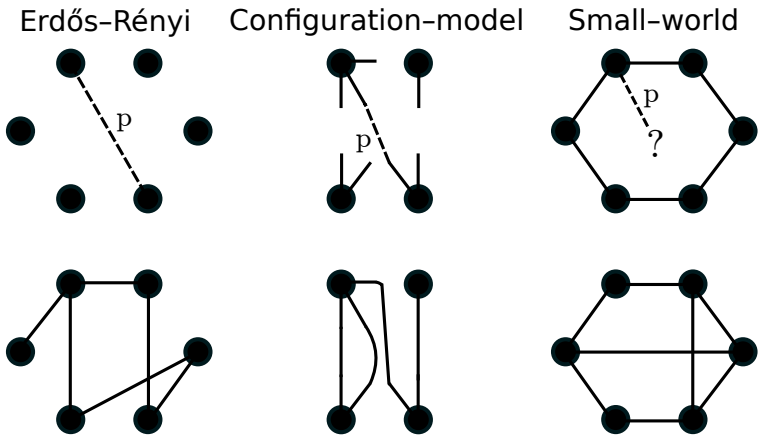

FIGURE 4.1: Illustration of the creation of three kinds of synthetic networks. The leftmost column illustrates the creation of Erdős–Rényi networks. Any link exists with a probability p. The middle column illustrates the creation of configuration-model networks. First, a degree sequence is defined, and nodes with an equivalent number of link stubs are created. Then, pairs of stubs are matched uniformly at random. The rightmost column illustrates the creation of Newman-Watts small-world networks. First, a lattice is created. Then, each node gets linked to another node with probability p. For each link, the target node is chosen uniformly at random.

To create this $\mathcal{G}(N, p)$ network, one then independently draws a number between 0 and 1 uniformly at random for each pair of nodes. The link exists if the random number comes out smaller or equal to p. This rule is illustrated in the top-left panel of Figure 4.1. The bottom-left panel illustrates what an Erdős–Rényi network might look like.

Erdős–Rényi networks are also called "Poisson random graphs" or "Bernoulli random graphs" (Newman, 2018). These names refer to their degree distributions, which are binomial since each edge is created independently with equal probability. In the limit of large N and small p, the degree distribution is Poissonian with mean $\langle k \rangle = (N-1)p$.

Erdős–Rényi networks are simple to make, and their structural properties are known in great detail (Newman, 2018). Unfortunately, empirical networks rarely have Poissonian degree distributions. This realization was what drove Barabási and Albert to work on problems related to networks at the end of the previous millenium (Barabási and Albert, 1999). The Erdős–Rényi networks remain popular null-models nonetheless. In my work, I will consistently use the $\mathcal{G}(N, p)$ formulation to create them.

Configuration-model networks

Another class of synthetic, random networks are configuration-model networks. To create configuration-model networks with N nodes, one needs to define a degree sequence $\{k_n\}_{n=1}^{N}$ for the network. The network is then drawn uniformly-at-random from the space of networks with this given degree sequence (Bollobás, 1980; Newman, 2018; Fosdick et al., 2018). Configuration-model networks are especially popular as degree-preserving statistical null-models, and their structural properties have been thoroughly investigated (Newman, Strogatz, and Watts, 2001; Molloy and Reed, 1998; Molloy and Reed, 1995). Configuration models also exist for networks

with more complicated attributes, including temporal networks and networks with higher-order interactions (Holme and Saramäki, 2012; Holme, 2005; Karsai et al., 2011; Young et al., 2017; Chodrow, 2019). It is important to state that configuration-model networks are not just one thing. As argued in a recent paper by Fosdick et al., the way of drawing networks from the space of networks with the degree sequence in question should depend on the application one has in mind (Fosdick et al., 2018). This is particularly important if the networks are meant to constitute a statistical null-model.

In my work, all configuration-model networks are created in the same way. The configuration-model networks have not been systematically used as statistical null-models, but rather a convenient way of creating random networks with a given degree sequence. Therefore the subtleties of choosing the correct degree-preserving synthetic network are not relevant to my work.

Given a degree sequence, $\{k_n\}_{n=1}^{N}$, I create a network as follows. I create N nodes, and give node n k_n "half-edges" or "stubs" for every n between 1 and N. Pairs of stubs are then matched uniformly at random. If the sum of degrees is even, this procedure creates a network with the wanted degree sequence. In the created network, nodes may link to themselves, and parallel edges may occur. The frequency of these self-loops and parallel edges declines as N gets large. The creation of configuration-model networks is illustrated in the middle column of Figure 4.1.

Small-world networks

The third kind of synthetic network I have used in my research is a kind of small-world network. As previously mentioned, small-world networks were first introduced by Watts and Strogatz in a seminal paper approximately 20 years ago. To understand the fuzz about small-world networks, it might be helpful to recall the legend of "6 degrees of separation". In social networks, contacts tend to cluster: Many of your friends are also friends of your friends, and most of your friends probably live near you. In this light, the statement that you are only 6 or fewer social interactions from any person on earth might seem surprising.

Nonetheless, experiments have found that only a few intermediate steps (typically 4-6) are required for a person B to receive a package from another person A (Travers and Milgram, 1977; Milgram, 1967; Backstrom et al., 2012). This is true even if A and B live far apart, and if the person A is selected randomly among citizens of a particular city. This raises a question: How can the average shortest social distance between people be this small if social connections cluster together?

Watts and Strogatz came up with a way of creating networks with high clustering and low average shortest distance. To create a small-world network consisting of N nodes, they first created a regular lattice. The lattice could, in principle, be repeated geometrical arrangement of nodes and edges, like the squares on a chessboard or the circular pattern depicted in the top-right panel of Figure 4.1. In a regular lattice, every node has the same degree. Watts and Strogatz then rewired each link independently with some probability p, moving one end of the link to a node chosen uniformly at random. If $p = 0$, the lattice persisted. If $p = 1$, the network would be much more random. Intermediate p preserved some lattice structure, but shortcuts connected far-apart nodes. For such intermediate p, Watts and Strogatz found that the resulting network had high clustering and low average shortest distance between nodes.

The small-world properties of high clustering and low average shortest distances have turned up in many places, including the human brain, the world wide web, and

many others (Bassett and Bullmore, 2006; Adamic, 1999; Amaral et al., 2000). The properties of small-world networks have been studied continuously since Watts and Strogatz published their famous paper (Kleinberg, 2000; Latora and Marchiori, 2001; Barahona and Pecora, 2002; Santos, Rodrigues, and Pacheco, 2005; Lü, Chen, and Zhou, 2011; Xia, Fan, and Hill, 2010), and it remains a very influential piece of work. I will be creating small-world networks in a slightly different way than what Watts and Strogatz did originally. As is the case in the original model, I will start with a regular lattice. For each node in the lattice, I will then insert a new link to another node chosen randomly and uniformly with chance p. Newman and Watts (Newman and Watts, 1999) introduced this way of making small-world networks, and the method has the lovely property that the lattice structure remains unbroken in the final network. This property was mathematically convenient for Newman and Watts, and this convenience is why I will create small-world networks like this in Chapter 6.

4.2 Contagion in networks

Contagion is a concept that originated in epidemiology but is now used for anything that can spread between peers in a network. Examples of contagion include bank defaults (Cont, Moussa, and Santos, 2010; Haldane and May, 2011; Acemoglu, Özdaglar, and Tahbaz-Salehi, 2015), misinformation (Vosoughi, Roy, and Aral, 2018; Del Vicario et al., 2016), power failures (Brummitt, D'Souza, and Leicht, 2012; Buldyrev et al., 2010; Carreras et al., 2002), rumours (Banerjee et al., 2019; Banerjee et al., 2014; Jackson, Malladi, and McAdams, 2018; Shah and Zaman, 2011; Shah and Zaman, 2016; Shah and Zaman, 2012), innovations and other products (Mellor et al., 2015; Krapivsky, Redner, and Volovik, 2011; Rogers, 2010; Rogers, 1976; Mahajan, 2010; Hagerstrand, 1968; Hinz et al., 2011; Aral, Muchnik, and Sundararajan, 2013; Chin, Eckles, and Ugander, 2018; Iyer and Adamic, 2018), social behavior (Aral and Nicolaides, 2017; Crandall, 1988; Centola and Macy, 2007; Guilbeault, Becker, and Centola, 2018a; Centola, 2010), and communicable diseases (Pastor-Satorras et al., 2015; Keeling and Rohani, 2011; Lloyd-Smith et al., 2009; Anderson and May, 1992; Haydon et al., 2003; Fennell and Gleeson, 2019; Sanz et al., 2014; Salehi et al., 2015). Contagion is one of many dynamical processes that are studied on networks. One of the main reasons for doing this is to understand the impact of network properties on different aspects of contagion (Porter and Gleeson, 2016). The underlying network can for example influence how infectious a disease needs to be in order to spread widely (Boguná, Pastor-Satorras, and Vespignani, 2003; Eguiluz and Klemm, 2002; Pastor-Satorras and Vespignani, 2002; Pastor-Satorras et al., 2015) and which vaccination strategies are effective (Holme, 2004; Rushmore et al., 2014; Salathé et al., 2010; Miller and Hyman, 2007). In addition to network topology, nodes with special properties can also have an impact on dynamical processes on networks (Mellor et al., 2015; Klamser et al., 2017; Juul and Porter, 2019). One example of such nodes with special properties are "luddites" – nodes that oppose the spread of innovations (Mellor et al., 2015).

My primary interest has been studying how widespread contagions get under different conditions. These conditions include different models for the spreading process, different underlying network structures, and including different kinds of nodes in the network. I have also been interested in how the number of nodes that are infectious at the beginning of time ("the seed") influences the impact of contagion. The projects I introduce in the following 3 chapters deal with two overarching

kinds of contagion: "Simple contagion" and "complex contagion". In the following subsections, I introduce these two kinds of contagion.

4.2.1 Simple contagion

In simple contagion, a single contact between a susceptible and an infectious person is enough for the disease to be transmitted (Porter and Gleeson, 2016). Examples of simple contagion include spreading diseases.

The most prominent models of simple contagion are probably the so-called compartmental models (Pastor-Satorras et al., 2015). In such models, a person can be in different compartmental "states". Depending on the contagion dynamics, transitions between states can occur. Examples of such states could be "Susceptible" and "Infectious". A node in the susceptible state could then transition into the infectious state with some rate $n_I \lambda_{SI}$ where n_I is the number of infectious neighbours the susceptible node has. These rules define the *Susceptible-Infected model* (SI model). More complicated compartmental models also exist. For example, if nodes in the infectious state have a chance of transitioning back into the susceptible state with some rate of λ_{IS}, the resulting model is the *Susceptible-Infected-Susceptible model* (SIS model). If instead, infectious nodes are allowed to transition into a new, "recovered" state with a rate λ_{IR}, the model is the *Susceptible-Infected-Recovered model* (SIR model).

It is difficult to overstate the influence these compartmental models have had. Since their introduction near the beginning of the last century (Kermack and McKendrick, 1927), countless variants of compartmental models have come to exist, with applications to a wide range of problems (Pastor-Satorras et al., 2015; Mellor et al., 2015; Eilersen and Sneppen, 2019; Jensen, Uekermann, and Sneppen, 2019; Jensen et al., 2019; Shulgin, Stone, and Agur, 1998; Beretta and Takeuchi, 1995; Stopczynski, Pentland, and Lehmann, 2015; Miller, 2009; Kiss, Miller, Simon, et al., 2017; Volkening et al., 2018; Pastor-Satorras and Vespignani, 2001a; Watts et al., 2005; Dodds and Watts, 2004; Dodds and Watts, 2005; Pérez-Reche et al., 2011). Often models of simple contagion are formulated in terms of coupled, ordinary differential equations. In this case the underlying network is implicitly assumed to be "complete" – links exist between all nodes.

4.2.2 Complex contagion

A different kind of contagion is complex contagion. Complex contagions spread as a result of *social reinforcement*. In other words, instead of a single contact with an infectious person being sufficient to pass the contagion, multiple exposures could be necessary. Experimental evidence of complex contagion has been observed in Twitter retweets and other social-media dynamics (Mønsted et al., 2017; Ugander et al., 2012), innovation diffusion (Bandiera and Rasul, 2006; Oster and Thornton, 2012; Banerjee et al., 2013; Karsai et al., 2014) and social-media growth, and is a very active research topic in the social sciences (Centola and Macy, 2007; Weng, Menczer, and Ahn, 2013; Lehmann and Ahn, 2018; Ternovski and Yasseri, 2019).

The article "The strength of weak ties" (Granovetter, 1977) was arguably a historical milestone in the study of contagion in social systems. In this paper, Granovetter explored the effect of social network structure on diffusion of influence. Following this, Granovetter introduced a model of complex contagion, a so-called "threshold model" (Granovetter, 1978). A similar model was later introduced by Duncan Watts (Watts, 2002). This Watts Threshold Model (WTM) was mathematically well-defined, and Watts computed several interesting quantities for the model. These

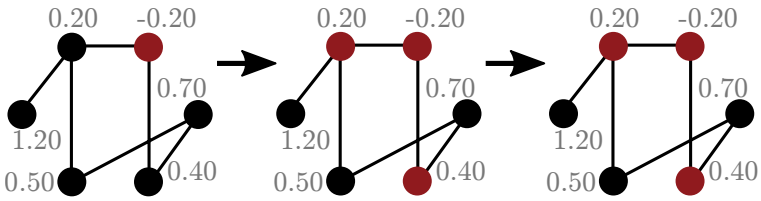

FIGURE 4.2: Illustration of the Watts Threshold Model (WTM). For each node, a threshold, ϕ, is drawn from some probability distribution. These thresholds are the grey numbers in the figure. Nodes can be either active (red) or inactive (black). A nodes turns active if Eq. (4.2) is satisfied. Here, nodes are updated synchronously, and time is discrete. Time progresses from left to right. One node has a negative threshold and acts as a seed.

included conditions under which the contagion would *cascade* through the underlying network. The papers of this and the following chapter investigate modified versions of the WTM. For this reason, I introduce the WTM formally below.

The Watts Threshold Model

In the WTM, nodes can be in either of two states, 0 or 1. I shall refer to these states as *inactive* and *active*, respectively. The dynamics are monotonic: An inactive node can turn active, but the reverse is not possible. How prone a node is to becoming active depends on its *threshold*, ϕ. Typically, these thresholds are drawn independently from some probability distribution $f(\phi)$. A node turns active if the fraction of its neighbours that are active is at least equal to its threshold. If n is the number of active neighbours a node of degree k has, this condition can be expressed as

$$\Xi_{\text{WTM}} := n/k \geq \phi. \tag{4.2}$$

I shall refer to the function $\Xi_{\text{WTM}} = n/k$ as the "peer-pressure function" of the WTM. After the creation of a network, and assignment of thresholds, simulations of the WTM typically proceed in the following way. First, some fraction of the nodes is chosen as seed – active at the beginning of the simulation. This choice of seed nodes can either be done explicitly by drawing a number of nodes randomly. It can also be done by letting thresholds take negative values; if a node has $\phi \leq 0$, Eq. (4.2) will be satisfied even for $n = 0$, and so the node is a seed. With seeds chosen, the states of nodes need to be updated as time progresses. The updating can, for example, be done for all node states simultaneously before proceeding to the next time step and repeating. This procedure is referred to as synchronous update in discrete time. Other choices include updating nodes one at a time instead of synchronously or updating only some randomly chosen nodes. When working with the WTM, I will be updating node states synchronously, and in discrete time steps. The updating continues until no more nodes can become active. Thus, the dynamics of the WTM are completely deterministic once seed nodes have been chosen and thresholds been drawn.

The WTM is a popular model for complex contagion. Many extensions of the model have been studied. These include extensions where nodes become active with some delay τ after they fulfill Eq.(4.2) (Oh and Porter, 2018), and ones where nodes influence their neighbours more if they have many active neighbours (Melnik et al., 2013). They also include ones in which the activation criterium of Eq. (4.2) is entirely based on the number of active neighbours a node has, rather than what fraction of its

neighbours are active (Centola and Macy, 2007; Centola, Eguíluz, and Macy, 2007). A large number of studies have focused on calculating the fraction of nodes that are active at the end of spreading (Gleeson, 2008; Gleeson and Cahalane, 2007; Gleeson, 2011; Melnik et al., 2011; Hackett, Melnik, and Gleeson, 2011; Melnik et al., 2013; Fennell and Gleeson, 2019; Hurd and Gleeson, 2013). Such analytical results can provide a deeper understanding of phenomena seen in numerical investigations of threshold models on networks. In both of my research articles concerning threshold models on networks, I develop analytical approximations for the fraction of k-degree nodes that are active at discrete time step t. The first of these papers studies a modification of the WTM including synergistic interaction. This model was inspired by models of synergistic interactions in simple contagion. The following section introduces this prior work on synergistic contagion.

4.3 Synergistic contagion in networks

In typical models of spreading processes, each infectious neighbour influences a susceptible node equally. For example, for compartmental models, the rate with which susceptible nodes become infected is linear in the number of infectious neighbours $\lambda_{SI} n$. Similarly, in the WTM, the lefthand side of Eq. (4.2) is linear in the number of infectious neighbours too. When the increase in influence is instead nonlinear in n, the joint effort of infectious nodes is *synergistic*. If the influence of n infectious nodes is smaller than it would be under a linear model, the synergy is interfering. Conversely, if the impact of n infectious nodes is larger, the synergy is constructive.

Pérez-Reche et al. (Pérez-Reche et al., 2011) were the first to introduce synergistic effects in spreading processes. They based their model on the SIR model and suggested two different ways in which synergy could be incorporated. The first, they named *r-synergy*. r is short for recipient. In this case, the rate with which each infectious neighbour infects a susceptible node is

$$\max\left(0, \alpha + \beta(n_r(t) - 1)\right). \tag{4.3}$$

Here, $n_r(t)$ is the number of infectious neighbours the susceptible node has at time t, α is a baseline rate, and β is a parameter describing the synergy. If a susceptible node has only a single infectious neighbour, $n_r = 1$, and no synergy is taking place between infectious neighbours. If the susceptible node has several infectious neighbours, the rate is increased or diminished depending on the sign of β. If $\beta > 0$, the rate increases compared to the synergy-free case, and the synergy is constructive; if $\beta < 0$, the synergy is interfering. For $\beta = 0$, the synergistic model reduces to the regular SIR model.

The second kind of synergy Pérez-Reche suggested, they called d-synergy. The d is short for "donor". In this case, an infectious node successfully infects a susceptible neighbour with rate

$$\max\left(0, \alpha + \beta(n_d(t) - 1)\right). \tag{4.4}$$

Here, $n_d(t)$ is the number of infectious neighbours of the infectious node. As was the case for r-synergy, $\beta > 0$ corresponds to constructive synergy, $\beta < 0$ corresponds to interfering synergy, and for $\beta = 0$ the model reduces to the ordinary SIR model. Figure 4.3 illustrates the two kinds of synergy.

Pérez-Reche et al. incorporated synergistic interaction because of experimental evidence that synergy could be present among colonizing bacterial and fungal pathogens and in the growth of tumors (Pérez-Reche et al., 2011). They found that,

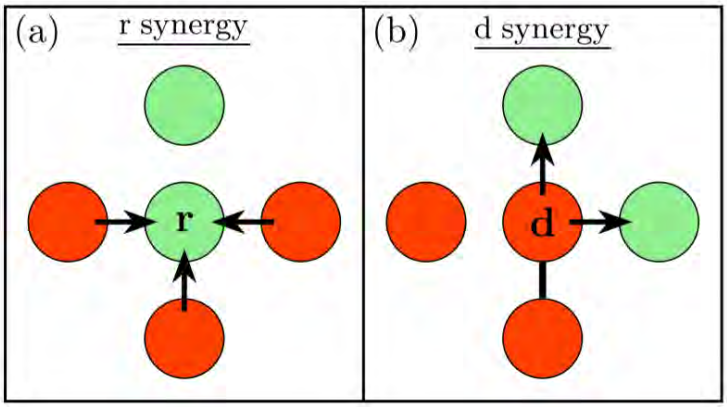

FIGURE 4.3: Illustration of the model of the models of synergistic contagion from (Pérez-Reche et al., 2011). The lefthand panel illustrates r-synergy. In this case, the rate with which a susceptible node gets infected by each of its infectious neighbours gets boosted by an amount proportional to the number of infectious neighbours the susceptible node has. The righthand panel illustrates d-synergy. In this case, the rate with which an infectious node infects neighbouring susceptible nodes gets boosted by an amount proportional to the number of infectious neighbours the infectious node has. Figure from (Pérez-Reche et al., 2011).

depending on the value of β, the spreading process would show "exploitative" or "explorative" behavior. Exploitative behavior is characterised by the pathogen invading many hosts, efficiently filling the space between infectious hosts. Explorative behavior is characterised by the pathogen spreading widely but infecting only a few hosts in the process.

Following the first model of synergistic spreading, several papers have examined details of synergy in spreading processes (Broder-Rodgers, Pérez-Reche, and Taraskin, 2015; Taraskin and Pérez-Reche, 2019; Taraskin and Pérez-Reche, 2013; Ogura, Mei, and Sugimoto, 2019). These studies have yielded further insights into the details of various aspects of synergistic spreading. These insights range from describing bifurcations to examining the impact of underlying spatial topology. All studies build upon compartmental models as the original paper by Pérez-Reche et al. did.

Synergy seems to be a phenomenon very related to social reinforcement, though. From this perspective, it seems natural to study models of complex contagion that include synergistic effects. With Mason A. Porter, I formulated synergistic versions of the Watts Threshold Model and studied how synergy effects affected cascades on different network topologies. In addition to being the first model of complex contagion incorporating synergy, it is also the first model of deterministic synergistic spreading. This makes the model particularly suited for analytical studies – most existing models relied primarily on numerical results.

4.4 Our results: Bifurcations caused by synergy

In the paper "Synergistic effects in threshold models on networks", published in Chaos (Juul and Porter, 2018), Mason A. Porter and I define two synergistic peer-pressure functions, $\Xi(n, \beta)$. These function take two arguments: n, which is the

number of active neighbours a nodes has, and β, a synergy parameter similar to the one used by Pérez-Reche et al. The peer-pressure functions both satisfy

$$\Xi(n,\beta) = \begin{cases} = 0, & \text{if} \quad n = 0, \\ > n, & \text{if} \quad \beta > 0 \quad \text{and} \quad n \geq 2, \\ = n, & \text{if} \quad \beta = 0 \quad \text{or} \quad n = 1, \\ = 0, & \text{if} \quad \beta < 0 \quad \text{and} \quad n \geq 2. \end{cases} \tag{4.5}$$

This formally expresses that 1) No peer-pressure exists if no neighbours are active; 2) synergy is only present if more than 1 neighbour is infectious; 3) Synergy is constructive if $\beta > 0$, interfering if $\beta < 0$, and nonexistent if $\beta = 0$.

Although the two peer-pressure functions are different, we find that they give rise to qualitatively similar behavior. In particular, we find that nodes of degree k can only be activated if β is above some critical value. We also find that the fraction of degree-k nodes that are active at equilibrium increases in discrete steps at certain β values. We argue that these discrete jumps are caused by bifurcations taking place at these β values.

If β is just above the critical β value that makes it possible for degree-k nodes to get activated, the degree-k node can only get activated if *all* (that is k) of its neighbours are active. Similarly, there is a larger value of β, above which degree-k nodes can get activated either if k or $k-1$ neighbours are active. As β gets larger and larger, fewer active neighbours are needed to activate degree-k nodes. For this reason, the final fraction of active degree-k nodes increases in sudden jumps at the bifurcation points in β. We show how to find the bifurcation points analytically for any synergistic peer-pressure function $\Xi(n,\beta)$. We also argue that identical bifurcation points will be present in all peer-pressure functions that are continuous and non-decreasing in β.

We successfully write down an analytical approximation for the fraction of degree-k nodes that are active at time step t. This approximation describes simulations well when the model is realised on synthetic networks. It also works well when the model is simulated on an empirical network of condensed-matter theory collaborations, but breaks down when a Facebook subgraph is used as the underlying network. The approximation is built on the assumption that neighbours of a node are connected only rarely. We show that the Facebook subgraph probably breaks this assumption to a larger degree than any of the other networks used in the study.

4.5 Paper: Synergistic effects in threshold models on networks

CHAOS **28**, 013115 (2018)

Synergistic effects in threshold models on networks

Jonas S. Juul[1,a)] and Mason A. Porter[2,3,4,b)]
[1]*Niels Bohr Institute, University of Copenhagen, Blegdamsvej 17, Copenhagen 2100-DK, Denmark*
[2]*Department of Mathematics, University of California, Los Angeles, Los Angeles, California 90095, USA*
[3]*Oxford Centre for Industrial and Applied Mathematics, Mathematical Institute, University of Oxford, Oxford OX2 6GG, United Kingdom*
[4]*CABDyN Complexity Centre, University of Oxford, Oxford OX1 1HP, United Kingdom*

(Received 23 January 2017; accepted 1 December 2017; published online 12 January 2018)

Network structure can have a significant impact on the propagation of diseases, memes, and information on social networks. Different types of spreading processes (and other dynamical processes) are affected by network architecture in different ways, and it is important to develop tractable models of spreading processes on networks to explore such issues. In this paper, we incorporate the idea of *synergy* into a two-state ("active" or "passive") threshold model of social influence on networks. Our model's update rule is deterministic, and the influence of each meme-carrying (i.e., active) neighbor can—depending on a parameter—either be enhanced or inhibited by an amount that depends on the number of active neighbors of a node. Such a synergistic system models social behavior in which the willingness to adopt either accelerates or saturates in a way that depends on the number of neighbors who have adopted that behavior. We illustrate that our model's synergy parameter has a crucial effect on system dynamics, as it determines whether degree-k nodes are possible or impossible to activate. We simulate synergistic meme spreading on both random-graph models and networks constructed from empirical data. Using a heterogeneous mean-field approximation, which we derive under the assumption that a network is locally tree-like, we are able to determine which synergy-parameter values allow degree-k nodes to be activated for many networks and for a broad family of synergistic models. *Published by AIP Publishing.*
https://doi.org/10.1063/1.5017962

Models of cascading processes on networks yield insights into a large variety of processes, ranging from the spread of information and memes in social networks to propagating failures in infrastructure and bank networks.[1–9] In the context of social networks, it is very popular to study models of social influence based on overcoming individuals' stubbornness thresholds with peer pressure or influence.[1–3,10–14] Most such models consider peer pressure only from nearest neighbors, but it is also important to explore the influence of nodes beyond nearest neighbors (e.g., in the context of the "three degrees of influence" that has been reported in some studies).[15] If the combined influence from several nodes is different than the sum of the influences from individual nodes, *synergy* is taking place, and such synergistic effects can exert a major influence on spreading processes on networks. For example, in some systems, the amount of influence per person applying peer pressure may depend on the number of people who are applying peer pressure, and our goal in this paper is to incorporate such ideas into a threshold model of social influence in an analytically tractable way. In our synergistic model, we examine social behavior in which the willingness to adopt either accelerates or saturates in a way that depends on the number of neighbors who have adopted some behavior. We illustrate that a synergy parameter can have a crucial effect on system dynamics (e.g., by determining whether degree-k nodes are possible or impossible to activate). We also develop an analytical approximation (in the form of a heterogeneous mean-field theory) that is effective at forecasting both the temporal development of cascades and the sizes of cascades in many networks.

I. INTRODUCTION

Examining the spread of opinions, actions, memes, information, and misinformation in a population has received intense scrutiny in sociology, economics, computer science, physics, and many other fields.[1,2,4,6–8,10–24] Such phenomena—including the spread of defaults of banks, norms in populations, and products or new practices in populations—are often modeled as contagion processes that spread from node to node in a network,[25–27] in analogy with the spread of infectious diseases in a population.

In addition to modeling spreading processes themselves, it is important to consider the effect of network structure on contagions.[1,4,5,28] For example, network architecture can have a significant impact on phenomena such as the peak size and temporal development of outbreaks.[5,14,26,29–35]

In the study of contagions, many studies suppose that some small fraction of the nodes is infected initially, and they examine when a meme or disease can spread widely in a network.[4,31] When many nodes have adopted the meme (or become infected, in the context of a disease), it is said that a *cascade* has occurred.[11,23] A cascade can either be good or bad: a game developer may dream about his/her app becoming viral, but bank defaults due to systemic risk is a source

a)Electronic mail: jonas.juul@nbi.ku.dk
b)Electronic mail: mason@math.ucla.edu

of fear and dread in the financial sector. Seemingly viral spread of misinformation was also a prominent aspect of the 2016 U.S. presidential campaigns and election.

In applications ranging from finance[25] to meme spreading on Twitter,[36] researchers are very interested in trying to identify what causes cascading behavior on networks.[23] In one prominent family of models, known as *threshold models*, nodes survey their neighborhoods and adopt a meme (i.e., change their state) if sufficiently many of their neighboring nodes have already adopted this meme.[2,4,10,11,31] In most such models (and in most compartmental models), nodes are influenced only by their immediate neighbors, but in many situations (e.g., including social media such as Facebook and LinkedIn), individuals are able to observe actions by individuals beyond those to whom they are connected directly by an edge. [In fact, the sizes of the observable neighborhoods are different in different media (e.g., Facebook versus LinkedIn), and this can have profound effects on user experience, company algorithms, and more.[37]] In such situations, *synergistic* effects can occur, as a node can be influenced by multiple nodes at the same time, and the combined influence differs from the sum of the individual influences. Synergistic effects can either increase or decrease the chance that a node will adopt a meme. The aim of our paper is to construct an analytically tractable threshold model that incorporates synergistic effects into spreading processes on networks. We show that synergy has important effects on system dynamics, and we illustrate our model's spreading dynamics on several different networks.

Synergistic effects can contribute to the dynamics of spreading processes in a diverse variety of contexts. Examples include the spread of behavior,[38] the transmission of pathogens,[39] and the spread of new opportunities for farm activities among vineyards that form a wine route together.[40] Other phenomena with synergistic effects include the classical psychological "sidewalk experiment" with people staring up at the sky,[41] increased value from the merging of companies (see, e.g., Ref. 42), and "learning" of delinquent and criminal behavior.[43]

A few years ago, Pérez-Reche *et al.*[44] introduced a simple model of synergistic spreading by augmenting a compartmental model for a biological contagion, and they examined its dynamics on a square lattice in two dimensions. Their model was based on the standard susceptible–infectious–removed (SIR) model,[4,5] in which an *infectious* (I) node infects a *susceptible* (S) neighbor at a constant rate $r_{SI} = \alpha$. In this SIR model, an infectious node is infectious for a time τ before it switches states to *removed* (R) (or "recovered", if one is less fatalistic), and then it can never become susceptible or infectious again. Pérez-Reche *et al.* generalized this SIR model so that r_{SI} includes not only the parameter α but also a synergy term $r_{syn} = \beta m_i$, where m_i is the number of nodes that contribute to the synergy when updating node i. They used a linear form of synergy: $r_{SI} = \max\{\alpha + r_{syn}, 0\} = \max\{\alpha + \beta m_i, 0\}$. For $\beta < 0$, the synergy is *interfering*, as synergy decreases the chance that node i becomes infectious; for $\beta > 0$, the synergy is *constructive*, as synergy increases the chance that node i becomes infectious. For $\beta = 0$, the model in Ref. 44 reduces to the standard SIR model; there is no synergy.

Pérez-Reche *et al.* defined two types of synergistic dynamics: (1) *r-synergy*, in which $m_i + 1$ is the total number of infectious nearest neighbors that simultaneously attempt to infect a focal susceptible node i; and (2) *d-synergy*, in which m_i is the number of infectious nodes that are adjacent to the infectious nearest neighbor that is attempting to infect the susceptible node i. In their simulations, only the node at the center of the square grid is infectious at time $t = 0$; all other nodes start in the susceptible state. An important feature that Pérez-Reche *et al.* illustrated is that the value of the synergy parameter can affect whether an infectious host can infect more than one node.

Several papers have built on Ref. 44 and produced additional insights on synergistic spreading dynamics on networks.[45–48] To our knowledge, all previous studies considered update rules for node states that include stochasticity, and most of them examined spreading on lattices rather than on more general network structures. To facilitate analytical treatment of problems and to help isolate the effects of novel features in a model, it is often convenient to use deterministic update rules,[4] so we will do this in our exploration of synergistic effects. Specifically, we examine a two-state deterministic model in the form of a linear threshold model[2,10,11] in which a node can be either *active* or *inactive*. In the context of social contagions, "inactive" nodes are susceptible, and "active" nodes are infected. Upon becoming active, a node remains active forever. This facilitates analytical treatment, which we will use to shed light on synergistic spreading processes on networks. We focus on what Pérez-Reche *et al.*[44] called "r-synergy" (which includes only nearest-neighbor interactions), although our approach can be generalized for models with next-nearest-neighbor interactions (what Pérez-Reche *et al.* called "d-synergy"). It can also be generalized to incorporate interactions in even larger neighborhoods.

The rest of our paper is organized as follows. In Secs. II–IV, respectively, we introduce our models for synergistic spreading on networks, examine this model on two empirical networks, and develop an analytical approximation to describe the fraction of active nodes with degree k and threshold ϕ in a network as a function of time. We also demonstrate that we expect certain values of a synergy parameter in the models to lead to abrupt changes in the dynamics. In Sec. V, we study synergistic spreading processes on several families of random networks. In Secs. V A and V B, we simulate synergistic spreading on 3-regular and Erdős–Rényi (ER) random networks and compare our analytical approximation to the simulated spreading processes. In Sec. V C, we simulate synergistic spreading on networks that we construct using a configuration model with degree distributions from two empirical networks. We conclude in Sec. VI.

II. SYNERGISTIC THRESHOLD MODELS

Probably the most popular type of deterministic model of meme spreading is *threshold models* of social influence.[1,2,4,8,10–12,14] In the simplest type of threshold model, which is a generalization of bootstrap percolation,[49,50] one chooses a threshold ϕ_i for each node independently from a

probability distribution $f(\phi)$ at time $t=0$ (in traditional bootstrap percolation, all nodes have the same threshold), and a node becomes "active" (i.e., it adopts the meme) if the fraction of its neighbors (or, in some variants, the number of its neighbors) that are active is at least this threshold. In the so-called *Watts threshold model* (WTM),[11] one considers the fraction of active neighbors. An inactive node i with degree k, threshold ϕ_i, and number n_i of active neighbors becomes active when it is updated if and only if $n_i/k_i \geq \phi_i$. Because of the simplicity of basic threshold models, one can derive analytical approximations for cascade conditions in a variety of settings and in various extensions of the model.[12,31,34,51–53]

We seek to develop a synergistic threshold model. We focus on r-synergy and hence on nearest-neighbor interactions. (It is also worth thinking about models with d-synergy, but we leave this for future work.) We examine networks that consist of unweighted, undirected N-node graphs. At each point in time, a node can be in one of two states: *inactive* (S_0) or *active* (S_1). Inactive nodes exert no influence on their neighbors, and active nodes exert some amount of influence on their neighbors. The total amount of influence exerted by all neighbors of a node i gives the *peer pressure* experienced by node i. Each node i has a stubbornness threshold ϕ_i drawn from a distribution $f(\phi)$ at time $t=0$. We also activate a seed set of nodes at $t=0$. In all of our simulations, the seed consists of a single node chosen uniformly at random. Whenever we consider updating node i (which we do in discrete time with synchronous updating), it becomes active if and only if the peer pressure on it is at least ϕ_i.

We now construct a response function $F(n_i, k_i, \phi_i, \beta)$ that depends on the number n_i of node i's active neighbors, its degree k_i, its threshold ϕ_i, and a global synergy parameter β that we will explain below. The response function, a non-decreasing function of n_i, encodes when a node switches from the inactive state to the active one.[32] One can use such a response function to describe numerous models of binary-state dynamics, such as bond and site percolation and the WTM.[31] We express the response function using a peer-pressure function $\Xi(n_i, \beta)$ by writing

$$F(n_i, k_i, \phi_i, \beta) = \begin{cases} 0\,, & \text{if} \quad \Xi(n_i, \beta) < \phi_i k_i\,, \\ 1\,, & \text{otherwise}\,. \end{cases} \tag{1}$$

We want to incorporate synergistic effects into $\Xi(n_i, \beta)$. With inspiration from Pérez-Reche *et al.*,[44] we require that

$$\Xi(n_i, \beta) \begin{cases} = 0\,, & \text{if} \quad n_i = 0\,, \\ > n_i\,, & \text{if} \quad \beta > 0 \quad \text{and} \quad n_i \geq 2\,, \\ = n_i\,, & \text{if} \quad \beta = 0 \quad \text{or} \quad n_i = 1\,, \\ < n_i\,, & \text{if} \quad \beta < 0 \quad \text{and} \quad n_i \geq 2\,. \end{cases} \tag{2}$$

The first line of (2) encodes the requirement that the peer pressure experienced by a node is 0 if it does not have any active neighbors. From the second line, we see that for a positive synergy parameter $\beta > 0$ with $n_i \geq 2$ active neighbors, the peer pressure experience by node i is larger than that in the WTM. This, therefore, amounts to a "constructive synergy." The third line encodes the fact that our synergistic model reduces to the WTM either when the synergy parameter $\beta = 0$ or when the number of active neighbors is $n_i = 1$. (Similarly, the synergistic SIR model of Pérez-Reche *et al.*[44] reduces to the standard SIR model for $\beta = 0$.) From the last line, we see that for a negative synergy parameter $\beta < 0$ and $n_i \geq 2$ active neighbors, the peer pressure experienced by node i is smaller than that in the WTM. This, therefore, amounts to "interfering synergy."

We consider the following two peer-pressure functions that satisfy these requirements:

$$\Xi_{\text{multiplicative}} = (1+\beta)^{n_i - 1} n_i\,, \tag{3}$$

$$\Xi_{\text{power}} = n_i^{1+\beta}\,. \tag{4}$$

Naturally, these are not the only two functions that satisfy the requirements in Eq. (2). Additionally, in Sec. V A, we will argue that any synergistic peer-pressure function that is non-decreasing and continuous in the synergy parameter β exhibits the same qualitative behavior as these two functions, in the sense of experiencing the same types of bifurcations.

If a node is *vulnerable* (i.e., it can be activated by a single active neighbor), it remains vulnerable if one introduces synergy using Eq. (3) or Eq. (4). Moreover, no non-vulnerable node can become vulnerable as a result of the synergy introduced using Eq. (3) or Eq. (4). We seek to examine when synergy effects, as encapsulated by the parameter β, change the number of active neighbors that can activate a degree-k node. That is, we seek to examine when synergy can assist or hinder the spread of a meme through a network. Let us calculate when a specific change like this occurs. Suppose that a node i with degree k_i can be activated when there are at least m_i active neighbors for $\beta = 0$. We wish to determine the values of β for which l_i active neighbors are sufficient to activate node i. For the power synergy model (4), we calculate

$$(l_i)^{1+\beta} \geq \phi_i k_i, \tag{5}$$

$$\Rightarrow \beta \geq \frac{\ln(\phi_i k_i)}{\ln(l_i)} - 1\,. \tag{6}$$

For the multiplicative synergy model (3), we obtain

$$\beta \geq \left(\frac{\phi_i k_i}{l_i}\right)^{1/(l_i - 1)}\,. \tag{7}$$

More generally, except for $m_i = 1$ or $l_i = 1$ (by construction, nodes cannot become vulnerable or stop being vulnerable due to synergistic effects), we can solve for the value at which any $l_i \in \mathbb{N}$ active neighbors can activate a node with degree k_i and threshold ϕ_i, given the synergy parameter β. We thereby examine how synergy alters the difficulty of activating nodes.

When we initiate our simulations with only a single node as a seed, there is a risk that this seed is surrounded—or is part of a small number of vulnerable nodes that are surrounded—by non-vulnerable nodes. Because such situations arise from the choice of threshold distribution $f(\phi)$ rather than from synergistic effects, we discard such simulations throughout this paper.

III. SYNERGY IN TWO EMPIRICAL NETWORKS

We start by examining the synergistic threshold model with power synergy (4) on the network of condensed-matter physics paper coauthorships from Ref. 54. (This network is available at https://snap.stanford.edu/data/.) In this network, a node represents an author, and there is an undirected edge between nodes i and j if the authors coauthored at least 1 paper. We suppose for simplicity that all nodes have a threshold of $\phi = 1/10$.

We show the results of our simulations in Fig. 1. We use power synergy (4), and we show results for interfering synergy (with $\beta = -0.80$) in panel (a) and constructive synergy (with $\beta = 0.15$) in panel (b). Data points correspond to the mean fraction of degree-k nodes that are active at each time step. Among our simulations, we include only realizations in which the meme activates at least 0.5% of the nodes in the network. For each degree, a smaller or equal fraction of nodes is activated for interfering synergy than for constructive synergy. In panel (b), we show the $k = 2$ curve from panel (a) for comparison. We see that it takes longer for the meme to spread in the network for interfering synergy than for constructive synergy.

We now examine our synergistic threshold model on another empirical network, the NORTHWESTERN25 network from the FACEBOOK100 data set.[55] This data set consists of the complete set of people and friendships of 100 different U.S. universities from one day in autumn 2005. NORTHWESTERN25 is the data for Northwestern University. We show results of our numerical simulations on the largest connected component of this network in Fig. 2. We suppose that all nodes have a threshold of $\phi = 1/33$, and we again examine power synergy with interfering synergy (with $\beta = -0.80$) in panel (a) and constructive synergy (with $\beta = 0.15$) in panel (b). For

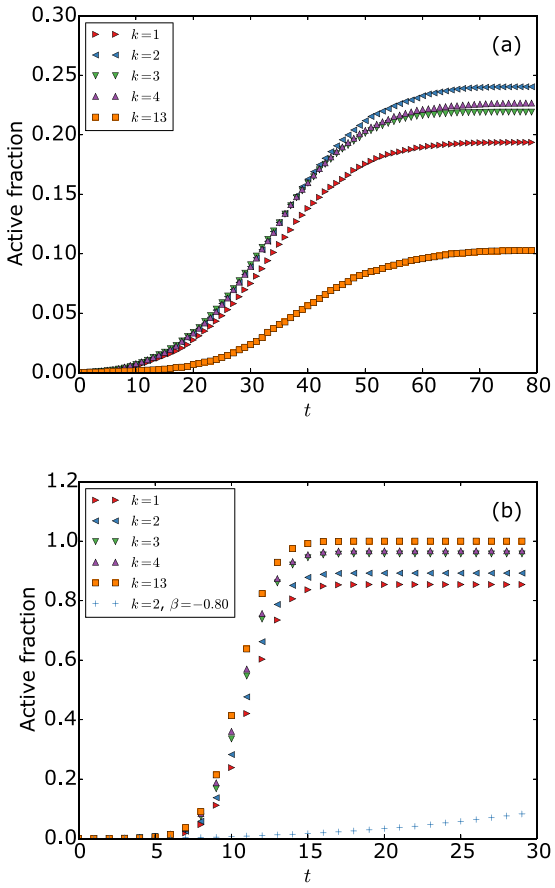

FIG. 1. Example behavior of the synergistic threshold model with power synergy (4) using (a) interfering synergy (with $\beta = -0.80$) and (b) constructive synergy (with $\beta = 0.15$). In panel (b), we show part of the curve for $k = 2$ from the case of interfering synergy for comparison. Because we choose the seed active node uniformly at random, there is a chance that only the seed is activated, and we do not take such runs into consideration. For the interfering synergy plot, only the seed was activated in 94 of our 110 runs; for constructive synergy, this occurred in 31 of 110 runs. For the simulations in this figure, we run the synergistic threshold model on the condensed-matter physics coauthor network from Ref. 54, and the threshold for each node is $\phi = 1/10$. For each degree, a smaller or equal fraction of nodes becomes active for interfering synergy than for constructive synergy. It also takes longer for the meme to spread in the network for interfering synergy than it does for constructive synergy.

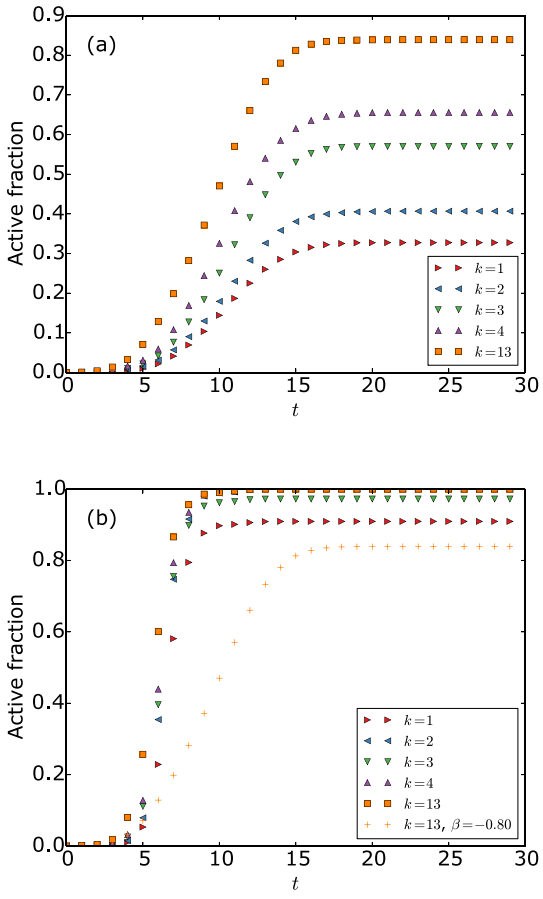

FIG. 2. Example behavior of the synergistic threshold model with power synergy (4) using (a) interfering synergy (with $\beta = -0.80$) and (b) constructive synergy (with $\beta = 0.15$). In panel (b), we show the curve for $k = 13$ for the case of interfering synergy for comparison. Because we choose the seed active node uniformly at random, there is a chance that only the seed is activated, and we do not take such runs into consideration. For the interfering synergy plot, only the seed was activated in 30 of 110 runs; for constructive synergy, this occurred in 24 of 110 runs. For the simulations in this figure, we run the synergistic threshold model on the NORTHWESTERN25 network from the FACEBOOK100 data set,[55] and the threshold for each node is $\phi = 1/33$. For each degree, a smaller or equal fraction of nodes becomes active for interfering synergy than for constructive synergy. It also takes longer for the meme to spread in the network for interfering synergy than it does for constructive synergy.

comparison, we include the curve for degree $k = 13$ for constructive synergy among our plots for interfering synergy. We again see that it takes longer for the meme to spread in the network for interfering synergy than it does for constructive synergy and that, for each degree, a smaller or equal fraction of nodes is activated for interfering synergy than for constructive synergy.

IV. ANALYTICAL APPROXIMATION OF THE NUMBER OF ACTIVE NODES VERSUS TIME

We now develop an analytical approximation that describes the fraction of active nodes in a network as a function of time, given a peer-pressure function, degree distribution, and threshold distribution. This approximation is a heterogeneous mean-field approximation,[56] and it assumes that neighbors of a node are independent of each other. In our derivation, we assume that networks are locally tree-like,[4,57] which treats such pairs of neighbors as independent (because, in the approximation, they are not adjacent to each other).

Recall that we employ synchronous updating in our simulations. Because our update rule is deterministic, synchronous updating and asynchronous updating yield the same final (i.e., steady state) fraction of active nodes.[58] At time $t = 0$, we activate one seed node of the N total nodes. For our theoretical analysis, this entails that the expected initially active fraction of nodes with degree k and threshold ϕ is $\psi_k^\phi = 1/N$ for all choices of k and ϕ.[59] See Refs. 32 and 60 for a discussion of the effects on cascade size of using a single active node (as opposed to a specified fraction of active nodes) as a seed for the WTM, and see Ref. 61 for a recent discussion of issues regarding synchronous versus asynchronous updating (where asynchronous updating, such as through a Gillespie algorithm, is meant to model continuous-time dynamics) for dynamical processes on networks.

To calculate the fraction $\rho_k^\phi(n+1)$ of active nodes with degree k and threshold ϕ at time $n+1$, we write the recursive formula (as in, e.g., Refs. 32, 34, and 60)

$$\rho_k^\phi(n+1) = \psi_k^\phi + (1-\psi_k^\phi)\sum_{j=0}^{k} B_j^k(\bar{q}_k{}^\phi(n))F(j,k,\phi,\beta)\,, \tag{8}$$

where $\bar{q}_k^\phi(n)$ is the probability that a neighbor (chosen uniformly at random) of a uniformly-randomly chosen inactive node with degree k and threshold ϕ is active at time n, and

$$B_j^k(p) = \binom{k}{j} p^j (1-p)^{k-j}\,. \tag{9}$$

The first term in Eq. (8) is the fraction of nodes that are active at time $t = 0$. The second term represents the nodes that are activated at a later time. The factor $1 - \psi_k^\phi$ is present because these nodes are not part of the seed, the sum encompasses the probabilities that a degree-k node can have $0, 1, \ldots, k$ active neighbors at time n, and the response function $F(j, k, \phi, \beta)$ encodes when an inactive node becomes active when its state is updated. The sum of the two terms in Eq. (8) gives the fraction of nodes with degree k and threshold ϕ that are active at time $n+1$. We write $\bar{q}_k^\phi(n)$ as a function of $q_{k'}^{\phi'}(n)$, the probability that, for a given inactive node, a neighbor with degree k' and threshold ϕ' is active at time n. This probability is

$$\bar{q}_k^\phi(n) = \frac{\sum_{k',\phi'} P\big((k,\phi),(k',\phi')\big) q_{k'}^{\phi'}(n)}{\sum_{k',\phi'} P\big((k,\phi),(k',\phi')\big)}\,, \tag{10}$$

where $P((k,\phi),(k',\phi'))$ is the probability that a node with degree k and threshold ϕ is adjacent to a node with degree k' and threshold ϕ'. For an inactive node, the probability that a neighboring node with degree k and threshold ϕ is active is

$$q_k^\phi(n+1) = \psi_k^\phi + (1-\psi_k^\phi)\sum_{j=0}^{k-1} B_j^{k-1}(\bar{q}_k{}^\phi(n))F(j,k,\phi,\beta)\,. \tag{11}$$

The only difference between Eq. (11) and Eq. (8) stems from the fact that the degree-k neighbor that we consider in (11) has a maximum of $k-1$ active neighbors if it is adjacent to at least one inactive node. In these equations, we have assumed that each neighbor of node i is independent of the others, because (as indicated above) we are assuming that the network is locally tree-like.[4,57] We also assume that all nodes with degree k and threshold ϕ have the same dynamics, so our approach constitutes a heterogeneous mean-field approximation.[56]

V. SYNERGY IN SYNTHETIC NETWORKS

To illustrate our theoretical results, we examine synergistic spreading in several families of random graphs. For each family of networks, we draw a new network from the ensemble (which is a probability distribution on graphs) for each simulation of a synergistic threshold model. For all networks except Erdős–Rényi (ER) networks, we specify a degree distribution $p(k)$. We use this to determine a degree for each of 10 000 nodes, and we then connect these nodes to each other using a configuration model (connecting ends of edges to each other uniformly at random).[62]

A. Synergy in 3-regular configuration-model networks

We first examine 3-regular random networks, in which every node has degree 3, which we construct by matching stubs (i.e., ends of edges) uniformly at random. We study how synergy affects meme spreading on these networks by examining several values of the parameter β for both multiplicative and power synergy. In our numerical simulations, we suppose that a fraction $p_0 = 0.8$ of the nodes have threshold $\phi = 0.32 < 1/3$ and that a fraction $1 - p_0 = 0.2$ of the nodes have threshold $\phi = 1$. Although our numerical simulations illustrate a rather specific scenario, having only two types of nodes facilitates a detailed investigation of the fraction of active nodes of each type as a function of β and time. Our particular choice of p_0 ensures that there is a large fraction of vulnerable nodes, but it is otherwise arbitrary. It is also worthwhile to do numerical explorations for a wide

variety of threshold distributions, but we leave those for future work.

We choose a single node uniformly at random as a seed and update nodes synchronously at each discrete time step. We stop the simulations when we reach steady state (i.e., when no more nodes can eventually activate). In Fig. 3, we consider multiplicative synergy and plot the steady-state active fractions of high-threshold and low-threshold nodes as a function of the synergy parameter β. Each data point is a mean over 10 realizations of the spreading process. For each realization, we create a new 3-regular configuration-model network.

When β surpasses the values 0 and 0.5, the final fraction of active nodes with threshold $\phi = 1$ increases dramatically. We can see this from Eqs. (7) and (1). For $\beta < 0$, it is not possible to satisfy $\phi_i k_i \geq (1+\beta)^{n_i-1} n_i$, because $n_i \leq k_i$. For $\beta \in [0, 0.5)$, the relation $\phi_i k_i \geq (1+\beta)^{n_i-1} n_i$ holds only for $n_i = k_i$. In this case, nodes with $\phi = 1$ can be activated, but they are never able to help activate a neighbor (unless they are part of the seed set of active nodes), as all of their neighbors are necessarily already active once they have been activated. For $\beta \geq 0.5$, the relation $\phi_i k_i \geq (1+\beta)^{n_i-1} n_i$ holds for $n_i = k_i$ and $n_i = k_i - 1$. In this case, nodes with $\phi = 1$ can be activated even when they still have an inactive neighbor. Hence, nodes with $\phi = 1$ can help spread the meme, resulting in more active nodes with both $\phi = 1$ and $\phi = 0.32$ than what occurs for $\beta < 0.5$. Rephrasing these observations, bifurcations occur at special values of β (which are $\beta = 0$ and $\beta = 0.5$ in this example) for the multiplicative peer-pressure function (3), and we calculate the bifurcation points by solving $\Xi(n_i, \beta) = k_i \phi_i$ for $n_i \in \{2, \ldots, k_i\}$ (where we exclude $n_i = 1$ because it corresponds to a vulnerable node, which by design, is vulnerable for any value of β). Such values of β exist for any non-decreasing peer-pressure function $\Xi(n_i, \beta)$ that is continuous in β. For different peer-pressure functions, the value of β that makes it possible for a specific number of active neighbors to activate a specific node can differ, but there is some value of β for each function. Hence, in this sense, all continuous, non-decreasing synergistic peer-pressure functions behave in qualitatively the same way. By contrast, the peer-pressure function $\Xi = n_i^{1+|\beta|}$ is not non-decreasing. This function is similar to Ξ_{power}, but with $\beta \to |\beta|$. For this peer-pressure function, we do not obtain the leftmost step that we observe in Fig. 3, so this choice entails different qualitative behavior than what we observe with Ξ_{power}.

In Figs. 4(a) and 4(b), we show how the meme spreads for $\beta = 0.4999$ and $\beta = 0.5001$, respectively. Each data point is a mean over 100 realizations of the spreading process. For each realization, we create a new 3-regular configuration-model network.

For any response function, such as ones that use the peer-pressure functions (3) or (4), one can compute when $n_i \leq k_i$ nodes can activate a node with threshold ϕ_i by solving the equation $\Xi(n_i, \beta) = \phi_i k_i$. Therefore, different response

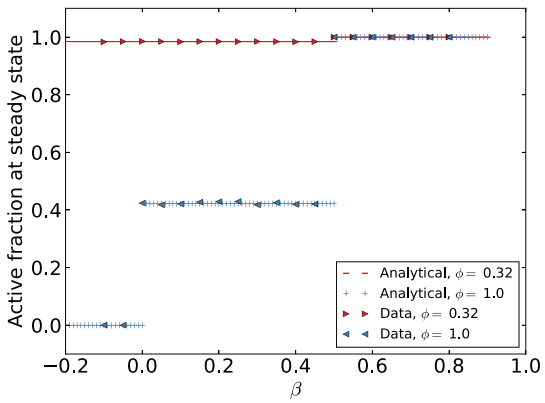

FIG. 3. Steady-state fraction of active nodes in 3-regular random networks of 10 000 nodes for our synergistic threshold model with the multiplicative synergistic peer-pressure function (3). A fraction $p_0 = 0.8$ of the nodes have threshold $\phi = 0.32 < 1/3$, and a fraction $1 - p_0 = 0.2$ of the nodes have threshold $\phi = 1$. Each data point is a mean of 10 realizations of the synergistic threshold model on 10 different 3-regular random networks, which we create using a configuration model. For each value of β, we construct 10 networks. (In doing these simulations, we discarded two total realizations due to the choice of seed node; the contagion did not spread enough in those cases.).

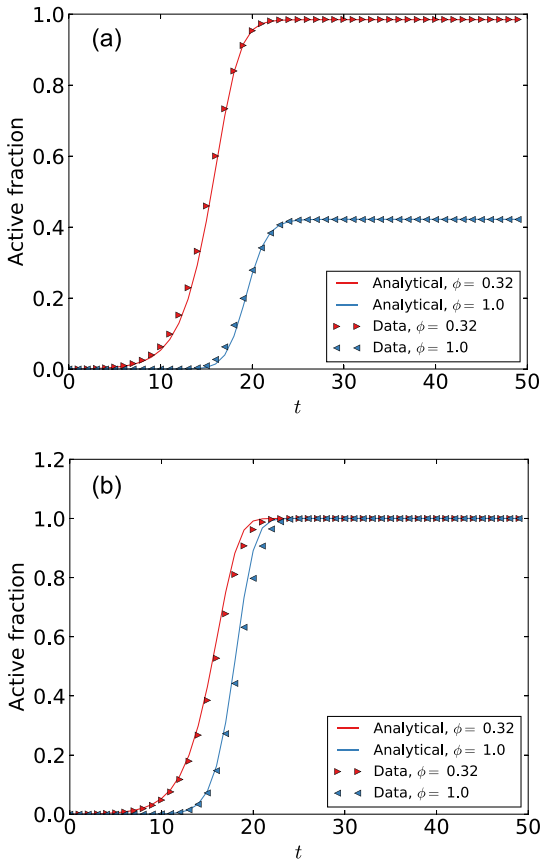

FIG. 4. Active fraction of nodes as a function of time for our synergistic threshold model with peer-pressure function (3) with constructive synergy in 3-regular random networks of 10 000 nodes. A fraction $p_0 = 0.8$ of the nodes have threshold $\phi = 0.32 < 1/3$, and a fraction $1 - p_0 = 0.2$ have threshold $\phi = 1$. In panel (a), the synergy parameter is $\beta = 0.4999$; in panel (b), it is $\beta = 0.5001$. In each panel, each data point is a mean over 100 realizations of the threshold model. We observe good agreement between the analytical approximation (8) and our simulations. (In these simulations, we did not need to discard any realizations due to the choice of seed node.) For each realization, we create a 3-regular random network using a configuration model. The sets of 100 networks are different in the two panels.

functions can have sudden increases in the steady-state fraction of active nodes at critical values of β for the same reason: at these values of β, it becomes possible for some nodes to be activated with fewer active neighbors than is the case for smaller values of β. Although these critical values of β can differ for different response functions, our two synergistic response functions exhibit qualitatively similar behavior, so we henceforth use only the response function that is specified by the power peer-pressure function (4).

B. Synergy in Erdős–Rényi networks

We now simulate the spread of memes with power synergy (i.e., using the peer-pressure function (4)) on ER networks. Specifically, we use $\mathcal{G}(N,p)$ networks, where N is the number of nodes and p is the probability that there is an edge between a pair of nodes. The expected mean degree of such an ER network is $z = p(N-1) \approx pN$. First, we consider ER networks with expected mean degree $z = 3$, and we then consider ER networks with expected mean degree $z = 8$. In both cases, all nodes are assigned the same threshold $\phi = 1/7$. In our simulations, we use $N = 10\,000$. These networks do not in general consist of a single component, and this is especially relevant for $z = 3$. However, components other than the largest connected component (LCC) are so small that if the seed node is part of one of these small components, the total number of activated nodes is so small that such a simulation is one that we discard. We also confirm with computations that the LCC is very large even for $z = 3$. For example, in one set of 100 realizations of ER networks with $N = 10\,000$ nodes and expected mean degree $z = 3$, the mean size of the LCC is 9409.61 ± 4.99 nodes, and the mean size of the second-largest component is 4.07 ± 0.95 nodes.

1. Expected Mean Degree z = 3

We use our analytical approximation (8) to find the expected steady-state active fraction of nodes as a function of their degree and the synergy parameter β for the response function with power peer-pressure function (4). We plot these quantities in Fig. 5. In Fig. 6, we plot the time series of the fraction of active nodes when the synergy parameter is $\beta = -0.93$, for which our model predicts different steady-state active fractions for nodes with degrees 1, 2, 3, and 8. We observe very good agreement between our simulations and the analytical approximation (8) for these four node degrees.

2. Expected Mean Degree z = 8

We now examine ER networks with expected mean degree $z = 8$. We simulate synergistic spreading with the power peer-pressure function (4) with a parameter value of $\beta = -0.835$. We choose this value of β so that the steady-state fraction of active nodes is different for nodes with different degrees. In Fig. 7, we show the fraction of active nodes as a function of time, and we observe good agreement between our computations and our analytical approximation (8).

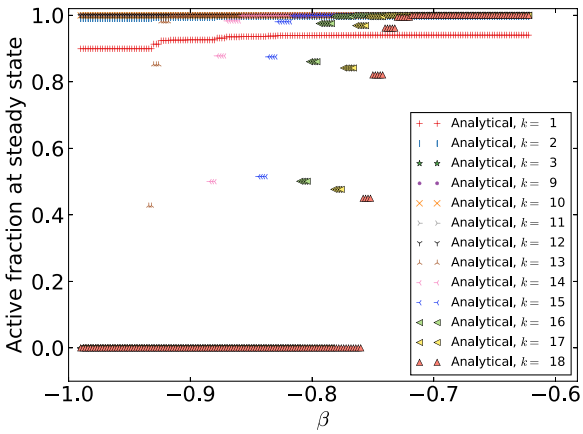

FIG. 5. Steady-state active fraction of degree-k nodes as a function of the synergy parameter β for a meme that spreads on ER networks with expected mean degree $z = 3$, homogeneous threshold $\phi = 1/7$, and a response function with the power peer-pressure function (4). Using Eq. (6), our analytical approximation (8) gives abrupt jumps that agree well with our numerical calculations (see Fig. 6).

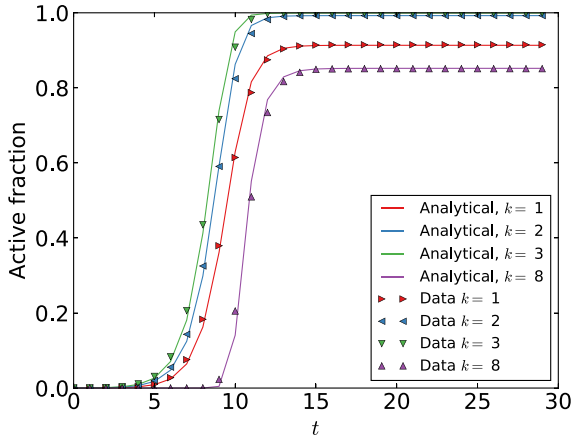

FIG. 6. Active fraction of nodes of degrees 1, 2, 3, and 8 as a function of time for synergistic spreading with the power peer-pressure function (4) in ER networks with interfing synergy $\beta = -0.93$, expected mean degree $z = 3$, and homogeneous threshold $\phi = 1/7$. Each data point is a mean over 31 realizations of the spreading process. Our analytical approximation (8) of the temporal activation of nodes of degrees 1, 2, 3, and 8 agrees very well with the results of our simulations. We obtain good matches for all node degrees that we examined in this way. We construct a new random ER network for each realization. (In doing these simulations, we discarded nine realizations due to the choice of seed node; the contagion did not spread enough in those cases.).

C. Synergy on networks with degree distributions from empirical data

We now simulate the spread of synergistic memes on two networks with degree distributions from empirical data. In Sec. V C 1, we consider random networks created using a configuration model with a degree distribution determined by the degree sequence of the network of coauthorships in condensed-matter physics papers[54] that we examined in Sec. III. This network has a mean degree of $z \approx 8$. In Sec. V C 2, we simulate the spread of synergistic memes on configuration-model networks with a degree distribution from the degree sequence of the NORTHWESTERN25 network

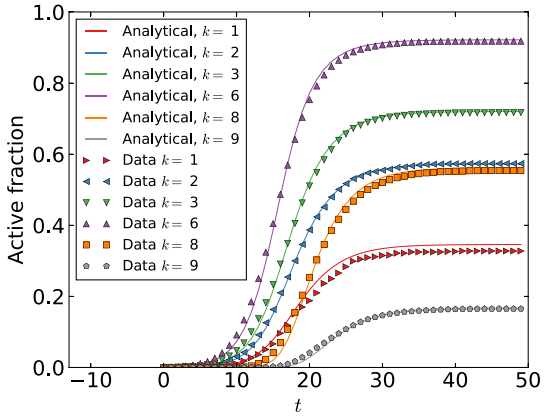

FIG. 7. Fraction of active degree-k nodes as a function of time for our synergistic threshold model with power peer-pressure function (4) and interfering synergy $\beta = -0.835$ for ER networks with expected mean degree $z = 8$. Each node has a threshold of $\phi = 1/7$. We average our numerical computations over 31 realizations of the dynamics. We observe a good match between our numerical computations and our analytical approximation, although there is a slight discrepancy for nodes with $k = 1$. (In doing these simulations, we discarded nine realizations due to the choice of seed node; the contagion did not spread enough in those cases.).

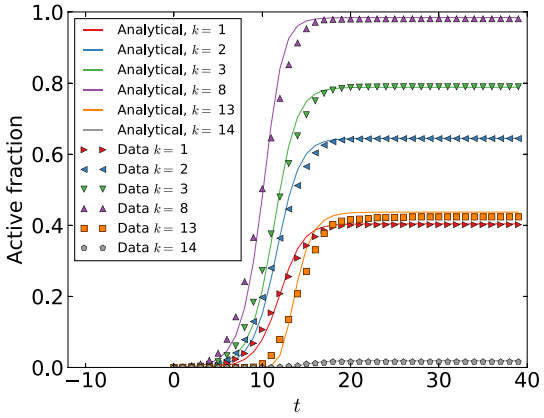

FIG. 8. Fraction of active nodes with degrees 1, 2, 3, 8, 13, and 14 as a function of time for our synergistic threshold model with power peer-pressure function (4) and interfering synergy $\beta = -0.85$ in configuration-model networks with a degree distribution determined from the degree sequence of the condensed-matter theory collaboration network from Ref. 54. Each node has a threshold of $\phi = 1/10$. We average the results over nine realizations of the dynamics, and we create a new configuration-model network for each realization. We observe good agreement between our analytical approximation and our numerical simulations. (In doing these simulations, we discarded one realization due to the choice of seed node; the contagion did not spread enough in that case.).

from the FACEBOOK100 data set.[55,63] This Facebook network has a mean degree of $z \approx 92$. For each realization, we create a new 10 000-node network using a configuration model and degree sequences drawn from the associated degree distribution.

1. Condensed-matter physics collaboration network

We draw the degree of each of the 10 000 nodes from the degree distribution of the condensed-matter physics collaboration network,[54] and we place edges using a configuration model. In Fig. 8, we plot the fraction of active nodes of degree k as a function of time. We average over nine simulations (we discarded one simulation because there was insufficient spreading from the seed node) of the spreading of a meme with the power synergy peer-pressure function (4) on these networks. For each of these realizations, we create a new random network using a configuration model.

As in Sec. III, we use the peer-pressure function (4) and a homogeneous threshold $\phi = 1/10$ for our simulations. We first consider interfering synergy with $\beta = -0.85$, which makes it impossible to activate any node whose degree is 16 or larger. Our analytical approximation gives good agreement with our numerical simulations. In Fig. 9, we examine the effect of constructive synergy with the peer-pressure function (4). In this case, we use $\beta = 0.20$ and $\phi = 1/7$. For all node degrees that we checked, the steady-state active fractions from our analytical predictions and numerical simulations are indistinguishable. However, in our analytical approximation, the active fraction increases earlier than what we observe in our simulations.

2. A Facebook network

We simulate the spread of synergistic memes on configuration-model networks that we construct using the degree sequence of the NORTHWESTERN25 network from the

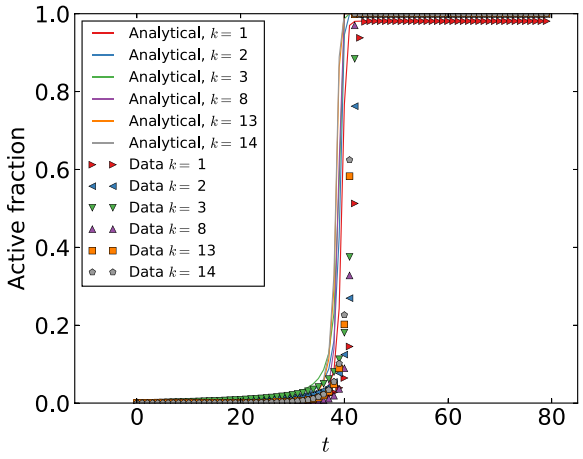

FIG. 9. Fraction of active nodes with degrees 1, 2, 3, 8, 13, and 14 as a function of time for our synergistic threshold model with power peer-pressure function (4) and constructive synergy $\beta = 0.20$ in configuration-model networks with a degree distribution determined from the degree sequence of the condensed-matter theory collaboration network from Ref. 54. Each node has a threshold of $\phi = 1/7$. We average the results over 10 realizations of the dynamics, and we create a new configuration-model network for each realization. In our analytical approximation, the fraction of active nodes increases slightly earlier than what we observe in our numerical simulations, but the resulting steady-state fractions of active nodes are visually indistinguishable. (In these simulations, we did not need to discard any realizations due to the choice of seed node.).

FACEBOOK100 data set.[55] The network has a mean degree of $z \approx 92$, a minimum degree of $d = 1$, and a maximum degree of $d = 2105$. We assign all nodes a degree from a degree distribution based on the degree sequence of the NORTHWESTERN25 network, and we again create edges using a configuration model. We suppose that each node has a

threshold of $\phi = 1/33$. In Fig. 10, we plot the fraction of active degree-k nodes as a function of time. As in our other simulations, each realization is a different draw of one of these configuration-model networks. We show results for both interfering synergy (with power peer-pressure function (4) and $\beta = -0.05$) and constructive synergy (with $\beta = 0.15$ and peer-pressure function (4)). For this family of networks, our analytical approximation departs from our numerical simulations for both the steady-state fractions of active nodes and the times at which the active fractions of degree-k nodes saturate. Additionally, our analytical approximation suggests that interfering synergy slows down the spreading process much more than is actually the case in our simulations.

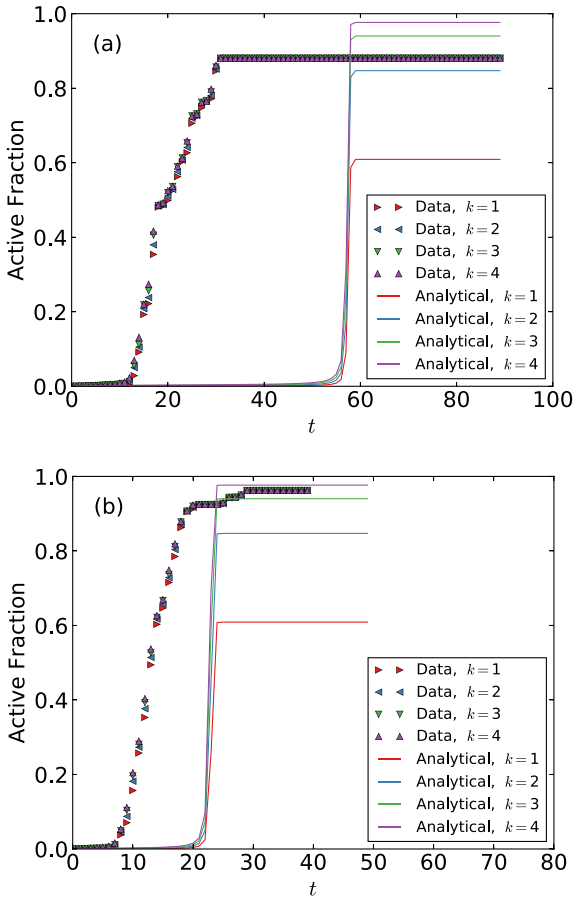

FIG. 10. Simulations of synergistic spreading on 10 000-node networks with a degree distribution determined from the degree sequence of the NORTHWESTERN25 network from the FACEBOOK100 data set.[55] The nodes have a homogeneous threshold of $\phi = 1/33$. (a) We examine interfering synergy (with power synergy (4) and $\beta = -0.05$) and plot the fraction of active nodes with degrees 1, 2, 3, and 4 as a function of time. All nodes with degree $k \geq 5$ exhibit similar behavior to those with the plotted degrees, and the final fractions of activated nodes are between 0.79 and 0.88. The time until the cascade occurs is very different in our analytical approximation (8) and numerical simulations, and there are also discrepancies in the steady-state fraction of active nodes between our analytics and numerics. We average our results over 51 realizations. (In doing these simulations, we discarded 149 realizations due to the choice of seed node; the contagion did not spread enough in those cases.) (b) We examine constructive synergy (with power synergy (4) and $\beta = 0.15$) and plot the fraction of active nodes with degrees 1, 2, 3, and 4 as a function of time. All nodes with degree $k \geq 5$ eventually have fractions of active nodes that are larger than 0.92. For this case as well, the time until the cascade occurs is very different in our analytical approximation (8) and our numerical simulations, and there are also discrepancies in the steady-state fraction of active nodes between our analytics and numerics. We average our results over 53 realizations. (In doing these simulations, we discarded 147 realizations due to the choice of seed node; the contagion did not spread enough in those cases.).

Our analytical approximation assumes that we are considering dynamics on a locally tree-like network, although such methodology can yield results that produce "unreasonably" effective matches between theory and computations (e.g., of the locations of phase transitions) even in many situations in which the hypotheses used to derive the theoretical approximations do not hold.[57] Melnik *et al*.[57] discussed various reasons why a tree-based theory may not provide a good description of the actual dynamics on a network (for a given dynamical system, such as a particular type of spreading process). For the FACEBOOK100 networks, they found for several spreading processes (including the WTM) that simulations with a homogeneous threshold distribution yield different results than what one obtains from a tree-based theory. (In our work, we usually use a homogenous threshold.) In contrast, they found for a Gaussian distribution of thresholds that WTM simulations with a seed consisting of all nodes with $\phi < 0$ yields results that are well-described by their tree-based approximation. In Ref. 57, all nodes with $\phi < 0$ were active at the beginning of simulations, because nodes with $\phi < 0$ are activated by any nonnegative fraction of active neighbors.[60] In our case, however, when using this threshold distribution, we obtain different results in simulations versus analytical approximations of cascades.

Two properties that may provide some indication of the effectiveness of tree-based theories for studying dynamical processes on a network are the mean geodesic (i.e., shortest) path length between nodes and the mean local clustering coefficient of the network. Although this is not something that is required mathematically (as there are counterexamples, such as a star graph), we expect that a "typical" tree-like network—in the extreme case, consider an ensemble of networks drawn uniformly at random from the set of all trees with a given number of nodes—to have larger mean geodesic path lengths than networks of the same size that are not tree-like. One also expects a locally-tree-like network to have a smaller mean local clustering coefficient than a network with the same number of nodes that is not locally tree-like. Averaging the mean geodesic path length between nodes in a set of 10 randomizations (based on a configuration model, as described above) of the NORTHWESTERN25 network yields 2.510 ± 0.007, which is somewhat smaller than in the original network and is much smaller than any other random network in our study (see Table I). Averaging the local clustering coefficient for the same 10 networks yields 0.02828 ± 0.00109, which is reasonably small but is much larger than for any other random network that we examine in this paper. This suggests that the randomized NORTHWESTERN25 networks are less tree-like than our other random networks. Additionally, the mean local clustering coefficient and the mean geodesic path length in the original NORTHWESTERN25 and condensed-matter collaboration networks are larger than those of the randomized networks that we construct from those networks. Unsurprisingly,

TABLE I. Mean geodesic path length between nodes and mean local clustering coefficient in the four random-network families that we examine. We construct the 3-regular random graphs using a configuration model (with stubs connected uniformly at random), and we also construct configuration-model networks using degree sequences (with associated degree distributions) from the condensed-matter collaboration network and NORTHWESTERN25 Facebook network. In each case, we average our results over 10 networks, and we indicate the mean values and the standard deviations of those means. We also indicate the values for the original NORTHWESTERN25 and condensed-matter collaboration networks. Observe that the mean geodesic path length between nodes is noticeably smaller in the NORTHWESTERN25 networks than in the other networks. Among the random networks, the mean local clustering coefficient is by far the largest in the NORTHWESTERN25 network, although the random network constructed from the condensed-matter collaboration network also has a much larger mean local clustering coefficient than the ER networks and 3-regular networks. The values of the mean geodesic path length and mean local clustering coefficients in the corresponding original empirical networks are larger (considerably so, for the clustering coeffecients) than those in the configuration-model networks with degrees drawn from the associated degree distributions.

Network	Mean geodesic path length	Mean local clustering coefficient
3-regular configuration model	6.359 ± 0.001	0.00033 ± 0.00011
Erdős–Rényi, $z = 3$	8.366 ± 0.043	0.00020 ± 0.00014
Erdős–Rényi, $z = 8$	4.664 ± 0.009	0.00079 ± 0.00008
Condensed-matter collaborations (original network)	5.352	0.64173
Condensed-matter collaborations (random networks)	4.091 ± 0.024	0.00471 ± 0.00049
NORTHWESTERN25 (original network)	2.723	0.23828
NORTHWESTERN25 (random networks)	2.509 ± 0.007	0.02828 ± 0.00109

randomization considerably decreases the value of the mean local clustering coefficients, especially for the condensed-matter collaboration network.

VI. CONCLUSIONS

It is important to study when diseases, information, memes, or other things (e.g., misinformation or "alternative facts") spread to a large number of nodes in a network.[4,15] For example, prior studies have suggested that some organisms and tumors spread via synergistic effects[64,65] and that synergistic effects can also be important for the spread of information on networks,[35] the spread of behavior in online social networks,[38] the transmission of pathogens,[39] and the spread of opportunities among vineyards on wine routes.[40]

In the present paper, we developed a deterministic threshold model with synergistic spreading, and we illustrated that constructive synergy speeds up the spreading process and that interfering synergy slows down the spreading process. Using both computations and a heterogeneous mean-field approximation (which assumes that a network is locally tree-like), we investigated the fraction of nodes, resolved by degree and as a function of a synergy parameter, that are activated for two empirical networks and several families of random graphs. We illustrated that the synergy functions (3) and (4) lead to critical values of a synergy parameter β, and we showed that such values also arise for any peer-pressure function that is continuous and non-decreasing in β. We found for non-vulnerable nodes with a specified degree k that there exist $k - 1$ critical synergy parameter values that indicate when a node is activated by at least $m \in \{2, 3, \ldots, k\}$ active neighbors. In all cases, we observed that constructive synergy speeds up the spreading process and that interfering synergy slows down the spreading process.

Investigating the influence of synergistic effects on spreading processes on networks is a promising area of study. It is an important feature to consider when studying the spread of information (and misinformation) on social networks,[35] the dynamics of certain biological organisms, and social processes in which the propensity for state changes either saturates or increases with the number of individuals who are trying to influence others in a network. It has interesting effects on spreading behavior in various types of networks, such as lattices[35] and modular networks,[47] and it can affect whether or not it is possible for certain nodes to adopt a certain meme or behavior.

In the future, it will be interesting to consider synergistic spreading processes—with both deterministic and stochastic update rules—on other types of networks, such as multilayer networks,[66–68] temporal networks,[69] and adaptive networks.[70]

ACKNOWLEDGMENTS

Part of this research was carried out at the Mathematical Institute at University of Oxford. We thank James Fowler, James Gleeson, Matthew Jackson, Mikko Kivelä, James Moody, and four anonymous referees for helpful comments. J.S.J. also thanks the Mathematical Institute for their hospitality. J.S.J. received funding through the University of Copenhagen, UCPH 2016 Excellence Programme for Interdisciplinary Research.

[1] *Spreading Dynamics in Social Systems*, edited by S. Lehmann and Y.-Y. Ahn (Springer-Verlag, forthcoming), https://socialcontagionbook.github.io.
[2] T. W. Valente, *Network Models of the Diffusion of Innovations* (Hampton Press, 1995).
[3] E. M. Rogers, *Diffusion of Innovations*, 3rd ed. (Free Press, 1983).
[4] M. A. Porter and J. P. Gleeson, *Dynamical Systems on Networks: A Tutorial (Frontiers in Applied Dynamical Systems: Reviews and Tutorials)* (Springer, 2016), Vol. 4.
[5] R. Pastor-Satorras, C. Castellano, P. Van Mieghem, and A. Vespignani, "Epidemic processes in complex networks," Rev. Mod. Phys. **87**, 925–979 (2015).
[6] J. Borge-Holthoefer, R. A. Baños, S. González-Bailón, and Y. Moreno, "Cascading behavior in complex socio-technical networks," J. Complex Networks **1**, 3–24 (2013).
[7] K. Dey, S. Kaushik, and L. V. Subramaniam, "Literature survey on interplay of topics, information diffusion and connections on social networks," preprint arXiv:1706.00921 (2017).
[8] D. Guilbeault, J. Becker, and D. Centola, "Complex contagions: A decade in review," in *Spreading Dynamics in Social Systems*, edited by S.

Lehmann and Y.-Y. Ahn (Springer-Verlag, forthcoming), https://socialcontagionbook.github.io.
[9]A. G. Haldane and R. M. May, "Systemic risk in banking ecosystems," Nature **469**, 351–355 (2011).
[10]M. Granovetter, "Threshold models of collective behavior," Am. J. Sociol. **83**, 1420–1443 (1978).
[11]D. J. Watts, "A simple model of global cascades on random networks," Proc. Natl. Acad. Sci. U. S. A. **99**, 5766–5771 (2002).
[12]D. Kempe, J. Kleinberg, and E. Tardos, "Maximizing the spread of influence through a social network," in *Proceedings of the 9th ACM SIGKDD International Conference on Knowledge Discovery and Data Mining*, KDD '03 (ACM, New York, NY, USA, 2003), pp. 137–146.
[13]P. S. Dodds and D. J. Watts, "A generalized model of social and biological contagion," J. Theor. Biol. **232**, 587–604 (2005).
[14]D. Centola and M. Macy, "Complex contagions and the weakness of long ties," Am. J. Sociol. **113**, 702–734 (2007).
[15]N. A. Christakis and J. H. Fowler, "Social contagion theory: Examining dynamic social networks and human behavior," Stat. Med. **32**, 556–577 (2013).
[16]M. O. Jackson and D. López-Pintado, "Diffusion and contagion in networks with heterogeneous agents and homophily," Network Sci. **1**, 49–67 (2013).
[17]M. O. Jackson and Y. Zenou, "Games on networks," in *Handbook of Game Theory*, edited by P. Young and S. Zamir (Elsevier, 2014), Vol. 4, pp. 95–163.
[18]E. Laurence, J.-G. Young, S. Melnik, and L. J. Dubé, "Exact analytical solution of irreversible binary dynamics on networks," preprint arXiv:1711.02721 (2017).
[19]C. Castellano, S. Fortunato, and V. Loreto, "Statistical physics of social dynamics," Rev. Mod. Phys. **81**, 591–646 (2009).
[20]N. A. Christakis and J. H. Fowler, "The spread of obesity in a large social network over 32 years," New England J. Med. **357**, 370–379 (2007).
[21]S. Aral, L. Muchnik, and A. Sundararajan, "Distinguishing influence-based contagion from homophily-driven diffusion in dynamic networks," Proc. Natl. Acad. Sci. U. S. A. **106**, 21544–21549 (2009).
[22]J. Ugander, L. Backstrom, C. Marlow, and J. Kleinberg, "Structural diversity in social contagion," Proc. Natl. Acad. Sci. U. S. A. **109**, 5962–5966 (2012).
[23]S. Goel, A. Anderson, J. Hofman, and D. J. Watts, "The structural virality of online diffusion," Manage. Sci. **62**, 180–196 (2016).
[24]D. Mollison, "Spatial contact models for ecological and epidemic spread," J. R. Stat. Soc. Ser. B **39**, 283–326 (1977).
[25]M. S. Helmut Elsinger and A. Lehar, "Risk assessment for banking systems," Manage. Sci. **52**, 1301–1314 (2006).
[26]D. Centola, R. Willer, and M. Macy, "The emperor's dilemma: A computational model of self-enforcing norms," Am. J. Sociol. **110**, 1009–1040 (2005).
[27]H. P. Young, "Innovation diffusion in heterogeneous populations: Contagion, social influence, and social learning," Am. Econ. Rev. **99**, 1899–1924 (2009).
[28]I. Z. Kiss, J. C. Miller, and P. L. Simon, *Mathematics of Epidemics on Networks: From Exact to Approximate Models* (Springer International Publishing, 2017).
[29]D. Taylor, F. Klimm, H. A. Harrington, M. Kramár, K. Mischaikow, M. A. Porter, and P. J. Mucha, "Topological data analysis of contagion maps for examining spreading processes on networks," Nat. Commun. **6**, 7723 (2015).
[30]E. Valdano, L. Ferreri, C. Poletto, and V. Colizza, "Analytical computation of the epidemic threshold on temporal networks," Phys. Rev. X **5**, 021005 (2015).
[31]J. P. Gleeson, "Binary-state dynamics on complex networks: Pair approximation and beyond," Phys. Rev. X **3**, 021004 (2013).
[32]J. P. Gleeson, "Cascades on correlated and modular random networks," Phys. Rev. E **77**, 046117 (2008).
[33]T. R. Hurd and J. P. Gleeson, "On Watts' cascade model with random link weights," J. Complex Networks **1**, 25–43 (2013).
[34]S. Melnik, J. A. Ward, J. P. Gleeson, and M. A. Porter, "Multi-stage complex contagions," Chaos **23**, 013124 (2013).
[35]M. Zheng, L. Lü, and M. Zhao, "Spreading in online social networks: The role of social reinforcement," Phys. Rev. E **88**, 012818 (2013).
[36]J. P. Gleeson, K. P. O'Sullivan, R. A. Baños, and Y. Moreno, "Effects of network structure, competition and memory time on social spreading phenomena," Phys. Rev. X **6**, 021019 (2016).
[37]C. Borgs, M. Brautbar, J. Chayes, S. Khanna, and B. Lucier, "The power of local information in social networks," in *Proceedings of the 8th International Workshop on Internet and Network Economics, WINE 2012, Liverpool, UK, December 10–12, 2012*, edited by P. W. Goldberg (Springer Berlin Heidelberg, Berlin, Heidelberg, 2012), pp. 406–419.
[38]D. Centola, "The spread of behavior in an online social network experiment," Science **329**, 1194–1197 (2010).
[39]J. J. Ludlam, G. J. Gibson, W. Otten, and C. A. Gilligan, "Applications of percolation theory to fungal spread with synergy," J. R. Soc. Interface **9**, 949–956 (2012).
[40]G. Brunori and A. Rossi, "Synergy and coherence through collective action: Some insights from wine routes in Tuscany," Sociologia Ruralis **40**, 409–423 (2000).
[41]S. Milgram, L. Bickman, and L. Berkowitz, "Note on the drawing power of crowds of different size," J. Pers. Soc. Psychol. **13**, 79–82 (1969).
[42]S. Sudarsanam, P. Holl, and A. Salami, "Shareholder wealth gains in mergers: Effect of synergy and ownership structure," J. Bus. Finance Accounting **23**, 673–698 (1996).
[43]C. Ballester, Y. Zenou, and A. Calvó-Armengol, "Delinquent networks," J. Eur. Econ. Assoc. **8**, 34–61 (2010).
[44]F. J. Pérez-Reche, J. J. Ludlam, S. N. Taraskin, and C. A. Gilligan, "Synergy in spreading processes: From exploitative to explorative foraging strategies," Phys. Rev. Lett. **106**, 218701 (2011).
[45]S. N. Taraskin and F. J. Pérez-Reche, "Effects of variable-state neighborhoods for spreading synergystic processes on lattices," Phys. Rev. E **88**, 062815 (2013).
[46]D. Broder-Rodgers, F. J. Pérez-Reche, and S. N. Taraskin, "Effects of local and global network connectivity on synergistic epidemics," Phys. Rev. E **92**, 062814 (2015).
[47]K. Chung, Y. Baek, D. Kim, M. Ha, and H. Jeong, "Generalized epidemic process on modular networks," Phys. Rev. E **89**, 052811 (2014).
[48]Q.-H. Liu, W. Wang, M. Tang, T. Zhou, and Y.-C. Lai, "Explosive spreading on complex networks: The role of synergy," Phys. Rev. E **95**, 042320 (2017).
[49]J. C. Miller, "Equivalence of several generalized percolation models on networks," Phys. Rev. E **94**, 032313 (2016).
[50]J. Chalupa, P. L. Leath, and G. R. Reich, "Bootstrap percolation on a Bethe lattice," J. Phys. C: Solid State Phys. **12**, L31–L35 (1979).
[51]A. Grönlund and P. Holme, "A network-based threshold model for the spreading of fads in society and markets," Adv. Complex Syst. **8**, 261–273 (2005).
[52]J. S. Juul and M. A. Porter, "Hipsters on networks: How a small group of individuals can lead to an anti-establishment majority," preprint arXiv:1707.07187 (2017).
[53]S.-W. Oh and M. A. Porter, "Complex contagions with timers," preprint arXiv:1706.04252 (2017).
[54]J. Leskovec, J. Kleinberg, and C. Faloutsos, "Graph evolution: Densification and shrinking diameters," ACM Trans. Knowl. Discovery Data **1**, 2 (2007).
[55]A. L. Traud, P. J. Mucha, and M. A. Porter, "Social structure of Facebook networks," Phys. A **391**, 4165–4180 (2012).
[56]S. Gómez, J. Gómez-Gardenes, Y. Moreno, and A. Arenas, "Nonperturbative heterogeneous mean-field approach to epidemic spreading in complex networks," Phys. Rev. E **84**, 036105 (2011).
[57]S. Melnik, A. Hackett, M. A. Porter, P. J. Mucha, and J. P. Gleeson, "The unreasonable effectiveness of tree-based theory for networks with clustering," Phys. Rev. E **83**, 036112 (2011).
[58]However, the temporal pattern of activation depends on the choice of asynchronous or synchronous updating. One can also generalize the WTM to other models in which the final fraction of active nodes does depend on this choice. For example, if nodes can be activated into different states as a function of their neighbors' states at the time of activation, then the steady-state fraction of nodes in a specific state can depend on whether one updates the nodes synchronously or asynchronously.
[59]The reason for this is as follows. We choose the single seed node uniformly at random from all nodes in a network, and we do not know the degree or the threshold of this node. Consider the fraction g_k^ϕ of nodes with degree k and threshold ϕ that are active, given that the seed is one of these nodes; and then multiply g_k^ϕ by the probability that the seed node has degree k and threshold ϕ. That is, $\psi_k^\phi = g_k^\phi p(k,\phi) = \frac{1}{Np(k,\phi)} p(k,\phi) = 1/N$.
[60]J. P. Gleeson and D. J. Cahalane, "Seed size strongly affects cascades on random networks," Phys. Rev. E **75**, 056103 (2007).
[61]P. G. Fennell, S. Melnik, and J. P. Gleeson, "Limitations of discrete-time approaches to continuous-time contagion dynamics," Phys. Rev. E **94**, 052125 (2016).
[62]B. K. Fosdick, D. B. Larremore, J. Nishimura, and J. Ugander, "Configuring random graph models with fixed degree sequences," SIAM Rev. (in press); preprint arXiv:1608.00607.

[63]A. L. Traud, E. D. Kelsic, P. J. Mucha, and M. A. Porter, "Comparing community structure to characteristics in online collegiate social networks," SIAM Rev. **53**, 526–543 (2011).
[64]E. Ben-Jacob, O. Schochet, A. Tenenbaum, I. Cohen, A. Czirok, T. Vicsek *et al*., "Generic modelling of cooperative growth patterns in bacterial colonies," Nature **368**, 46–49 (1994).
[65]L. A. Liotta and E. C. Kohn, "The microenvironment of the tumour–host interface," Nature **411**, 375–379 (2001).
[66]M. De Domenico, C. Granell, M. A. Porter, and A. Arenas, "The physics of spreading processes in multilayer networks," Nat. Phys. **12**, 901–906 (2016).
[67]M. Salehi, R. Sharma, M. Marzolla, M. Magnani, P. Siyari, and D. Montesi, "Spreading processes in multilayer networks," IEEE Trans. Network Sci. Eng. **2**, 65–83 (2015).
[68]M. Kivelä, A. Arenas, M. Barthélemy, J. P. Gleeson, Y. Moreno, and M. A. Porter, "Multilayer networks," J. Complex Networks **2**, 203–271 (2014).
[69]P. Holme and J. Saramäki, "Temporal networks," Phys. Rep. **519**, 97–125 (2012).
[70]G. Demirel, F. Vázquez, G. A. Bhöme, and T. Gross, "Moment-closure approximations for discrete adaptive networks," Phys. D **267**, 68–80 (2014).

Chapter 5

How a minority group of individuals can lead to an anti-establishment majority

On Friday, June 24, 2016 Britons and the rest of the world woke up to some startling news. The day before, the British people had voted to leave the European Union. "Brexit" was to become a reality. Approximately 5 months later, the final result of the 2016 presidential election was equally astonishing. Donald Trump beat Hillary Clinton despite her being a clear favorite in many influential organizations analysing and providing polls (*FiveThirtyEight 2016 final forecast*; *RealClearPolitics 2016 final forecast*).

In both the British referendum and the American presidential elections, the victors were seen as being in opposition to an establishment. A British publisher of news formulated this anti-establishment nature of the victors of the referendum as follows (Watts, 2018),

> "...at the 2016 referendum Leave was bolstered by its image as an anti-establishment crusade, while Remain was hindered by the perception that it was the campaign of the government and business elite."
>
> Joe Watts, Political Editor, The Independent (2018)

Bernie Sanders, one of the runner-ups for the Democratic nomination and a prominent political opponent of Donald Trump, said in his post-election statement (Levin et al., 2016),

> "Donald Trump tapped into the anger of a declining middle class that is sick and tired of establishment economics, establishment politics and the establishment media."
>
> Bernie Sanders, US senator (2016)

If these statements are to be trusted, it would seem that people voted *against* an establishment in both the UK referendum and the 2016 US presidential election. Indeed, in both cases, anti-establishment opinions appear to have spread to large fractions of the populations (Hobolt, 2016; Oliver and Rahn, 2016).

It seems paradoxical if every person voting for the victors should be inherently anti-establishment. So did a smaller fraction of the population successfully spread their anti-establishment opinions to a substantial fraction of the population? This question immediately leads one to ask whether such spreading is likely to happen.

Another relevant question seems to be whether such spreading would be likely to happen happen on a large enough scale to allow for an anti-establishment outcome of an election or referendum. With Mason A. Porter, I examined whether a few anti-establishment nodes could change which of two spreading products would get the most widespread in a population. The central idea of this work was incorporating anti-establishment nodes into the WTM.

5.1 Anti-establishment nodes in network dynamics

That some nodes actively oppose to align with a majority is not a new idea. Such nodes have previously been incorporated into mathematical models of human behavior, and empirical studies have reported manifestations of anticonformity in various forms. Examples include motivations to share political rumours (Petersen, Osmundsen, and Arceneaux, 2018) and how expert statements and data are misinterpreted to align with the beliefs group members (Guilbeault, Becker, and Centola, 2018b; Jamieson and Hardy, 2014).

In the literature, anti-establishment traits are often referred to by other names such as anti-conformism or contrarianism. The models incorporating anti-establishment behavior have very different scopes. Galam and collaborators have been particularly interested in such models, using them to investigate phenomena such as "hung elections" (where no political party can form a majority of legislators) or describe how outcomes of debates are influenced by stubbornness or inflexibility (Galam, 1986; Galam, 2004; Galam and Jacobs, 2007; Galam, 2016; Galam and Cheon, 2019; Jacobs and Galam, 2019). These works rarely study the effect of underlying network structures.

Other studies have examined the impact of anticonformists in relation to fashion cycles and advertising in duopoly markets. It has also been examined how such nodes change the dynamics of well-known models (Nyczka, Sznajd-Weron, and Cisło, 2012; Nyczka and Sznajd-Weron, 2013; Khalil and Toral, 2019; Sznajd-Weron and Weron, 2003). In these studies, models are typically simulated on only a single kind of network. A rare instance of a study incorporating nodes similar to anticonformists and systematically investigating the effect of network topology is (Mellor et al., 2015). They incorporated "luddites" into a compartmental model of innovation spreading. The luddites would choose to reject an innovation all together with a probability proportional to the adoption rate of the innovation in the node's neighbourhood. Simulating their model on Erdős–Rényi networks, complete networks, and one-dimensional lattices, they showed that luddites could cause fast-spreading innovations to spread less far in the long run. Slow spreading made innovations more likely to spread far.

5.1.1 Touboul's model of hipsters

In a preprint first published in 2014, Jonathan Touboul investigated the effect of anti-conformism in a spin-glass model (Touboul, 2014). In the model, agents can be in either of two states. Most agents are conformists and prefer to align with the majority. The remaining agents are anti-conformists that prefer to misalign with the majority. Agent i observes the states of other agents with some delay τ_{ij}, and assigns that state a weight J_{ij}. The parameters τ_{ij} and J_{ij} are assigned from some distributions and independently drawn from these for each node.

Touboul referred to the anti-establishment nodes as *hipsters* and showed that a phase transition exists beyond which the hipsters end up looking the same. In other words, although all hipsters prefer to misalign with other agents, all of these anti-conformists end up synchronising with each other. In this way, they all successfully misalign with the majority but still end up looking identical to many other nodes. In a recent update to this preprint, the bifurcations of the model are investigated in greater detail (Touboul, 2019).

5.2 Our results: How a minority group of individuals can lead to an antiestablishment majority

In the paper, "Hipsters on networks: How a minority group of individuals can lead to an antiestablishment majority" published in Physical Review E (Juul and Porter, 2019), Mason A. Porter and I study a variant of the WTM. In this model, we assume that nodes are either conformists or hipsters. An adjustable fraction of the population p_{Hip} is chosen uniformly at random to be hipsters. Two different products are spreading in the population. A node adopts one of the products if the fraction of its neighbours that have adopted *any* product is larger than or equal to its threshold ϕ. As in the WTM, thresholds are drawn independently from a distribution $f(\phi)$.

If a node adopts a product, it must specify which of the two possible products it would like to adopt. Conformists adopt whichever product is the most adopted among their neighbours at the preceding time step $t-1$. Hipsters instead adopt the product, which is least adopted in the total population at some previous time step $t-\tau$. τ can serve as a time delay. If $\tau = 1$, hipsters know the distribution of products at the preceding time step, and there is no time delay. If $\tau \geq 2$, their knowledge is outdated.

In the paper, we ask 3 questions: "1) How does a large fraction of a population decide to choose something different from the established standard?; 2) How can a small fraction of individuals spread their anti-establishment opinions to a majority (or at least a very large minority) of the rest of a population?; 3) Can we capture these ideas using a simple mathematical model of a spreading process on a network?" (Juul and Porter, 2019). To answer these questions, we need to have a well-defined "established standard". We get this by only letting one of the two products, product A, be adopted at the beginning of simulations. In this way, as long as only conformists adopt products, only product A spreads in the network. The other product, product B, is only introduced when the first hipster adopts a product. The model proceeds in discrete time steps; every node is updated synchronously in each time step.

Simulating our model on several classes of networks, we are interested in the average outcome over many simulations. We find that a tiny fraction of hipsters can make the two products equally widespread at equilibrium. In synthetic networks, we find the smallest fraction of the population that needs to be hipsters for the two products to be equally prevalent at equilibrium to be strikingly small. The fraction is as low as 0.06 in one type of network, and below 0.10 in all cases. The needed fraction of hipsters is higher when the model is simulated on an empirical network of Facebook friendships. Depending on τ, we find that the final fraction of product-A and product-B adopters depend non-monotonously on p_{Hip}. We analytically approximate these adoption fractions and obtain good agreement for low fractions of hipsters. We also show that the findings are insensitive to seed size for some values of the delay, τ, and more sensitive for other values of τ.

We are mainly interested in the dynamics for low p_{Hip} and investigate these in more depth analytically. Using a recursive argument, we argue that the reason why few hipsters can impact the popularity of the two products so much is rooted in *adoption paths*. If a hipster is located close to the seed of product A adopters, it will effectively influence a large part of the population to adopt product B. This is the case because the down-stream conformist neighbours of the hipster will adopt the same product as the hipster did: product B. The conformist neighbours of this product-B adopting conformist will then adopt product B too. In this way, a cascade of product-B adoption is started by the rare event of a hipster being located close to the seed. These extraordinary events drive the expected fraction of product-B adopters up, even for small values of p_{Hip}. This makes a minority group of individuals capable of leading to an anti-establishment majority. The recursive calculation used in this calculation is in good agreement with simulations. The paper constitutes the following section, which concludes the present chapter.

5.3 Paper: How a minority group of individuals can lead to an anti-establishment majority

PHYSICAL REVIEW E **99**, 022313 (2019)

Hipsters on networks: How a minority group of individuals can lead to an antiestablishment majority

Jonas S. Juul*
Niels Bohr Institute, University of Copenhagen, Blegdamsvej 17, Copenhagen 2100-DK, Denmark

Mason A. Porter†
Department of Mathematics, University of California, Los Angeles, California 90095, USA;
Oxford Centre for Industrial and Applied Mathematics, Mathematical Institute, University of Oxford, Oxford OX2 6GG, United Kingdom;
and CABDyN Complexity Centre, University of Oxford, Oxford OX1 1HP, United Kingdom

(Received 28 November 2018; published 26 February 2019)

The spread of opinions, memes, diseases, and "alternative facts" in a population depends both on the details of the spreading process and on the structure of the social and communication networks on which they spread. One feature that can change spreading dynamics substantially is heterogeneous behavior among different types of individuals in a social network. In this paper, we explore how *antiestablishment* nodes (e.g., *hipsters*) influence the spreading dynamics of two competing products. We consider a model in which spreading follows a deterministic rule for updating node states (which indicate which product has been adopted) in which an adjustable probability p_{Hip} of the nodes in a network are hipsters, who choose to adopt the product that they believe is the less popular of the two. The remaining nodes are conformists, who choose which product to adopt by considering which products their immediate neighbors have adopted. We simulate our model on both synthetic and real networks, and we show that the hipsters have a major effect on the final fraction of people who adopt each product: even when only one of the two products exists at the beginning of the simulations, a small fraction of hipsters in a network can still cause the other product to eventually become the more popular one. To account for this behavior, we construct an approximation for the steady-state adoption fractions of the products on k-regular trees in the limit of few hipsters. Additionally, our simulations demonstrate that a time delay τ in the knowledge of the product distribution in a population, as compared to immediate knowledge of product adoption among nearest neighbors, can have a large effect on the final distribution of product adoptions. Using a local-tree approximation, we derive an analytical estimate of the spreading of products and obtain good agreement if a sufficiently small fraction of the population consists of hipsters. In all networks, we find that either of the two products can become the more popular one at steady state, depending on the fraction of hipsters in the network and on the amount of delay in the knowledge of the product distribution. Our simple model and analysis may help shed light on the road to success for antiestablishment choices in elections, as such success—and qualitative differences in final outcomes between competing products, political candidates, and so on—can arise rather generically in our model from a small number of antiestablishment individuals and ordinary processes of social influence on normal individuals.

DOI: 10.1103/PhysRevE.99.022313

I. INTRODUCTION

The study of spreading phenomena on networks has received considerable attention in many disciplines, including sociology, economics, physics, biology, computer science, mathematics, and others [1–18]. In analogy with the spread of infectious diseases in populations of susceptible individuals, the spread of social phenomena (such as opinions, actions, memes, information, misinformation, and alternative facts) is often viewed as a contagion process that spreads through a network's nodes, which are connected to each other via one or more types of edges. The nodes can represent entities such as people or institutions [19–21] (or other things); and the edges can represent physical proximity, communication channels, sociological interactions (e.g., different types of relationships), or something else. An important goal of many studies of the spread of social contagions is the identification of criteria that determine when the phenomenon that is spreading reaches a large fraction of a population or subpopulation [1,2].

Scholars have used various approaches for studying contagions on networks. These include game theory [7], statistical physics [10], agent-based models [22], and systems of coupled differential equations or stochastic processes [2,23–27]. The temporal dynamics and peak size of an outbreak are influenced both by the specific model of a contagion and by the structure of the network on which it spreads [12,20,25,27–34]. A key idea is to examine when a disease or idea—perhaps one that initially is present in a small fraction of nodes—can become widespread in a network. When a large fraction of a population or subpopulation becomes infected (or adopts an idea), one says that a *cascade* has occurred. Cascading phenomena have been studied in a wide variety of systems,

*jonas.juul@nbi.ku.dk
†mason@math.ucla.edu

ranging from financial networks [21] to social media like Twitter [35]. For example, a failing financial institution can cause a cascade of failures of numerous other financial institutions, a tweet can result in a cascade of tweets that promotes the opinion of the original tweeter (perhaps influenced by the actions of "bot" or sockpuppet accounts [17]), and widely spread alternative facts can influence the opinions of a large population of voters [36]. Notwithstanding these dystopian examples, cascading behavior can be beneficial, neutral, or harmful.

Models of cascading behavior on networks can have either stochastic or deterministic state-update rules, and the update rules in most models only consider nodes that are adjacent to a focal node. One example of models that traditionally have deterministic update rules is *threshold models* for social contagions. The simplest example is the Watts threshold model (WTM) [5,6,9], a type of bootstrap percolation [37], in which each node is assigned a threshold from some distribution. When considering a node for updating, if the fraction of its neighbors that are adopters is at least as large as its threshold, it too becomes an adopter. There are numerous variants and generalizations of the WTM, including ones with adoption thresholds that are based on the number (rather than the fraction) of neighbors who are adopters [12,38], ones with multiple adoption stages [25], ones with "synergy" from other nearby adopters [27], and ones with timers in addition to adoption thresholds [39].

Efforts to develop mathematical models for the spread of products or innovations date at least as far back as the 1960s. Rogers [40] gave a qualitative description (as a sigmoidal shape) of the number of adopters as a function of time. Bass [41] developed a model for the adoption of innovations that was inspired by models for biological contagions. Bass's model results in sigmoidal-shaped adoption curves, and it has been generalized in various ways [42–45]. More recent studies have considered models in which agents of different types can have significant effects on the final distributions of products or innovations in a population. For example, Gordon *et al.* [46] showed that temporal cycles of adoption can occur if some nodes are allowed to regret adopting an innovation while other ("contrarian") nodes resist adopting innovations. References [47,48] found rich behavior (including chaotic dynamics) in a social contagion model that incorporates an aversion to complete conformity.

Contrarian agents, a key aspect of the present paper, have been incorporated into various types of models of opinion dynamics and hierarchy formation. In the 1980s, Galam [49] illustrated a hierarchical mechanism that allows a minority community to elect its preferred candidate instead of that of the majority. Galam and collaborators have also examined the effects of contrarian [50] and stubborn [51,52] agents on opinion dynamics (though typically without any network structure). Nyczka *et al.* [53] and Nyczka and Sznajd-Weron [54] studied various opinion models (e.g., q-voter models) on a complete graph to highlight an important distinction between two types of nonconformity—anticonformity and independence—that have distinct implications for social dynamics. Khalil and Toral [55] incorporated contrarians into a noisy voter model, and they illustrated that a few contrarians can substantially alter the dynamics of the model. Apriasz *et al.* [56] examined an opinion model that includes "snobs," who conform to nodes in their own community but anticonform to nodes in others, to examine how the density of connections between two communities can affect phenomena such as fashion cycles. One can also consider contrarian individuals in the context of economic markets, such as in work by Sznajd-Weron and Weron [57], who studied an Ising model on a rectangular lattice to model advertising in duopoly markets. More recent work related to contrarian agents, in addition to [46–48], includes that of Mellor *et al.* [58], who examined a population in which nodes can either adopt a product or become "luddites," who oppose the spread of innovation. They found that luddites greatly limit adoption if the adoption rate is high but not if it is low. Gambaro and Crokidakis [59] illustrated that contrarian agents can be a source of disorder in opinion dynamics, and Ferrara and collaborators have investigated how individual social-media accounts controlled by bots can exert a considerable influence on political elections and social cascades [17,60,61].

Anticonformity can manifest in a variety of ways in society. For example, it has been reported that partisan bias can result in some groups of individuals misinterpreting data and explanations of experts (e.g., with respect to the issue of climate change), in conflict with the intended message, such that it fits with the personal beliefs of the group [62,63]. In a recent example about information spreading, Petersen *et al.* [64] provided psychological assessment of motivations to share hostile political rumors (e.g., in the form of "fake news") among citizens of democratic societies, concluding that such rumors are often shared by individuals because they believe it can mobilize their audience against a disliked establishment (rather than because they think that these rumors are true).

In the present paper, we examine the influence of *antiestablishment* nodes, such as *hipsters*, on spreading processes in a social network. Individuals who specifically prefer something other than the established standard in society have manifested in several ways over the last decade. They include members of antiestablishment movements in Western Europe and the United States of America, who have hugely impacted the geopolitical landscape, to the curious style of hipsters in cities throughout the world. In some cases, such as the 2016 "Brexit" vote [65] and the 2016 American presidential election [66], antiestablishment opinions appear to have spread to so many people that they exerted a major influence on political outcomes. In this paper, we ask the following questions: (1) How does a large fraction of a population decide to choose something different from the established standard? (2) How can a small fraction of individuals spread their antiestablishment opinions to a majority (or at least to a very large minority) of the rest of a population? (3) Can we capture these ideas using a simple mathematical model of a spreading process on a network?

A few years ago, a statistical-physics approach was used to examine how anticonformists (i.e., hipsters) who make decisions that differ from that of a majority, perhaps in an attempt to stand out from the crowd, may all end up "looking the same" [67] (wearing the same clothes, buying the same products, having the same opinions, and so on). This study observed that the dynamics of a population was influenced greatly by delays in the knowledge of hipsters and by how

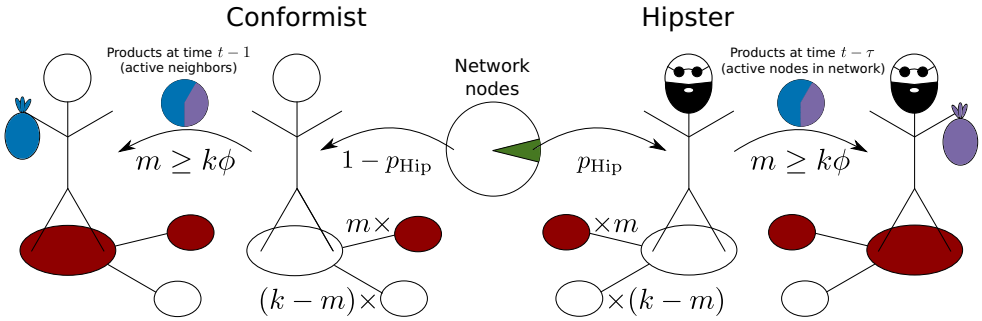

FIG. 1. Illustration of our model of a threshold-based social contagion with hipsters. A node is a hipster with probability p_{Hip}, and it is a conformist with probability $1-p_{\mathrm{Hip}}$. If at least a fraction ϕ_i of the neighbors of node i are active (as indicated by the red coloring) at discrete time step $t-1$, the node activates and adopts a product at time step t (for $t \geqslant 1$). We then need to consider which products have been adopted by node i's neighbors and the relative popularity of different products in the whole network. If node i is a conformist, it adopts the product that is more popular among its active neighbors at time $t-1$. However, if node i is a hipster, it adopts the product that is less popular among the active nodes in the network at time step $t-\tau$ (where $\tau \in \mathbb{N}$). For both node types, a tie results in a node choosing one of the two products (blue versus purple) with equal probability.

large a fraction of the population are hipsters. In the model in [67], individuals interact with their environments and switch between two states with a probability that depends on this environment and on whether an individual is a conformist (preferring to be aligned with its environment) or a hipster (preferring to be opposite to its environment). The model has a phase transition that determines whether or not hipsters ultimately attain the same state. Touboul [67] referred to the anticonformists with delayed knowledge as "hipsters." Because the model that we introduce in this study includes anticonformists with delayed knowledge of the global product distribution, we adopt this terminology. However, our approach, focus, and type of model—which builds on threshold models for social contagions—are rather different from those in [67].

We will explore how anticonformists (i.e., hipsters) affect the spreading of competing products in a network by generalizing the WTM to a network with two types of nodes—hipsters and conformists—who respond differently to adoptions. Conformists prefer to adopt the product (or meme, opinion, message, etc.) that is more popular among their active neighbors at time $t-1$. Hipsters, however, prefer to adopt the product that is the less popular of the two products in the whole network at some previous time $t-\tau$. Their choice to adopt a product uses the same adoption condition as that of the conformists. This is a strong assumption, and we make it partly for simplicity (as it allows us to build from the WTM) and partly because it reflects a scenario in which an anticonformist may more actively rebel on an issue that is sufficiently established in its neighborhood in a network. In our model, both conformists and hipsters first choose to buy some product or form an opinion, and then they choose which one to adopt. In their study of the effect of luddites, Mellor *et al.* [58] assumed that the probability of a node becoming a luddite is proportional to the rate of change in the density of adopters of its neighbors. This resembles our choice that a node's neighborhood influences whether or not it elects to adopt a product, but it differs from our choice that each of our nodes is either inherently a conformist or inherently a hipster. The delay τ in our model encodes the fact that knowledge about the total population is not instantly available; instead, it is collected over some time before it is available. See Gleeson *et al.* [68] for a model (without network structure) that illustrates another type of competition between local information (in the form of a social-media feed) and global information (in the form of a bestseller list).

The rest of our paper is organized as follows. In Sec. II, we introduce our model for the spreading of two competing products on networks under the influence of hipster nodes. In Sec. III, we examine our model on a Facebook network. In Sec. IV, we develop an analytical approximation to describe the time-dependent fractions of nodes that adopt the products (where each adopter chooses one of the two competing products) as a function of their degree k and an adoption threshold ϕ. In Sec. V, we examine our model on several classes of empirical networks and investigate the final fractions of nodes that adopt the products as a function of the time delay τ and the hipster probability p_{Hip}. In Sec. VI, we explain the observed behavior in the limit of few hipsters, and we obtain an approximation for the fraction of nodes that adopt the products as a function of the number of hipsters. We conclude and discuss our results in Sec. VII.

II. A THRESHOLD MODEL WITH HIPSTERS

Threshold models of social influence are a popular type of spreading process to study on networks [1,2,6]. To set up a simple example of a threshold model, consider a network with N nodes, and suppose that each node i has an independently assigned threshold ϕ_i that we draw from a distribution $f(\phi)$. We also suppose that a node can be in one of two states: *active* or *inactive*. An active node has adopted a product (or meme, opinion, etc.) that is spreading in a population, and an inactive node has not adopted the product. (We will use the term "product" from now on.) Once a node becomes active, it stays active forever. The threshold of a node determines how difficult it is to activate that node, so one can construe a node's threshold value as its stubbornness level. Node i becomes active if a peer pressure, which in the WTM is equal to the fraction of active nodes among i's neighbors, is greater than or equal to its threshold ϕ_i.

We seek to develop a model for competing products that spread in a population that includes hipsters. Therefore, in our

model, each node i has a value $H_i \in \{0, 1\}$, such that $H_i = 0$ indicates that node i is a *conformist* and $H_i = 1$ indicates that node i is a *hipster*. We update nodes synchronously. At each discrete time $t \geqslant 1$, we assume that conformists know the distribution of products among their immediate neighbors at the previous time step $t' = t - 1$, whereas hipsters know the distribution of products in the total population at an earlier time step $t_\tau = t - \tau$ (where $\tau \in \mathbb{N}$). The first updating step occurs at $t = 1$. If $t - \tau < 0$, we let $t_\tau = 0$.

A node chooses to adopt a specific product in two steps. First, the node must become active, which occurs if sufficiently many of its neighbors are active. If the fraction of neighbors that are active at time $t - 1$ is at least as large as the node's threshold, it becomes active at time t. If node i becomes active, it immediately adopts one of two possible products. If $H_i = 0$, node i is a conformist and thus adopts the product that is more popular among its active neighbors at time step $t - 1$. However, if $H_i = 1$, node i is a hipster and thus adopts the product that is less popular in the total population at time $t_\tau = t - \tau$. For both values of H_i, a tie results in the node choosing one of the two products with equal probability. Each node can adopt only a single product, and once it has adopted a product, it never switches to the other product or becomes inactive. To keep track of the product distribution, we associate a variable S_i with each node i. If $S_i = 0$, node i is inactive; if $S_i = 1$, node i has adopted product A; and if $S_i = 2$, node i has adopted product B. We summarize our model and the decision process in Fig. 1 and its caption. See [79] for a PYTHON script to simulate our model.

At $t = 0$, we activate a single node with product A, and we introduce product B when the first hipster chooses to adopt a product. In principle, it is possible to generalize our model to consider arbitrarily many products spreading on a network, but we consider only the case of two products for simplicity.

Although it may seem somewhat artificial that the conformists in our model use only local information to decide which product to adopt, whereas the hipsters use only global information, it is both convenient and illustrative (because the WTM has been studied so meticulously) to generalize the WTM model by adding one specific feature. This is also appropriate for exploring the competition between local and global forms of influence. We examine our hipster model both on synthetic networks and on empirical social networks. Our main goal is to examine whether (and when) a small probability p_{Hip} of hipster nodes can lead to a majority of a network's nodes adopting a product that is less popular than another product at the beginning of a spreading process. We find that the fraction of nodes that adopt the less popular of our two products depends in an interesting way on the delay τ in the hipsters' knowledge of the product distribution in the total population.

III. SIMULATION OF OUR MODEL ON A FACEBOOK NETWORK

We start by simulating our model on the NORTHWESTERN25 network from the FACEBOOK100 data set [69]. This network consists of the friendship relationships on Facebook at Northwestern University on one day in autumn 2005. The network has 10 537 nodes, a mean degree of $\langle k \rangle \approx 92$, and a maximum degree of $k_{\max} = 2105$. We assign a threshold of $\phi = 1/33$ to each node. In addition to this threshold, we independently assign each node a value $H_i \in \{0, 1\}$ with some hipster probability p_{Hip} to be $H_i = 1$. Therefore, different simulations of our model with a specified hipster probability do not in general have the same number of hipster nodes. We examine our model with two different time delays and two different values for the probability of hipsters in the network. We consider $\tau = \{1, 4\}$ and $p_{\text{Hip}} = \{0.04, 0.30\}$, and we conduct simulations for the four combinations of these parameter choices.

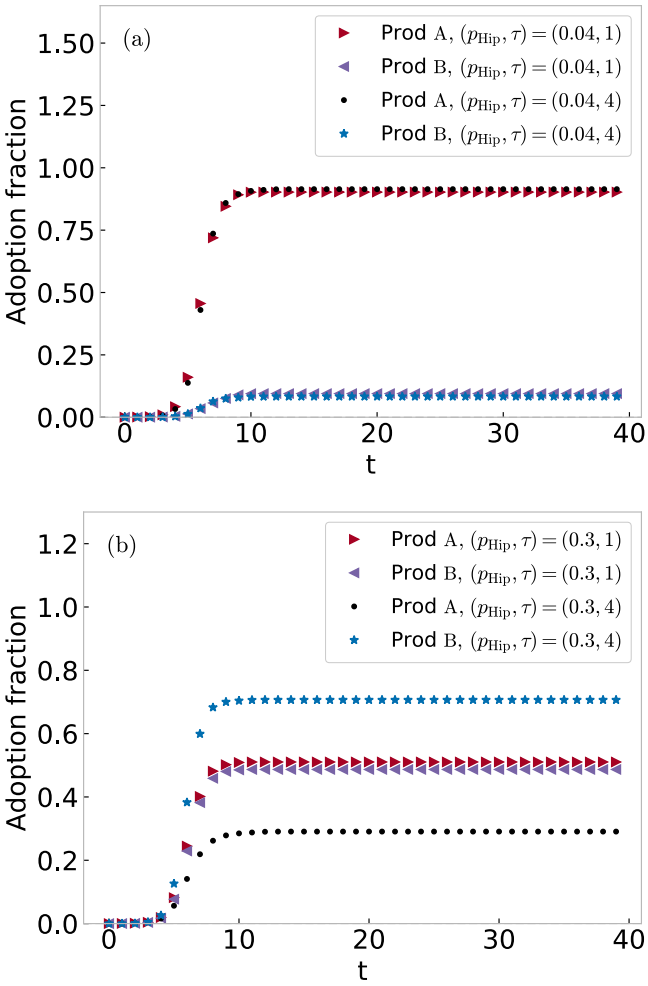

FIG. 2. Example of the behavior of our hipster threshold model on a Facebook network for delay values $\tau = \{1, 4\}$ for (a) a hipster probability of $p_{\text{Hip}} = 0.04$ and (b) a hipster probability of $p_{\text{Hip}} = 0.30$. In each panel, we show the fraction of nodes in the network that are adopters of each of the two products as a function of time. In panel (a), the curves from the two different values of τ are almost indistinguishable from each other. In panel (b), the adoption fractions of the two products are clearly different when we use different delays ($\tau = 1$ and $\tau = 4$). For $\tau = 1$, the final fractions that are adopters of products A and B are approximately equal. However, for $\tau = 4$, product B becomes more popular than product A. For both panels, each data point is a mean over 200 simulations on the same network (the NORTHWESTERN25 network of the FACEBOOK100 data set [69]), where we choose seed nodes and hipster nodes uniformly at random for each of the simulations.

For each parameter pair, we choose a single node uniformly at random and suppose that it has adopted product A at time $t = 0$. This node acts as a seed for the spreading process on the network. We introduce another product, labeled B, when the first hipster node is activated. Thus, product B will never be adopted by any node if the network has no hipsters, and product A has a head start when product B is adopted for the first time. We stop our simulations after the dynamics reaches a steady state, in which no further adoptions occur. At each time step, we track the fraction of the nodes that are adopters of each of the two products. We conduct 200 simulations—each with a seed chosen uniformly at random, with new hipster nodes for each simulation—and, at each time step t, we average the fraction of nodes that are adopters of each product over these 200 simulations. We show the results of these simulations in Fig. 2.

In Fig. 2(a), we plot the fraction of nodes in the adopted state for each of the products at time t for simulations in which the hipster probability is 0.04. For these parameters, the curves are indistinguishable for the two values of the delay time τ. A much larger fraction of nodes adopts product A than product B. In Fig. 2(b), we show the corresponding curves for simulations in which the hipster probability is 0.30. The results for different delay times τ are now clearly distinguishable. For $\tau = 1$, the fraction of nodes that have adopted the two products are approximately equal; for $\tau = 4$, however, the fraction of nodes that have adopted product B is much larger than the fraction that have adopted product A.

IV. ANALYSIS

We approximate the temporal spreading of products on a network using a pair approximation (as in [25,27,32,70]) that relies on the hypothesis that the network is locally tree-like [71,72]. Let $\rho_\lambda^{(\phi,k)}(t)$ denote the density of nodes with threshold ϕ and degree k that are in the adopted state, for a product $\lambda \in \{A, B\}$, at time step t. We write the recursion relation

$$\rho_\lambda^{(\phi,k)}(t+1) = \rho_\lambda^{(\phi,k)}(t) + \left[1 - \rho_\lambda^{(\phi,k)}(t)\right] \sum_{k'=1}^{k} F(k,k',\phi) B_{k'}^{k}\left(\sum_{\beta\in\{A,B\}} \bar{q}_\beta^{(\phi,k)}(t) \right)$$
$$\times \left[(1-p_{\rm Hip}) \sum_{k''=1}^{k'} \Theta\left(k'' - \frac{k'}{2}\right) B_{k''}^{k'}\left(\frac{\bar{q}_\lambda^{(\phi,k)}(t)}{\sum_{\beta\in\{A,B\}} \bar{q}_\beta^{(\phi,k)}(t)} \right) \right.$$
$$\left. + p_{\rm Hip} \prod_{\beta\neq\lambda} \Theta\left(\sum_{k,\phi} \rho_\lambda^{(\phi,k)}(\max\{t-\tau,0\}) - \sum_{k,\phi} \rho_\beta^{(\phi,k)}(\max\{t-\tau,0\}) \right) \right], \tag{1}$$

where $\bar{q}_\beta^{(\phi,k)}(t)$ is the probability that a neighbor, chosen uniformly at random, of an inactive node with threshold ϕ and degree k is active and has adopted product $\beta \in \{A, B\}$; the "response function" $F(k,k',\phi) = 1$ if $k'/k \geqslant \phi$ and $F(k,k',\phi) = 0$ otherwise; $\Theta(x)$ is the step function (it equals 1 for $x > 0$, it equals $1/2$ for $x = 0$, and it equals 0 otherwise); and

$$B_l^k(p) = \binom{k}{l} p^l (1-p)^{k-l} \tag{2}$$

is the binomial function for probability p. The product over $\beta \neq \lambda$ in Eq. (1) is in fact a product over a single value (so we did not need to use the product symbol), but one must take a product over all values of β except for λ in a model with three or more competing products. In this more general case, it is also necessary to take the sums over β over a larger set of products (and to replace the step function in the product with a more complicated function).

We write $\bar{q}_k^{(\phi,k)}(t)$ as a function of $q_i^{(\phi',k')}(t)$, the probability that, for a given inactive node, a neighbor with degree k' and threshold ϕ' is active at time step t. This probability is given by

$$\bar{q}_\lambda^{(\phi,k)}(t) = \frac{\sum_{k',\phi'} P((k,\phi),(k',\phi')) q_\lambda^{\phi',k}(t)}{\sum_{k',\phi'} P((k,\phi),(k',\phi'))}, \tag{3}$$

where $P((k,\phi),(k',\phi'))$ is the probability that a node with degree k and threshold ϕ is adjacent to a node with degree k' and threshold ϕ'. Given an active node, the probability that a particular neighbor with degree k and threshold ϕ is active is

$$q_\lambda^{(\phi,k)}(t+1) = \rho_\lambda^{(\phi,k)}(t) + \left[1 - \rho_\lambda^{(\phi,k)}(t)\right] \sum_{k'=1}^{k-1} F(k,k',\phi) B_{k'}^{k}\left(\sum_{\beta\in\{A,B\}} \bar{q}_\beta^{(\phi,k)}(t) \right)$$
$$\times \left[(1-p_{\rm Hip}) \sum_{k''=1}^{k'} \Theta\left(k'' - \frac{k'}{2}\right) B_{k''}^{k'}\left(\frac{\bar{q}_\lambda^{(\phi,k)}(t)}{\sum_{\beta\in\{A,B\}} \bar{q}_\beta^{(\phi,k)}(t)} \right) \right.$$
$$\left. + p_{\rm Hip} \prod_{\beta\neq\lambda} \Theta\left(\sum_{k,\phi} \rho_\lambda^{(\phi,k)}(\max\{t-\tau,0\}) - \sum_{k,\phi} \rho_\beta^{(\phi,k)}(\max\{t-\tau,0\}) \right) \right]. \tag{4}$$

TABLE I. Summary statistics of the discarded realizations of our hipster threshold model on each network family (or individual network, for NORTHWESTERN25). The second column gives the total number of discarded realizations. In it, we sum the instances from all parameter values, because the values of τ and p_{Hip} do not influence the fraction of nodes that activate in a given realization. We show the mean fraction of nodes that are active at steady state for discarded realizations and the standard deviation of this mean. For all networks, the mean fraction of active nodes is much smaller than the threshold fraction of 0.10, below which we discard realizations. For each choice of parameter values and network, we keep 200 realizations for our samples.

Network	Number of discarded realizations	Mean	Standard deviation of the mean
5-regular configuration model	36	0.0001	0.0000
3-regular configuration model	1843	0.0002	0.0001
Erdős–Rényi $[G(N, p)]$	52214	0.0072	0.0010
NORTHWESTERN25	35171	0.0001	0.0001

The only difference between Eq. (4) and Eq. (1) stems from the following: in Eq. (1), we consider any degree-k node; however, in Eq. (4), we consider a degree-k neighbor of an inactive node. The latter has a maximum of $k-1$ active neighbors, which is therefore the maximum value of the index of the first sum in Eq. (4). In these equations, we have assumed that each neighbor of node i is independent of the others, so we are assuming that this process is occurring on a locally treelike network [2,71]. However, the Facebook network that we used in Sec. III has a large local clustering coefficient [69], so it is not locally treelike.

V. HIPSTER THRESHOLD MODEL ON SYNTHETIC NETWORKS

We now test our analytical approximations of Sec. IV by simulating our model on various synthetic networks with $N = 10\,000$ nodes. We assign each node i a threshold ϕ_i from some probability distribution $f(\phi)$, which we specify in the following subsections. We also independently assign each node i a value $H_i \in \{0, 1\}$ to determine if it is a hipster. As before, p_{Hip} denotes the probability of being assigned the hipster value $H_i = 1$.

As with our simulations on the Facebook network in Sec. III, we select a single node uniformly at random to have adopted product A at time $t = 0$. This node is the seed of the spreading process. There is a risk that the chosen seed node is located in a neighborhood of very few vulnerable nodes. (A node that can be activated by a single active neighbor is known as a "vulnerable" node [9].) With such a seed, few nodes are activated in that realization of the dynamical process, and we do not observe a cascade of adoptions (in which many nodes adopt a product).

To focus on situations in which many nodes adopt (either of the products), we consider only realizations in which at least some minimal fraction of nodes eventually adopt a product. We take this minimal threshold to be 0.10. (Another way to examine situations with a lot of spreading is through "cluster seeding" [29], in which one considers initial conditions in which some node and all of its neighbors start out as adopters.) In Table I, we indicate the number of discarded realizations, the mean fraction of adopting nodes in these simulations, and the standard deviation of this number of adopters for several types of networks. The threshold 0.10 is much larger than the mean fraction of adopters in discarded realizations, and it is much smaller than the fraction of adopting nodes in realizations that we keep. Therefore, this choice of threshold entails a clear separation between realizations with cascades of adoption and those without such cascades. In many of our networks, the number of discarded simulations (in which there are few adoptions) is very large, consistent with the empirical study of Goel *et al.* [73].

A. 5-regular configuration-model networks

We consider configuration-model networks [74] in which every node has degree 5. As described in [74,75], we match stubs (i.e., ends of edges) uniformly at random. We suppose that each node has a threshold of $\phi_i = 0.19$ with probability $p_0 = 0.8$ and a threshold of $\phi_i = 0.8$ with probability $1 - p_0 = 0.2$. Therefore, on average, 80% of the nodes are vulnerable, and 20% of the nodes can adopt only when 4 or more of their nearest neighbors are adopters. We select these parameter values because this choice entails that some nodes are vulnerable, whereas other nodes need to have two or more active neighbors to adopt a product; and it ensures that a cascade of product adoptions occurs in most of our simulations.

We examine our hipster threshold model on the networks for time delays $\tau \in \{1, 2, 3, 4, 5, 6\}$ and hipster probabilities of $p_{\text{Hip}} \in [0, 1]$ (in increments of 0.01). For each parameter pair (τ, p_{Hip}), we simulate our model on 200 different networks. We independently draw the specific sets of networks for different parameter values, so in general they are not the same networks. For each realization, we stop the simulations after the distribution of product adoptions reaches a steady state, and we track the adoption fractions of the two competing products. From these values, we calculate the mean fraction of nodes that adopt each product over the 200 realizations and the corresponding standard deviations of the means. We plot these values in Fig. 3.

For all hipster delay times τ, the steady-state fraction $\rho_{B,\text{tot}}(t \to \infty)$ of nodes that are adopters of product B increases rapidly for small p_{Hip}. For $\tau = 1$ [see Fig. 3(a)], the hipsters have access to information without any delays, and their behavior leads to a balancing of the adoptions of products A and B. If a sufficiently large fraction of the nodes are hipsters, the mean final fraction of nodes that are adopters of one product is almost indistinguishable from the other. This occurs for $p_{\text{Hip}} \gtrapprox 0.09$.

In all examined cases, $\rho_{B,\text{tot}}(t \to \infty)$ approximately equals $\rho_{A,\text{tot}}(t \to \infty)$ (i.e., the steady-state fraction of nodes

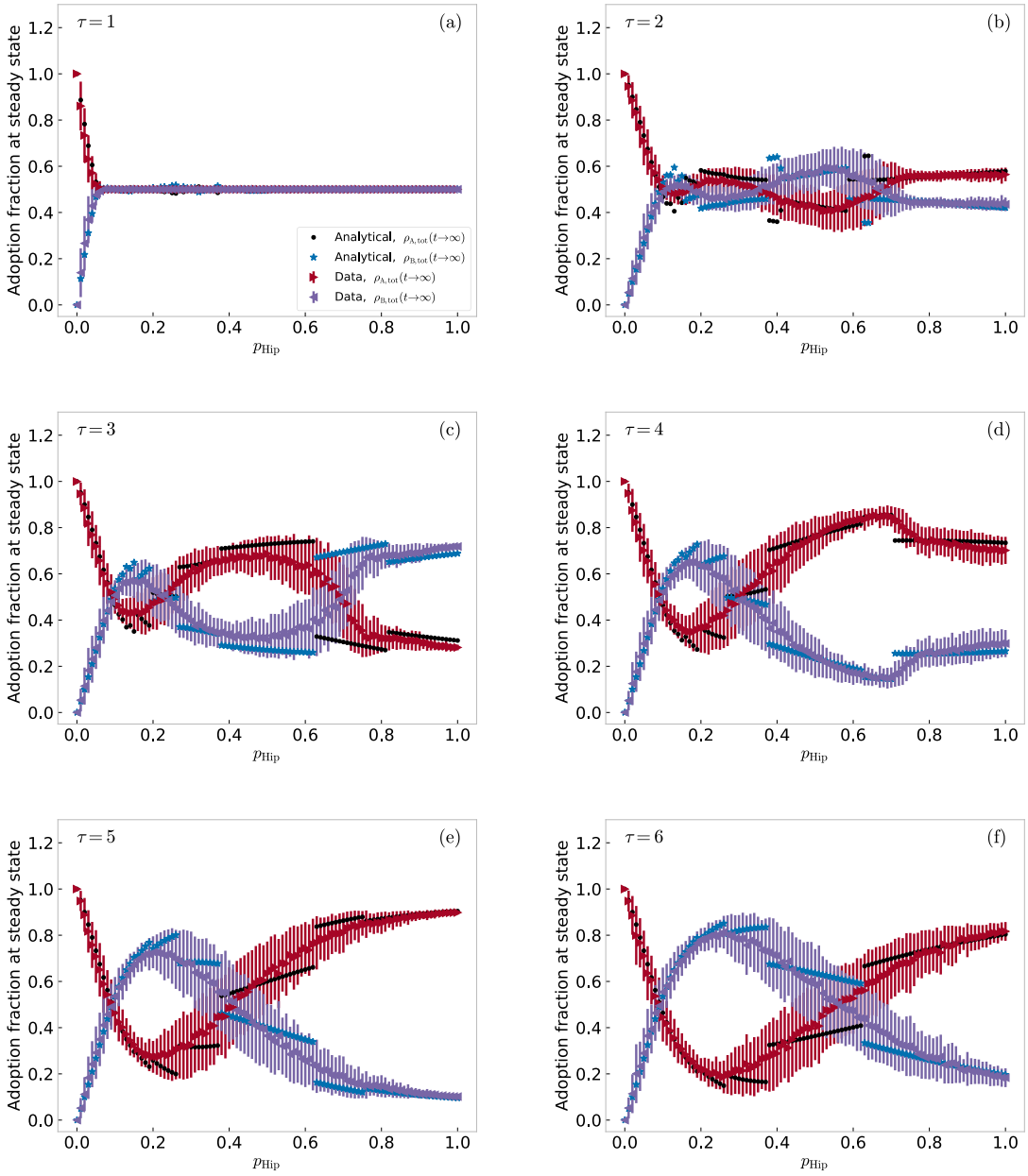

FIG. 3. Distribution of products at steady state for 10 000-node 5-regular configuration-model networks. The different panels give results of simulations of our hipster threshold model with different delay times τ for the hipster nodes. For each value of τ, we consider hipster probabilities $p_{\text{Hip}} \in [0, 1]$ in increments of 0.01. For each (p_{Hip}, τ) parameter pair, we simulate the hipster threshold model on 200 different networks that we construct using a configuration model (in which we connect stubs uniformly at random). The nodes have a threshold of $\phi = 0.19$ with probability $p_0 = 0.8$ and threshold of $\phi = 0.8$ with probability $1 - p_0 = 0.2$. For each simulation, we activate a single node, chosen uniformly at random, with product A at time $t = 0$. We stop each simulation when product adoptions are no longer occurring. We plot the mean fraction of nodes that adopt products A and B in the 200 realizations and the corresponding standard deviations of the means. [For each (τ, p_{Hip}) parameter pair, we independently construct 200 networks, and we also independently determine the initial condition for each network.] For all values of τ, the fraction of nodes that are adopters of product B at steady state increases rapidly with p_{Hip} for small p_{Hip}, reaching 0.5 at $p_{\text{Hip}} \approx 0.09$. For $\tau = 1$, which we show in panel (a), hipsters have information about the product distribution in the network without any delay, and the steady-state fractions of nodes that adopt products A and B are almost indistinguishable for $p_{\text{Hip}} \gtrapprox 0.09$. For larger values of τ, which we show in panels (b)–(f), the steady-state fraction of nodes that adopt each product varies for $p_{\text{Hip}} \gtrapprox 0.09$. The steady-state fraction of nodes that adopt product B is larger than that for product A for an interval of p_{Hip} values whose left end is at about $p_{\text{Hip}} \approx 0.09$. For $\tau \in \{2, 3\}$ [see panels (b) and (c)], we also observe that more nodes adopt product B for large values of p_{Hip}. The height of the peak in the fraction of product-B adopters above $p_{\text{Hip}} \approx 0.09$ increases with τ, reaching a value above 0.80 for $\tau = 6$ [see panel (f)]. We also plot our analytically estimated product-adoption fractions from Eq. (1). Our analytical approximation matches the behavior well for small values of p_{Hip} and large values of p_{Hip}. Between these extremes, however, our approximation has jumps in the steady-state adoption fractions of products; these discontinuities do not arise in our numerical computations.

that are adopters of product A) for $p_{\text{Hip}} \approx 0.09$. For $\tau \geqslant 2$ [see Figs. 3(b)–3(f)] and $p_{\text{Hip}} \gtrapprox 0.09$, there exists an interval of p_{Hip} values in which $\rho_{B,\text{tot}}(t \to \infty) > \rho_{A,\text{tot}}(t \to \infty)$. This interval is larger for larger values of τ, and the peak of $\rho_{B,\text{tot}}(t \to \infty)$ in this interval grows with τ, taking a value above 0.8 for $\tau = 6$ [see Fig. 3(f)]. In other words, the fraction of hipsters must be larger than about 0.09 for product B to be adopted by a larger fraction of the population than product A at steady state.

For $\tau = 2$ [see Fig. 3(b)], we observe another (and wider) p_{Hip} interval (specifically, at about [0.35,0.69]) in which product B beats product A. For $p_{\text{Hip}} \gtrapprox 0.69$, product A dominates. Hence, for $\tau = 2$, product B dominates in two p_{Hip} intervals, and product A dominates in three p_{Hip} intervals. However, $\tau = 3$ [see Fig. 3(c)] results in two intervals of dominance for each product. Product B is the more-popular product at steady state in hipster-probability intervals starting at $p_{\text{Hip}} \approx 0.09$ and $p_{\text{Hip}} \approx 0.69$. Our simulations with $\tau \geqslant 4$ result in a single p_{Hip} interval in which product B is more popular than product A at steady state. From the standard deviations, we see that different realizations with the same parameter values can yield rather different results.

Our analytical approximation and numerical computations match well for small and large p_{Hip}. However, our approximation includes jumps in the fraction of adopters for each of the products, and we do not observe such discontinuities in our simulations. The mean fraction of nodes that adopt a product in the discarded realizations is 0.0001, which is much less than the threshold of 0.10.

B. 3-regular configuration-model networks

We now examine our hipster threshold model on 3-regular configuration-model networks. Suppose that a probability $p_0 = 0.8$ of the nodes have a threshold of $\phi = 0.3$ and that the remaining probability $1 - p_0 = 0.2$ of the nodes have a threshold of $\phi = 0.65$. We perform simulations as in the 5-regular configuration-model networks (see Sec. V A) and show our results in Fig. 4.

Our results on 3-regular configuration-model networks differ from those on 5-regular configuration-model networks in several ways. One interesting result is that the fractions that adopt products A and B are very similar for $\tau = 2$ [see Fig. 4(b)] and $p_{\text{Hip}} \in [0.06, 0.93]$. Additionally, for all examined $\tau \geqslant 3$ [see Figs. 4(c)–4(f)], the $\rho_{B,\text{tot}}(t \to \infty)$ curve on 3-regular networks has one more maximum as a function of the hipster probability than the corresponding curve on the 5-regular configuration-model networks.

On 3-regular configuration-model networks with $\tau \geqslant 2$, we observe that $\rho_{B,\text{tot}}(t \to \infty)$ first becomes larger than $\rho_{A,\text{tot}}(t \to \infty)$ at about $p_{\text{Hip}} \approx 0.06$, which is lower than the hipster probability that we observed for the analogous result for 5-regular configuration-model networks. As we show in Fig. 5, this transition sometimes changes with seed size, depending on the value of the delay τ. For $\tau = 2$, the transition occurs at the same probability when we seed more nodes with product A; however, for the larger delay value $\tau = 6$, the transition moves towards larger probabilities for progressively larger sets of seed nodes who adopt product A. When the seed size is 1, we observe in Fig. 4 that the height of the first peak is lower when we simulate our model on 3-regular configuration-model networks than was the case for 5-regular configuration-model networks. For large p_{Hip}, the more-popular product at steady state is the same for $\tau = \{3, 4\}$ [see Figs. 4(c) and 4(d)] as it is for the same delay times on the 5-regular configuration-model networks, while it is opposite to that on the 5-regular configuration-model networks for $\tau = \{5, 6\}$ [see Figs. 4(e) and 4(f)]. For many parameter pairs, the standard deviations of the outcomes are large, indicating that realizations with identical parameters can yield very different outcomes.

Our analytical approximation and numerical simulations match well for $p_{\text{Hip}} \lessapprox 0.05$. However, for values of p_{Hip} that are larger than about 0.05, our analytical approximation again has jumps that we do not observe in computations. Our analytical approximation also does not match the fraction of nodes that adopt each product for $p_{\text{Hip}} = 1$ as well as it did on 5-regular configuration-model networks. This may be because 3-regular configuration-model networks have a higher edge density than 5-regular configuration-model networks, so the former depart rather significantly from satisfying a local-tree hypothesis (on which our analytical approximation relies). The mean fraction of nodes that adopt a product in the discarded realizations is 0.0002, which is much less than the threshold of 0.10.

C. Erdős–Rényi networks

We now examine our hipster threshold model on Erdős–Rényi (ER) networks. Specifically, we examine $G(N, p)$ graphs, in which one specifies the total number N of nodes, and each pair of nodes is linked independently with probability p. We choose the expected mean degree of the networks to be $z = 5$ (so the probability of an edge between any two nodes is $p = z/N$) to match the mean degree of the 5-regular configuration-model networks that we examined in Sec. V A.

We assign the same threshold $\phi_i = \phi^* = 0.2$ to each node. With this threshold, all nodes with degree $k \leqslant 5$ are vulnerable. We again consider $p_{\text{Hip}} \in [0, 1]$ (in increments of 0.01) and $\tau \in \{1, 2, 3, 4, 5, 6\}$. For each parameter pair (τ, p_{Hip}), we simulate the dynamics on 200 different networks, stop the simulations after reaching a steady state, track the final fractions of nodes that are adopters of each of the products, and calculate the corresponding mean and standard deviation of the mean from these data. As in prior simulations, we use a different set of 200 networks for each parameter value. We plot our results in Fig. 6.

As with our simulations on 5-regular and 3-regular configuration-model networks, the absence of time delay (i.e., $\tau = 1$) in the information possessed by hipsters results in $\rho_{B,\text{tot}}(t \to \infty)$ being almost indistinguishable from $\rho_{A,\text{tot}}(t \to \infty)$ [see Fig. 6(a)]. For all examined values of τ, we observe that $\rho_{B,\text{tot}}(t \to \infty)$ again increases rapidly for small values of p_{Hip}. For $p_{\text{Hip}} \approx 0.07$, we observe that $\rho_{A,\text{tot}}(t \to \infty)$ and $\rho_{B,\text{tot}}(t \to \infty)$ have similar steady-state fractions, although one can also observe rather interesting dynamics. For large values of p_{Hip}, the same product becomes the more-popular one at steady state as with the 3-regular configuration-model networks for delay times $\tau = \{4, 5, 6\}$ [see Figs. 6(d)–6(f)], but product A is the more-popular one

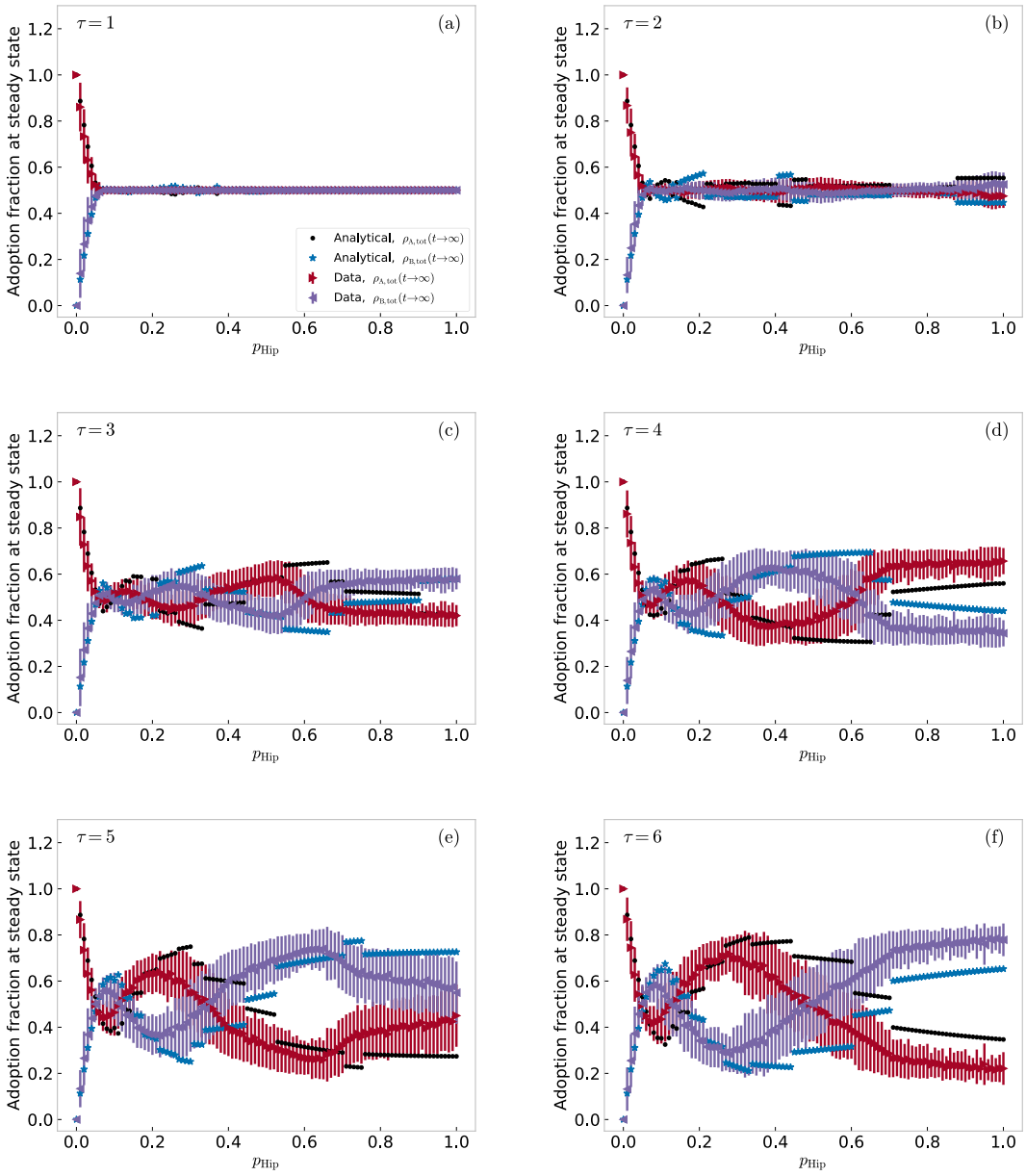

FIG. 4. Distribution of products at steady state for 10 000-node 3-regular configuration-model networks. The different panels give results of simulations of our hipster threshold model with different delay times τ for the hipster nodes. For each value of τ, we consider hipster probabilities $p_{\text{Hip}} \in [0, 1]$ in increments of 0.01. For each (p_{Hip}, τ) parameter pair, we simulate the model on 200 different networks that we construct using a configuration model (in which we connect stubs uniformly at random). The nodes have a threshold of $\phi = 0.3$ with probability $p_0 = 0.8$ and threshold of $\phi = 0.65$ with probability $1 - p_0 = 0.2$. For each simulation, we activate a single node, chosen uniformly at random, with product A at time $t = 0$. We stop each simulation when product adoptions are no longer occurring. We plot the mean steady-state fraction of nodes that adopt products A and B in the 200 realizations and the corresponding standard deviations of the means. [For each (τ, p_{Hip}) parameter pair, we independently construct 200 networks, and we also independently determine the initial condition for each network.] For all values of τ, the steady-state fraction of nodes that adopt product B increases rapidly with p_{Hip} for small p_{Hip}, reaching 0.5 at $p_{\text{Hip}} \approx 0.06$. For $\tau = 1$, which we show in panel (a), hipsters have information about the product distribution in the network without any delay, and the steady-state fractions of nodes that adopt products A and B are almost indistinguishable for $p_{\text{Hip}} \gtrapprox 0.06$. For $\tau = 2$, which we show in (b), the fractions of nodes that adopt the two products are similar (though one can see some interesting dynamics) until $p_{\text{Hip}} \approx 0.93$, above which product B is the more-popular product. For larger values of τ [see panels (c)–(f)], the fraction of nodes that adopt each product varies for $p_{\text{Hip}} \gtrapprox 0.05$. The height of the peak, which occurs at $p_{\text{Hip}} \approx 0.08$, of the node fraction that adopts product B increases with τ, reaching a value of over 0.6 for $\tau = 6$ [see panel (f)]. For all time delays $\tau \geqslant 2$ [see panels (b)–(f)], the maximum steady-state fraction that adopts product B does not take place at p_{Hip} values near 0.08; instead, it occurs for much larger values of p_{Hip}. We also plot our analytically estimated fractions of product adoption from Eq. (1). Our approximation matches well with our computations for small values of p_{Hip}. For $p_{\text{Hip}} \gtrapprox 0.06$, however, our approximation does not do well. Our analytical solution includes jumps in the steady-state adoption fractions of the products, but these do not arise in our numerical simulations.

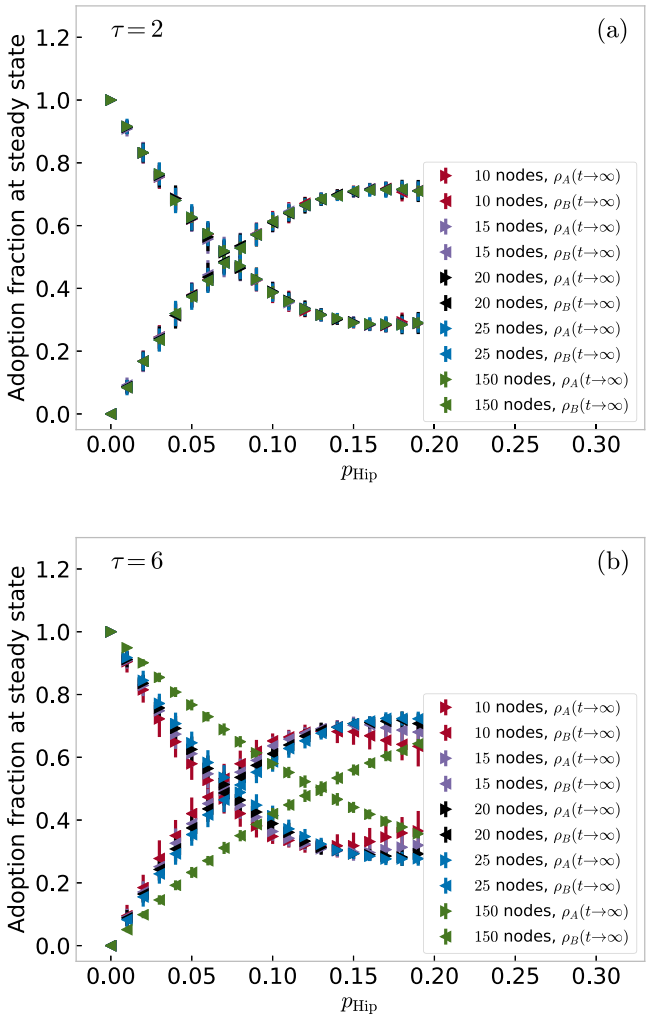

FIG. 5. Distribution of products at steady state for 10 000-node 3-regular configuration-model networks with different seed sizes, where all seed nodes adopt product A. We show the distribution of products for delays of (a) $\tau = 2$ and (b) $\tau = 6$. With $\tau = 2$, the adoption fraction is indistinguishable for the different seed sizes. For $\tau = 6$, our results vary for different seed sizes, but the qualitative behavior is consistent across all cases: the steady-state fraction of nodes that adopt product B increases rapidly with p_{Hip}, and equal fractions adopt products A and B at a value of p_{Hip} that increases slowly with seed size. For seed sets with 10 to 25 nodes, equal fractions of nodes adopt the two products at $p_{\mathrm{Hip}} \approx 0.07$. For a seed set with 150 nodes, equal fractions adopt the two products at $p_{\mathrm{Hip}} \approx 0.13$.

for $\tau = 3$ [see Fig. 6(c)]. We generally observe large standard deviations of the outcomes of realizations with given parameter values. The mean fraction of nodes that adopt a product in the discarded realizations is 0.0072. This is larger than what we observed for 3-regular and 5-regular configuration-model networks, but it is still much smaller than the threshold of 0.10.

Our analytical approximation and numerical simulations once again match well for small values of p_{Hip} (specifically, for $p_{\mathrm{Hip}} \lessapprox 0.07$). For larger values of p_{Hip}, our analytical approximation has jumps in the fraction that adopt each product; we again do not observe this phenomenon in our simulations. One possibility, which we suggested in our discussion of 3-regular configuration-model networks in Sec. V B, is whether our analytical approximation is running into problems because we are considering networks that are not locally treelike (although similar approximations are known to be effective for many networks that are not locally treelike [71]). Additionally, note that the mean local clustering coefficient for our ER networks with $z = 5$ is 0.00058 ± 0.00018, so our networks have very few 3-cycles. If we ignore which product is adopted and pretend that the two products are the same, we recover the usual WTM model; the present paper uses an analytical approximation that is known to work in that situation [31]. Our own recent work has demonstrated that this type of analytical approximation is also effective for a WTM augmented with "synergistic" social influence from nodes other than nearest neighbors [27], so the incorporation of different types of nodes (rather than the lack of a locally treelike network structure) appears to be the likely cause of the breakdown of the approximation, especially given that our approximation becomes worse as we increase the hipster probability p_{Hip}.

D. The NORTHWESTERN25 Facebook network

In Sec. V B, we showed simulations of our hipster threshold model model on the NORTHWESTERN25 network from the FACEBOOK100 data set for two choices of the (p_{Hip}, τ) parameter pair. We now examine our model on the NORTHWESTERN25 network more systematically by considering more initial conditions and a wider variety of parameter values. Suppose that each node has a threshold of $\phi^* = 1/33$. In each of our simulations, we use a single node, chosen uniformly at random, as a seed at $t = 0$ and consider $\tau \in \{1, 2, 3, 4, 5, 6\}$ and $p_{\mathrm{Hip}} \in [0, 1.0]$ (in increments of 0.01).

In Fig. 7, we show the mean fraction of nodes that are adopters of products A and B at steady state. For each choice of parameters, we choose a set of 200 initial conditions, and we calculate means over these simulations. The most striking difference between these plots compared to those for our model on synthetic networks in previous sections is that now it takes more hipsters to obtain equal steady-state fractions of adopters of the two products. In the NORTHWESTERN25 network, the fractions that adopt the two products become equal when roughly one fifth of the nodes are hipsters. We also observe that the height of the first peak of $\rho_{B,\mathrm{tot}}(t \to \infty)$ increases with τ, as was also the case in the synthetic networks that we examined, and the standard deviations are once again large for most parameter pairs. The mean fraction of nodes that adopt a product in the discarded realizations is 0.0001, which again is much less than the threshold of 0.10.

VI. MAJOR IMPACT OF A FEW INDIVIDUALS: APPROXIMATION ON k-REGULAR TREES

In Sec. V, we observed that even just a few hipster nodes can cause product B to become the more-popular product at steady state, but we have not yet explored how this phenomenon can occur. In this section, we argue why even just a few antiestablishment nodes can have a major impact on

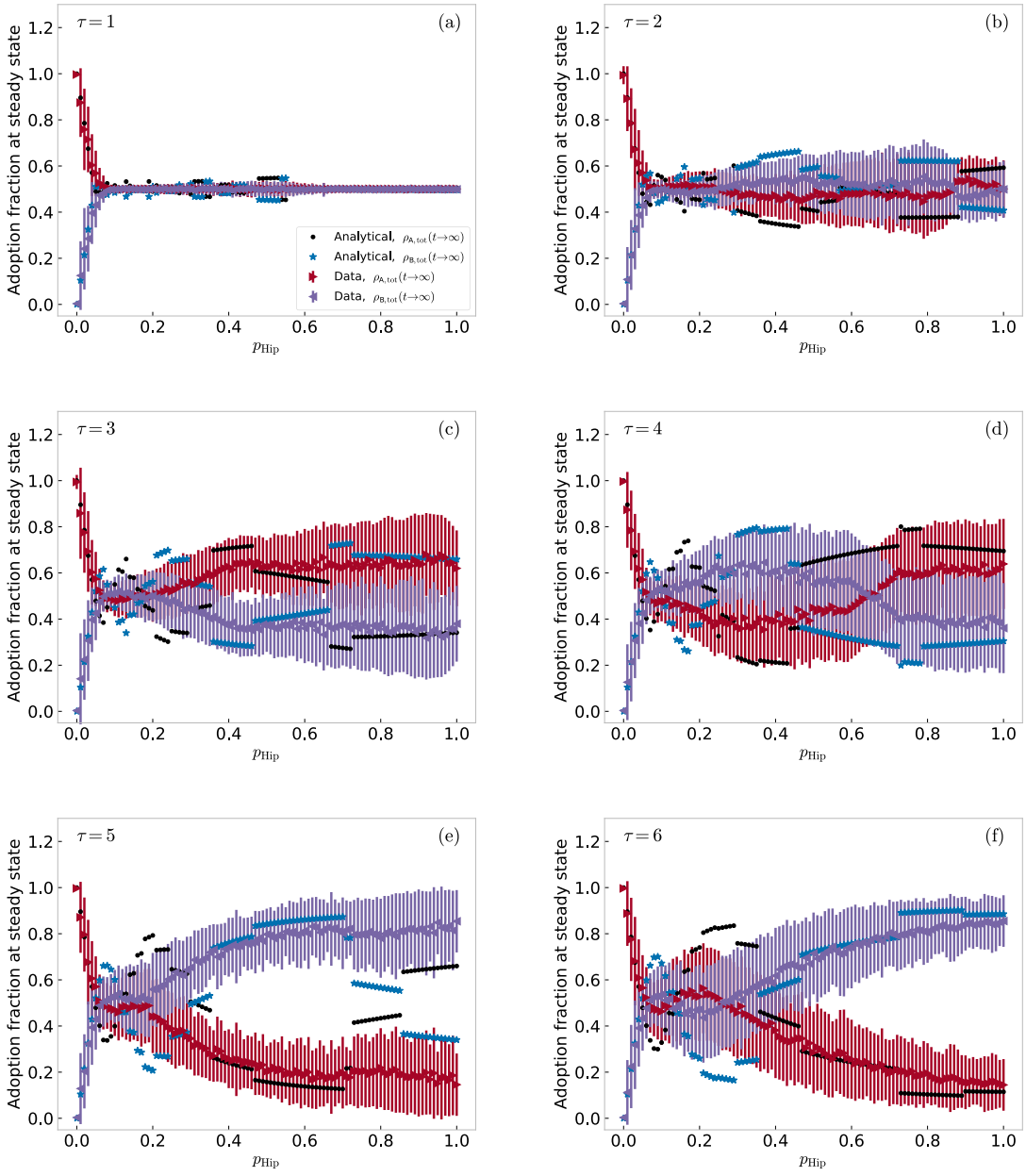

FIG. 6. Distribution of products at steady state for 10 000-node Erdős–Rényi networks with an expected mean degree of $z = 5$. The different panels give results of simulations of our hipster threshold model with different delay times τ for the hipster nodes. For each value of τ, we consider hipster probabilities $p_{\text{Hip}} \in [0, 1]$ in increments of 0.01. For each (τ, p_{Hip}) parameter pair, we simulate the model on 200 different networks and initial conditions. Each node has a threshold of $\phi = 0.2$. For each simulation, we activate a single node, chosen uniformly at random, with product A at time $t = 0$. We stop each simulation when product adoptions are no longer occurring. We plot the mean steady-state fraction of nodes that adopt products A and B in the 200 realizations and the corresponding standard deviations of the means. [For each (τ, p_{Hip}) parameter pair, we independently construct 200 networks, and we also independently determine the initial condition for each network.] For all values of τ, the fraction of nodes that adopt product B increases rapidly with p_{Hip} for small p_{Hip}, reaching 0.5 at $p_{\text{Hip}} \approx 0.07$. For $\tau = 1$, which we show in panel (a), hipsters have information about the product distribution in the network without any delay, and the steady-state fractions of nodes that adopt products A and B are almost indistinguishable for $p_{\text{Hip}} \gtrapprox 0.07$. For larger values of τ [see panels (b)–(f)], the steady-state fraction of nodes that adopt each product varies for $p_{\text{Hip}} \gtrapprox 0.07$. For all $\tau \geqslant 3$ [see panels (c)–(f)] the fraction of nodes that adopt product B is largest for a small interval of p_{Hip} around $p_{\text{Hip}} \approx 0.10$. For $\tau \geqslant 4$ [see panels (d)–(f)], we observe an additional, large-p_{Hip} interval in which a majority of the nodes adopt product B. We also plot our analytically estimated fractions of product adoption from Eq. (1). Our analytical curves and numerical simulations match well for small values of p_{Hip}. For larger hipster probabilities, however, our analytical approximation is not accurate. For $\tau = 5$ [see panel (e)], it predicts incorrectly that product A is the more-popular product at steady state for large values of p_{Hip}. Our analytical results also include jumps in the steady-state adoption fractions of products that are not present in our numerical simulations.

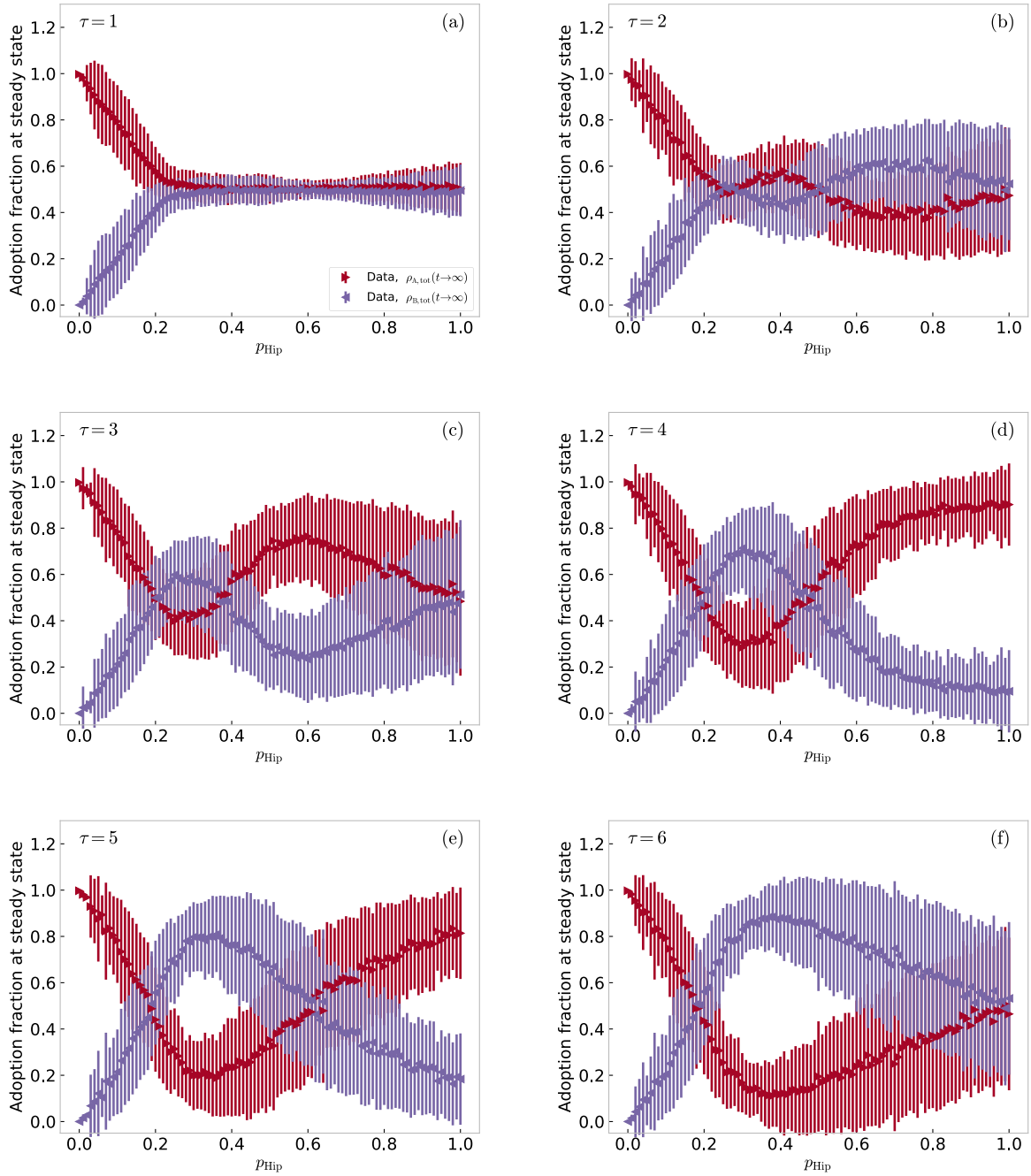

FIG. 7. Distribution of products at steady state for the NORTHWESTERN25 network from the FACEBOOK100 data set. The different panels give results of simulations of our hipster threshold model with different delay times τ for the hipster nodes. For each value of τ, we consider hipster probabilities $p_{\text{Hip}} \in [0, 1]$ in increments of 0.01. For each (τ, p_{Hip}) parameter pair, we simulate the hipster threshold model on the NORTHWESTERN25 network with 200 choices for the seed node, chosen uniformly at random, which adopts product A at $t = 0$. We use a different set of 200 nodes for different parameter values. Each node has a threshold of $\phi = 1/33$. We plot the mean fractions of nodes that are adopters of products A and B at steady state in the 200 realizations and the corresponding standard deviations of the means. For all values of τ, the steady-state fraction of nodes that adopt product B increases rapidly with p_{Hip} for small p_{Hip}, reaching 0.5 at $p_{\text{Hip}} \approx 0.2$ for $\tau \geqslant 3$ [see panels (c)–(f)] and for larger values of p_{Hip} for $\tau \leqslant 2$ [see panels (a) and (b)]. For $\tau = 1$, which we show in panel (a), hipsters have information about the product distribution in the network without any delay, and the steady-state fractions of nodes that adopt products A and B are very similar for $p_{\text{Hip}} \gtrapprox 0.3$. For larger values of τ [see panels (b)–(f)], the fraction of nodes that adopt each product varies nonmonotonically for $p_{\text{Hip}} \gtrapprox 0.2$. For $\tau \geqslant 3$ [see panels (c)–(f)], the fraction of nodes that adopt product B is largest for a small interval of p_{Hip} around $p_{\text{Hip}} \approx 0.3$. This is the single peak in the adoption of product B in the mean over these simulations. For $\tau = 2$ [see panel (b)], product B is the more-popular product for large values of p_{Hip}. For $\tau \geqslant 2$ [see panels (b)–(f)], product B is the more-popular product for a p_{Hip} interval starting at $p_{\text{Hip}} \approx 0.20$. The length of this interval increases with τ, and both the hipster probability that produces the peak fraction in this interval and (especially) the value of the peak fraction increase with τ. For $\tau = 6$ [see panel (f)], the maximum fraction of nodes that adopt product B is about 0.90.

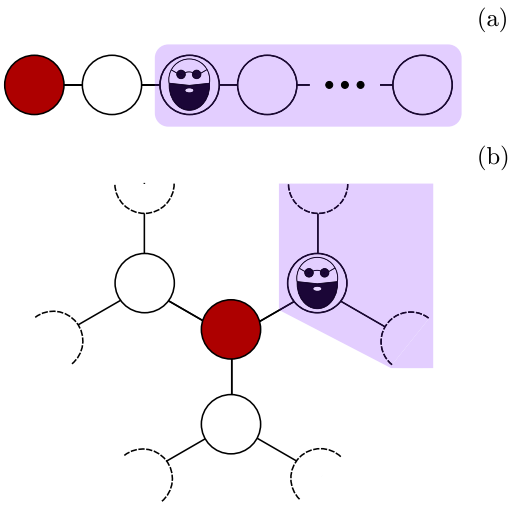

FIG. 8. (a) A line graph in which the leftmost node is the only seed. (It adopts product A.) If all nodes are vulnerable and exactly one node is a hipster, all nodes to the hipster's right eventually adopt product B. (b) A 3-regular tree in which the central node is the only seed. (It adopts product A.) If the tree has a single hipster, all nodes that are descendants of the hipster eventually adopt product B.

steady-state adoptions in our model. From studying this mechanism, we expect that some similar qualitative phenomena occur in many other models, including ones with stochastic update rules.

To understand why even a few hipster nodes can dramatically increase the number of product-B adopters at steady state, we first consider a line of N nodes, which we number from one end to the other with the labels $0, 1, 2, \ldots, N-1$. Each node is adjacent to its immediate neighbors, with 2 neighbors each, except for nodes 0 and $N-1$ (which each have degree 1). For the sake of the argument, we assume that all nodes are vulnerable and that there is no delay in information (so that $\tau = 1$). We also suppose that node 0 is the only seed, so it has adopted product A at time $t = 0$ [see Fig. 8(a)]. If there are no hipsters in the line, all nodes in this scenario eventually adopt product A. If, by contrast, a single node i is a hipster, then all nodes $j \geqslant i$ eventually adopt product B. Therefore, if each node has the same independent probability of being a hipster, the expected steady-state fraction of product-B adopters approaches $1/2$ as $N \to \infty$. In this case, the presence of a single hipster node increases the expected steady-state fraction of nodes that adopt product B from 0 nodes to half of the nodes. The main idea is that early adopters can influence later adopters in a way that depends on the adoption paths that are available [39]. Moreover, although the expected steady-state fraction of product-B adopters is $1/2$, a single simulation of the model is equally likely to result in any number of product-B adopters, because each node is equally likely to be the hipster. This may be a reason why we observe large standard deviations in different realizations of our model on the various types of networks. For more complicated network topologies, although it is no longer true in general that different steady-state fractions of product-B adopters are equally probable, the steady-state adoption fraction in a given simulation depends significantly on where hipsters are located in a network.

With this simple example in mind, we now turn to a more difficult example: a k-regular tree of vulnerable nodes in which the central node (which we label as node 0) is the only seed [see Fig. 8(b)]. As usual, the seed has adopted product A. As in the above example on a line graph, if a certain node is a hipster, it will force the nodes that follow it in an adoption path to adopt product B, rather than product A. We can divide the tree into hierarchical "levels." The central node is 0, and it is adjacent to k nodes in level 1. Each node in level 1 is adjacent to $k-1$ nodes in level 2, each node in level 2 is adjacent to $k-1$ nodes in level 3, and so on. Hence, level $l \geqslant 1$ includes $n_l = k(k-1)^{l-1}$ nodes, and all nodes except those in the last level (which have degree 1) have degree k. Such a k-regular tree with L levels has $N = 1 + \sum_{l=1}^{L} k(k-1)^{l-1}$ nodes. In the limit of infinitely many levels, a k-regular tree is a Bethe lattice.

Suppose that there is a single hipster in the network. By construction, we can view any hipster as the root in a rooted tree. We can then make the following approximation. If all nodes have an equal, independent probability of being a hipster, the probability for there to be a hipster in level l is equal to the fraction of nodes (n_l/N) that are in that level. If a hipster is present in level l, all nodes in an adoption path after that hipster (i.e., all of its descendants) eventually adopt product B. Because level l has n_l nodes, a single hipster in level n_l causes $1/n_l$ of the nodes in later levels ($l' \geqslant l+1$) to adopt product B. Therefore, one can approximate the expected steady-state fraction of product-B adopters as

$$\bar{\rho}_B(n_{\mathrm{Hip}} = 1) \approx \sum_{s=1}^{L} \frac{n_s}{N} \frac{1}{n_s} \left[\frac{1}{N} \sum_{l=s}^{L} k(k-1)^{l-1} \right] = \frac{1}{N^2} \sum_{s=1}^{L} \sum_{l=s}^{L} k(k-1)^{l-1}. \quad (5)$$

For a spreading process on a network, one can construct a dissemination tree, which describes how a contagion spreads through the network [39]. For a k-regular tree with only vulnerable nodes, the dissemination tree is the same k-regular tree, except that all edges are directed from the center towards the periphery. The above analysis indicates that the fraction of nodes that a single hipster can cause to adopt product B is related to the properties of a dissemination tree. For dissemination trees with a progressively larger number of mean descendants per node, we expect a progressively larger fraction of nodes in an associated network to adopt product B when a single hipster is present in the network. Equation (5) illustrates that, for a given network, increasing the number of hierarchical levels in a dissemination tree tends to result in a larger number of product-B adopters from a single hipster.

To obtain a naive estimate of the fraction of product-B adopters as a function of n_{Hip} when $n_{\mathrm{Hip}} \ll N$, we multiply Eq. (5) by n_{Hip}/N, thereby assuming that adding a second hipster to the network leads to as many product-B adopters as the number that resulted from the original hipster [76]. However, the second hipster may be a descendant of the existing hipster, such that it does not lead to any additional product-B

adoptions. To account for this, we develop a recursive formula that takes this possibility into account.

Imagine adding hipsters to a network one at a time (allowing the possibility of choosing the same node multiple times when attempting to add hipsters). We seek to approximate the expected fraction of product-B adopters at steady state in a network with n_{Hip} hipsters as a function of the expected fraction of product-B adopters at steady state in a network with $n_{\text{Hip}} - 1$ hipsters. Let P_{desc} denote the probability that the additional hipster is a descendant of another hipster in the network. Adding a hipster has two possible outcomes: (1) the hipster is a descendant of another hipster, such that it does not yield additional product-B adopters; or (2) the hipster is not a descendant of another hipster, so on average it yields another $\bar{\rho}_B(n_{\text{Hip}} = 1)$ fraction of product-B adopters at steady state. We summarize this reasoning in the formula

$$\bar{\rho}_B(n_{\text{Hip}}) \approx \bar{\rho}_B(n_{\text{Hip}} - 1)P_{\text{desc}} + \left[\bar{\rho}_B(n_{\text{Hip}} - 1) + \bar{\rho}_B(n_{\text{Hip}} = 1)\right](1 - P_{\text{desc}}) . \tag{6}$$

In a k-regular tree with sufficiently few hipsters, all descendants of a hipster are product-B adopters at steady state, so the probability that the nth hipster descends from one of the previous $n - 1$ hipsters equals the expected fraction of nodes that are product-B adopters at steady state in a network with $n_{\text{Hip}} = n - 1$ hipsters. We thus insert $P_{\text{desc}} = \bar{\rho}_B(n_{\text{Hip}} - 1)$ into Eq. (6) to obtain

$$\bar{\rho}_B(n_{\text{Hip}}) \approx \bar{\rho}_B(n_{\text{Hip}}-1) + \left[1-\bar{\rho}_B(n_{\text{Hip}} - 1)\right]\bar{\rho}_B(n_{\text{Hip}} = 1) . \tag{7}$$

In Fig. 9, we compare the analytical expression in Eq. (7) to computations using 3-regular and 5-regular trees. Our analytical approximation is a good match for our simulations when n_{Hip}/N is small. For larger n_{Hip}/N, Eq. (7) overestimates the steady-state fraction of nodes that adopt product B. Hipsters need not always adopt product B; with more hipsters, it becomes increasingly likely that product B is not always the less-popular product.

Our analysis has several interesting consequences. For example, it yields some understanding of how the delay τ affects the steady-state adoption fractions of each product. To illuminate the impact of τ, it is helpful to consider the following situation. Suppose that, because of hipsters, product B becomes more popular than product A at some point during a simulation of our model. A delay of $\tau \geqslant 2$ postpones this time, at which hipsters start adopting product A rather than product B, so we expect hipsters who adopt product A to have fewer descendants than if $\tau = 1$. This provides an argument for why the height of the peak of the fraction of product-B adopters as a function of p_{Hip} increases with the delay, and it sheds some light on the effects of the delay. If there is no delay (i.e., $\tau = 1$) and there are many hipsters, then hipsters tend to balance the popularities of the two products, leading to roughly equal fractions of the two products at steady state (as we saw in our simulations on all networks in Sec. V).

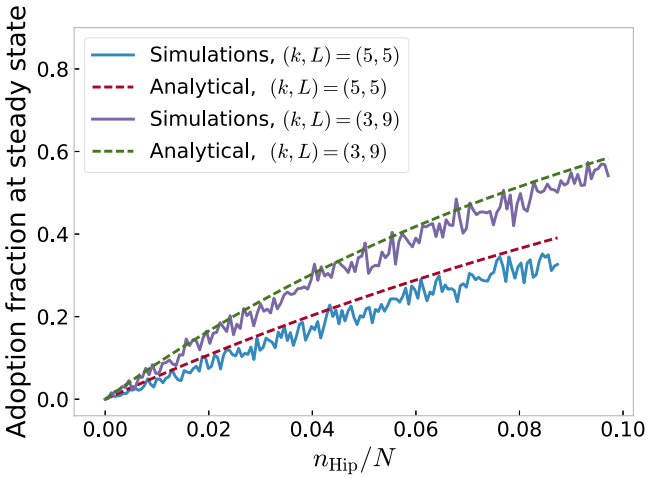

FIG. 9. Fraction of nodes in k-regular trees with L levels that are adopters of product B at steady state. We show results for 3-regular trees with 9 levels (and hence with $N = 1534$ nodes in total) and for 5-regular trees with 5 levels (and hence with $N = 1706$ nodes in total). We plot the recursive approximation from Eq. (7) and show our simulation results, averaged over 100 realizations, for the steady-state fraction of nodes that adopt product B as a function of the fraction n_{Hip}/N (with $n_{\text{Hip}} \in \{0, 1, \ldots, 150\}$) of hipsters in the network. As expected, our approximation is good for $n_{\text{Hip}} \ll N$.

Our analysis also improves our understanding of how various changes to our hipster model can affect steady-state results. For example, suppose that we use a stochastic updating rule instead of a deterministic one. Although the above analysis does not rely on the deterministic nature of our updating rule, it does indicate that adoption order is important, and anything that changes the adoption order (such as using a stochastic update rule or updating node states asynchronously instead of synchronously) may change the outcome of simulations [77]. However, from our analysis, we do expect some features of our results to be robust even with different update rules and update orders. For example, for either stochastic update rules or asynchronous updating, we expect an increase in the number of steady-state product-B adopters with increasing p_{Hip} for small values of p_{Hip}, followed by a decrease (or stall) in the number of steady-state product-B adopters when enough hipsters are present in a network (as some of them will now adopt product A). However, the rate at which the steady-state fraction of product-B adopters increases with p_{Hip} for small p_{Hip} is likely to be influenced by stochastic update rules and asynchronous updating. For instance, suppose that we use the same rules for product selection but that we employ an asynchronous updating process in which, during each time step, we select a node uniformly at random to update; we repeat this selection process some number of times during the same time step; and we then advance time by one step. We then continue with this process in our simulations until no further spreading occurs. In this case, every node in a network can potentially adopt a product even in the first time step, and the process tends to spread at a different rate—it can be either faster or slower—than in synchronous updating. Because the hipsters are distributed uniformly at random

and the rules governing product choice are the same as in our original model, changing the number of adopters during each time step can directly affect hipsters, as their product choice is time-dependent. (Other nodes are affected indirectly, as they can experience a different product distribution in their neighborhoods.) Consequently, a faster initial spreading would increase early product-B adoption for a delay $\tau \geqslant 2$, as all hipsters are guaranteed to choose product B for time steps $t \leqslant \tau$. To test this, we simulate the spreading of products on 5-regular configuration-model networks with $\tau = 2$ and a single product-A adopter as a seed. We use the asynchronous updating procedure that we just described above. Averaging our results over 100 realizations [which we determine as in Fig. 3(b)], we find that the steady-state product-B adoption fraction increases faster as we increase p_{Hip} for small values of p_{Hip} than what was the case for synchronous updating [see Fig. 3(b)]. As we expected, we also find that the product-B steady-state adoption fraction decreases as we increase p_{Hip} for larger values of p_{Hip}. More generally, different update mechanisms and update orders can yield different dissemination trees, which describe how a contagion spreads through a network [39]. This can, in turn, impact steady-state product popularities.

Another aspect that tends to alter a dissemination tree is changes in the threshold distribution of nodes in a network. For example, with a threshold distribution in which all nodes are vulnerable, a spreading process can reach a steady state very quickly, and there are then few hierarchical levels in the associated dissemination tree. By contrast, a threshold distribution for which a network starts with fewer vulnerable nodes may take longer to reach a steady state, and one thus expects more levels in an associated dissemination tree. From our analysis, we see that this in turn can increase the steady-state adoption fraction of product B for small values of p_{Hip}. Performing simulations on 5-regular configuration model networks with $\tau = 2$ [as in Fig. 3(b)] and 150 seed nodes with probabilities $p_0 = 1.00$, $p_0 = 0.90$, and $p_0 = 0.80$ supports this intuition. When we examine small values of p_{Hip}, the steady-state fraction of product-B adopters increases slightly more slowly for larger values of p_0 as we increase p_{Hip}.

For some network families, we expect networks with different numbers of nodes to have different fractions of product-B adopters at steady state. To illustrate this point, we again consider line networks and k-regular trees. For a line network with a single hipster and a seed node that adopts product A at one end, the expected steady-state fraction of product-B adopters is roughly $1/2$ for a line with any number of nodes. However, adding another level to a k-regular tree with a single seed node that adopts product A affects the expected steady-state fraction of product-B adopters. For example, a 3-regular tree with 3 levels (and hence with 10 nodes in total) has an expected steady-state fraction $\bar{\rho}_B = 15/100$ of product-B adopters, whereas a 3-regular tree with 4 levels (and hence with 22 nodes in total) has $\bar{\rho}_B = 1/10$. This difference occurs because adding another level to the 3-regular tree increases the fraction of nodes that are leaves. Therefore, the randomly distributed hipsters have fewer descendants on average in a dissemination tree, decreasing the expected fraction of product-B adopters at steady state. In simulations on regular configuration-model networks with 10^3 nodes (using several values of τ for 3-regular networks and $\tau = 3$ for 5-regular ones) for small values of p_{Hip}, we observe the same fast increase in steady-state product-B adopters as we increase p_{Hip} that we observed previously for these networks with 10^4 nodes (see, e.g., Fig. 4). However, for large values of p_{Hip}, the steady-state product-B adopter fraction can differ substantially in simulations on networks with 10^3 nodes and 10^4 nodes. More generally, our analysis demonstrates that the number of nodes in a network can affect steady-state product distributions. Even taking seed-size scaling into consideration (see [70]), dissemination trees can still change, potentially affecting qualitative steady-state results.

Changing the way that nodes choose which product to adopt can also drastically influence simulation outcomes. For example, consider a modification of our model in which a hipster that becomes active at time step t adopts the product that is less popular among its neighbors at time $t - \tau$. Furthermore, suppose that two competing products are spreading in a k-regular tree in which the central node is the only seed. As usual, the seed has adopted product A. When we constructed our approximation (7) for the steady-state distribution of products in the limit of few hipsters, we assumed that every hipster adopts product B. In the modified hipster model in our current discussion, this approximation may be very bad. Hipsters who descend from other hipsters may adopt product A. We thus expect the product-B steady-state adoption fraction to increase more slowly with p_{Hip} for small p_{Hip} if a hipster adopts the product that is less popular among its neighbors, rather than the less-popular product among all active nodes in a network. Performing simulations of the modified hipster model on 5-regular configuration-model networks with $p_0 = 0.80$ vulnerable-node probability, $\tau = 1$, and a single seed node [as in Fig. 3(a)] for $p_{\text{Hip}} \leqslant 0.14$, we find that a smaller (or equal, for $p_{\text{Hip}} = 0$) steady-state fraction of nodes adopts product B than in our observations for our focal hipster model.

VII. CONCLUSIONS

It is important to study what makes information, opinions, diseases, memes, products, misinformation, alternative facts, and other things that originate in a small subpopulation spread to a large fraction of nodes in a network. Such scenarios can arise in the adoption of products and the spreading of memes, and they can also occur in antiestablishment behavior, which can significantly impact the geopolitical landscape.

We developed a threshold model to examine the impact of anticonformists (so-called "hipsters") on the spreading of two competing products (one of which, labeled B, is not adopted by any node at the beginning of our simulations). We examined our hipster threshold model on various types of networks, and we considered different probabilities of the hipster nodes and different amounts of time delay in the global information that the hipsters possess. In the absence of a time delay, we found that hipsters tend to balance the adoption of the two competing products. For all other delay values and all examined types of networks, we observed that the steady-state fraction of nodes that adopt product B (i.e., the

product that would not be adopted in the absence of hipsters) grows rapidly with the probability of hipsters. Surprisingly, for all of our networks, we needed only a small probability of hipsters to observe many situations in which product B is comparably popular, or even more popular, than product A at steady state. In our simulations on a variety of synthetic networks, we found that it is often sufficient for fewer than 10% of the nodes to be hipsters for product B to become at least as widespread as product A (the only product that has any adopters at time $t = 0$). For the NORTHWESTERN25 Facebook network, roughly 20% of the nodes need be hipsters for product B to be as widespread as product A at steady state.

Using a line network and k-regular trees, we illustrated why the fraction of nodes that adopt product B increases rapidly for small values of p_{Hip}. On these networks, we obtained good agreement between simulations and an approximation of the steady-state fraction of nodes that adopt product B in the limit of few hipsters. From our analytical approximation in the few-hipster regime, we observed that the steady-state product-B adoption fraction increases with the distance between the seed node and other nodes. This gives some insight into why there is a much slower increase in product-B adopters for the spreading process on the Facebook network than in the examined synthetic networks, as the former has a smaller mean geodesic (i.e., shortest) path length than our synthetic networks. It also suggests that different realizations with identical parameter values may result in very different steady-state adoption fractions, given that we use random processes to choose hipsters and seed nodes. One consequence of such sensitivity to initial conditions is large standard deviations in the mean steady-state adoption fraction of each product, which is what we observed in most cases. The same mechanistic insight suggests that a larger delay τ results in more hipsters adopting product B early in a simulation, and each of these early adopters influences the product choice of later adopters. We believe that postponing the time at which hipsters choose product A instead of product B is the main reason that a progressively larger delay τ results in a progressively larger peak of the expected product-B adoption fraction as a function p_{Hip}. Finally, the mechanistic insight from our approximation in the few-hipster limit also helps illustrate that the properties—such as threshold distributions, the number of nodes in a network, and update rules—of an update rule or network that affect dissemination trees (which describe how a contagion spreads through a network) can affect observations at steady state, although some qualitative observations should be robust under such variations.

Our hipster threshold model exhibits a variety of fascinating dynamics on different types of networks. For example, when there is a delay in global information (i.e., $\tau \geqslant 2$) and the hipster probability p_{Hip} is large, we observed nontrivial characteristics in the number of intervals of hipster probabilities for which a given product is more popular at steady state. The quality of the match between our pair approximation and numerical simulations also depends both on network structure and on the hipster probability. For example, our approximation was effective for small values of p_{Hip}, and it correctly produced a fast increase in product-B adopters with increasing values of small p_{Hip}; it did reasonably well for large values of p_{Hip} for 5-regular configuration-model networks (except for abrupt jumps that are not present in the simulations); it achieved mixed results for 3-regular configuration-model networks (although it yielded the correct result for the more-popular product at steady state for $p_{\text{Hip}} \approx 1$ in all but one instance); and it was ineffective for Erdős–Rényi networks (where it was incorrect about which product is more popular at steady state for $p_{\text{Hip}} \approx 1$ in roughly half of the cases).

When there is a delay (i.e., $\tau \geqslant 2$) in the global adoption information that is available to hipsters, we also found that the steady-state fraction of nodes that adopt a product varies nonmonotonically with the probability of hipsters. For some delay values, this steady-state fraction peaks for multiple, disparate values of the probability of hipsters; for other delay values, however, there is only a single peak. This behavior also depends on the network type on which spreading occurs. If there is no delay in the global adoption information that is available to hipsters (i.e., $\tau = 1$), we found that the steady-state fraction of nodes that adopt product B first increases rapidly with p_{Hip} and then stabilizes, such that approximately half of the nodes adopt each product.

In summary, in our hipster model, even when only one of two products is adopted when spreading begins, small probabilities of antiestablishment nodes can lead to a competitor product being adopted by a majority in a population. Our simple model and numerical experiments may help shed light on the road to success for antiestablishment choices in elections and competition between products, as such success (and qualitative differences in final outcomes between competing products, political candidates, and so on) can arise rather generically from a small number of antiestablishment individuals and ordinary processes of social influence on normal individuals. In our model, the hipsters always choose to adopt the product that is less popular at time step $t - \tau$. If all hipsters regard product A as the established choice at all time steps—regardless of the actual distribution of adopted products—the steady-state adoption fractions of product B become even larger, and the antiestablishment choice (which is product B, in our example) becomes even more successful than what we observed in our simulations. This more extreme situation may be relevant in elections in which the conception of who is part of the establishment may not change during weeks of campaigning and polls that forecast which candidate will win and take office.

In future work, it would be interesting to study our hipster model in more detail, including investigating whether the fraction of hipsters is connected to any notion of criticality, and to extend the model in various ways. Generalizations of our model may be helpful for studying the impact of antiestablishment hubs, such as alt-right broadcasting services or alt-right Twitter accounts with many followers. Understanding what makes a large population of voters vulnerable to the views of a few antiestablishment nodes may help guard populations from manipulation and fake information during elections and other scenarios.

ACKNOWLEDGMENTS

Part of this work was carried out at the Mathematical Institute at University of Oxford. We thank James Gleeson, Kameron Decker Harris, Shankar Iyer, and Mikko Kivelä for

helpful discussions, and M.A.P. thanks Ben Williamson for early inspiration to study hipsters. We also thank Serge Galam for bringing his work to our attention. J.S.J. thanks the Mathematical Institute at University of Oxford for hospitality and Mogens H. Jensen (Niels Bohr Institute, University of Copenhagen) for making this project possible; and he acknowledges funding through the University of Copenhagen UCPH 2016 Excellence Programme for Interdisciplinary Research.

[1] S. Lehmann and Y.-Y. Ahn (eds.), *Complex Spreading Phenomena in Social Systems: Influence and Contagion in Real-World Social Networks* (Springer International Publishing, Cham, Switzerland, 2018); preprints of some chapters are available at https://socialcontagionbook.github.io.

[2] M. A. Porter and J. P. Gleeson, Dynamical systems on networks: A tutorial, Front. Appl. Dyn. Syst.: Rev. Tutorials **4**, 1 (2016).

[3] N. A. Christakis and J. H. Fowler, Social contagion theory: Examining dynamic social networks and human behavior, Stat. Med. **32**, 556 (2013).

[4] J. Borge-Holthoefer, R. A. Baños, S. González-Bailón, and Y. Moreno, Cascading behavior in complex socio-technical networks, J. Complex Networks **1**, 3 (2013).

[5] M. Granovetter, Threshold models of collective behavior, Am. J. Soc. **83**, 1420 (1978).

[6] T. W. Valente, *Network Models of the Diffusion of Innovations* (Hampton Press, Creskill, NJ, USA, 1995).

[7] M. O. Jackson and D. López-Pintado, Diffusion and contagion in networks with heterogeneous agents and homophily, Network Sci. **1**, 49 (2013).

[8] D. Kempe, J. Kleinberg, and É. Tardos, Maximizing the spread of influence through a social network, in *Proceedings of the Ninth ACM SIGKDD International Conference on Knowledge Discovery and Data Mining*, KDD '03 (ACM, New York, NY, USA, 2003), pp. 137–146.

[9] D. J. Watts, A simple model of global cascades on random networks, Proc. Natl. Acad. Sci. U.S.A. **99**, 5766 (2002).

[10] C. Castellano, S. Fortunato, and V. Loreto, Statistical physics of social dynamics, Rev. Mod. Phys. **81**, 591 (2009).

[11] N. A. Christakis and J. H. Fowler, The spread of obesity in a large social network over 32 years, New Engl. J. Med. **357**, 370 (2007).

[12] D. Centola and M. W. Macy, Complex contagions and the weakness of long ties, Am. J. Soc. **113**, 702 (2007).

[13] P. S. Dodds and D. J. Watts, A generalized model of social and biological contagion, J. Theor. Biol. **232**, 587 (2005).

[14] S. Aral, L. Muchnik, and A. Sundararajan, Distinguishing influence-based contagion from homophily-driven diffusion in dynamic networks, Proc. Natl. Acad. Sci. U.S.A. **106**, 21544 (2009).

[15] J. Ugander, L. Backstrom, C. Marlow, and J. Kleinberg, Structural diversity in social contagion, Proc. Natl. Acad. Sci. U.S.A. **109**, 5962 (2012).

[16] S. Goel, A. Anderson, J. Hofman, and D. J. Watts, The structural virality of online diffusion, Manage. Sci. **62**, 180 (2016).

[17] B. Mønsted, P. Sapieżyński, E. Ferrara, and S. Lehmann, Evidence of complex contagion of information in social media: An experiment using Twitter bots, PLoS One **12**, e0184148 (2017).

[18] D. Mollison, Spatial contact models for ecological and epidemic spread, J. R. Stat. Soc.: Ser. B (Methodol.) **39**, 283 (1977).

[19] H. P. Young, Innovation diffusion in heterogeneous populations: Contagion, social influence, and social learning, Am. Econ. Rev. **99**, 1899 (2009).

[20] D. Centola, R. Willer, and M. W. Macy, The emperor's dilemma: A computational model of self-enforcing norms, Am. J. Soc. **110**, 1009 (2005).

[21] H. Elsinger, A. Lehar, and M. Summer, Risk assessment for banking systems, Manage. Sci. **52**, 1301 (2006).

[22] J. Juul and K. Sneppen, Locally self-organized quasicritical percolation in a multiple-disease model, Phys. Rev. E **84**, 036119 (2011).

[23] P. S. Dodds and D. J. Watts, Universal Behavior in a Generalized Model of Contagion, Phys. Rev. Lett. **92**, 218701 (2004).

[24] I. Z. Kiss, J. C. Miller, and P. L. Simon, *Mathematics of Epidemics on Networks: From Exact to Approximate Models* (Springer International Publishing, Cham, Switzerland, 2017).

[25] S. Melnik, J. A. Ward, J. P. Gleeson, and M. A. Porter, Multi-stage complex contagions, Chaos **23**, 013124 (2013).

[26] F. J. Pérez-Reche, J. J. Ludlam, S. N. Taraskin, and C. A. Gilligan, Synergy in Spreading Processes: From Exploitative to Explorative Foraging Strategies, Phys. Rev. Lett. **106**, 218701 (2011).

[27] J. S. Juul and M. A. Porter, Synergistic effects in threshold models on networks, Chaos **28**, 013115 (2018).

[28] R. Pastor-Satorras, C. Castellano, P. Van Mieghem, and A. Vespignani, Epidemic processes in complex networks, Rev. Mod. Phys. **87**, 925 (2015).

[29] D. Taylor, F. Klimm, H. A. Harrington, M. Kramár, K. Mischaikow, M. A. Porter, and P. J. Mucha, Topological data analysis of contagion maps for examining spreading processes on networks, Nat. Commun. **6**, 7723 (2015).

[30] E. Valdano, L. Ferreri, C. Poletto, and V. Colizza, Analytical Computation of the Epidemic Threshold on Temporal Networks, Phys. Rev. X **5**, 021005 (2015).

[31] J. P. Gleeson, Binary-State Dynamics on Complex Networks: Pair Approximation and Beyond, Phys. Rev. X **3**, 021004 (2013).

[32] J. P. Gleeson, Cascades on correlated and modular random networks, Phys. Rev. E **77**, 046117 (2008).

[33] T. R. Hurd and J. P. Gleeson, On Watts' cascade model with random link weights, J. Complex Networks **1**, 25 (2013).

[34] M. Zheng, L. Lü, and M. Zhao, Spreading in online social networks: The role of social reinforcement, Phys. Rev. E **88**, 012818 (2013).

[35] J. P. Gleeson, K. P. O'Sullivan, R. A. Baños, and Y. Moreno, Effects of Network Structure, Competition, and Memory Time on Social Spreading Phenomena, Phys. Rev. X **6**, 021019 (2016).

[36] X. Qiu, D. F. M. Oliveira, A. S. Shirazi, A. Flammini, and F. Menczer, Limited individual attention and online virality of low-quality information, Nat. Hum. Behav. **1**, 0132 (2017).

[37] J. Chalupa, P. L. Leath, and G. R. Reich, Bootstrap percolation on a Bethe lattice, J. Phys. C: Solid State Phys. **12**, L31 (1979).
[38] D. Centola, V. M. Eguíluz, and M. W. Macy, Cascade dynamics of complex propagation, Physica A **374**, 449 (2007).
[39] S.-W. Oh and M. A. Porter, Complex contagions with timers, Chaos **28**, 033101 (2018).
[40] E. M. Rogers, *Diffusion of Innovations* (Simon and Schuster, New York, NY, USA, 2010).
[41] F. M. Bass, A new product growth for model consumer durables, Manage. Sci. **15**, 215 (1969).
[42] F. M. Bass, The relationship between diffusion rates, experience curves, and demand elasticities for consumer durable technological innovations, J. Bus. **53**, S51 (1980).
[43] J. V. Nevers, Extensions of a new product growth model, Sloan Manage. Rev. **13**, 77 (1972).
[44] F. M. Bass, T. V. Krishnan, and D. C. Jain, Why the Bass model fits without decision variables, Marketing Sci. **13**, 203 (1994).
[45] F. M. Bass, Comments on "A new product growth for model consumer durables: The Bass model", Manage. Sci. **50**, 1833 (2004).
[46] M. B. Gordon, M. F. Laguna, S. Gonçalves, and J. R. Iglesias, Adoption of innovations with contrarian agents and repentance, Physica A **486**, 192 (2017).
[47] P. S. Dodds, K. D. Harris, and C. M. Danforth, Limited Imitation Contagion on Random Networks: Chaos, Universality, and Unpredictability, Phys. Rev. Lett. **110**, 158701 (2013).
[48] K. D. Harris, C. M. Danforth, and P. S. Dodds, Dynamical influence processes on networks: General theory and applications to social contagion, Phys. Rev. E **88**, 022816 (2013).
[49] S. Galam, Majority rule, hierarchical structures, and democratic totalitarianism: A statistical approach, J. Math. Psychol. **30**, 426 (1986).
[50] S. Galam, Contrarian deterministic effects on opinion dynamics: The hung elections scenario, Physica A **333**, 453 (2004).
[51] S. Galam and F. Jacobs, The role of inflexible minorities in the breaking of democratic opinion dynamics, Physica A **381**, 366 (2007).
[52] S. Galam, Stubbornness as an unfortunate key to win a public debate: An illustration from sociophysics, Mind Society **15**, 117 (2016).
[53] P. Nyczka, K. Sznajd-Weron, and J. Cisło, Phase transitions in the q-voter model with two types of stochastic driving, Phys. Rev. E **86**, 011105 (2012).
[54] P. Nyczka and K. Sznajd-Weron, Anticonformity or independence? Insights from statistical physics, J. Stat. Phys. **151**, 174 (2013).
[55] N. Khalil and R. Toral, The noisy voter model under the influence of contrarians, Physica A **515**, 81 (2019).
[56] R. Apriasz, T. Krueger, G. Marcjasz, and K. Sznajd-Weron, The hunt opinion model—An agent based approach to recurring fashion cycles, PLoS One **11**, e0166323 (2016).
[57] K. Sznajd-Weron and R. Weron, How effective is advertising in duopoly markets? Physica A **324**, 437 (2003).
[58] A. Mellor, M. Mobilia, S. Redner, A. M. Rucklidge, and J. A. Ward, Influence of Luddism on innovation diffusion, Phys. Rev. E **92**, 012806 (2015).
[59] J. P. Gambaro and N. Crokidakis, The influence of contrarians in the dynamics of opinion formation, Physica A **486**, 465 (2017).
[60] E. Ferrara, Disinformation and social bot operations in the run up to the 2017 French presidential election, First Monday **22**, 8 (2017).
[61] A. Bessi and E. Ferrara, Social bots distort the 2016 US Presidential election online discussion, First Monday **21**, 11 (2016).
[62] D. Guilbeault, J. Becker, and D. Centola, Social learning and partisan bias in the interpretation of climate trends, Proc. Natl. Acad. Sci. U.S.A. **115**, 9714 (2018).
[63] K. H. Jamieson and B. W. Hardy, Leveraging scientific credibility about Arctic Sea ice trends in a polarized political environment, Proc. Natl. Acad. Sci. U.S.A. **111**, 13598 (2014).
[64] Michael Bang Petersen, Mathias Osmundsen, and Kevin Arceneaux, A "Need for Chaos" and the Sharing of Hostile Political Rumors in Advanced Democracies (2018), PsyArXiv, https://doi.org/10.31234/osf.io/6m4ts.
[65] S. B. Hobolt, The Brexit vote: A divided nation, a divided continent, J. Eur. Public Policy **23**, 1259 (2016).
[66] J. E. Oliver and W. M. Rahn, Rise of the Trumpenvolk: Populism in the 2016 election, Ann. Am. Acad. Political Social Sci. **667**, 189 (2016).
[67] J. Touboul, The hipster effect: When anticonformists all look the same, arXiv:1410.8001.
[68] J. P. Gleeson, D. Cellai, J.-P. Onnela, M. A. Porter, and F. Reed-Tsochas, A simple generative model of collective online behavior, Proc. Natl. Acad. Sci. U.S.A. **111**, 10411 (2014).
[69] A. L. Traud, P. J. Mucha, and M. A. Porter, Social structure of Facebook networks, Physica A **391**, 4165 (2012).
[70] J. P. Gleeson and D. J. Cahalane, Seed size strongly affects cascades on random networks, Phys. Rev. E **75**, 056103 (2007).
[71] S. Melnik, A. Hackett, M. A. Porter, P. J. Mucha, and J. P. Gleeson, The unreasonable effectiveness of tree-based theory for networks with clustering, Phys. Rev. E **83**, 036112 (2011).
[72] Pair approximations have also been employed in other types of opinion models, such as for a q-voter model in [78].
[73] S. Goel, D. J. Watts, and D. G. Goldstein, The structure of online diffusion networks, in *Proceedings of the 13th ACM Conference on Electronic Commerce*, EC '12 (ACM, New York, NY, USA, 2012), doi:10.1145/2229012.2229058.
[74] B. K. Fosdick, D. B. Larremore, J. Nishimura, and J. Ugander, Configuring random graph models with fixed degree sequences, SIAM Rev. **60**, 315 (2018).
[75] M. E. J. Newman, *Networks*, 2nd ed. (Oxford University Press, Oxford, UK, 2018).
[76] The original hipster was in the network before it was popular.
[77] P. G. Fennell, S. Melnik, and J. P. Gleeson, Limitations of discrete-time approaches to continuous-time contagion dynamics, Phys. Rev. E **94**, 052125 (2016).
[78] A. Jedrzejewski, Pair approximation for the q-voter model with independence on complex networks, Phys. Rev. E **95**, 012307 (2017).
[79] Our code is available at https://sid.erda.dk/share_redirect/hZOCeo4qU5.

Chapter 6

Scaling law for the impact of mutant contagion

In the classic child game "Chinese whispers", also known as "Telephone", a word or a phrase is slowly spreading among participants. The participants first form a line. One person then chooses a phrase, which she whispers to the ear of the next person in the line. This person then repeats the phrase to the next in line, who then shares it with the next in line, etc. In this way, the phrase slowly makes its way through the whole group of participants. The person who is told the phrase last loudly repeats the phrase as he was told it. The phrase the last person proclaims is usually very different from what was whispered by the first person in line. The message *mutated* as it travelled.

The mutation of messages is not confined to the world of child games. As illustrated by Hans Christian Andersen in the fairytale "No doubt about it!" (Andersen, 2004; Andersen, 2004), rumours can mutate as they spread. In this fairytale, a little feather comes out as a hen plucks herself with her beak. She jokingly tells her neighbour on the roost that she removed the feather to improve her looks. The neighbour tells the story to another hen, who then passes the tale on, etc. By the next morning, the innocent joke about removing a feather to look good has turned into a tragedy. The story now goes

> "Five hens (...) have plucked out all their feathers to show which of them had grown leanest for love of the cock, and then they all pecked at each other till the blood ran down and they fell down dead (...)"
>
> Hans Christian Andersen, excerpt from "No doubt about it!"

Perhaps the most critical kind of mutation in spreading processes happens in communicable diseases. During the summer of 1918, a flu spread across the world, like so many times before. From the Americas to the trenches of Western Europe, people fell ill with the contagious disease. Evidence from Scandinavian cities (Andreasen, Viboud, and Simonsen, 2008) shows that the disease spread quickly because the population was to a good approximation fully susceptible. A substantial number of people succumbed to the illness. By the end of the summer, it looked like the disease had released its grip on urban populations in Scandinavia. Then it took off.

After a quiet period following the summer wave, a new wave of influenza hit the world. Compared to the summer wave, the case-fatality rate in Copenhagen increased about one order of magnitude. Although investigations suggest that the first wave provided some immunity to the more lethal second wave, the epidemic successfully spread widely in populated areas. After this lethal wave, another followed during the winter of 1919. Although 24% of the influenza-related excess hospitalizations in Copenhagen happened during the summer of 1918, less than 5% of

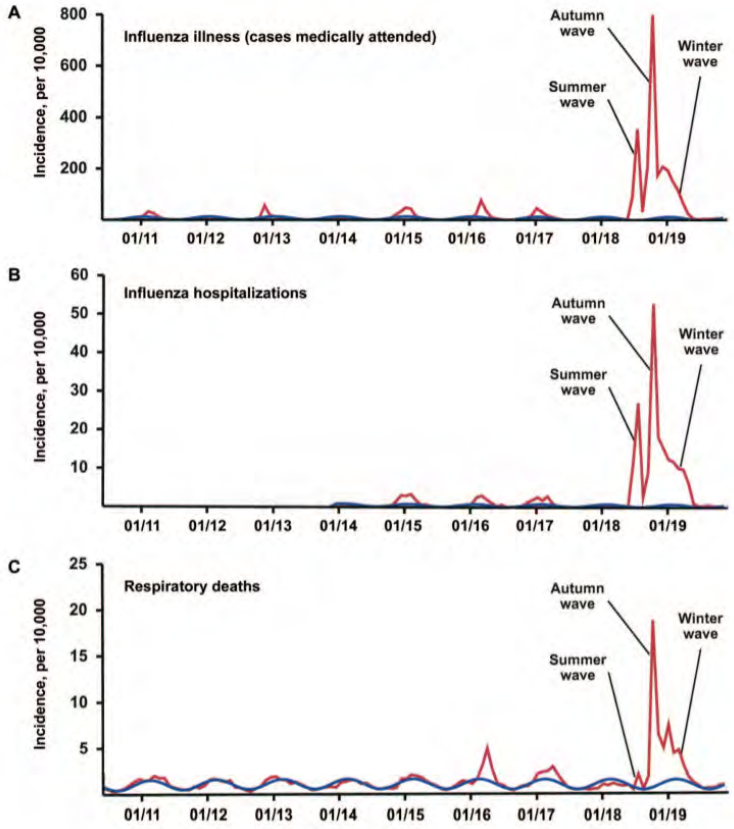

FIGURE 6.1: The impact of influenzas in Copenhagen, 1911-1919. The top figure shows the number of medically-attended influenza cases plotted in numbers per 10,000 citizens as a function of time. Three peaks stand out – the summer, autumn, and winter waves of the Spanish flu. Similar peaks are visible in the middle panel, plotting the number of influenza hospitalisations per 10,000 citizens. The bottom panel plots the number of respiratory deaths. Peaks are only visible for the autumn and winter waves. A less deadly strain of flu was spreading during the summer. Figures from (Andreasen, Viboud, and Simonsen, 2008).

the corresponding deaths happened in this period. For every 20 influenza-related deaths during these first 3 waves of the "Spanish" flu, about 19 happened during the last two waves (Andreasen, Viboud, and Simonsen, 2008). Figure 6.1 illustrates these astonishing statistics.

The more lethal version of the 1918 flu came to exist because the influenza mutated as it travelled through the global human contact network. How widespread a mutated form of a spreading disease will get is not obvious. For the Spanish flu, the second and third waves would have been effectively contained had the summer wave spread to every susceptible person. The chance of the mutation happening after most of the world was immune probably depends on the details of the contagion. The details could be the properties of the human contact network, the rate of mutation, and the rate with which the flu spreads.

Likewise, Telephone is a great ice breaker because the underlying network topology, a line, makes the message extremely vulnerable to distortions. If the game were instead played by making the first person whisper the same phrase to every other participant, message mutations would probably be less frequent. So how prevalent

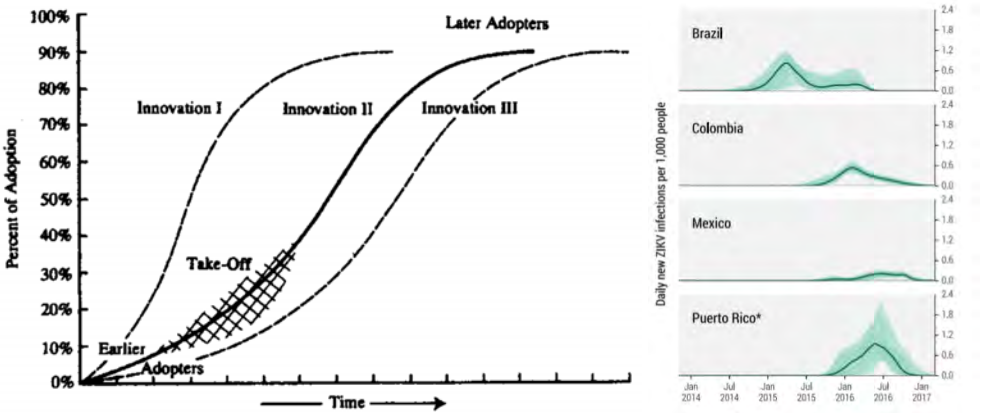

FIGURE 6.2: Two examples of studies focusing on the number of adopters/infected cases. Lefthand panel plots the adoption of an innovation as a function of time. The adoptions follow s-shaped curves. Righthand panel shows the number of daily new Zika infections in countries in the Americas as a function of time. This amounts to plotting the derivative of curves like the ones in the lefthand panel. Figures first published in (Rogers, 2010) (left) and (Zhang et al., 2017) (right).

should we expect the next Spanish flu to get? Is it likely to become a worldwide pandemic with more than 50 million fatalities? Or will most such mutant contagions die out quickly? If the disease does get widespread, how likely is it to infect 500 million people instead of 50 million people? The paper of the present chapter quantifies the impact of very contagious mutant contagion in different network structures. Computing this impact is complicated by the need for knowing not only the *number* of people that get infected, but also who infects whom. We need to quantify the *diffusion paths*.

6.1 Epidemic trees and the structure of diffusion

When studying the spread of contagion, scholars typically focus on quantifying the *number* of nodes that get infected. In many ways, this is a natural choice. The number of people infected with a disease can give some idea about what impact the disease will have on society — both economic and human. For companies, the number of adopters of an innovation is proportional to the revenue the company will make. What is more, it is much easier to collect data on who is infected or who bought a product compared to, for example, who infected whom. Figure 6.2 shows two figures from the contagion literature. One figure is from a classic paper on innovation diffusion; the other is from a recent article studying the spread of the Zika virus in the Americas. Both figures quantify the number of people "infected" by the contagion as a function of time. The leftmost panel plots the number of infected people directly, while the rightmost panel quantifies the number of newly infected cases per day as a function of time.

In some cases, knowing only the number of infected cases is not sufficient. Who infected who is essential to know if *causality* plays a vital role in the system of interest. When studying mutant contagion, causality is imperative: only people influenced by the "Patient Zero" of the mutated strain will eventually carry the mutant disease. We can think about the contagion making a kind of family tree as it spreads;

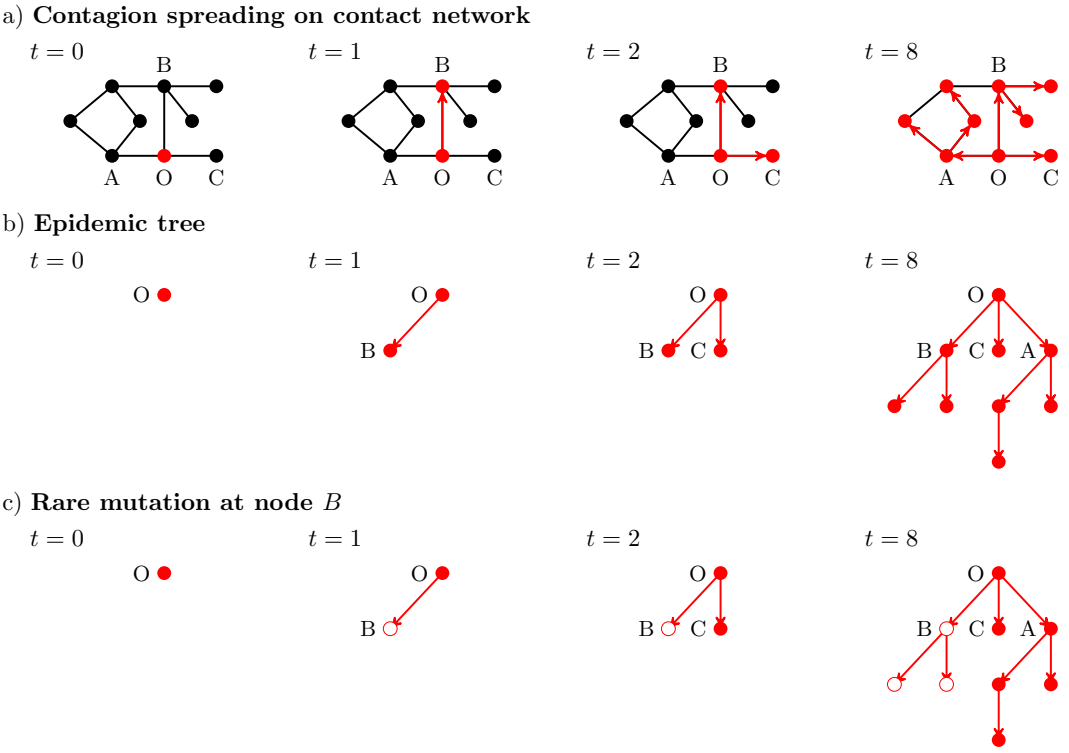

FIGURE 6.3: Epidemic trees and their relation to the impact of mutant contagion. The top panel shows a network (black nodes and links) in which contagion is spreading (red nodes and directed links). Time progresses from left to right. The middle panel plots the Epidemic tree of the contagion. In the top row, the seed is plotted. In the second row, the children of the seed are plotted. In the third row, the children of the children are plotted, etc. In the bottom panel, the contagion mutates as node B gets infected. Node B and all of its descendants will get this mutated variant of the contagion. Figure from (Juul and Strogatz, 2019).

a distant ancestor of every infected node is the first person to catch the disease. That person can be thought of as having a number of children: the people infected directly by this eldest. These children have offspring of their own, and these children are *descendants* of the first person to catch the disease. Figure 6.3 illustrates such a family tree and its importance in relation to mutant contagion. We will refer to this family tree as the "*epidemic tree*". This term is inspired from an epidemiological study of causality in the UK foot-and-mouth outbreak in 2001 (Haydon et al., 2003).

Although most studies focus on the total number of nodes infected by a contagion, Epidemic trees have been considered in some cases. However, this literature is scattered, and the number of names used to refer to Epidemic trees illustrates this. These names include adoption paths (Juul and Porter, 2019), dissemination trees (Oh and Porter, 2018; Liben-Nowell and Kleinberg, 2008), spreading patterns (Liu et al., 2015; Jang et al., 2018), patterns of information diffusion (Chierichetti, Liben-Nowell, and Kleinberg, 2011), causal trees of disease transmission (Vázquez, 2004), diffusion structure patterns (Zhang et al., 2016), the network structure of diffusion processes (Goel, Watts, and Goldstein, 2012), structure of diffusion (Golub and Jackson, 2010), the structure of information cascades (Cheng et al., 2014), information spreading trees (Wang et al., 2011), cascade scructure (Anderson et al., 2015) and the structure of diffusion events (Goel et al., 2015). Most studies focusing on Epidemic

trees do so out of academic interest and do not mention any applications.

Arguably one of the two the most influential papers on Epidemic trees is a recent paper by Goel et al. called "The structural virality of online diffusion" (Goel et al., 2015). This is also the one paper that most directly puts forward a possible application of Epidemic trees. In this paper, the authors define a measure they call "structural virality", which they report can measure to what degree the diffusion on a network can be described as "viral". If the measure takes a large value, the Epidemic tree is deep and broad, reminiscent of what one might find for a communicable disease spreading in a network. If the measure takes a small value, the Epidemic tree is more similar to what one would see if a few "broadcasters" were responsible for the spreading. The structural-virality measure is equal to the average distance between pairs of nodes in the epidemic tree,

$$v(T) = \frac{1}{|T|(|T|-1)} \sum_{i,j \in T} d(i,j), \tag{6.1}$$

where T denotes the Epidemic tree and $d(i,j)$ is the shortest path (graph geodesic) between nodes i and j in T. This is a normalized version of the "Wiener index" in graph theory (Goel et al., 2015). Goel et al. analyze roughly a billion Epidemic trees of retweet cascades on Twitter and find that the large cascades have considerably diverse structural virality. So far, no study has suggested a coupling between mutant contagion and Epidemic trees.

6.2 Mutations

Mutations are central to evolutionary biology. There are many aspects to study about mutations. In this section, I will limit myself to mentioning works that are directly relevant to the research article of Section 6.4. I will first mention a theoretical model introduced by Udny Yule at the beginning of the previous century (Yule, 1925). Next, I go through some fascinating experimental results on mutations in meme spreading on Facebook. These empirical findings support the existence and relevance of the scaling law we derived in our paper.

6.2.1 The Yule process

The Yule process is a simple model of a biological system. The process contains two ingredients: replication and mutation. The Yule process starts with just a single cell and describes its development into a diverse population of cells. Each cell has the same probability of dividing next. When a division happens, there is a risk of errors occurring. The likelihood of giving birth to a mutant copy is given by m. Consequently, the probability of a division being error-free is $1-m$.

The main reason to study the Yule process is to understand the diversity of biological systems. Depending on the chosen parameters, how many cell variants are present at large times, and how widespread is each of these variants? In the article I coauthor with Steven H. Strogatz, we are interested in situations where mutations are rare. In this case, $m/(1-m) \ll 1$, and the probability of each mutant constituting a fraction c of the total population at very large times approaches

$$P(c) = \frac{1}{c(c-1)}. \tag{6.2}$$

The Yule process has been used to model diversity in several biological systems including bacteria (Mandelbrot, 1974), structures of phylogenetic trees (Steel and McKenzie, 2001; Scott et al., 2019), and protein structures (Koonin, Wolf, and Karev, 2002; Qian, Luscombe, and Gerstein, 2001).

6.2.2 Empirical study of meme spreading on Facebook

Before proceeding to describe the results of our paper, it is worthwhile to understand some recent fascinating results concerning meme spreading on Facebook. In the paper "Information Evolution in Social Networks", Adamic et al. presented a thorough study of how memes spread and mutate on Facebook (Adamic et al., 2016). They studied thousands of memes on Facebook. To share a meme, a person would have to copy and paste the text before sharing it. Sometimes, the person would choose to edit the text before resharing, thereby giving rise to a new *variant* of the meme. In this way, a mutant version of the meme could be born.

The memes studied by Adamic et al. were pretty diverse. Some memes would mutate often, and some only rarely. Examples of memes with high mutation rates included memes that specifically asked the person sharing the meme to edit it, e.g. [1]

> "it s national book week the rules grab the closest book to you go to page 56 copy the 5th sentence as your status don t mention the book post these rules as part of your status"
>
> The M2 meme from (Adamic et al., 2016).

Other memes would change more rarely. The part of the study directly relevant to our research is the frequency with which different variants of the same meme occurred on Facebook. Adamic et al. found that, just as in biological processes, some mutant variants of memes would become very widespread, whereas others would only be shared a limited number of times. The left-hand panel of Figure 6.4 shows their findings. The color of the curves indicate the mutation rate of the memes. Fitting power-laws to the tails of the curves, they found that the power-law exponents were distributed around -2. Specifically, a Kolmogorov-Smirnov test confirmed that the data was consistent with a power-law fit with exponents 2.01 ± 0.15 for 121 of the 123 memes with more than 10^5 different variants. When they extended the analysis to the 435 memes with more than 10^4 different variants, the exponents came out 1.99 ± 0.21. The histogram of these exponents is shown as the inset in the lefthand panel of Figure 6.4. The authors note that this analysis primarily entails memes with a low mutation rate.

That the power-law exponents come out close to -2 for memes with low mutation rates is captivating. This is exactly what Eq. (6.2) shows happens for the Yule process. Adamic et al. therefore investigated whether the Yule process could model the meme spreading. The right-hand panel of Figure 6.4 shows simulations of the Yule process, and the similarity to the empirical results are apparent. They also carried out other tests and found that the Yule process was a good approximation in these cases.

It is indeed interesting that the Yule process can model the mutating memes on Facebook. It seems strange, however, that a stochastic process with no underlying network structure is a good model for the spreading and mutation happening on a complicated network such as the Facebook graph. Is this some universality at

[1] Note that punctuation was removed as part of the study.

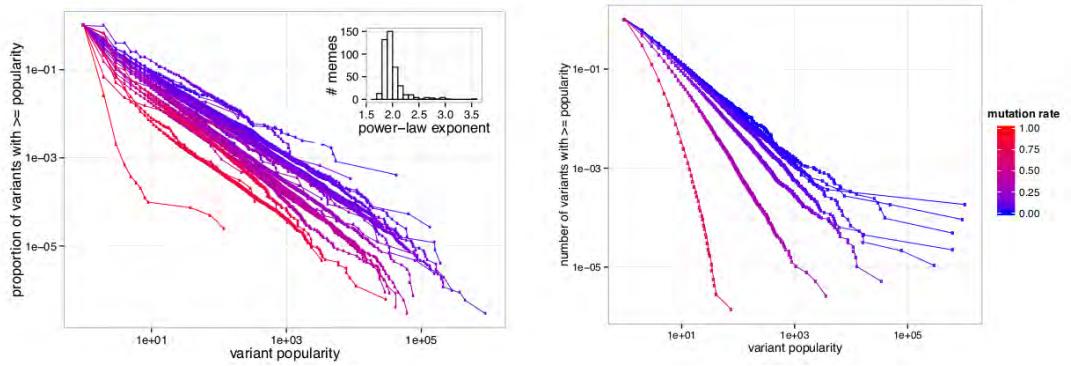

FIGURE 6.4: The lefthand panel shows the popularity of different variants of memes spreading on Facebook. (Adamic et al., 2016) found that popularity of variants of rarely mutating memes had power-law tails with exponent of approximately -2 (see inset). The righthand panel shows power laws obtained from simulations of the Yule process. Figure from (Adamic et al., 2016).

work? Does network structure simply not matter? These are some of the questions we ended up answering in the paper presented in this chapter.

6.3 Our results: A scaling law for the impact of mutant contagion

In the paper "Scaling law for the impact of mutant contagion", which we have submitted and is available as a preprint online (Juul and Strogatz, 2019), Steven H. Strogatz and I quantify the impact of mutant contagions spreading in various networks. We do this by studying a simple model of contagion in networks analytically and with simulations.

In the model, we assume that nodes can be either susceptible or infected and that only a single node starts infectious. After the seed is chosen, we assume that a single node gets infected at a time – two nodes never get infected at exactly the same time. In our model, any link between a susceptible and an infectious node is equally likely to be the next link the contagion traverses. We keep track of who gets infected by whom, and in our simulations, we stop the spreading after a specified number of nodes are infected. In most cases, we specify this number of nodes to be equal to the total number of nodes in the network.

From the obtained data of who infected whom, we construct an epidemic tree. If a mutation were to happen as a random node in the network got infected, every node downstream of that random node would get the mutant contagion. We call the nodes downstream of a node A *descendants* of node A. For each simulation, we count the number of descendants of every node and compile a histogram of the number of nodes that had n descendants. We then average these histograms over many simulations to obtain an average *descendant distribution*. The descendant distribution for the contagion realised on some network is a probability distribution expressing the probability that a node chosen uniformly-at-random from the infected nodes will end up having d descendants. If mutations happen at nodes chosen uniformly at random, the descendant distribution quantifies the probability that d nodes will get infected with the mutant contagion.

We find that on several kinds of networks, the descendant distribution declines proportional to d^{-2} for large d. We analytically calculate the descendant distributions for the contagion spreading on complete networks, Erdős–Rényi networks, configuration-model networks, and small-world networks. For all networks, we obtain functions of the form $B(f(d, \boldsymbol{p}), 2)$, where $B(x, y)$ is the beta function. $f(d, \boldsymbol{p})$ is some function of the parameters used to create the networks, $\boldsymbol{p}$, and the number of descendants, d. $f(d, \boldsymbol{p})$ is non-decreasing in d. These beta functions all approach d^{-2} for large d, as our simulations indicated.

Using our analytical calculation we argue that the descendant distribution will have the form $B(f(d, \boldsymbol{p}), 2)$ for the contagion spreading on *any* infinite-dimensional network. Consequently, we predict the probability that a mutant version of a spreading entity infects d people to decline proportional to d^{-2} on any effectively infinite-dimensional network. We show that previously published data on meme spreading on Facebook agrees with our prediction. We also simulate our spreading process on subgraphs of Twitter and Facebook and find that the descendant distributions indeed decline according to the predicted scaling law. Finally, we show that the descendant distribution for the contagion spreading on a $2D$ square grid does not follow the scaling law we derived for infinite-dimensional networks.

6.4 Paper: Scaling law for the impact of mutant contagion

Scaling law for the impact of mutant contagion

Jonas S. Juul*

Niels Bohr Institute, University of Copenhagen, Blegdamsvej 17, Copenhagen 2100-DK, Denmark

and

Center for Applied Mathematics, Cornell University, Ithaca, New York 14853, USA

Steven H. Strogatz†

Center for Applied Mathematics, Cornell University, Ithaca, New York 14853, USA

(Dated: October 3, 2019)

* jonas.juul@nbi.ku.dk

† strogatz@cornell.edu (corresponding author)

Contagion, broadly construed, refers to anything that can spread infectiously from peer to peer[1–5]. Examples include communicable diseases[6–10], rumors[11], misinformation[12], ideas[13], innovations[14–16], bank failures[17], and electrical blackouts[18]. Sometimes, as in the 1918 Spanish flu epidemic[19], a contagion mutates as it propagates. Here, using a simple mathematical model, we quantify the downstream impact of a contagion that mutates exactly once as it travels. Assuming that this mutation occurs at a random node in the contact network, we calculate the distribution of the number of "descendants," d, downstream from the initial "Patient Zero" mutant. We find that the tail of the distribution decays as d^{-2} for complete graphs, random graphs, small-world networks and other infinite-dimensional networks. This prediction agrees with the observed statistics of memes propagating and mutating on Facebook[20], and is expected to hold universally for other effectively infinite-dimensional networks, such as the global human contact network. In a wider context, our approach suggests a possible starting point for a mesoscopic theory of contagion. Such a theory would focus on the paths traced by a spreading contagion, thereby furnishing an intermediate level of description between that of individual nodes and the total infected population. For every discipline concerned with contagion and its prevention, we anticipate that contagion pathways hold valuable lessons, given their role as the conduits through which single mutations, innovations, or failures can sweep through a network as a whole.

When a contagion spreads, it propagates from one or more "parent" nodes to a number of "descendant" nodes. Enumerating the descendants in all the paths stemming from a parent can reveal important and useful information. In particular, suppose the contagion mutates into a more pernicious form at some point along its travels. Then counting its descendants would tell us how many nodes will be confronted by this nastier strain. A mutation event of this sort occurred in 1918, and gave rise to the Spanish flu epidemic that killed millions of people worldwide[19]. Similar (but less consequential) mutations happen online when users modify memes to make them funnier or stickier before sharing them with their peers[20].

To quantify the impact of such mutations, consider a simplified model of contagion in

which each node is either susceptible or permanently infected (Fig. 1). As the contagion spreads (Fig. 1(a)), we record which nodes caught it from which, and plot the resulting paths of infection as an epidemic tree (Fig. 1(b)). Then we count how many nodes would be affected by a mutation occurring at a random "Patient Zero" node. In the example shown in Fig. 1(c), the mutant infection occurs at node B and is passed along to the two nodes below it. Of course, if the mutation had occurred elsewhere, it could have produced either more descendants (e.g., three descendants, had the mutation occurred at A) or fewer (zero descendants, had it occurred at C). Thus, the natural statistical quantity to study is the *distribution* of the number of descendants, aggregated over all possible Patient Zero nodes.

In one sense, the dynamics assumed here are trivial: one node after another gets infected until no susceptibles remain. But what is far from trivial are the descendant distributions implied by this model, as they depend on the network's structure. To learn what to expect, we first compute descendant distributions numerically from Monte Carlo simulations. For a given random realization of the contagion process on a given network, like the one shown in Fig. 1(b), we count the number of descendants of each node and compile a histogram. This histogram, however, merely gives the descendant distribution for one realization of the dynamics. To extract a more robust statistical measurement, we average over the random location of the initially infected seed node, as well as the random decisions of whom to infect at each step, to obtain an average descendant distribution.

Figure 2 shows the average descendant distribution for the simplest possible network structure: a complete graph, in which each node is connected to all the others. The downward slope of the plot indicates that many nodes have few descendants, and a few nodes have many descendants. Of course, the seed O has every other node as its descendant, as an artifact of the assumed initial conditions. Its corresponding data point in Fig. 2 lies off the curve for this reason.

The most striking feature of the descendant distribution in Fig. 2 is its apparent power-law decay for $d \gg 1$. To explain this scaling law intuitively, recall that one way of getting power-law distributions is through rich-get-richer effects[21–24], and observe:

(i) If node i infected node j, the ancestors of j will be i *and* all the ancestors of i.

(ii) A node i can acquire a new descendant j if it passes the infection on to j, or if one of its descendants passes the infection on to j.

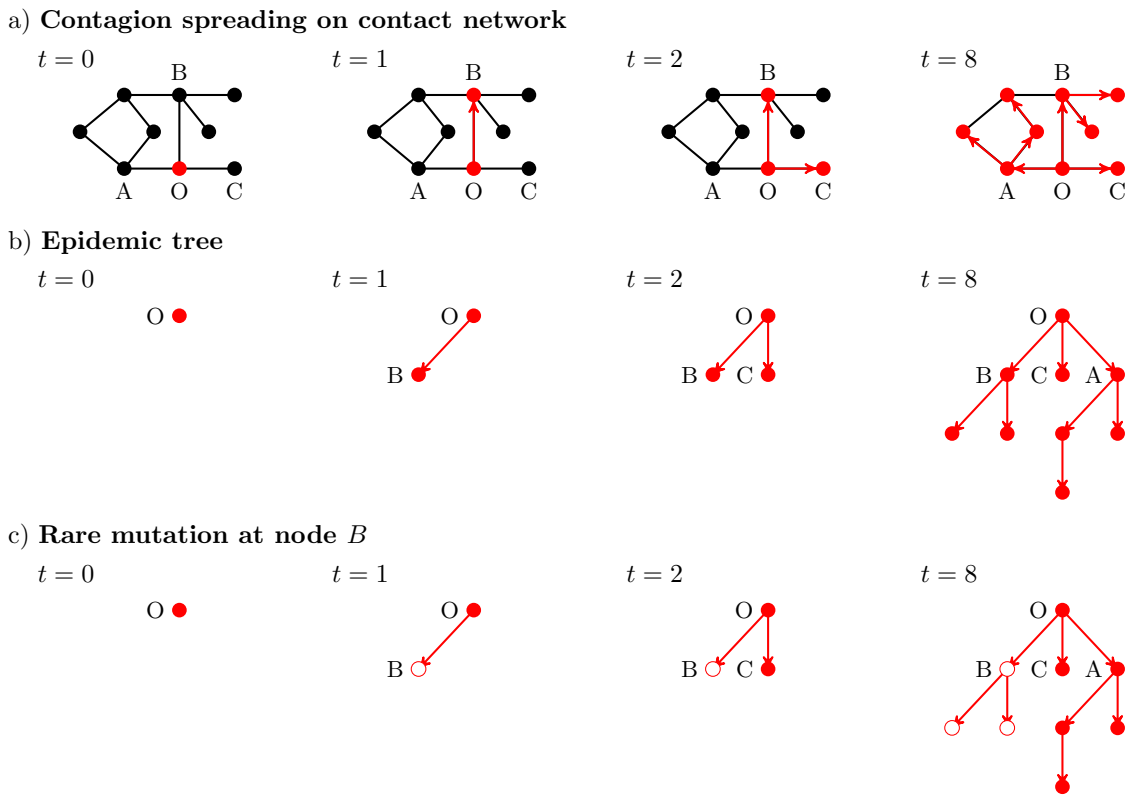

FIG. 1. **Simple model of contagion spreading on a network and its corresponding epidemic tree.** Black filled circles denote susceptible nodes; red filled circles, infected nodes; red open circles, nodes infected by a mutant strain of the infection. **a)** Starting with a single infected seed O at time $t = 0$, another node gets infected at random at the next time step. Any edge between an infected node and a susceptible node has an equal chance of being the next edge over which the contagion spreads. We keep track of which nodes transmitted and received the infection at every time step, until ultimately every node is infected. **b)** The epidemic tree shows who infected whom in the contagion process depicted in **a)**. We draw this tree with the seed on top. The nodes that the seed infected are drawn in the second layer, and so on. A descendant of node i is defined as any node that directly or indirectly received the infection from node i. Such a descendant node j can be reached by starting at node i and following a sequence of directed edges downward through the epidemic tree until the path ends at j. **c)** If a mutant infection occurs at some node (B, in the example shown here), that node passes the mutated strain on to all its descendants (two descendants, in this example).

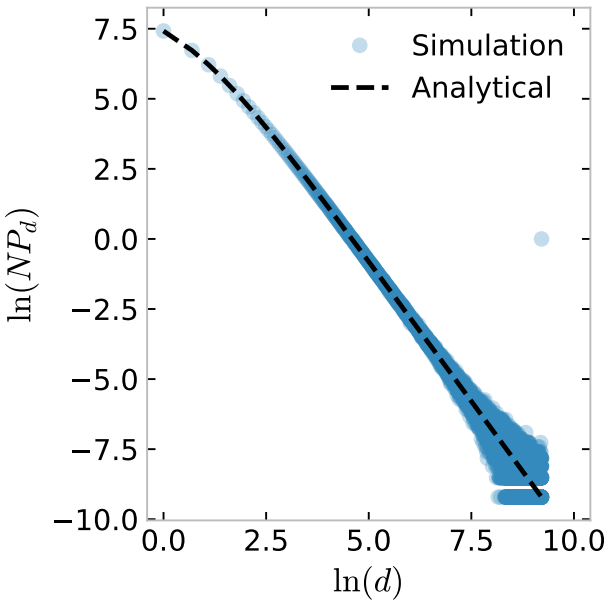

FIG. 2. **Descendant distribution for the contagion process on a complete graph.** We simulated the simple contagion model on complete graphs of $N = 10^4$ nodes, and averaged the resulting descendant distributions over 10^3 realizations of the random contagion process, each of which started with a single seed node. Filled circles show the numerically computed distribution of the number, d, of descendants of each node in the network. This distribution quantifies the impact that a mutant infection would have on the rest of the population, had it started at a random "Patient Zero" node. The dashed line shows the analytical result (1). For large values of d, the descendant distribution declines proportional to d^{-2}.

The first point means that our model contagion process is equivalent to a network that grows by node copying[25]. The second point suggests that the probability of a node acquiring more descendants should grow, loosely speaking, in proportion to the number of descendants it already has, thereby making the rich richer.

To sharpen this intuition, we calculate the descendant distribution P_d analytically for some exactly solvable networks (for derivations, see Supplementary Sections 2, 3, 4, and 5). First, for a complete graph in the limit $N \to \infty$, we find

$$P_d = \frac{1}{(d+2)(d+1)}. \tag{1}$$

Figure 2 shows that this result agrees well with our simulation data. Likewise, for several

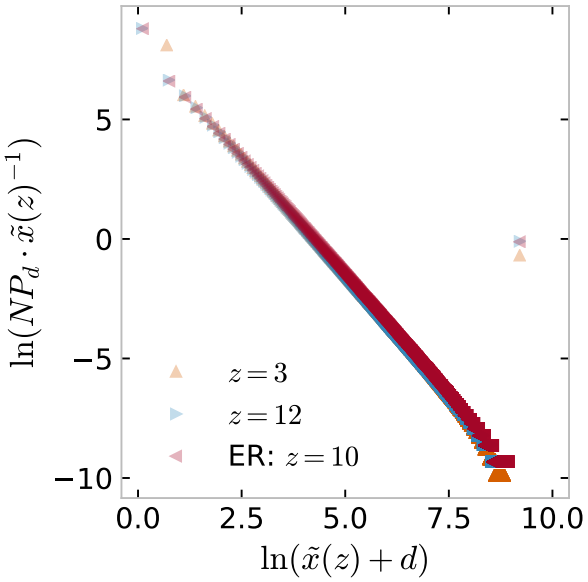

FIG. 3. **Descendant distributions for the simple contagion process on random networks.** We simulated the simple contagion process on z-regular configuration models and Erdős–Rényi (ER) networks of $N = 10^4$ nodes. The descendant distributions have been rescaled to collapse on the analytical solution (2). This rescaling involved adding $\tilde{x}(z) = (z-1)/(z-2)$ to d, and multiplying P_d by $\tilde{x}(z)^{-1}$, the inverse of the scaling factor of P_d (see Supplementary Section 3).

classes of random networks, the descendant distributions can be derived in the limit of infinite network size. We obtain the infinite-N solution

$$P_d = \frac{z-1}{z-2} B\left(\frac{z-1}{z-2} + d, 2\right), \tag{2}$$

where $B(a, b)$ denotes the beta function and z is the average degree. Figure 3 shows the simulation results for z-regular configuration models and Erdős–Rényi random graphs of size $N = 10^4$. When plotted in a manner suggested by equation (2), the simulation data for the different random networks collapse onto a single curve (Fig. 3), consistent with the analytical approximation. Finally, for a small-world network created by inserting random shortcuts in a ring lattice, with probability p of connecting a node with a node chosen uniformly at random[26], the analytical solution (Supplementary Section 4 and Extended Data Fig. 1) is

$$P_d = \frac{2p+1}{2p} B\left(\frac{2p+1}{2p} + d, 2\right). \tag{3}$$

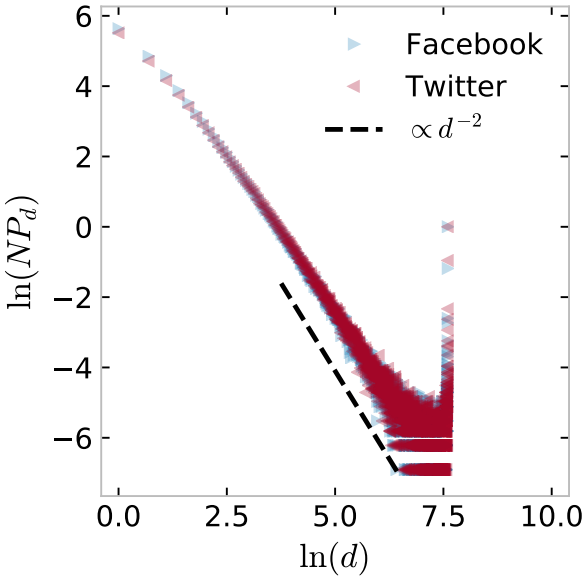

FIG. 4. **Descendant distributions of a contagion process simulated on real networks.** We ran simulations of the contagion process on two empirical undirected networks (see Supplementary Section 6): one with $N = 81,306$ nodes consisting of the combined edges of 973 Twitter ego-networks[27]; and another with $N = 13,866$ nodes consisting of Facebook pages of athletes[28], in which edges indicate mutual likes among them. In both cases, we started the contagion at a random seed node, and let exactly $2,000$ nodes get infected. Then we stopped the spreading, obtained the descendant distribution for the realization, and started a new simulation with a seed chosen uniformly at random. The descendant distributions shown here are averaged over 10^3 such simulations. The tail of the distribution declines with an exponent close to -2.

Remarkably, all the descendant distributions we have calculated so far turn out to decay asymptotically according to the same power law:

$$P_d \propto d^{-2} \tag{4}$$

for $d \gg 1$. Further analysis (Supplementary Section 5) indicates that this inverse-square scaling follows from a property that the complete graph shares with the random networks: they all become infinite dimensional as $N \to \infty$. On this basis, we expect that the same d^{-2} scaling should hold for other infinite-dimensional networks, but not for one-dimensional

chains, two-dimensional grids, three-dimensional lattices, or other networks whose dimensionality remains finite as the number of nodes tends to infinity. Simulations of the model contagion on two-dimensional square grids support this prediction: descendant distributions deviate significantly from the d^{-2} scaling (Extended Data Fig. 2).

Conveniently, many real-world networks are effectively infinite dimensional. Consider the social network Facebook, which as of June 2019 had more than 2.4 billion active users. In a fascinating study, Adamic et al.[20] examined memes spreading from friend to friend on the Facebook social graph. Typically, memes would propagate from one user to another without being altered, but occasionally a user would change the content of the meme before resharing it. This would make a new variant of the meme, which would then spread on the network along with previously existing copies. Adamic et al.[20] examined the frequency of different variants of rarely-changing memes, and found that the frequency distribution of the most widely shared variants followed an inverse-square law. Specifically, they found the exponent to be -2.01 ± 0.15. This exponent matched the prediction of a mean-field model (the Yule process), but it remained unclear why a model without any underlying network structure could account for the exponent obtained from the actual Facebook network.

Our work suggests that the observed exponent of -2 is a consequence of the approximate infinite-dimensionality of the Facebook network. Indeed, when we simulate our simple contagion process on sub-networks of Facebook or Twitter, an approximate power-law tail with a slope close to -2 emerges (Fig. 4 and Supplementary Section 6).

Our analysis can be viewed as a step toward a mesoscopic theory of contagion, in which infection pathways and epidemic trees would play the leading role, operating at a scale in between the local level of individual nodes and the global level of the entire network. To clarify these distinctions, consider the transition to a giant component in a susceptible-infected-removed model of contagion on a network[10]. Above the transition, there exists a giant infected component of size proportional to N. Such macroscopic phenomena have been extensively and fruitfully studied in the literature on network contagion[1,5,10]. But sizes of giant components and other macroscopic quantities lump all infected nodes together, and thus discard information about which nodes infected which. Such causal information is retained in epidemic trees, which show the pathways of contagion.

In this letter we have shown one way that epidemic trees can be used: they allow us to calculate descendant distributions, which quantify the impact of a mutant contagion

occurring at a random place in the network. Our finding that the distribution has a universal d^{-2} tail (for infinite-dimensional networks) means that the expected size of a mutant infected component is of size comparable to $\log N$ for $N \gg 1$. This size is intermediate in a precise sense; it is large compared to the $O(1)$ scale of individual nodes, but small compared to the $O(N)$ scale of giant infected components and the network itself. Note, however, that the variance of the mutant infected component size also diverges as $N \to \infty$. Hence the mean and variance do not adequately summarize the overall distribution, underscoring that one should rely only on the descendant distribution itself, as calculated here.

We expect that notions like contagion pathways, epidemic trees, and descendant distributions are just the beginning of a mesoscopic theory of contagion. Much remains to be discovered about the geometry and statistics of these and other quantities, both empirically for real contagions, and theoretically for a wide range of infection dynamics and network structures. Understanding this middle ground might also have practical benefits for the control of contagion processes, in contexts ranging from vaccination strategies for communicable diseases to methods for combating the spread of misinformation on social media.

Code availability

All scripts necessary to reproduce the simulated results are available at https://sid.erda.dk/wsgi-bin/ls.py?share_id=F8JmKmQryb.

Acknowledgements

J.S.J. acknowledges funding through the University of Copenhagen UCPH 2016 Excellence Programme for Interdisciplinary Research, the Danish Council for Independent Research, and thanks the Center for Applied Mathematics at Cornell University for hospitality while this work was carried out. S.H.S. was supported by NSF Grant CCF-1522054.

Author Contributions

J.S.J. and S.H.S. designed the study. J.S.J. performed the simulations and calculations. J.S.J. and S.H.S. wrote the manuscript.

Competing Interests

The authors declare that they have no competing financial interests.

Materials & Correspondence

Should be addressed to S.H.S.

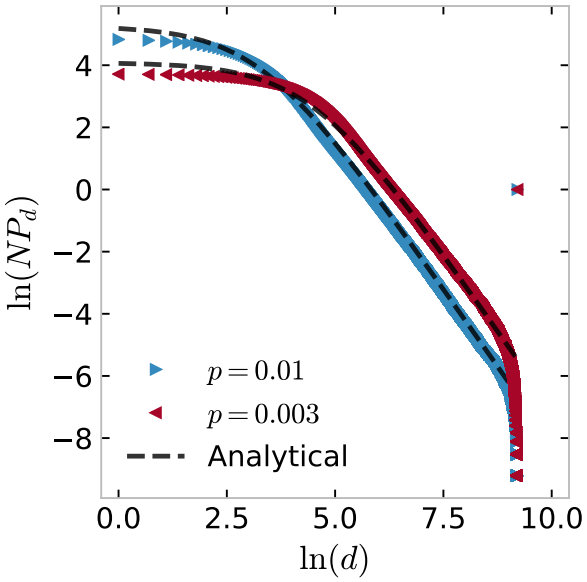

Extended Data Fig. 1. **Descendant distributions of a contagion process on Newman-Watts small-world networks.** The networks are created by starting out with a ring in which every node is connected to its two nearest neighbors, and then connecting each node with probability p to another node chosen uniformly at random[26]. The resulting descendant distributions, plotted here for networks of size $N = 10^4$ nodes, show the same universal behavior discussed in the main text: the distribution P_d decays in proportion to d^{-2} for large d, followed by a finite-size cutoff. We simulate the system for two values of p and plot the resulting descendant distributions P_d along with the analytical approximation (3) derived in Supplementary Section 4.

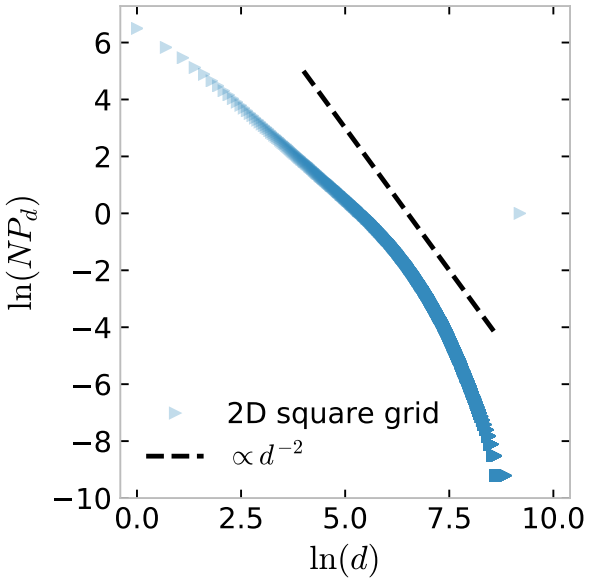

Extended Data Fig. 2. **Descendant distributions of a contagion process on two-dimensional square grids with periodic boundary conditions.** The networks consist of $N = 99^2$ nodes, and 10^3 random realizations of the spreading process were simulated. Because the underlying network is two-dimensional rather than infinite-dimensional, the resulting descendant distributions do not show the scaling law discussed in the main text: the distribution P_d does not decay in proportion to d^{-2} for large d.

Supplementary Information: Scaling law for the impact of mutant contagion

Jonas S. Juul*

Niels Bohr Institute, University of Copenhagen, Blegdamsvej 17*, Copenhagen 2100-DK, Denmark*

and

Center for Applied Mathematics, Cornell University, Ithaca, New York 14853, USA

Steven H. Strogatz †

Center for Applied Mathematics, Cornell University, Ithaca, New York 14853, USA

(Dated: October 3, 2019)

* jonas.juul@nbi.ku.dk

† strogatz@cornell.edu (corresponding author)

I. PRIOR WORK ON CONTAGION PATHS AND EPIDEMIC TREES

The contagion paths and epidemic trees constructed in Fig. 1 in the main text have been studied previously in diverse disciplines. They have been called adoption paths[15], dissemination trees[29,30], spreading patterns[31], causal trees of disease transmission[32], diffusion structure patterns[33], the structure of diffusion events[34], and epidemic trees[35]. We adopt the latter term, which comes from epidemiology, with a single caveat: Generally the graph of the propagation paths for a contagion need not be a directed tree; in the case of a complex contagion[36], where each child node has two or more parents, the graph could be a directed graph with no cycles. But for the simple contagions studied in this paper, where each child is assumed to have only one parent, the graph of the propagation paths is always a tree.

In the following sections, we show the details of our calculations of descendant distributions on complete graphs, configuration models, Erdős–Rényi random networks, small-world networks, and infinite-dimensional networks in general. In each case, we assume a simplified model of contagion dynamics in which each node is in one of two states: susceptible, or permanently infected and infectious, as described in the main text. The final section of the Supplementary Information contains information about the maximum-likelihood fit we performed on the descendant distributions for the spreading process on empirical networks.

II. COMPLETE GRAPH

In this section, we calculate the descendant distribution for a complete graph of N nodes, with $N \gg 1$.

Suppose that nodes are infected one at a time, and that the descendant distribution after t nodes have been infected is given by $P_{d,t}$. We wish to calculate the equilibrium distribution of descendants, $P_d := \lim_{t\to\infty} P_{d,t}$. To do this, it is helpful to use language from network growth[37]. When a new node is infected, a number of already-infected nodes will gain this node as a descendant in the epidemic tree. If, say, 14 nodes acquire this node as a descendant, let us refer to this as introducing 14 descendants in the epidemic tree and then distributing these 14 descendants among the infected nodes. With this terminology in place, we proceed with the calculation.

First, because any edge that connects a susceptible and infected node is equally likely to

be the next edge over which the infection is transmitted, and because the graph is complete, the expected *fraction* of newly introduced descendants that nodes with d descendants get is

$$\frac{(d+1)P_{d,t}}{\sum_d (d+1)P_{d,t}} = \frac{(d+1)P_{d,t}}{(m_t+1)}, \tag{S1}$$

where

$$m_t := \sum_d dP_{d,t} \tag{S2}$$

is the mean number of descendants in the epidemic tree at time t. The numerator in Eq. (S1) expresses point (ii) in the main text, and the denominator is a normalisation factor. Next, to go from the expected fraction in Eq. (S1) to the expected *number* of new descendants that a node with d descendants gets in the following time step, we must multiply the expected fraction (S1) by the total expected number of new descendants, aggregated over nodes with *any* number of descendants, that are added during the time step.

To find this total, we observe that every infected node has equal probability of being the next to pass on the infection, and there are t infected nodes at time t. Thus the probability that nodes with d descendants will get a new descendant is $(d+1)P_{d,t}/t$. Summing over all d then gives us the expected fraction of the infected nodes in total that will get a new descendant in the following time step; multiplying by t gives us the corresponding expected number. This argument tells us, then, that

$$t\sum_d \frac{(d+1)P_{d,t}}{t} = m_t + 1 \tag{S3}$$

is the expected number of infected nodes, in total, that will get a new descendant in the following time step. Note that the underlying network did not influence this last part of the calculation.

By combining Eqs. (S1) and (S3) we find that, for the complete graph, the expected number of new descendants that a node with d descendants gets in time step t is

$$\frac{(d+1)P_{d,t}}{(m_t+1)}(m_t+1) = (d+1)P_{d,t}. \tag{S4}$$

This result leads us to the following master equation, which expresses the expected gain and loss of nodes with d descendants between time steps t and $t+1$:

$$(t+1)P_{d,t+1} - tP_{d,t} = \begin{cases} 1 - P_{0,t} & \text{for } d = 0, \\ dP_{d-1,t} - (d+1)P_{d,t} & \text{for } d \geq 1. \end{cases} \tag{S5}$$

The case $d = 0$ is different from other values of d since the newly infected node will have no descendants when it is added to the epidemic tree, thereby making the gain term in the master equation equal to 1. An equilibrium distribution must satisfy $P_{d,t} = P_{d,t+1} =: P_d$. Applying this condition and solving for P_d, we get:

$$P_0 = \frac{1}{2}, \qquad P_d = \frac{d}{d+2} P_{d-1}. \tag{S6}$$

From this we conclude that the distribution of the expected number of descendants on the complete graph is

$$P_d = \frac{d!}{(d+2)!} = \frac{1}{(d+2)(d+1)}. \tag{S7}$$

As mentioned in the main text, keeping track of descendants can be mapped to growing a network by node copying[25]. For the complete graph, this mapping means that equation (S7) is identical to the formula for the in-degree distribution calculated by Krapivsky & Redner[25]. In their paper on network growth with node copying, Krapivsky & Redner derive geometrical properties of the grown networks. We refer the interested reader to the paper, and continue with calculating descendant distributions below.

III. CONFIGURATION MODEL AND ERDŐS–RÉNYI RANDOM NETWORKS

In this section, we turn to two classes of random networks: configuration-model networks, and Erdős–Rényi random graphs.

In the configuration model that we consider, each of N nodes has a certain number of "half edges" (or "stubs") sticking out of it, with the number of stubs being chosen at random from a prescribed degree distribution. The network is then generated by connecting pairs of stubs, chosen uniformly at random from the list of all stubs, to make the full edges of the resulting network.

The Erdős–Rényi networks are constructed by considering each pair of nodes independently and, with probability p, connecting that pair with an undirected edge.

To understand Fig. 3 shown in the main text, we now calculate the descendant distribution for these random networks, using the same method as in the previous section. At time steps $t \geq 1$, an infected node with degree k has at least one infected neighbor (its "parent"). If the infected node (denoted I), or one of its descendants, infects a neighbor, then I loses one edge over which it could infect another node. By doing this, however, it gets a new

descendant, which might have a number of edges connecting it to susceptible nodes. If we assume that every one of the $k-1$ edges that could connect an infectious degree-k node with a susceptible node has equal probability of doing so (equal to 1 in the infinite-network limit), and if we assume that this probability is the same for every infected node, then an infected node has on average $(z-2)d+(z-1)$ edges which could connect it to susceptible nodes. Here z is the mean degree of the network.

So the mean number of new descendants that a node with d descendants gets when a new node is infected is

$$\frac{\left[(z-2)d+z-1\right]P_{d,t}}{(z-2)m_t+z-1}\left(m_t+1\right). \tag{S8}$$

Using this result, we can write down a master equation as we did when calculating the descendant distribution for the spreading process on the complete graph, and solve for a steady-state descendant distribution P_d, in the limit of infinite network size. After some algebra (see Supplementary Section V for details), we find that

$$P_d=\begin{cases}\frac{z-2}{2z-3} & \text{for } d=0,\\ \frac{z-2}{2z-3}\left[B\left(\frac{z-1}{z-2},2\right)\right]^{-1}B\left(\frac{z-1}{z-2}+d,2\right) & \text{for } d\geq 1.\end{cases} \tag{S9}$$

Here $B(a,b)$ is the beta function, which declines as a^{-b} as $a\to\infty$ for fixed b. In our case, this means

$$\begin{aligned}P_d &\propto B\left(\frac{z-1}{z-2}+d,2\right),\\ &\propto d^{-2},\end{aligned} \tag{S10}$$

for $d\gg 1$. By invoking identities for the beta function, we can rewrite the expression (S9) for the descendant distribution as

$$P_d=\frac{z-1}{z-2}B\left(\frac{z-1}{z-2}+d,2\right), \tag{S11}$$

which is the expression we list in the main text. Figure 3 in the main text collapses the simulated data on the curve $B(\tilde{d},2)$, where

$$\tilde{d}:=\tilde{x}(z)+d=\frac{z-1}{z-2}+d. \tag{S12}$$

Given a simulated data point (d,P_d), this collapse is made by plotting the data point at $(d+\tilde{x}(z),[\tilde{x}(z)]^{-1}P_d)$ instead.

IV. A RING AND A SMALL-WORLD NETWORK

The networks of the previous section are related to each other, in that edges between nodes are created according to a random procedure. They all show the inverse-square scaling mentioned in the main text: $P_d \propto d^{-2}$ for large d.

On the other hand, some non-random graphs do not have this limiting behavior. If we consider the spreading process taking place on a ring, in which every node has only two neighbours, one to its left and one to its right, we can write down the expected distribution of number of descendants immediately. Starting from only a single seed, in each time step there will be exactly one possibility for the process to spread on the right hand side of the seed, and one possibility to spread on the left hand side. The resulting distribution of descendants in a ring consisting of N nodes is

$$P_d = \mathcal{N} \sum_{L=0}^{N} \left[\Theta\left(d \leq L-1\right) P_L + \Theta\left(d \leq N-L+1\right) P_L \right], \tag{S13}$$

where $\mathcal{N}$ is a normalization constant, $\Theta(x)$ is the Heaviside function equal to 1 if $x \geq 0$ and 0 otherwise, and P_L is the probability of the contagion process spreading exactly L times to the left along the periphery of the ring, given by

$$P_L = \binom{N}{L} \left(\frac{1}{2}\right)^N. \tag{S14}$$

One natural question to ask is then: How random does a network have to be to show the limiting behavior $P_d \propto d^{-2}$ we observed in the previous sections? In the rest of this section we analytically estimate the descendant distribution for the contagion process on small-world networks. Specifically, the small-world networks are Watts-Newman small-world networks in which all nodes are connected to their two immediate neighbours on a ring lattice, and each node gets a shortcut to a neighbour chosen uniformly at random with probability p.

First, we must estimate the expected number of new descendants that a node with d descendants gets when a node gets infected. If the underlying network was simply a ring and no shortcuts had been added, every node would have equal chance of getting new descendants. This changes when the shortcuts are inserted: For each descendant a node has, the chance that one of its descendants has a shortcut increases. If the infection traverses such a shortcut link successfully, it can spread both to the right and to the left in this newly discovered part of the network. Hence, two more boundaries between infectious nodes and

susceptible nodes have been created, and every node that has descendants on this boundary now has a higher chance of getting more descendants. This effect alters the expected number of descendants received by a node with d descendants when a new node gets infected. The expected number now becomes

$$\frac{P_{d,t}(1+2p(d+1))}{1+2p(m_t+1)}(m_t+1). \tag{S15}$$

Here the first term represents the shortcut-independent probability that every node has to get a new descendant, and the terms that are proportional to p correspond to the increased probability of getting new descendants that nodes get via shortcuts. With this, we can write down the master equation as in the two sections above. After some algebra (see Supplementary Section V below for details), we find

$$P_d = \begin{cases} \frac{2p}{1+4p} & \text{for } d=0, \\ \frac{2p}{1+4p}\left[B\left(\frac{2p+1}{2p},2\right)\right]^{-1} B\left(\frac{2p+1}{2p}+d,2\right) & \text{for } d\geq 0. \end{cases} \tag{S16}$$

For large d, this analytical solution declines as

$$P_d \propto B\left(\frac{2p+1}{2p}+d,2\right), \tag{S17}$$

$$\propto d^{-2}. \tag{S18}$$

In Extended Data Fig. 1, we see that the analytical solution indeed is in qualitative agreement with the simulations.

V. UNIVERSAL BEHAVIOR AND WHEN IT BREAKS DOWN

We have studied the descendant distributions for simple contagion on different networks: complete graphs, configuration-model networks, Erdős–Rényi networks, and small-world networks. On all of these networks, we have discovered a striking universality: The distributions decline as a power law with exponent -2 for large d. A natural question to ask is, then, what unifies these graphs: When does the universality exist, and when does it break down?

One thing that is true for all the graphs we have studied is that the probability of getting more descendants is linearly proportional to the number of descendants the node already has.

In other words, the expected number of descendants received by a node with d descendants, when a new node gets infected, is of the form

$$\frac{P_{d,t}\,(c+fd)}{\sum_d P_{d,t}\,(c+fd)}\,(m_t+1) = \frac{P_{d,t}\,(c+fd)}{c+fm_t}\,(m_t+1)\,, \tag{S19}$$

for $c, f > 0$. We will now show that this, and $m_t \to \infty$ as $t \to \infty$, is sufficient to make the resulting distribution of the number of descendants decline as the power law with exponent -2 for large d. The condition $m_t \to \infty$ is true for all the classes of random graphs we have examined, since the fewer edges compared to the complete graph decreases the interface between susceptible and infectious nodes. This makes the probability of nodes with many descendants getting additional descendants increase compared to the spreading process on the complete graph. Because m_t diverges for the complete graph, m_t also diverges for the random graph in question by the comparison test. As $m_t \to \infty$, the right hand side of equation (S19) approaches $P_{d,t}(d/f + d)$. With this, we get the master equation,

$$(t+1)P_{d,t+1} - tP_{d,t} = \begin{cases} 1 - P_d\frac{c}{f} & \text{for } d = 0, \\ \left[P_{d-1,t}\left(\frac{c}{f}+d-1\right)\right. & \\ \quad \left. -P_{d,t}\left(\frac{c}{f}+d\right)\right] & \text{for } d \geq 1. \end{cases} \tag{S20}$$

Looking for steady-state solutions $P_{d,t+1} = P_{d,t} =: P_d$, we obtain

$$P_0 = \frac{f}{f+c}, \qquad P_d = \frac{c/f - 1 + d}{1 + c/f + d}P_{d-1}, \tag{S21}$$

where the expression for P_d is valid for $d \geq 1$. Denoting $c/f - 1 =: \alpha$, we can use the recursive nature of the expression to rewrite P_d as follows:

$$\begin{aligned} P_d &= P_0 \prod_{\lambda=1}^{d} \frac{\alpha+\lambda}{\alpha+2+\lambda} \\ &= P_0 \frac{\Gamma(\alpha+3)\Gamma(\alpha+d+1)}{\Gamma(\alpha+1)\Gamma(\alpha+3+d)}. \end{aligned} \tag{S22}$$

If we increase the terms of the fraction by a factor of $\Gamma(2)$, and use the relation between gamma functions and beta functions, $\Gamma(x)\Gamma(y)/\Gamma(x+y) = B(x,y)$, we get

$$P_d = \frac{f}{f+c}\left[B(\alpha+1,2)\right]^{-1} B(\alpha+d+1,2), \tag{S23}$$

$$= \frac{c}{f} B\left(\frac{c}{f}+d, 2\right). \tag{S24}$$

The final step was made by inserting the value of α and evaluating $B(c/f, 2) = f^2/[c(c+f)]$. The asymptotic behavior for large d is

$$\begin{aligned} P_d &\propto (c/f + d)^{-2} \\ &\propto d^{-2}. \end{aligned} \tag{S25}$$

Therefore, if the probability of getting more descendants increases linearly with the number of descendants a node already has, the descendant distribution will decline as d^{-2} for large d. If we interpret the number of descendants an infected node has as a volume, and the interface separating infectious and susceptible nodes as a surface area, the descendant distribution will show the observed universality if the surface area and the volume increase equally fast (proportional to d); in other words, if the graph is infinite dimensional.

VI. EMPIRICAL NETWORKS AND MAXIMUM-LIKELIHOOD FIT

The two empirical networks discussed in the main text were obtained from the SNAP database[38]. For the Twitter network, we converted all directed edges into undirected ones, not allowing parallel edges. To estimate the power-law exponent of the tail of the distributions, we used a maximum-likelihood method to fit a power-law to the data for $d \in [100, 1900]$ (not including the extreme data points caused by the choice of having a single seed). We used the approximate expression for the maximum-likelihood power-law exponent $\hat{\alpha}$ for binned data[39]

$$\hat{\alpha} \approx 1 + n \left[\sum_{i=1}^{n} \ln \frac{d_i}{d_{\min} - 1/2} \right]^{-1}, \tag{S26}$$

and checked that direct numerical evaluation gave a similar result. In this formula, n is the total number of data points, d_i is the i^{th} data point, and $d_{\min}$ is the smallest value for the data (in this case, 100). We estimated the standard error on $\hat{\alpha}$ by using the corresponding formula,

$$\sigma_{\hat{\alpha}} = \frac{1}{\sqrt{n \left[\frac{\zeta''(\hat{\alpha}, d_{\min})}{\zeta(\hat{\alpha}, d_{\min})} - \left(\frac{\zeta'(\hat{\alpha}, d_{\min})}{\zeta(\hat{\alpha}, d_{\min})} \right)^2 \right]}}, \tag{S27}$$

where prime indicates differentiation with respect to the first variable. For both networks we obtained $\hat{\alpha} \approx 2.04 \pm 0.01$.

---

[1] Watts, D. J. A simple model of global cascades on random networks. *Proceedings of the National Academy of Sciences* **99**, 5766–5771 (2002).

[2] Dodds, P. S. & Watts, D. J. A generalized model of social and biological contagion. *Journal of theoretical biology* **232**, 587–604 (2005).

[3] Castellano, C., Fortunato, S. & Loreto, V. Statistical physics of social dynamics. *Reviews of Modern Physics* **81**, 591 (2009).

[4] Christakis, N. A. & Fowler, J. H. The spread of obesity in a large social network over 32 years. *New England Journal of Medicine* **357**, 370–379 (2007).

[5] Lehmann, S. & Ahn, Y.-Y. *Complex spreading phenomena in social systems* (Springer, 2018).

[6] Anderson, R. M. & May, R. M. *Infectious diseases of humans: dynamics and control* (Oxford university press, 1991).

[7] Keeling, M. J. & Rohani, P. *Modeling infectious diseases in humans and animals* (Princeton University Press, 2011).

[8] De Domenico, M., Granell, C., Porter, M. A. & Arenas, A. The physics of spreading processes in multilayer networks. *Nature Physics* **12**, 901 (2016).

[9] Fennell, P. G. & Gleeson, J. P. Multistate dynamical processes on networks: analysis through degree-based approximation frameworks. *SIAM Review* **61**, 92–118 (2019).

[10] Pastor-Satorras, R., Castellano, C., Van Mieghem, P. & Vespignani, A. Epidemic processes in complex networks. *Reviews of Modern Physics* **87**, 925 (2015).

[11] Daley, D. J. & Kendall, D. G. Stochastic rumours. *IMA Journal of Applied Mathematics* **1**, 42–55 (1965).

[12] Vosoughi, S., Roy, D. & Aral, S. The spread of true and false news online. *Science* **359**, 1146–1151 (2018).

[13] Bettencourt, L. M., Cintrón-Arias, A., Kaiser, D. I. & Castillo-Chávez, C. The power of a good idea: Quantitative modeling of the spread of ideas from epidemiological models. *Physica A: Statistical Mechanics and its Applications* **364**, 513–536 (2006).

[14] Mellor, A., Mobilia, M., Redner, S., Rucklidge, A. M. & Ward, J. A. Influence of luddism on innovation diffusion. *Physical Review E* **92**, 012806 (2015).

[15] Juul, J. S. & Porter, M. A. Hipsters on networks: How a minority group of individuals can lead to an antiestablishment majority. *Physical Review E* **99**, 022313 (2019).

[16] Krapivsky, P. L., Redner, S. & Volovik, D. Reinforcement-driven spread of innovations and fads. *Journal of Statistical Mechanics: Theory and Experiment* **2011**, P12003 (2011).

[17] Haldane, A. G. & May, R. M. Systemic risk in banking ecosystems. *Nature* **469**, 351 (2011).

[18] Brummitt, C. D., D'Souza, R. M. & Leicht, E. A. Suppressing cascades of load in interdependent networks. *Proceedings of the National Academy of Sciences* **109**, E680–E689 (2012).

[19] Andreasen, V., Viboud, C. & Simonsen, L. Epidemiologic characterization of the 1918 influenza pandemic summer wave in Copenhagen: implications for pandemic control strategies. *The Journal of Infectious Diseases* **197**, 270–278 (2008).

[20] Adamic, L. A., Lento, T. M., Adar, E. & Ng, P. C. Information evolution in social networks. In *Proceedings of the Ninth ACM International Conference on Web Search and Data Mining*, 473–482 (ACM, 2016).

[21] Yule, G. U. A mathematical theory of evolution, based on the conclusions of dr. j. c. willis, f.r.s. *Philosophical Transactions of the Royal Society of London. Series B, containing papers of a biological character* **213**, 21–87 (1925).

[22] Simon, H. A. On a class of skew distribution functions. *Biometrika* **42**, 425–440 (1955).

[23] De Solla Price, D. A general theory of bibliometric and other cumulative advantage processes. *Journal of the American Society for Information Science* **27**, 292–306 (1976).

[24] Barabási, A.-L. & Albert, R. Emergence of scaling in random networks. *Science* **286**, 509–512 (1999).

[25] Krapivsky, P. L. & Redner, S. Network growth by copying. *Physical Review E* **71**, 036118 (2005).

[26] Newman, M. E. J. & Watts, D. J. Renormalization group analysis of the small-world network model. *Physics Letters A* **263**, 341–346 (1999).

[27] Leskovec, J. & McAuley, J. J. Learning to discover social circles in ego networks. In *Advances in neural information processing systems*, 539–547 (2012).

[28] Rozemberczki, B., Davies, R., Sarkar, R. & Sutton, C. Gemsec: Graph embedding with self clustering. *arXiv preprint arXiv:1802.03997* (2018).

[29] Oh, S.-W. & Porter, M. A. Complex contagions with timers. *Chaos: An Interdisciplinary Journal of Nonlinear Science* **28**, 033101 (2018).

[30] Liben-Nowell, D. & Kleinberg, J. Tracing information flow on a global scale using internet chain-letter data. *Proceedings of the National Academy of Sciences* **105**, 4633–4638 (2008).

[31] Jang, S. M. *et al.* A computational approach for examining the roots and spreading patterns of fake news: Evolution tree analysis. *Computers in Human Behavior* **84**, 103–113 (2018).

[32] Vázquez, A. Causal tree of disease transmission and the spreading of infectious diseases. In *Discrete Methods in Epidemiology*, 163–180 (2004).

[33] Zhang, Z.-K. *et al.* Dynamics of information diffusion and its applications on complex networks. *Physics Reports* **651**, 1–34 (2016).

[34] Goel, S., Anderson, A., Hofman, J. & Watts, D. J. The structural virality of online diffusion. *Management Science* **62**, 180–196 (2015).

[35] Haydon, D. T. *et al.* The construction and analysis of epidemic trees with reference to the 2001 uk foot–and–mouth outbreak. *Proceedings of the Royal Society of London. Series B: Biological Sciences* **270**, 121–127 (2003).

[36] Mønsted, B., Sapieżyński, P., Ferrara, E. & Lehmann, S. Evidence of complex contagion of information in social media: An experiment using twitter bots. *PloS one* **12**, e0184148 (2017).

[37] Newman, M. E. J. The structure and function of complex networks. *SIAM Review* **45**, 167–256 (2003).

[38] Leskovec, J. & Krevl, A. SNAP Datasets: Stanford large network dataset collection. `http://snap.stanford.edu/data` (2014).

[39] Clauset, A., Shalizi, C. R. & Newman, M. E. J. Power-law distributions in empirical data. *SIAM review* **51**, 661–703 (2009).

6.5 Conclusions of Part II and perspectives for further research

We have studied two extensions of the Watts Threshold Model and the impact of mutant variants of simple contagion spreading in various networks. For the WTM with synergistic effects, we found that the synergy could make it possible or impossible to activate degree-k nodes. Synergy could also decrease the number of active neighbours needed to activate nodes with degree k. We provided explicit formulas for these bifurcation points and an analytical approximation that described the fraction of active degree-k nodes as a function of time. This approximation worked well for all networks but broke down when the model was simulated on a Facebook subgraph. We argued that this was caused by the network being less locally tree-like.

For the WTM with anti-establishment nodes, we found that anti-establishment nodes constituting tiny fractions of the population could cause an otherwise insignificant product to become adopted by a majority of the network at equilibrium. We found this tiny fraction to be smaller than 10% in every synthetic network we chose. We argued that the large impact of the anti-establishment nodes was due to adoption paths. The small chance that a hipster having many descendants drives up the expected number of product-B adopters.

Finally, we found that the impact of mutant contagion follows a probability distribution $B(f(d, \boldsymbol{p}), 2)$ for all infinite dimensional networks. In particular, the tail of the distribution declines proportional to d^{-2}. We assumed that the contagion was simple, mutated rarely, and that the mutation did not impact the rate of infection. We also argued that this will hold for any effectively infinite-dimensional network. Two examples of such effectively infinite-dimensional networks are the global human contact network and Facebook. We argued that evidence of this scaling law for the impact of mutant contagion was previously observed in meme-spreading on Facebook. We also showed that the impact of mutant contagion in a 2-dimensional network did not follow the same scaling law.

There are several promising directions for future research. The model of synergistic spreading we provided was based on the so-called r-synergy. One could create similar models of d-synergy and investigate what effect such donor synergy would have on spreading dynamics. An educated guess on the results would be that bifurcations, similar to the ones we uncovered, would be present in the d-synergistic threshold models. Another direction would be to further analyse the models by simulating them on other types of networks: multi-layer networks, temporal networks, or modular networks.

By including hipsters in the WTM, we wanted to investigate the formation of anti-establishment majorities. It is not clear, however, that opinion dynamics seen in elections are well-approximated by threshold models of complex contagion. It might be that citizens continuously update their opinions as time progresses. Hence, including hipster nodes in other dynamical models could inform us more about how such anti-establishment majorities in elections come to be. One class of models that would be an obvious choice for such implementation of hipsters is voter models. A recent study suggested doing this (Kureh and Porter, 2019).

The most promising directions, however, I think come from the final paper I presented in this part of the dissertation. Epidemic trees have not been studied in detail, and therefore much work needs to be done. First, the impact of mutant contagion in finite-dimensional networks has not been understood yet. Is there a scaling law in 2 dimensions, similar to the one found for inifinite dimensions? How about other

finite dimensions? Finite dimensions are common in biological systems, and hence this research track could be of great importance.

It would also be interesting to study what impact mutant contagions would have, if the mutations altered traits of the contagion. What if the mutation changed the rate of infection? In our study, we assumed that the contagion could be described as an SI model. What if the contagion were instead described by an SIR model? How would choices of the rates of infection and removal affect the dynamics? And what if mutations caused the contagion to be more lethal and increased the rate of removal? Finally, we have only suggested one application of epidemic trees. Perhaps epidemic trees have other applications, waiting to be uncovered.

Part III

Patterns in telecommunication

Chapter 7

Investigating homophily and network centrality among narcissists using telecommunication data

7.1 A day in the life

Darkness still covered the land when the alarm went off. Still half asleep, Bob fumbled for his phone, eventually succeeding in stopping the screaming of the device. After dragging himself to the kitchen to make his morning cup of coffee, he turned on the radio via the sound system controller app and made a bowl of cereal. With a steaming cup of coffee and a bowl of breakfast, he quickly browsed through the latest online news before heading out for his daily commute to work.

While the landscape drifted past outside the train cabin, Bob listened to his favourite podcast. While the host gave exceedingly detailed descriptions of the consistency, color, and flavour of the soup he was making, Bob made the day's first attempt to empty his email inbox. Finally at work, Bob found his desk exactly as he left it. While trading the mug from the day before for a new one full of coffee, he found the time to reply to a text message from a sick coworker while the coffee machine was buzzing away.

Bob, being an enthusiastic worker, resisted the siren song of the little bump in his right pocket for most of the day. A few exceptions to this were his occasional visits to the coffee machine or the bathroom. During these short intermissions of an otherwise busy day, he found the time to "like" pictures and status updates on social media.

On his train ride home, he called his old mother. She told him everything about the most recent football transfers in the Premier League, and how a courier had delivered a package to her neighbour earlier that day. Back in his apartment, he brought his microwaved meal with him to the living room. Accompanied by the shrinking mountain of noodles, he streamed the night's international football game. After a spectacular goal, he called his mother again. She assured him that the player leaving for a competing club at the end of the season would be tough for his old club.

Having turned off the connection between phone and television, Bob went to bed. The last thing he did before going to sleep was setting the alarm for the next morning.

7.2 Using telecommunication data to study humans

As the made-up day of Bob illustrates, phones are part of almost every minute of modern lives. Before Bob goes to sleep, he sets the alarm. The first thing he does in the morning is to turn it off. He uses his phone to read the news and connect to his stereo. He uses his phone for leisure and for work. Even his coffee and bathroom breaks can be inferred from when he uses his phone.

His phone is also a means of communicating with his social contacts. He calls his mom and replies to text messages from sick colleagues using the same device. As a football team scores, he calls his mom in excitement.

Because phones are such integrated parts of our lives, they might be good candidates for tools through which we can understand human behavior. Instead of giving people questionnaires about their eating, sleeping, and social habits, smartphone usage can provide data with a resolution of mere seconds. If we can develop the right measures and successfully filter signal from noise, the data holds almost unfathomable research potential.

During my Ph.D. I have worked with two different telecommunication data sets. With an interdisciplinary team of scientists, I have investigated human behavior in two very different situations. I have studied patterns in social connections aggregated over a long time interval and behavioral change following a sudden perturbation to the social system – in the form of a terror attack. In both projects, I have examined how differences among individuals influence emerging behavioral patterns. In the study on behavioral change following terror attacks, we compare the behavior of participants of different genders. In the other project, we investigate whether people with high scores on a specific personality trait tend to connect to other people with high scores on this same trait.

This third part of the dissertation is structured as follows. The present chapter introduces our research on the statistics of social ties of *narcissists*. The manuscript constitutes Section 7.6. Before proceeding to this section, however, I will introduce the concept of narcissism and give a brief introduction to *homophily* – one of the main things analysed in our manuscript. In the next chapter, Chapter 8, I present our manuscript on behavioral patterns following attacks. Chapter 8 also briefly motivates why we should study the behavior of populations following terror attacks and mentions prior results on such behavioral patterns.

7.3 Narcissism

Disposition-based behavior explanations have long been used in psychology (Ajzen, 2005). One way of describing dispositions is through personality traits. Among the many personality traits, humans can have, narcissism is perhaps the most infamous. This status of narcissism is perhaps most visible in narcissism being part of ancient mythology. According to the legend, Narcissus, a character from Greek mythology, fell in love with his own image. At the present day, the relevance of narcissism is illustrated by psychologists having public discussions about whether the current president of the United States suffers from "Narcissistic personality disorder" (Barber, 2016). But what does narcissism mean, and how is it quantified? This is an interesting question, the answer to which is currently under intense scrutiny.

The modern perception views narcissists as having "an overarching goal of maintaining a grandiose self". Half a decade ago, a group of psychologists suggested that a "grandiose self" is created by two mechanisms: narcissistic admiration (ADM) and

rivalry (RIV) (Back et al., 2013). They designed a questionnaire to test for rivalry. This Narcissistic Admiration and Rivalry Questionnaire (NARQ) contains 18 items. 9 of these items are related to the admiration dimension, whereas the remaining 9 items probe the rivalry dimension. Participants answer each question with an integer ranging from 1 to 6. 1 means "*not agree at all*"; 6 means "*agree completely*". The 18 items are listed in (Back et al., 2013), and I repeat them here to give a sense of the psychological phenomenon of narcissism.

The 9 items related to Narcissistic Admiration are (quote from (Back et al., 2013)),

1. I am great.
2. I will someday be famous.
3. I deserve to be seen as a great personality.
4. I show others how special I am.
5. I enjoy my successes very much.
6. Being a very special person gives me a lot of strength.
7. Most of the time I am able to draw people's attention to myself in conversations.
8. I manage to be the center of attention with my outstanding contributions.
9. Mostly, I am very adept at dealing with other people.

The first three probe a facet of ADM called "grandiosity". The next three test for "uniqueness". The final three questions test for the facet "charmingness".

The other narcissistic dimension is Narcissistic Rivalry. The 9 items to Narcissistic Rivalry are (quote from (Back et al., 2013)),

1. Most people won't achieve anything.
2. Other people are worth nothing.
3. Most people are somehow losers.
4. I secretly take pleasure in the failure of my rivals.
5. I want my rivals to fail.
6. I enjoy it when another person is inferior to me.
7. I react annoyed if another person steals the show from me.
8. I often get annoyed when I am criticized.
9. I can barely stand it if another person is at the center of events.

Here the first 3 test a facet "devaluation". The middle 3 probe for a facet "supremacy". The final 3 probe for "aggressiveness".

Because this splitting of narcissism into 2 dimensions was done so recently, much remains unknown concerning the correlation between narcissistic personality traits and social behavior. The manuscript presented in this chapter investigates *homophily* in narcissism, network centrality in narcissism, and the duration of social connections for narcissists. By doing this, we test current hypotheses in personality psychology.

	Black	Hispanic	White	Other
Black	506	32	69	26
Hispanic	23	308	114	38
White	26	46	599	68
Other	10	14	47	32

TABLE 7.1: Table of partner race. Couples from (Catania et al., 1992). Presented in a table after (Mollison and Denis, 1995; Newman, 2003b).

Recent research reported that certain personality traits, like empathy, correlate with centrality in some social networks (Morelli et al., 2017). Narcissists view themselves as special and deserving of being at the center of attention. Whether narcissists actually do receive more attention than others remains an open question. This is the motivation for investigating network centrality in narcissism.

Another hypothesis in the existing narcissism literature is related to the popularity of narcissists over time. It was suggested that popularity decreases over time, but is high in short-term relationships (Grosz et al., 2015; Back, Küfner, and Leckelt, 2018). By measuring how the frequency of long and short-term friendships in social networks correlate with ADM and RIV scores, we can test these hypotheses.

The final thing we set out to investigate – homophily – has a long history in the social sciences. I dedicate the following subsection to introduce this concept of homophily.

7.4 Homophily

Homophily is the tendency to form links to nodes with similar traits as oneself. One classic example of such homophily is in the choice of partner. Table 7.1 illustrates the race and ethnicity of each partner in couples participating in a health study (Catania et al., 1992). In each row, the diagonal entry takes the largest value. This indicates a high frequency of same-race or same-ethnicity couples – it indicates homophily!

Homophily is studied in many different systems. One particularly relevant study to quote here is the one by Møllgaard et al. (Mollgaard et al., 2016). Using the same dataset as we will be studying, they investigated homophily in "the Big Five" personality traits and social variables. These social variables were, e.g., consumption of alcohol and whether people smoked. They found homophily in social variables like gender, alcohol consumption, and smoking. In contrast, they found no evidence of homophily in any of the Big Five personality traits.

(Lee et al., 2017) recently reported that homophily in social networks influences the creation of perception biases such as filter bubbles and majority illusions. In another recent study, (Karimi et al., 2018) showed that homophily could make it more difficult for minorities to get influential in social networks.

Whether homophily exists in narcissism is interesting because there is no theoretical consensus on the topic. On the one hand, dominant narcissistic behavior might be best paired with more submissive personality traits (Orford, 1986). This would lead to homophily being absent in narcissism. On the other hand, one study reported that narcissists perceive it as difficult to find other people with greatness comparable of their own (Foster and Campbell, 2007). This longing could cause narcissists to frequently connect to other narcissists, thereby giving rise to homophily in narcissism.

In the past, psychologists did carry out a few studies on homophily in narcissism. One study asked participants to rate the attractiveness of hypothetical partners for short-term or long-term relationships. This study found homophily in both dimensions of narcissism (Grosz et al., 2015). Other studies have found homophily in grandiose narcissism in pairs of best friends and romantic couples (Lavner et al., 2016; Maaß et al., 2016). However, no one studied homophily in narcissism on a large scale with real-time social-network data.

In our paper, we will measure homophily in large social networks. In network science, homophily is often referred to as *assortative mixing* (Newman, 2002a; Newman and Girvan, 2003; Newman, 2003a; Newman, 2003b; Newman, 2018). Assortative mixing can be computed in different ways. The main idea in such quantifications is estimating how scores of linked nodes correlate with each other. If this correlation is larger than should be expected, if scores were distributed randomly among network nodes, homophily is present in the scores.

The way we will measure homophily in the article presented by the end of this chapter was first done by (Mollgaard et al., 2016). They generalised the intraclass correlation coefficient to take network structure into account. They expressed their homophily measure as a fraction,

$$r = \frac{t^2}{s^2}. \tag{7.1}$$

Here t^2 computes the correlation and s^2 takes into account the variation in the trait score. For a network with link weights w_{ij}, the mathematical expressions for t^2 and s^2 used to compute homophily in trait scores $\{x_i\}$ are

$$t^2 = \frac{\sum_{i>j} w_{ij}(x_i - \bar{x})(x_j - \bar{x})}{\sum_{i>j} 2w_{ij}}, \tag{7.2}$$

$$s^2 = \frac{\sum_{i>j} w_{ij}\left((x_i - \bar{x})^2 + (x_j - \bar{x})^2\right)}{\sum_{i>j} 2w_{ij}}. \tag{7.3}$$

The $\bar{x}$ is an expected value of the trait score which takes link weight into account ,

$$\bar{x} = \frac{\sum_{i>j} w_{ij}(x_i + x_j)}{\sum_{i>j} 2w_{ij}}. \tag{7.4}$$

In the following section, I present the results we obtained when studying homophily, link duration, and network centrality in relation to narcissism trait scores in our telecommunication data.

7.5 Our results: Correlations between narcissism scores and social behavior

The manuscript of the present chapter is still in preparation and entitled "Investigating Homophily, Network Centrality, and Social-Connection Duration of Grandiose Narcissists: Narcissistic Admiration and Rivalry in Big Data Social Networks". I coauthor this manuscript with psychologists and computational scientists.

In the study, we analyse behavioral patterns of narcissists using a data set of telecommunication and physical proximity between undergraduate students. All participants filled out questionnaires. Among the questions on these questionnaires

were the 18 NARQ questions listed in Section 7.6. We count the number of interactions between each pair of students. Interactions can take place via text messages, calls, and physical proximity, and we use these to create social networks, which we then analyse.

In the networks, we assign weights to social interactions using a social-amplification parameter $\alpha \in \mathbb{R}$. When $\alpha = 0$ the social network we create does not take into account the number of interactions between students – if a pair of students had *any* interaction, we create a link between them with weight 1. This makes the adjacency matrix of the form expressed by Eq. (4.1). When $\alpha = 1$, the link weight between a pair of nodes is precisely proportional to the number of interactions between them. Whereas $\alpha = 0$ did not take the frequency of interactions into account in assigning link weights, choosing $\alpha = 2$ amplifies the number of social interactions. In this case, the social network only effectively contains links between the very strongest-interacting dyads. The intermediate values of α interpolate between these extremes.

When investigating correlations between behavior and ADM scores, we find evidence for homophily in ADM when only the most active links are considered (high α). We see this in the networks created using text-message data and physical proximity. We also find that ADM scores correlate with the number of different people participants are in touch with via text messages and calls.

Psychologically the homophily in ADM can be understood as people high in ADM seeking to par up with others "signalling greatness", in agreement with one hypothesis in the field. The high degree centrality in networks where all contacts are weighted equally could indicate that people high in ADM like being at the center of attention and successfully attract attention from others.

For RIV, we do not find any evidence of homophily. This could make sense psychologically, with high RIV scores indicating a tendency for these people to rival. For the RIV analysis, we find a mismatch between outgoing and ingoing communication for high social amplification in the text-message networks. Our analysis indicates that high RIV scores correlate with a high volume of outgoing communication. Psychologically, this aligns with the hypothesis that, although people with high RIV scores would like to be at the center of attention (and thus seek out attention), they do not attract it from others.

We do not find evidence that the duration of social connections correlate with any of the narcissism scores.

7.6 Paper: Investigating Homophily, Network Centrality, and Social Connnection Duration of Grandiose Narcissists

In preparation:

Investigating Homophily, Network Centrality, and Social Connnection Duration of Grandiose Narcissists: Narcissistic Admiration and Rivalry in Big Data Social Networks

Ingo Zettler[1], Jonas S. Juul[2], Mitja D. Back[3], Jochen E. Gebauer[4], Albrecht C. P. Küfner[5], Jesper Dammeyer[6], Sune Lehmann Jørgensen[7], and Joachim Mathiesen[8]

[1] Department of Psychology, University of Copenhagen, ingo.zettler@psy.ku.dk

[2] Niels Bohr Institute, University of Copenhagen, jonas.juul@nbi.ku.dk

[3] Department of Psychology, University of Münster, mitja.back@wwu.de

[4] Mannheim Centre for European Social Research, University of Mannheim, and Department of Psychology, University of Copenhagen, mail@jochengebauer.info

[5] Department of Psychology, University of Münster, albrecht.kuefner@uni-muenster.de

[6] Department of Psychology, University of Copenhagen, jesper.dammeyer@psy.ku.dk

[7] Department of Applied Mathematics and Computer Science, Technical University of Denmark, sljo@dtu.dk

[8] Niels Bohr Institute, University of Copenhagen, mathies@nbi.ku.dk

Author Notes:

Correspondence concerning this manuscript should be directed to Ingo Zettler, Department of Psychology, University of Copenhagen, Øster Farimagsgade 2A, 1353 København K, Denmark. Fon: +45 35324850, e-mail: ingo.zettler@psy.ku.dk

Investigating Homophily, Network Centrality, and Social Connection Duration of Grandiose Narcissists: Narcissistic Admiration and Rivalry in Big Data Social Networks

The construct of narcissism has attracted attention from researchers, practitioners, and laypeople alike. From a subclinical personality psychology perspective, “narcissism is a multifaceted personality trait encompassing individual differences in feelings of grandiosity and entitlement, and in striving for attention and superiority” (Back & Morf, 2019, p. X). On the most general level, people high in narcissism can be characterized by strong feelings that they are grandiose, unique, and entitled to deserve special. Under this umbrella—that is, people high in narcissism share these feelings—three aspects (or manifestations) of narcissism can be distinguished: agentic, antagonistic, and neurotic narcissism (Back, 2018; see also Crowe, Lynam, Campbell, & Miller, 2019).

Whereas neurotic narcissism mainly refers to one’s need to get positive feedback from others, we herein focus on the aspects of Narcissistic Admiration (ADM; representing agentic narcissism) and Rivalry (RIV; representing antagonistic narcissism; Back, 2018). ADM and RIV refer to different social strategies how people high in narcissism aim to maintain their self-view of being grandiose: ADM captures “the tendency to approach social admiration by means of self-promotion” via striving for uniqueness or charmingness, for instance. RIV, by contrast, captures “the tendency to prevent social failure by means of self-defense” (both Back et al., 2013, p. 1015) via striving for supremacy or aggressiveness, for instance.

By linking people’s levels in ADM and RIV to Big Data derived from three smartphone activities indicating social interactions between people—sending/receiving text messages, making/receiving phone calls, and scanned Bluetooth connections indicating spatial proximity—we herein investigate three research questions. First, is there homophily in ADM and RIV? That is, do people with similar levels in ADM and RIV, respectively, interact more

often with each other as compared to people with less similar levels in ADM and RIV, respectively? Second, are certain levels in ADM and RIV related to network centrality? That is, do people with certain levels in ADM or RIV hold central positions in social networks? Finally, are certain levels in ADM or RIV related to the duration of social connections between people? That is, do people with certain levels in ADM or RIV tend to have unusually brief or long connections with others? Although all research questions are tested from an exploratory point of view (because the data already existed when we started developing the research questions), we sketch the theoretical background concerning each research question in the following.

Narcissistic Admiration and Rivalry

According to the Narcissistic Admiration and Rivalry Concept (NARC; Back, 2018; Back et al., 2013), ADM and RIV capture different motivational and behavioral dynamics on how people high in narcissism seek to maintain their self-view of being grandiose. Specifically, people high in ADM are typically driven by assertive self-enhancement and can accordingly be characterized by feelings and behavior that boost their ego such as having grandiose fantasies, striving for uniqueness, and being charming and winning when interacting with others. People high in RIV, by contrast, are typically driven by antagonistic self-protection and can accordingly be characterized by feelings and behavior that protect their ego such as striving for supremacy over others, and being aggressive and devaluating when interacting with others.

The idea of the NARC to disentangle ADM and RIV has been supported by several studies. For instance, Lange, Crusius, and Hagemeyer (2016) found that both ADM and RIV are related to envy, but that ADM is rather related to benign, whereas RIV is rather related to malicious envy. In a similar vein, Zeigler-Hill et al. (2019) found that both ADM and RIV indicate people’s pursuit of status, but whereas high levels in ADM indicate a use of

dominance- or prestige-based strategies to seek status, high levels in RIV indicate a use of dominance-based strategies only. Further, Wurst et al. (2017) found that short-term romantic appeal of narcissists can primarily be linked to ADM, whereas long-term romantic problems of narcissists can primarily be linked to RIV. And as a final example, Benson, Jeschke, Jordan, Bruner, and Arnocky (2019) found that people high in ADM tend to show self-enhancing group affiliation (e.g., higher levels of social identity following ingroup success), whereas people high in RIV tend to show self-protective group devaluation (e.g., higher likelihood to expel group members following ingroup failure).

Overall, although the NARC was introduced relatively recently (Back et al., 2013), the so far accumulated evidence strongly points at the importance to differentiate between ADM and RIV. Both ADM and RIV refer to people's inclination towards a grandiose self-view, explaining why correlations between these two narcissism aspects typically range around .30 and .50 (Back, 2018). But whereas people high in ADM can be characterized by a more charming and assertive manner in order to seek self-promotion in particular, people high in RIV can be characterized by a more aggressive and devaluating manner in order to seek self-defense in particular. Next, we speculate how ADM and RIV might be linked to homophily, network centrality, and the duration of social connections.

Homophily

Homophily occurs if people with similar characteristics are more likely to be socially connected with each other as compared to people with less similar characteristics. Stated briefly, the main idea behind homophily—reflecting the idiom that *birds of feather flock together*—is that people who connect with each other (e.g., friends, romantic partners) share similar characteristics because similarity matches one's need for a shared understanding and breeds liking (e.g., Byrne, 1971; Klohnen & Mendelsohn, 1998; McPherson, Smith-Lovin, & Cook, 2001). Importantly, it is theorized that homophily can occur as a blend of people's

tendency to form social relations with similar others (i.e., social selection) as well as of people's tendency to become similar to others with whom they have social relations (i.e., social influence; De Klepper, Sleebos, Van de Bunt, & Agneessens, 2010; Kandel, 1978).

Several studies have investigated the occurrence of homophily, covering very different both characteristics and types of social relations. Concerning the former, sociodemographic factors (e.g., age, gender, height, weight), behavioural patterns (e.g., drinking, exercising, smoking), attitudes and worldviews (e.g., about politics and religion), as well as personality traits (e.g., the Big Five) have been considered. Concerning the latter, homophily has been investigated with regard to, e.g., intimate partners (often referred to as assortative mating; e.g., Luo, 2017), best friends (e.g., Giletta et al., 2011), rather closed school or military groups (e.g., Ilmarinen, Lönnqvist, & Paunonen, 2016), large social networks (e.g., Ahmed, Jaidka, & Cho, 2018), or even owner-dog dyads (Turcsán, Range, Virányi, Miklósi, & Kubinyi, 2012).

Summarizing the vast amount of findings on homophily rather roughly, it seems that it is particularly pronounced in sociodemographic factors, followed by behavioural patterns. Homophily has also been observed relatively consistently, although weaker, with regard to attitudes and worldviews, whereas results concerning personality traits are rather mixed (e.g., DeLay, Laursen, Kiuru, Salmela-Aro, & Nurmi, 2013; Lee, Ashton, Pozzebon, Visser, Bourdage, & Ogunfowora, 2009; Møllgaard et al., 2016; Rushton & Bons, 2005; Wu, Stillwell, Schwartz, & Kosinski, 2017).

Narcissism and Homophily

Narcissism is a particularly fascinating personality trait with regard to homophily, because two opposing theoretical ideas have been put forward. On the one hand, research on interpersonal complementarity suggests that friendly-dominant behaviors are complementary with friendly-submissive behaviors (Orford, 1986). Thus, narcissists whose striving for dominance is expressed in a friendly manner may particularly affiliate with people high on

submissiveness, i.e., non-narcissists. Correspondingly, this line of theorizing suggests that complementarity rather than homophily governs the social relations of (friendly) narcissists.

On the other hand, research on narcissists' feelings of greatness suggests that narcissists often bemoan that they cannot find others on a par with their own greatness (Campbell & Foster, 2007). Consequently, they may be particularly interested in affiliating with others who, too, broadcast a sense of greatness. Correspondingly, this line of theorizing suggests that homophily might govern the social relations of (grandiose) narcissists.

A few studies have studied homophily with regard to narcissism, so far. Grosz, Dufner, Back, and Denissen (2015), for instance, investigated whether homophily in ADM and RIV occurs in potential and actual intimate partners. In a vignette-study about the attractiveness of a fictitious partner for a short- (one-night stand) or long-term committed relationship, they found homophily for both narcissism aspects. That is, people high in ADM tend to find people high in ADM more attractive, and people high in RIV tend to find people high in RIV more attractive (although much less so with regard to a long-term committed relationship, which we will discuss later). These homophily effects for ADM and RIV could be replicated in a second study with heterosexual couples, although for RIV the effects did not reach the threshold for statistical significance (arguably due to the relatively low sample size of $N = 91$ couples). In a similar vein, Lamkin, Campbell, van Dellen, & Miller (2015) found some support for homophily in grandiose narcissism in a sample of undergraduate couples. Also focusing on overall grandiose narcissism (i.e., not differentiating between agentic and antagonistic aspects), but considering best friends' dyads, Maaß, Lämmle, Bensch, and Ziegler (2016) found support for homophily in narcissism as well. Overall, findings across these and other (e.g., Lavner, Lamkin, Miller, Campbell, & Karney, 2016) studies suggest a small, but existent occurrence of homophily among grandiose narcissists.

Importantly, however, to the best of our knowledge no study to date has investigated homophily among narcissists—differentiating between ADM and RIV—in large social networks, and thus not focusing on close social relations (e.g., intimate partners, best friends) only. As stated above, we test for homophily in ADM and RIV in a large social network from an exploratory point of view. Considering previous theorizing and results, though, one might not expect to find homophily in RIV, because people high in this narcissism aspect can be characterized by devaluating others, which is arguably at odds with other narcissists' (including those high in RIV) aim to maintain a grandiose self-view. Concerning ADM, it seems more difficult to state a clear expectation. On the one hand, the evidence so far indicates a relatively consistent support for (few) homophily in narcissism, which might apply to ADM in social networks, too. The reasoning behind this could be that people high in ADM signal a sense of greatness and believe that only great others are on par with them—and because the self-view of being great is signaled in a rather positive, charming way towards others (as compared to RIV), people high in ADM might feel especially connected to each other. On the other hand, people high in ADM strive for uniqueness (even though in a charming way) and might thus particularly connect with others who do not share—and, in turn, question—such feelings of uniqueness, but who welcome that narcissists' self-view of being grandiose is expressed in a socially positive way. From this perspective, there might be no homophily in ADM.

Narcissism and Network Centrality

Grandiose narcissists (in both ADM and RIV) can be characterized by the self-view of being special and great. This self-view results in a desire to be and feelings of being entitled to be in the center of attention, as reflected in typical narcissism items such as "I manage to be the center of attention with my outstanding contributions", "I can barely stand it if another person is at the center of events" (both Back et al., 2013), or "I hate being the center of

attention" (reverse-coded; Jones & Paulhus, 2014). Surprisingly, though, whether narcissists actually happen to be in the center of attention (in terms of social networks) has hardly been investigated, so far. That is, it is an open question whether narcissists' desire matches reality.

Indirect evidence about whether narcissists might happen to be in the center of social networks can be derived from the large body of research on narcissists' popularity. In this regard, several studies have shown that narcissists are well-liked by others at zero and short-term acquaintance, but that this popularity decreases over time. Moreover, Back, Küfner, and Leckelt (2018) recently summarized the current evidence on the (early) impressions of grandiose narcissists, again illustrating the importance to distinguish between agentic and antagonistic aspects of narcissism: Whereas agentic narcissism is typically evaluated positively and thus increasing popularity, antagonistic narcissism is typically evaluated negatively and thus decreasing popularity.

Combining this evidence with the conceptualization of ADM and RIV, one might speculate that people high in ADM hold network centrality: They strive for social admiration by others, and their social strategies to reach this aim typically go along with increased popularity. Together, this should result in that people high in ADM are approached by more people (given their popularity) as well as that they approach more people (given their desire for social admiration), and, thus, network centrality overall. Concerning RIV, one might—again—consider different links. Specifically, people high in RIV might not desire to be in the center of attention so strongly (although they do not think that somebody else would deserve it) and their aggressive, devaluating manner in dealing with others might lead to social conflicts and less popularity overall. Consequently, it seems unlikely that people high in RIV are approached by many others; we can only speculate about whether they actively approach many others—they might do it in order to devaluate them or they might refrain from it in order to avoid their ego be threatened by social exposure.

Narcissism and Duration of Social Connections

As already mentioned, research on the popularity of narcissism strongly suggests that narcissists are popular at zero and short-term acquaintance, but that this popularity decreases over time (Back et al., 2018), including that narcissists are considered to be a less attractive partner in the long run (Grosz et al., 2015). Studies relying on the NARC also suggest that the short-term popularity is rather driven by ADM, whereas the continuingly decreasing popularity is rather driven by RIV. Based on these findings, we finally investigate whether people's levels in ADM or RIV are related to unusually brief or long social connections. In this regard, one might wonder whether narcissists have rather brief social connections with others overall, because people in social networks might turn away from narcissists once their egotistic self-views are (too) clearly reflected in behavior. Such a pattern might occur with RIV in particular, because this aspect goes along with less socially behavior. To put it bluntly: It appears unlikely that many people in a social network tend to continue having social connections with people high in RIV, if they are being aggressively devaluated over time. Concerning ADM, it seems more difficult to state clearer expectations. It might be that others turn away from people high in ADM, too, but it might as well be that people high in ADM are able to maintain their social relations normally, because they do not repel others that actively. At the same time, people high in ADM (as well as in RIV) might also turn to other people from time to time, simply because they might strive to get social admiration from (additional) others (ADM) and because they might aim to devaluate (additional) others, respectively.

The Present Investigation

Overall, we link people's levels in ADM and RIV to (1) homophily, (2) network centrality, and (3) duration of social connections, derived from Big Data across three modes of communication (text messages, calls, spatial proximity) in a large social network. In so doing, we are fully in line with recent narcissism research, consistently corroborating the

importance to distinguish between agentic and antagonistic narcissism aspects. We further crucially contribute to the literature by making use of Big Data from a large social network, as compared to the vast majority of studies focusing on homophily or popularity of narcissists with regard to romantic partners (e.g., Wurst et al., 2018)), best friend-dyads (e.g., Maaß et al., 2016), or smaller groups (e.g., Leckelt et al., 2015).

Open Science Statement

As described in the Methods section in more detail, we investigate our research questions using a data set that was collected from September 2013 onwards. Before the start of the data collection, no hypotheses concerning narcissism in general or ADM and RIV in particular were stated. The research questions were developed at the end of the year 2018, after all data had been collected already. Although the research questions were derived from previous literature and although no analyses involving ADM and RIV had been conducted before finalizing the research questions, we thus conducted all analyses from an exploratory point of view.

On the Open Science Framework (OSF), we provide the full list of the administered questionnaires, the analysis script (in Python), and results from additional analyses. We do not provide the data set used for the analyses, though, because this would make it possible to identify participants. Specifically, the Bluetooth information (see below) would allow to locate participants at a certain time, e.g., facilitating to locate their place of living.

Methods

Procedure and Participants

Data for this investigation stem from the SensibleDTU experiment. This experiment ran from 2013 to 2017 as part of the Social Fabric project (https://sodas.ku.dk/projects/social-fabric/), a collaborative project of two Danish universities (the Technical University of Denmark, DTU; the University of Copenhagen, UCPH). Participants of the SensibleDTU

experiment were 730 DTU first-year bachelor students from the natural and technical sciences. Each participant received a smartphone at the beginning of the academic year 2013-2014. The smartphones came with an app that collected information about participants' smartphone activities. Relevant for our study, the app registered how many text messages a participant sent or received to other participants, how many phone calls a participant made to or received from other participants, as well as when two smartphones from the participant pool showed a Bluetooth connection.

For this investigation, we use the same dataset as in Møllgard et al. (2016) that includes questionnaire responses and smartphone activities from 659 students (76% male, mean age = 21.5, *SD* = 2.8 years). This dataset only includes participants for which smartphone activities could be recorded for a minimum of three months and for which a minimum amount of communication activities could be recorded. Specifically, Møllgard et al. required for each participant to be included that min. 950 text messages, 170 calls, and 200 hours of Bluetooth interactions were recorded. These thresholds were based on the average communication activities that could be observed for one person in a three-month period in the SensibleDTU data. For the sample used herein (as well as in Møllgard et al.), smartphone activities could be retrieved for 530 days on average starting on September 1st 2013.

Prior to receiving a smartphone, participants completed an online questionnaire, including demographic items as well as the Narcissistic Admiration and Rivalry Questionnaire (Back et al., 2013).[1] Table 1 in the OSF provides an overview of all measures included in the online questionnaire. The Danish Data Protection Agency provided ethical

1 Participants were also asked to fill out three follow-up surveys. For the current investigation, we use questionnaire data from the first measurement occasion only, (1) because this allows to more clearly test whether ADM and RIV affect homophily and network centrality, and (2) because high drop-out rates of the follow-up questionnaires hamper investigating bidirectional or change-oriented patterns nonetheless.

approval for the SensibleDTU experiment (reference number: 2012-41-0664), and each participant provided informed consent before both filling out the questionnaire and receiving the smartphone.

Dataset

Several studies across fields have already used data from the SensibleDTU experiment (e.g., Mønsted, Møllgaard, & Mathiesen, 2018; Sekara, Stopczynski, & Lehmann, 2016; Stopczynski et al., 2014). Notably, none of those studies reported any results on narcissism. Fortunately, though, one study investigated homophily (regarding demographics, behaviors, attitudes, and basic personality traits, but not regarding narcissism; Møllgard et al., 2016). We could thus adopt that study's data analytic strategy for the analyses concerning homophily. None study using this dataset linked personality characteristics to network centrality or the social connection duration, though.

Measures

Narcissistic admiration and rivalry. Narcissistic admiration and rivalry were measured via the 18-item Narcissistic Admiration and Rivalry Questionnaire (NARQ, Back et al., 2013), including the 9-item Narcissistic Admiration (ADM) and the 9-item Narcissistic Rivalry (RIV) subscales. Sample items are "I am great" (ADM) and "Most people are somehow losers" (RIV). Participants responded on a 6-point Likert scale ranging from 1 (*not agree at all*) to 6 (*agree completely*). The NARQ was translated from English into Danish for the SensibleDTU experiment. For ADM, the mean in our sample is 3.31 (SD = 0.78), and for RIV, the mean is 2.16 (SD = 0.70). The intercorrelation between ADM and RIV was r = .33 (CI: [0.27,0.40]) and, thus, similar to the intercorrelation found in previous studies (Back, 2018).

In the light of the empirical and theoretical—both ADM and RIV are aspects of grandiose narcissism—overlap, previous research has discussed the implications of using

either the ‘pure’ measures of ADM and RIV or estimates controlling for the shared variance between them (e.g., Leckelt, Richter, Wetzel, & Back, 2019). More precisely, when the pure—i.e., non-residualized—measures are used, both measures represent people’s levels in maintaining a grandiose self, complemented by individual differences in doing so via agentic narcissistic self-presentation in the ADM scale, and complemented by individual differences in doing so via antagonistic narcissistic self-defense in the RIV scale, respectively. By contrast, when the residualized measures are used—i.e., when each of the measures ADM and RIV is controlled for the shared variance between ADM and RIV—, the measures particularly reflect individual differences in the different social strategies to maintain a grandiose self: agentic narcissistic self-presentation (ADM) and antagonistic narcissistic self-defense (RIV), respectively. Herein, we deem it more important to focus on the different social strategies, because all homophily, network centrality, and social interaction duration theoretically refer to *how* people with different levels of narcissism approach and are approached by others. Consequently, in the main document, we present the analyses for the ADM and RIV estimates controlled for the shared variance between them. To do so, we rely on the residulization method (see Paulhus & John, 1998); that is, predicting ADM by RIV and using the residual for the following analyses, and vice versa. On the OSF, we present the analyses using the pure (non-residualized) measures of ADM and RIV.

Homophily.

Interactions between participants. In order to measure homophily (as well as network centrality and social interaction duration), we use the same three indicators of interactions between participants as Møllgard et al. (2016). Specifically, interactions between participants were assessed via text messages, phone calls, and spatial proximity. Text messages refer to the number of texts exchanged via short message service sent to/received from other participants (average number of text messages sent/received 247, *SD* = 557, range 1-7,734). Phone calls

refer to the number of phone calls made to/received from other participants (average number of phone calls made/received 53, *SD* = 89, range 1-1,029).[2] Finally, spatial proximity refers to scanned Bluetooth connections. Specifically, each smartphone scanned every five minutes through the Bluetooth ports for smartphones belonging to other participants. The strength of the Bluetooth signal scanned is subsequently converted to a measure of proximity. Note that one cannot determine who "approached" whom via the proximity data (that is, there are no senders or recipients for these data). In line with Møllgard et al., we treat the data and resulting networks from the three interaction indicators separately, and simply refer to them as SMS, call, and Bluetooth data or network in the following. Generally, any interaction between a participant and a person outside the participant pool is not considered for the analyses.

Measuring homophily in networks created using the social-amplification parameter α. Based on the interactions between participants, we measure homophily using the homophily measure introduced by Møllgaard et al. (2016). To measure homophily, we first need to convert the raw data into a social network. To this end, we use a tunable link weight α, to which we refer to as the social-amplification parameter. Whereas the social-amplification parameter was briefly—and with a focus on the statistical details—introduced by Møllgaard et al. (2016) already, we provide a more detailed introduction in the following.

The social-amplification parameter controls how interactions with different strengths are weighted. Specifically, people in the network can interact more or less strongly with each other (e.g., Participant A might have exchanged 100 text messages with Participant B, but only 20 with Participant C). Now, each edge in the network—i.e., interaction between two people *i* and *j*—gets some weight, $w_{ij}(\alpha)$, and to which degree this weight mirrors the different strengths of the interactions is tunable via the social-amplification parameter α.[3]

2 We could not assess the number of text messages and phone calls exchanged via third-party apps (e.g., Facebook, Skype, Telegram, WhatsApp)

Measuring homophily in the SMS and call networks. For the SMS and call networks, the following weight is assigned to the edge describing communication going from participant *i* to participant *j*,

$$w_{ij}(\alpha) = n_{ij}^{\alpha} / \sum_{i,j} n_{ij}^{\alpha}.$$

In this formula, n_{ij} is the observed number of text messages (or calls respectively) going from participant *i* to participant *j* over the course of the study. α is the tunable social-amplification parameter that can take any value, but we will only consider positive values herein. Depending on the value of α, relations between people of different strengths dominate the homophily analysis. Specifically, a large value of α increases the weight of the strongest links compared to the weight of weaker ones. In such an analysis (with a large value of α), measuring homophily in the resulting network represents measuring homophily between the strongest connected individuals in the network (i.e., dyads that exchanged many text messages with each other or that had many phone calls with each other, respectively), and practically ignoring weaker ties (dyads who hardly interacted with each other). In an analysis with a low, positive value of α, by contrast, weights of strong and weak ties are considered similarly. Thus, measuring homophily in the resulting network represents measuring

3 Other measures of homophily have been used in the literature (e.g., Maaß et al., 2016; Schönbrodt, Humberg, & Nestler, 2018; Van Zalk, Nestler, Geukes, Hutteman, & Back, 2019). For our data and research questions, though, the measure of homophily as introduced by Møllgaard et al. (2016) is particularly suited. The main reasons are that (a) this measure represents a homophily measure for an entire network at once—and, e.g., not only considers homophily with regard to a few explicitly stated interaction partners such as one's three best friends. Further, the measure is tunable with regard to how to weigh interactions (social relations) of different strengths, allowing to investigate homophily at different intensity levels of social interactions.

homophily between all people, while to some degree disregarding the strength of the tie between the people in question. If α equals unity (i.e., 1), the weight of a link between two people is exactly proportional to the frequency of the interaction between them. Figure 1 illustrates the social amplification parameter with the example of the actual data from the call network, and Table 1 summarizes how to interpret values of the social-amplification parameter.

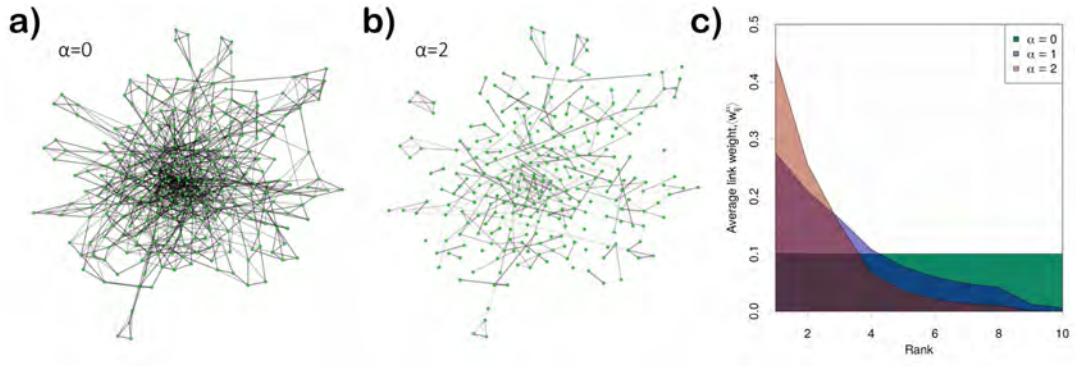

Figure 1. Illustration of the social-amplification parameter α via the actual data from the call network. In panel a) and b) we show the call network for the 50% most strongly connected participants (i.e., those 50% dyads of participants that called each other more often than the other 50% of the dyads). In panel a), the links all have the same weight with $\alpha = 0$. Consequently, it does not matter whether people have called each other, say, 60 or 600 times, each edge is considered equally. In panel b), α is set to 2, so that only a few—namely, the strongest—links dominate the network (we have colored the links according to weight such that the darkest links have the largest weights). In panel c), we consider the average weight for the 10 strongest links for all participants in the study. Before doing the average, the links have been ranked according to weight such that in the plot, the links with the largest weights are leftmost (having the lowest rank). Again, when $\alpha = 0$, the 10 links have the same weight, and for $\alpha = 2$, the link with the largest weight dominates over the others.

Table 1

Interpretation of Values of the Social-amplification parameter (α)

Social-amplification parameter (α)	Interpretation	Fictitious example (referring to the call network)	Implications for homophily measure
$\alpha = 0$ very small	All links with any activity carry equal weight in the analysis.	Dyads that called each other 10 times get the same weight as dyads that called each other 100 times.	Reflects whether homophily is present when all interactions are considered equally.
$\alpha = 1$ intermediate	All links carry weight exactly proportional to observed activity.	Dyads that called each other 10 times get a weight being 10% of the weight of dyads that called each other 100 times.	Reflects whether homophily is present when the network mirrors exactly the actually observed frequency of social interactions between people.
$\alpha = 2$ very large	Links with much activity carry disproportionally larger weights than links with no or little activity. Effectively, only the strongest links are considered in the analyses.	Dyads that called each other very often (say, more than 100 times) get a disproportionally large weight; dyads that called each other less often get a disproportionally small or even effectively no weight at all.	Reflects whether homophily is present at dyads having many social interactions.

Estimating homophily in the Bluetooth data. The Bluetooth data are different than the SMS and call data in that they consist not of a number of timestamps indicating when messages or calls were received by participant *i.* Instead, the data consist of a number of Bluetooth scans, separated by time intervals Δt . For each scan, all devices registered by the phone of the user are saved together with the time of the scan, and a parameter indicating the distance between the two devices. If two consecutive scan register the same device within a distance of *3* meters, we assume that the two users have spent the full Δt in proximity of each other. We define T_{ij} as the total amount of time user *i* and *j* spent together over the course of the data collection according to this definition, and create the proximity network by assigning the link between nodes (i.e., participants) the weight

$$w_{ij}(\alpha) = T_{ij}^{\alpha} / \sum_{i,j} \square \, T_{ij}^{\alpha}.$$

Besides not being able to differentiate between sender and receiver, however, the proximity data can be interpreted similarly than the text message and the call network.

Using α, Møllgaard et al. (2016; Figure 4) also reported the correlations between the three different networks. They observed that the SMS and call networks correlated around . 70-.80 across all levels of α (with a peak at rather small levels of α, < .5). Further, the correlation between the SMS and Bluetooth networks and the correlation between the call and Bluetooth networks were very similar to each other. However, these correlations were much smaller than the correlation between the SMS and call networks. Specifically, for SMS/Bluetooth and call/Bluetooth, the correlations increased from around .10 at low levels of α (0) to around .50 at levels of α of around .7. Then, the correlations dropped gradually (up to α = 2) to around .30. Overall, the SMS and call networks might thus be considered as relatively similarly to each other, whereas the Bluetooth network is a bit more different, especially at lower levels of α.

Testing for significance of homophily. As described above, for each network—SMS, call, and Bluetooth—we can get a homophily measure for the entire sample, depending on how interactions with different strengths between participants are weighted. We then check for the significance of the homophily measure by comparing it to the measure of simulated null models. Specifically, we simulate null models in which the network structure is kept—i.e., that the overall number and kind of interactions remains the same—, but the participants shuffle node positions (i.e., with whom they interact how often) randomly on the network. We then test if the homophily measure on the original network (for any of the tunable α) is more extreme than the typical measure obtained from the simulated networks (i.e., the networks with randomly assigned network positions to people). An illustration of how homophily is tested in the analyses is presented in Figure 2.

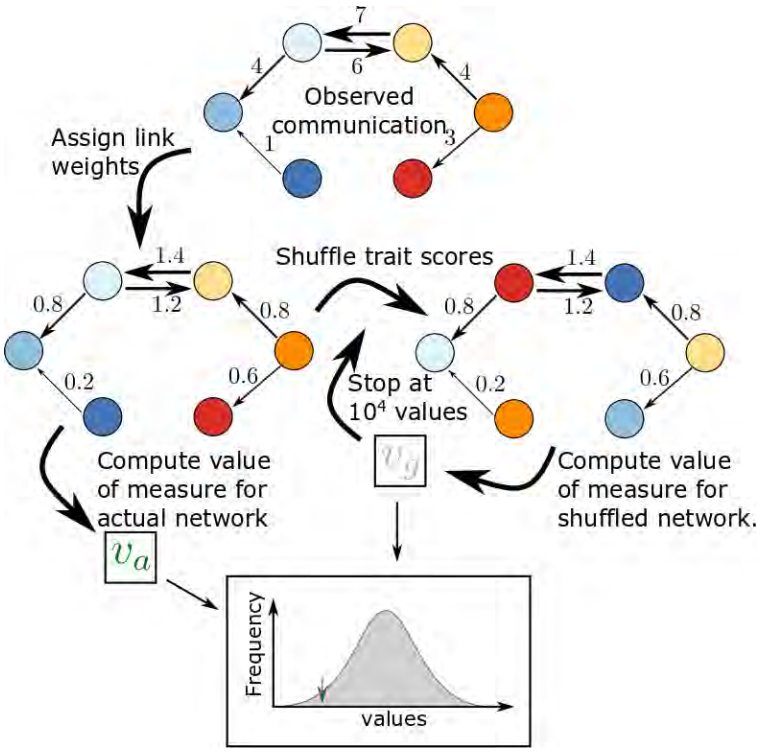

Figure 2. Illustration of testing for the significance of homophily in the data (see text for details).

At the top of Figure 2, one can see that the observed communication network consists of an integer number of interactions between people. For the SMS and call data the direction of each interaction is known, and this is indicated by a directed arrow in the figure (in the drawn example, the orange node initiated interaction with the red node 3 times). From these raw data, we create a network for the analyses by specifying link weights w_{ij} using the known interactions, and a chosen value of the social-amplification parameter α. With the resulting network, we can compute the actual value for the homophily measure of the observed network. To get a null-distribution for the homophily measure, we take the network created using the chosen value of the social-amplification parameter, and shuffle participants' ADM and RIV scores, respectively, among the nodes (one could shuffle participants based on any characteristic, of course). In other words, we keep the nodes and links fixed, but redistribute the ADM or RIV scores between the nodes. Computing the homophily measure for this network and distribution of participants' ADM or RIV yields one out of the 10^4 homophily measures that we use for the null distribution. We thus save the resulting homophily measure, shuffle the participants' ADM or RIV scores again, compute the new homophily measure, and repeat this process until all 10^4 measures that make up the computed null distribution are obtained. The null distribution serves as a null hypothesis: It indicates the frequency with which different values would be obtained, if the ADM and RIV scores were randomly distributed among the people in the social network. The null hypothesis is thus 'there is no more homophily than if the ADM or RIV scores were randomly distributed'. If the actually observed ('real') homophily measure is sufficiently extreme relative to the random scores, we reject the null hypothesis that there is no homophily in the network.

Network Centrality. In order to investigate network centrality, we use a simple measure for centrality: the degree of the node. This measure is usually referred to as ”degree centrality”, and in the SMS and call network, two degrees exist for each node: in-degree (receiving text messages and phone calls, respectively) and out-degree (sending text messages and calling others, respectively). Given link weights $w_{ij}(\alpha)$, the alpha-dependent in-degree of node *i* is $d_i^{recipient}(\alpha)=\sum_j w_{ji}(\alpha)$ and the alpha-dependent out-degree of node *i* is $d_i^{sender}(\alpha)=\sum_j w_{ij}(\alpha)$. To assess whether degree centrality correlates with scores in ADM or RIV, we define the following measure

$$r_d^X(\alpha)=\sum_i (s_i-\acute{s})d_i^X(\alpha).$$

In this formula, X can be replaced by either ”sender” or ”recipient” depending on which kind of degree we use, s_i is the respective ADM or RIV score of node *i*, and $\acute{s}$ is the average ADM or RIV score of the participants. A link will contribute positively to the sum if the focal node (i.e., target participant in question) has an ADM or RIV score above the average ADM or RIV score in the population and vice versa. Replacing X by ”sender” makes the focal node the node initiating the communication, and replacing X by ”recipient” makes the focal node the node that is being contacted by others. For the proximity network, we do not know which node initiates the proximity, and therefore $d_i^{sender}(\alpha)=d_i^{recipient}(\alpha)$, and consequently $r_d^{sender}(\alpha)=r_d^{recipient}(\alpha)$ in for the proximity network.

Social interaction duration. In order to assess whether a specific ADM or RIV score correlates with having social interactions with shorter or longer duration, we measure the average in-link duration of each node. For the SMS and call networks, we define the duration of a link from node *i* to node *j* as being the length of the time interval between message

number $n_{ij}/4$ and message (call) number $3n_{ij}/4$. The first number rounded up, and the second down to the nearest integer. We denote the average in-link duration for node *i* as t_i, and define the following measure to assess whether average in-link duration correlates with ADM or RIV scores,

$$\tau = \sum_i (s_i - \acute{s}) t_i .$$

Results

Homophily.

Figure 3 shows the results concerning homophily in ADM and RIV in the three different networks (SMS, call, and Bluetooth), depending on different values of the tunable social-amplification parameter α. In each plot, there is a full, colored curve as well as a colored area with three different shades. The full, colored curve indicates the actual value for the homophily measure, and the shaded areas indicate commonly chosen confidence intervals derived from the null distribution of the 10^4 homophily estimates. The darkest shade of the marked area indicates the 68% of the null distribution closest to the median of the null-distribution. These are the “least extreme” values of the null distribution. The two darkest shades cover the 95% least extreme values, and all three shades cover the 99% least extreme values of the null distribution. Practically speaking, the estimate for homophily is significant when the full colored curve is above or beyond (i.e., “outside”) the three shades on a $p < .01$ level, and on a $p < .05$ level when it is outside the middle shaded area.

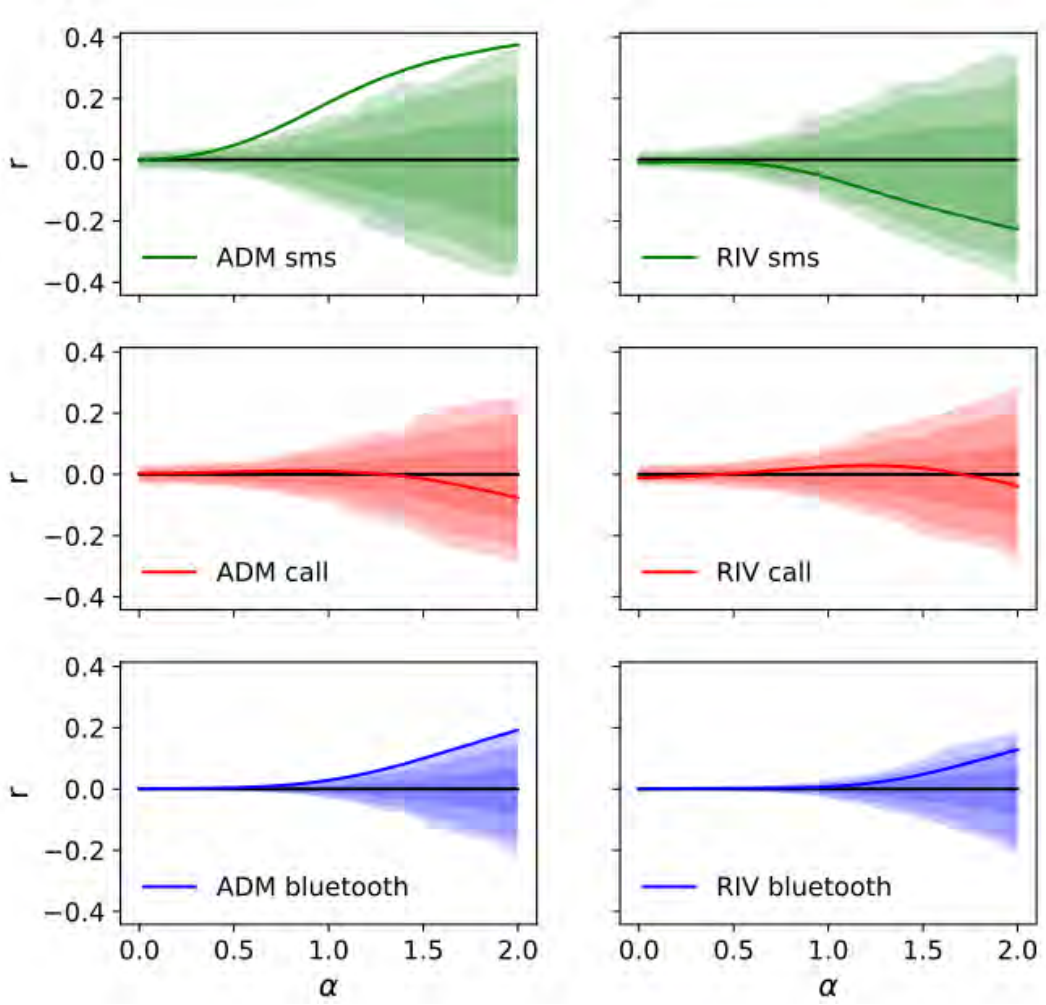

Figure 3. Homophily estimate (*r*) as a function of the social-amplification parameter *α*.

Concerning Narcissistic Admiration, Figure 3 shows that people generally tend to exchange more text messages with similar than dissimilar others, and that this is particularly pronounced when interactions between people are weighted in line with their strengths (around $\alpha = 1$) or when only edges with many interactions are considered (i.e., further increasing α values). Further, there is evidence that people interact more often with others having similar ADM-levels as themselves in the Bluetooth network, again particularly when α is 1 or higher. By contrast, there is no indication of homophily in the call network whatsoever.

Overall, data from the SMS and Bluetooth network support that there is homophily for ADM, especially when weak links between people are disregarded or neglected.

Concerning RIV, there is again no indication of homophily in the call network. Further, but contrary to the results concerning ADM, there is also no indication of homophily in either the SMS or proximity network. Concerning the latter, though, when dyads who show a high level of proximity are considered in particular (α-levels of around 1.5 or higher), homophily tends to get closer to the threshold of $p < .05$. Overall, there is strong indication for homophily of ADM in the SMS and the proximity network, but not in the call network. Also, there is no observed homophily concerning RIV across the networks.

Network Centrality

With regard to network centrality, Figure 4 shows the correlations between the ADM and RIV scores and in-degree centrality in the SMS and call networks (i.e., receiving text messages and phone calls), as well as the centrality in the proximity network (in which one cannot distinguish between in- and out-degree centrality), depending on the social-amplification parameter α.

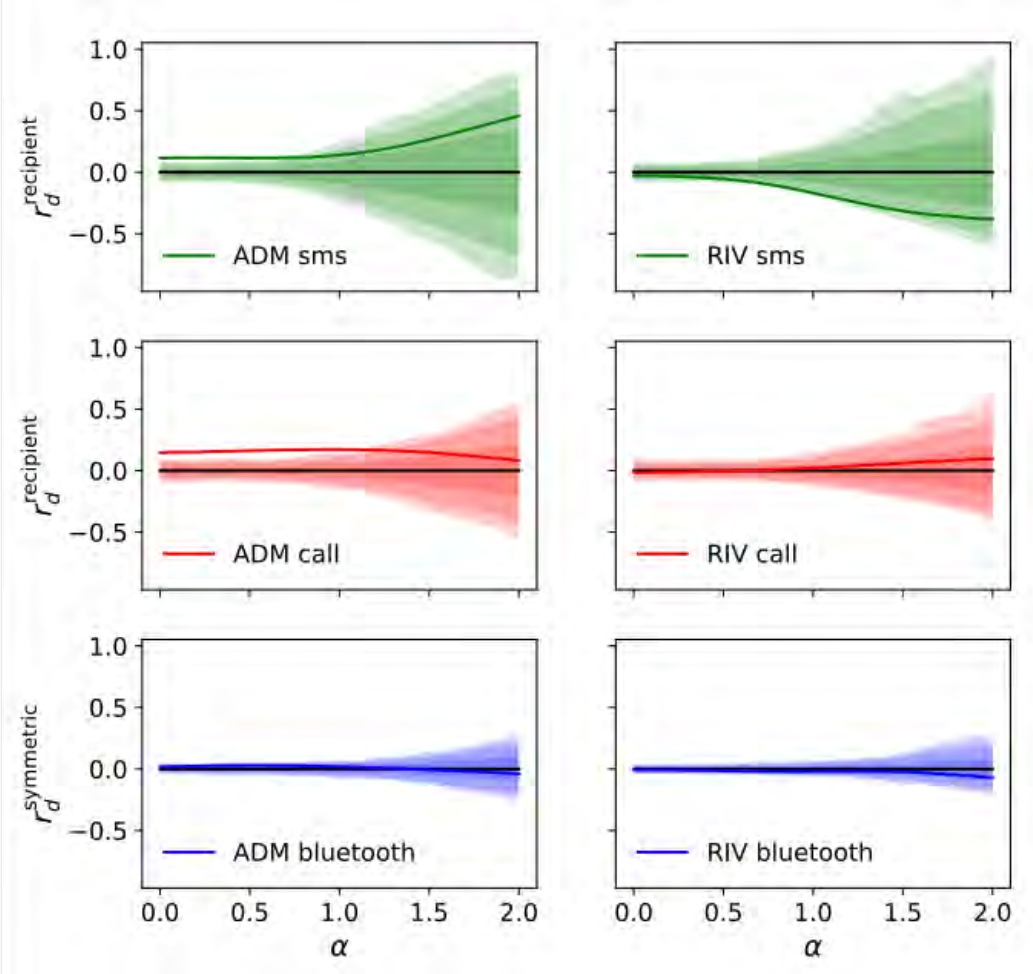

Figure 4. Correlation between in-degree centrality (in the SMS and call networks) as well as centrality (in the Bluetooth network) and ADM and RIV scores for networks depending on the social-amplification parameter α .

As can be seen in Figure 4, in-degree centrality correlates more with ADM than would be expected for a population with randomly distributed ADM scores in both the SMS and the call network with low values of α . With increasing values of α, this effect vanishes in both networks. That is, when all—including less frequently occuring—interactions between people are considered, those with higher levels in ADM receive more text messages and calls by others (than expected by chance). Concerning, RIV, there is no indication of a correlation with

in-degree centrality in the call network (irrespective of α), whereas there is an indication that RIV scores correlate negatively with the number of text messages received for an intermediate range of values of the social-amplification parameter (α between approx. 0.5 and 1.5). Concerning the proximity network, there is no indication of network centrality for either ADM or RIV, irrespective of how links are weighted. Thus, people with particular ADM or RIV-levels are not more often in physical proximity with others, irrespective of whether dyads with weak links are in- or excluded in the analyses.

Next, Figure 5 shows the results for out-degree centrality, i.e., sending text messages and calling others, respectively.

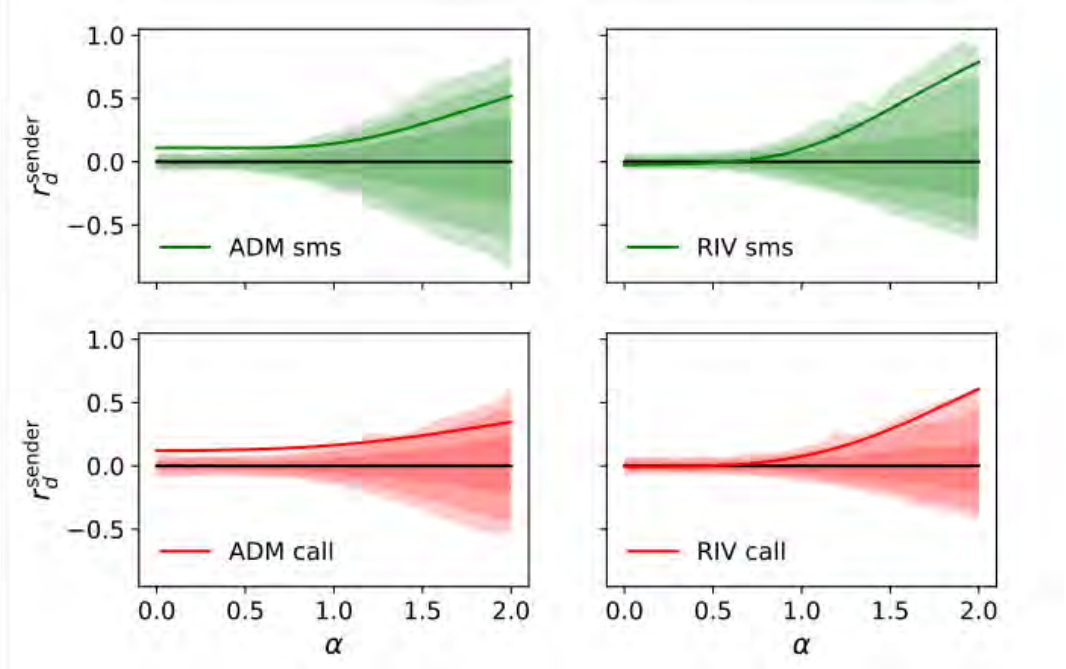

Figure 5. Correlation between out-degree centrality and ADM and RIV scores for networks depending on the social-amplification parameter α.

The plots in Figure 5 strongly indicate that out-degree correlates positively with ADM scores in both the SMS and the call network with low values of α. That is, if dyads are weighted equally (i.e., no matter how many calls or text messages were sent across these

dyads), high out-degree correlates with high ADM scores. With increasing levels of α, though, these effects vanish. In other words, people with higher levels in ADM tend to send text messages to a larger number of people as well as call a larger number of people than would be expected by chance if and only if all interactions between people are considered and weighted equally, thus independent of frequency.

With regard to RIV, there is indication in both the SMS and the call network that for increasing values of α (starting around ≈ 1.5) out-degree positively correlates more with RIV scores than would be expected at random. That is, when weak links between people are neglected, RIV scores correlate positively with the number of text messages sent and calls made to other people. In the call network, this finding falls even on the border of $p < .01$ at high values of α.

Overall, the results concerning network centrality indicate that both in- and out-degree centrality correlate with ADM in both the SMS and the call network for low values of *α*. More practically, people with high levels in ADM tend to receive and send more text messages to others as well as receive from and make more phone calls to others when all interactions are considered equally, independent of frequency. Concerning RIV, the pattern is more mixed: For in-degree centrality, there is no effect in the call network, but around α ≈ 1.5, people with higher values in RIV tend to receive less text messages. For out-degree centrality, though, people *high* in RIV send more text messages to others and make more phone calls to others, again when weak ties are neglected. There is no indication that specific levels in ADM or RIV are related to specific levels in proximity between people whatsoever.

Social interaction duration

Finally, Figure 6 shows the results concerning the correlation between ADM and RIV scores and social interaction duration. That is, the question is whether specific scores in ADM

or RIV are related to a specific duration of an interaction between people. Vertical black lines are actual τ -values—i.e., the actual average duration of an interaction between two people in the corresponding network—, and the histograms indicate null distributions consisting of 10^4 τ -values obtained by redistributing ADM or RIV scores uniformly at random. Again, we indicate how large a fraction of the null distribution takes more extreme values than the observed, actual value as the *p*-value, and color the more extreme values with grey. As can be seen in Figure 6, there is no indication that specific levels in ADM are linked to a particularly brief or long time of interaction with others (p = .21 in the SMS, p = .22 in the call network, and p = .06 in the Bluetooth network). In other words, the actually observed values concerning the link duration of people with specific levels in ADM is not more extreme than could be expected from the null distribution. The same—null—finding applies to levels of RIV in the call (p = .23) and Bluetooth (p = .37) networks: Specific levels in RIV are not related to a specific link duration between people. On the other hand, there is indication in the SMS network that people with higher levels in RIV send to and receive from people a higher number of text messages over a longer time period.

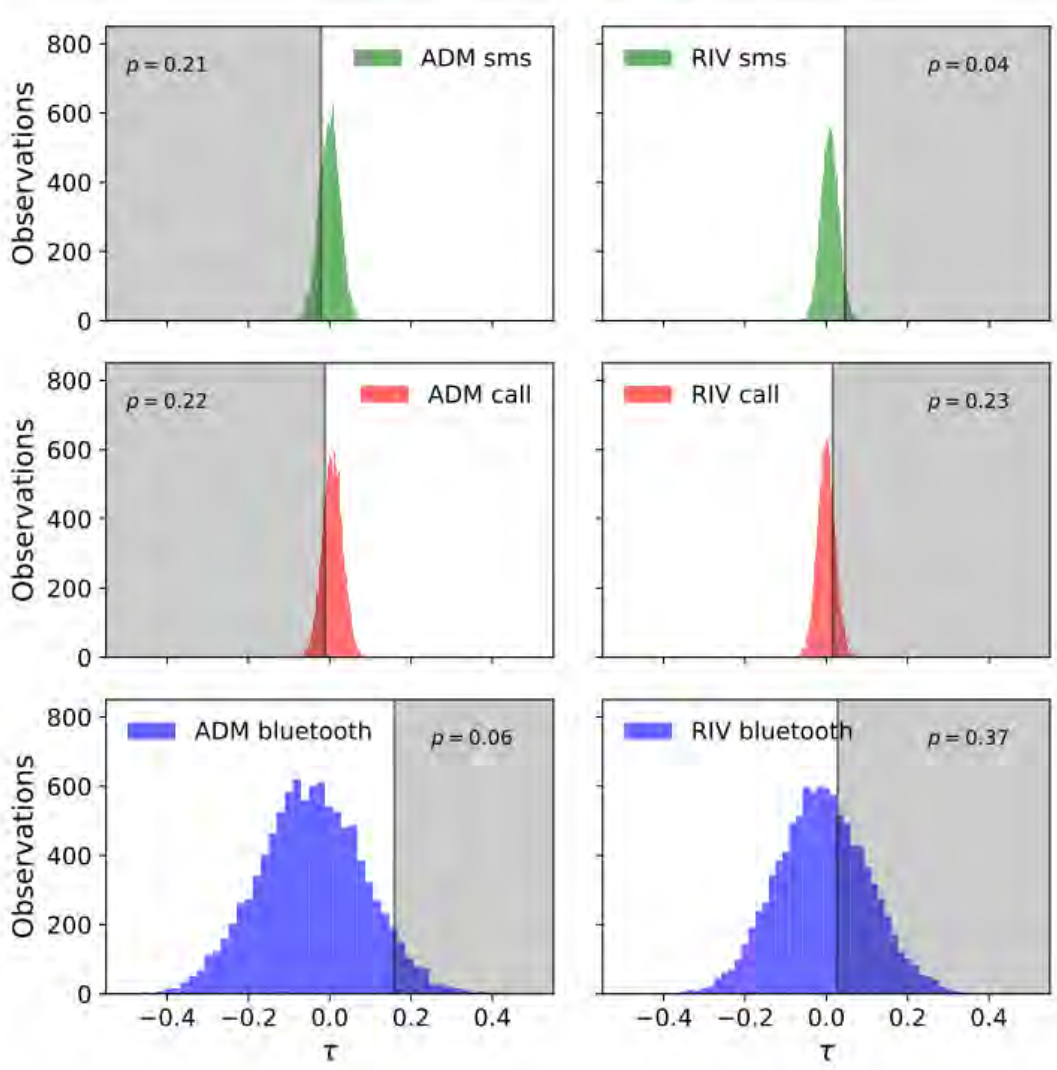

Figure 6. Correlation between in-link duration and ADM and RIV scores. The vertical black line indicates the actual value of the measure τ, and the histograms are 10^4 values obtained by distributing the ADM and RIV scores uniformly at random among the network nodes. The grey area marks the values more extreme than the actual observed τ value, and the *p* value is the fraction of histogram values that are located in the grey area.

General Discussion

The personality construct of narcissism has been linked to various outcomes for individuals, groups, and societies. Correspondingly, research has for a long time accumulated knowledge on the structure and core components of narcissism (e.g., Crowe et al., 2019). Currently, it is well accepted that three aspects of narcissism can be distinguished: Next to neurotic narcissism, this is agentic and antagonistic narcissism. For these, the respective subscales of the NARC (Back, 2018)—Narcissistic Admiration (ADM) representing agentic narcissism and Narcissistic Rivalry (RIV) representing antagonistic narcissism—are well-established operationalizations.

Whereas research on Narcissism in general and on ADM and RIV in particular has been flourishing recently, the current investigation contributes to the literature by linking people's levels in ADM and RIV to social outcomes in a freshmen population followed for some months. Specifically, via deriving Big Data from three modes of communication—namely, text messages, calls, and spatial proximity—, we investigated whether ADM and/or RIV are linked to homophily, network centrality, and the duration of social connections.

Overall, results indicated some links between ADM and/or RIV to homophily, network centrality, and the duration of social connections. Importantly, though, such links appeared not across all networks consistently. For instance, we found support for homophily of ADM in the SMS and the proximity network, but we found neither an indication for homophily concerning ADM in the call network, nor for homophily concerning RIV at all. Relatedly, we found both in- and out-degree centrality for both ADM and RIV. Again, however, results were neither fully consistent across the narcissism aspects, nor across the three networks. With regard to the duration of social connections, results were more consistent such that we observed hardly any support for the idea that ADM or RIV are linked to the duration of social networks; with the exception that people with higher levels in RIV send to and receive from people a higher number of text messages over a longer time period.

Strengths and Limitations

Our study has several strengths and limitations. From a conceptual perspective, a main strength is that we linked the timely, but already widely supported aspects of ADM and RIV to "objective" Big Data. That is, we linked people's self-reports in ADM and RIV to observed, and thus clearly objectively measurable behavior (e.g., how many calls a person makes). In the Big Data, we were even able to use data from three modes of communication (SMS, call, proximity), allowing to test whether any observed finding generalizes across the modes of communication. Finally, we targeted the analyzing methods to the research questions and data and hand, thereby overcoming limitations from previous methods. In particular, we provided a more detailed introduction of the social-amplification parameter α (which has been introduced by Mollgard et al., 2016) which allows to investigate homophily and network centrality while considering (or rather: weighing) different strengths of social interactions differently. We believe that the social amplification parameter provides a strong contribution to the (psychological) literature, given that homophily has typically been investigated by focusing on a small number of well-defined dyads only (e.g., best friends dyads; e.g., Maaß et al., 2016).

On the other hand, two limitations of our investigation deserve attention. First, our sample was rather specific (mostly male freshmen from a Technical University), which might not automatically show a generalizable variety in terms of ADM and RIV, and, even more, communication patterns. Second, we had to focus on homophily, network centrality, and the duration of social interaction within the sample. However, it might be that some participants showed homophily or network centrality outside the university setting. In concert, both limitations suggest aiming to replicate our investigation with a more diverse sample: concerning both the composition of the sample and the different social networks in which a person can show homophily and network centrality.

Conclusion

This study sheds light on some aspects concerning narcissists, with regard to agentic and antagonistic narcissism. Concerning ADM, we found that people's levels can be linked to homophily, namely in the SMS and Bluetooth network – in particular, when only strong links (i.e., a high social amplification parameter) are considered. So, agentic narcissists tend to interact more strongly with each other (via SMS) and to show higher levels of proximity. We further found that, when all interactions are considered equally (i.e., low social amplification parameter), agentic narcissists tend to receive and send more text messages to others as well as receive from and make more phone calls to others. These findings can be explained by previous theorizing suggesting that narcissists tend to believe to par up with others who also signal greatness (i.e., homophily) as well as that agentic narcissists not only want to be the center of attention, but also attract attention by others (arguably due to their attractive, charming manner). Concerning RIV, we found no strong signs of homophily, which fits to the idea that these people are antagonistic (and do not want to pair up with a specific kind of others). Concerning network centrality, we found that at around $\alpha \approx 1.5$, people with higher values in RIV tend to receive less text messages. Further, we found that people high in RIV send more text messages to others and make more phone calls to others (when weak ties are neglected). Together, these findings are in line with the idea that people high in RIV seek for attention (due to the underlying narcissistic theme), but have to actively aim for it, because. their antagonistic manner makes it less likely that others actively aim to communicate with them. Clearly, future research might pick up these findings and further illuminate how ADM and RIV are different aspects of narcissism. More generally, this study illustrates how linking established personality constructs to objective Big Data is a fruitful path for increasing our understanding of human behavior.

References

Ahmed, S., Jaidka, K., & Cho, J. (2018). Do birds of different feather flock together? Analyzing the political use of social media through a language-based approach in a multilingual context. *Computers in Human Behavior*, *86*, 299-310. https://doi.org/10.1016/j.chb.2018.04.051

Asendorpf, J. B., Conner, M., De Fruyt, F., De Houwer, J., Denissen, J. J. A., Fiedler, K., . . . Wicherts, J. M. (2013). Recommendations for increasing replicability in psychology. *European Journal of Personality, 27*, 108-119. http://dx.doi.org/10.1002/per.1919

Back, M. D. (2018). The Narcissistic Admiration and Rivalry Concept. In A. D. Hermann, A. Brunell, & J. Foster (Eds.), *The Handbook of trait narcissism: Key advances, research methods, and controversies* (pp. 57–67). New York, NY: Springer.

Back, M. D., Küfner, A. C. P., Dufner, M., Gerlach, T. M., Rauthmann, J. F., & Denissen, J. J. A. (2013). Narcissistic admiration and rivalry: Disentangling the bright and dark sides of narcissism. *Journal of Personality and Social Psychology, 105*, 1013–1037. http://dx.doi.org/10.1037/a0034431

Back, M. D., Küfner, A. C. P., & Leckelt, M. (2018). Early impressions of grandiose narcissists: A dual-pathway perspective. In A. D. Hermann, A. Brunell, & J. Foster (Eds.), *The Handbook of trait narcissism: Key advances, research methods, and controversies* (pp. 309–316). New York, NY: Springer.

Back, M. D., & Morf, C. C. (in press). Narcissism. In V. Zeigler-Hill & T. K. Shackelford (Eds.), *Encyclopedia of personality and individual differences*. New York, NY: Springer.

Benson, A. J., Jeschke, J., Jordan, C. H., Bruner, M. W., & Arnocky, S. (2019). Will they stay or will they go? Narcissistic admiration and rivalry predict ingroup affiliation and devaluation. *Journal of Personality*, *87*, 871-888. doi:10.1111/jopy.12441

Byrne, D. (1971). *The Attraction Paradigm*. New York, US: Academic Press.

Campbell, W. K., & Foster, J. D. (2007). The narcissistic self: Background, an extended agency model, and ongoing controversies. In C. Sedikides & S. J. Spencer (Eds.), *Frontiers of social psychology. The self* (pp. 115–138). New York, NY: Psychology Press.

Crowe, M. L., Lynam, D. R., Campbell, W. K., & Miller, J. D. (2019). Exploring the structure of narcissism: Toward an integrated solution. *Journal of Personality*, 87, 1151-1169. https://doi.org/10.1111/jopy.12464

De Klepper, M., Sleebos, E., van de Bunt, G., & Agneessens, F. (2010). Similarity in friendship networks: Selection or influence? The effect of constraining contexts and non-visible individual attributes. *Social Networks*, *32*, 82–90. https://doi.org/10.1016/j.socnet.2009.06.003

DeLay, D., Laursen, B., Kiuru, N., Salmela-Aro, K., & Nurmi, J.-E. (2013). Selecting and retaining friends on the basis of cigarette smoking similarity. *Journal of Research on Adolescence*, *23*, 464–473. https://doi.org/10.1111/jora.12017

Giletta, M., Scholte, R. H. J., Burk, W. J., Engels, R. C. M. E., Larsen, J. K., Prinstein, M. J., & Ciairano, S. (2011). Similarity in depressive symptoms in adolescents' friendship dyads: Selection or socialization? *Developmental Psychology*, *47*, 1804–1814. https://doi.org/10.1037/a0023872

Grosz, M. P., Dufner, M., Back, M. D., & Denissen, J. J. A. (2015). Who is open to a narcissistic romantic partner? The roles of sensation seeking, trait anxiety, and

similarity. *Journal of Research in Personality, 58,* 84–95. http://dx.doi.org/10.1016/j.jrp.2015.05.007

Ilmarinen, V-J., Lönnqvist, J-E., & Paunonen, S. (2016). Similarity-attraction effects in friendship formation: Honest platoon-mates prefer each other but dishonest do not. *Personality and Individual Differences*, *92*, 153-158. https://doi.org/10.1016/j.paid.2015.12.040

John, O. P., Donahue, E. M., & Kentle, R. L. (1991). *The Big Five Inventory—Versions 4a and 54*. Berkeley, US: Berkeley Institute of Personality and Social Research, University of California.

Jones, D. N., & Paulhus, D. L. (2014). Introducing the Short Dark Triad (SD3): A brief measure of dark personality traits. *Assessment*, *21*, 28–41. https://doi.org/10.1177/1073191113514105

Klohnen, E. C., & Mendelsohn, G. A. (1998). Partner selection for personality characteristics: A couple-centered approach. *Personality and Social Psychology Bulletin*, *24*, 268–278. https://doi.org/10.1177/0146167298243004

Lamkin, J., Campbell, W. K., van Dellen, M. R., & Miller, J. D. (2016). An exploration of the correlates of grandiose and vulnerable narcissism in romantic relationships: Homophily, partner characteristics, and dyadic adjustment *Personality and Individual Differences*. *79*, 166-171. DOI: 10.1016/j.paid.2015.01.029

Lange, J., Crusius, J., & Hagemeyer, B. (2016). The evil queen's dilemma: Linking narcissistic admiration and rivalry to benign and malicious envy. *European Journal of Personality*, *30*, 168-188. doi:10.1002/per.2047

Lavner, J. A.,Lamkin, J. Miller, J. D.,Campbell, W. K.,& Karney, B. R. (2016). Narcissism and newlywed marriage: Partner characteristics and marital trajectories. *Personality Disorders: Theory, Research, and Treatment*, *7*, 169-179.

Leckelt, M., Küfner, A. C. P., Nestler, S., & Back, M. D. (2015). Behavioral processes underlying the decline of narcissists' popularity over time. *Journal of Personality and Social Psychology, 109*, 856–871. http://dx.doi.org/10.1037/pspp0000057

Leckelt, M., Richter, D., Wetzel, E., & Back, M. D. (2019). Longitudinal Associations of Narcissism with Interpersonal, Intrapersonal, and Institutional Outcomes: An Investigation Using a Representative Sample of the German Population. Collabra: Psychology, 5(1), 26. http://doi.org/10.1525/collabra.248

Lee, K., Ashton, M. C., Pozzebon, J. A., Visser, B. A., Bourdage, J. S., & Ogunfowora, B. (2009). Similarity and assumed similarity in personality reports of well-acquainted persons. *Journal of Personality and Social Psychology, 96*(2), 460–472. https://doi.org/10.1037/a0014059

Luo, S. (2017). Assortative mating and couple similarity: Patterns, mechanisms, and consequences. *Social and Personality Psychology Compass, 11*(8), 1–14. https://doi.org/10.1111/spc3.12337

Maaß, U., Lämmle, L., Bensch, D., & Ziegler, M. (2016). Narcissists of a feather flock together: Narcissism and the similarity of friends. *Personality and Social Psychology Bulletin, 42*, 366–384. https://doi.org/10.1177/0146167216629114

McPherson, M., Smith-Lovin, L., & Cook, J. M. (2001). Birds of a feather: Homophily in social networks. *Annual Review of Sociology, 27*, 415–444. https://doi.org/10.1146/annurev.soc.27.1.415

Møllgaard, A., Zettler, I., Dammeyer, J., Jensen, M. H., Lehmann, S., & Mathiesen, J. (2016). Measure of node similarity in multilayer networks. *PLoS One, 11* [e0157436]. https://doi.org/10.1371/journal.pone.0157436

Mønsted, B., Mollgaard, A., & Mathiesen, J. (2018). Phone-based metric as a predictor for basic personality traits. *Journal of Research in Personality, 74*, 16–22. https://doi.org/10.1016/j.jrp.2017.12.004

Orford, J. (1986). The rules of interpersonal complementarity: Does hostility beget hostility and dominance, submission? *Psychological Review, 93*, 365–377. http://dx.doi.org/10.1037/0033-295X.93.3.365

Paulhus, D. L., & John, O. P. (1998). Egoistic and moralistic biases in self-perception: The interplay of self-deceptive styles with basic traits and motives. *Journal of Personality, 66*(6), 1025–1060. https://doi.org/10.1111/1467-6494.00041

Rushton, J. P., & Bons, T. A. (2005). Mate Choice and Friendship in Twins: Evidence for Genetic Similarity. *Psychological Science*, *16*(7), 555–559. https://doi.org/10.1111/j.0956-7976.2005.01574.x

Schönbrodt, F. D., Humberg, S., & Nestler, S. (2018). Testing similarity effects with dyadic response surface analysis. *European Journal of Personality*. doi:10.1002/per.2169

Sekara, V., Stopczynski, A., & Lehmann, S. (2016). Fundamental structures of dynamic social networks. *PNAS Proceedings of the National Academy of Sciences of the United States of America*, *113*(36), 9977–9982. https://doi.org/10.1073/pnas.1602803113

Stopczynski, A., Sekara, V., Sapiezynski, P., Cuttone, A., Madsen, M. M., Larsen, J. E., & Lehmann, S. (2014). Measuring Large-Scale Social Networks with High Resolution. Plos One, 9(4): e95978. https://doi.org/10.1371/journal.pone.0095978

Turcsán, B., Range, F., Virányi, Z., Miklósi, Á., & Kubinyi, E. (2012). Birds of a feather flock together? Perceived personality matching in owner–dog dyads. *Applied Animal Behaviour Science, 140*(3-4), 154–160. https://doi.org/10.1016/j.applanim.2012.06.004

van Zalk, M. H. W., Nestler, S., Geukes, K., Hutteman, R., & Back, M. D. (in press). The co-development of extraversion and friendships: Bonding and behavioral interaction mechanisms in friendship networks. *Journal of Personality and Social Psychology.* . doi: 10.1037/pspp0000253

Chapter 8

Gender-specific behavior change following terror attacks

> *"Acts of terrorism constitute one of the most serious violations of the universal values of human dignity, freedom, equality and solidarity, and enjoyment of human rights and fundamental freedoms on which the Union is founded. They also represent one of the most serious attacks on democracy and the rule of law, principles which are common to the Member States and on which the Union is based."*
>
> — European Parliament and Council of the European Union, 2017

Terrorist attacks constitute severe threats against civilians and societies. The quote opening this chapter illustrates the seriousness with which the European Union treats this threat. Although authorities take the threat seriously, terror attacks frequently happen in Europe and the rest of the world. In the period from 1950 to 2004, 11,245 terror events took place in Western European countries (Engene, 2007). Figure 8.1 illustrates the frequency of these terror attacks as a function of time. We do not find evidence that the duration of social connections correlate with any of the narcissism scores.

In their definition of terrorist offences, the European Parliament and Council of the European Union list 3 aims (Parliament and European Union, 2017). If an offence is committed with any of these aims, it qualifies as a terrorist offence. These aims (quoted from (Parliament and European Union, 2017)) are,

1. seriously intimidating a population;
2. unduly compelling a government or an international organisation to perform or abstain from performing any act;
3. seriously destabilising or destroying the fundamental political, constitutional, economic or social structures of a country or an international organisation.

The first of these aims is very interesting. While some consequences of an attack, such as fatalities, injuries, and material costs, are easy to quantify, the impact the attack has on the general population is more challenging to compute. In fact, how the broader population reacts to terror attacks remains an open question. In collaboration with psychologists at the University of Copenhagen, computational scientists at the Technical University Denmark and Department of Social Sciences, University of Copenhagen, and Joachim Mathiesen at the Niels Bohr Institute, I have sought to quantify how terror attacks affect the behavior of citizens in Western Europe.

FIGURE 8.1: The frequency of terror attacks in 18 Western European countries as a function of time. Figure from (Engene, 2007).

8.1 Previous work on behavior following terror attacks

Many of the existing studies on the impact of terror attacks on the broader population rely on data collected following the event. Two questionnaire-based studies investigated, among other things, the impact that living in Israeli areas with high exposure to terror attacks has on behavior and emotions (Oppenheimer, Villa, and Apter, 2011; Korn and Zukerman, 2011). The participants with high exposure to terror events perceived themselves as more cautious, one study concluded, while the other found the participants to show a higher degree of avoidance behavior. One of these studies, a self-report study focusing on adolescents, found a higher degree of terror-related stress responses among females and news consumers (Oppenheimer, Villa, and Apter, 2011). Gender differences were reported in other questionnaire-based studies with Israeli participants, too. These include increased self-reported risk-taking behavior among men frequently exposed to terrorism (Pat-Horenczyk et al., 2007) and increased depressive and post-traumatic symptoms among women (Solomon, Gelkopf, and Bleich, 2005).

Some psychological studies have focussed on the impact of the 9/11 attacks in New York City, 2001. In a nationwide online survey, one team of researchers found some demographic factors to correlate with psychological outcomes (Silver et al., 2002). The authors found that, among other things, high levels of symptoms of post-traumatic stress were associated with being female and with having pre-attack diagnosed depression or anxiety. Another study reported that after single events, such as the 9/11 attack, stress-symptom frequency returns to ordinary levels after only a short period of time (Schlenger, 2005).

Some studies have examined the behavioral impact of terror attacks using objective data or real-time data. One study found that the use of the New York subway decreased when the terror-alert level was increased (Montes, 2006). Another study

reported that the number of fatal traffic accidents in Israel fell shortly after terror attacks, and spiked 3 days following terror attacks (Stecklov and Goldstein, 2004). Lastly, telecommunication data following a bombing was part of a broader study on behavior following large-scale emergencies (Bagrow, Wang, and Barabási, 2011). In this study, the authors reported an increase in call volume for female participants. In addition to these examples, objective real-time data have been used to study behavior patterns following natural disasters (Bengtsson et al., 2011; Lu, Bengtsson, and Holme, 2012) and other emergencies such as disasters involving crowds of people (Helbing, Johansson, and Al-Abideen, 2007; Johansson et al., 2008). The objective of our study was to use objective, real-time data to systematically study behavioral patterns following several terror attacks. In particular, we aimed to test whether gender differences were present in our data. We also wanted to develop a statistical methodology well-suited for testing for gender differences and which went beyond binning data and analysing only the volume of telecommunication events.

8.2 Our results: Gender differences in behavior change following terror attacks

In the paper "Gender-specific behavior following terror attacks", which we have submitted but not yet received any comments on, we analyse telecommunication of citizens following terror attacks. We do this with three different aims in mind, 1) To understand whether the telecommunication patterns are significantly different following attacks, compared to days with no attacks; 2) To examine whether some groups of citizens behave differently following terror attacks; 3) If groups do indeed behave differently, to tell if these differences are consistent with differences observed on ordinary days, or if the differences are magnified following terror attacks. Specifically, we investigate gender differences, as some evidence of such differences was reported in previous studies.

Focussing on 6 different terror attacks carried out in Western Europe in the period 2015-2017, we examine telecommunication patterns of citizens living in the affected cities. We compare the communication patterns in the first 24 hours following an attack with the average behavior on 8 comparable weekdays before the attack. Our analysis goes beyond analysing call volume. Instead, we measure the deviation of the telecommunication timing from the characteristic diurnal communication patterns on ordinary days. We find that the communication patterns of both males and females are significantly different following terror attacks, as compared to regular days. We also find that differences in communication patterns between males and females are greater following the attack than would be expected if the gender labels carried no information. Furthermore, we find that the observed gender differences are significantly elevated following the terror attacks as compared to ordinary days.

8.3 Paper: Gender-specific behavior change following terror attacks

Gender-specific behavior change following terror attacks

Jonas S. Juul,[1,*] Laura Alessandretti,[2,3] Jesper Dammeyer,[4]
Ingo Zettler,[4] Sune Lehmann,[2,3] and Joachim Mathiesen[1,†]

[1] *Niels Bohr Institute, University of Copenhagen, Blegdamsvej* 17*, Copenhagen 2100-DK, Denmark*
[2] *Centre for Social Data Science, University of Copenhagen, DK-1353 Kgs. København K, Denmark*
[3] *Technical University of Denmark, DK-2800 Kgs. Lyngby, Denmark*
[4] *Department of Psychology, University of Copenhagen,*
Øster Farimagsgade 2A, 1353 København K, Denmark

Abstract

Terrorists use violence in pursuit of political goals. While terror often has severe consequences for victims, it remains an open question how terror attacks affect the general population. We study the behavioral response of citizens of cities affected by 7 different terror attacks. We compare real-time mobile communication patterns in the first 24 hours following a terror attack to the corresponding patterns on days with no terror attack. On ordinary days, the group of female and male participants have different activity patterns. Following a terror attack, however, we observe a significant increase of the gender differences. Knowledge about citizens' behavior response patterns following terror attacks may have important implications for the public response during and after an attack.

* jonas.juul@nbi.ku.dk
† mathies@nbi.dk

I. INTRODUCTION

Terror attacks affect all parts of the world and are often carried out in attempts to communicate political messages or to dictate a political change [1, 2]. The European Parliament and Council of the European Union defines an offence as terror if it has one of three aims; the first of these is "seriously intimidating a population" [3]. While the direct consequences of an attack are easily quantified in terms of human casualties or material damage, the implications for the populations more broadly remains an open question. Of particular interest is how terror attacks impact the behavior of citizens. How do people react? Do people significantly change their behavior? If they do, is this change in behavior similar for all citizens, or are particular groups of individuals especially susceptible? Knowledge on such questions is sparse, yet valuable in making informed decisions about public response following terror attacks.

Previous studies have shown that exposure to terror increases the level of psychological stress as well as the frequency of disorders such as post traumatic stress, anxiety, and depression. For example, in the month following the 9/11 attacks, 12% of the U.S. population experienced significant distress, about 30% reported symptoms of anxiety and 27% reported that they avoided situations that reminded them of 9/11 [4]. Exposure to terror through media or from knowing a victim also results in higher levels of avoidance behavior, a subjective feeling of insecurity, emotional distress, as well as changes of daily routines such as the choice of transportation [5, 6]. Whereas repeated exposure is known to be a physical health risk [7], studies have shown that for isolated events, the frequency of stress symptoms quickly return to normal levels – for instance among citizens in New York City following the 9/11 terror attacks [8]. Individual differences, and to some extent gender differences, have been reported to be factors in the response to terror [9–13]. For example, in a survey study women expressed symptoms of posttraumatic stress and depression more frequently than men [14]. Women's likelihood of developing posttraumatic stress symptoms were six times higher than those for men. It has also been reported that continuous threat of a terror attack promotes risk taking behaviors in men [13].

Objective real-time data have been used to analyze behavior patterns following e.g. natural disasters [15, 16], emergencies [17], and crowd disasters [17–19]. Whereas objective data have been used in studies on the frequency and size of terror attacks [20, 21] and

structural properties of operational networks [22, 23], systematic studies on the behavioral impact of terror typically have relied on post-terror and self-report data. Consequently, quantitative studies of terror-related behavioral changes are much needed [24]. In fact, the use of objective data to understand peoples response is limited to a few studies, for example in observations of correlations between the terror alert level and the number of people using public transportation [25], in observations of an increase of fatal traffic accidents in the days following a terror attack [26], and the behavioral response to a bombing with several injured and no fatalities [17]. In the latter case, the authors found that females were more likely to make a call following the emergency, than expected on normal days. Here, we analyze behavior patterns in telecommunication following several recent terror attacks throughout Europe. We rigorously test for gender differences in the behavioral response to terror attacks and explicitly compare with ordinary days with no terror attacks.

II. RESULTS

Our study uses data on telecommunication activity following 7 terror attacks in 6 different cities: Paris, Nice, Berlin, London($\times$2), Stockholm, and Barcelona. The attacks were carried out in the period November 14, 2015 - August 17, 2017, and although the attacks varied in size, all attacks resulted in several casualties (see Material and Methods). Figure 1 shows that following a terror attack the activity deviates significantly from the normal diurnal rhythm [27, 28] (see Supplementary Section SII). In our analysis, we focus on the deviation in the 24 hour window following terror attacks. We calculate the cumulative telecommunication activities for the female and male population separately, with notation $C_F(t)$ and $C_M(t)$, where the subscripts F and M refer to females and males, respectively. We normalize the cumulative activity such that for both populations, $C_{F/M}(0h) = 0$ and $C_{F/M}(24h) = 1$. We compute the area Δ_{FM} between the two curves, $C_F(t)$ and $C_M(t)$, and use this area to quantify the difference in behavior change (See Materials & Methods for details on our statistical analysis). Figure 2 shows an example of the activity on an ordinary day (panel A) and on a day following a terror attack (panel C). The corresponding cumulative activities are shown in panels B and D. Note that in Fig. 2A, the telecommunication activity of females is higher. Averaging over all participants in our study, we find that females in general are 18% more active than the male participants (see Supplementary Section SII). However, the

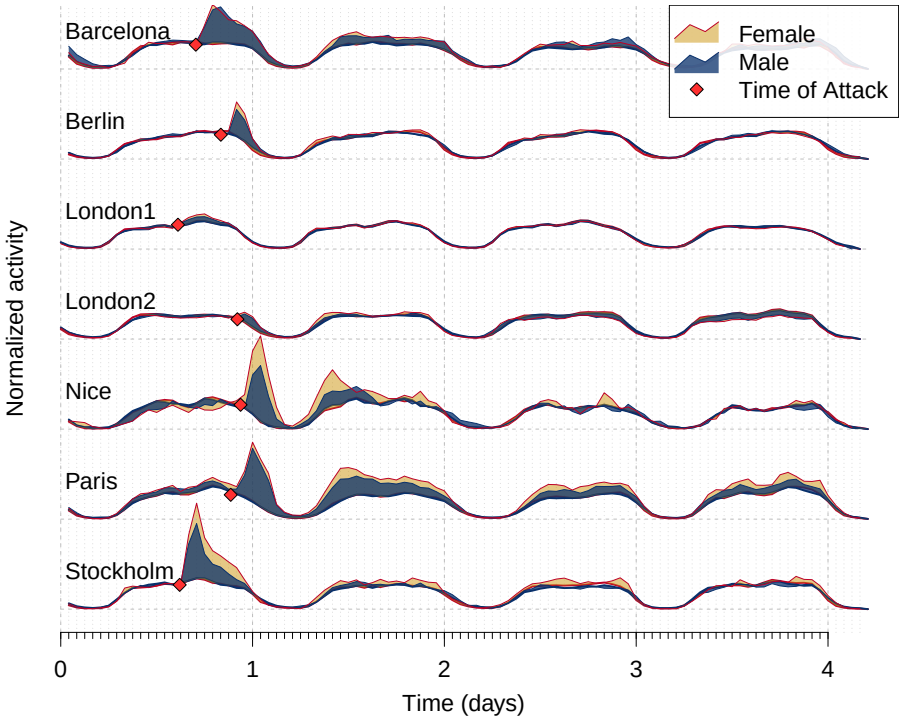

FIG. 1. **Normalized communication activity at the day of the terror attack and the three consecutive days.** The activity of the genders are normalized separately by their respective mean activities over 8 background weeks. The colored area under the curves shows the increased activity relative to the background weeks.

normalized cumulative activity (Fig. 2B) shows that the only difference between the diurnal rhythm of the genders is the volume of the activity. Following a terror attack, however, the response of the female participants is significantly different to that of the males as illustrated in Fig. 2D and quantified by the area between the normalized cumulative activities.

Following each terror attack, we probe the difference between the gender specific communication patterns by computing the area Δ_{FM}. We compare this area with a null distribution computed in the following way. First, we split the total population of both genders in two groups chosen at random: one group, $\tilde{F}$, which has a number of individuals equal to the number of females in the original population and a group $\tilde{M}$, consisting of the remaining individuals. Note that these two groups will contain a mix of both genders. Second, we compute an area $\Delta_{\tilde{F}\tilde{M}}$ between the normalized cumulative activities of the two new groups using the same 24 hour window following an attack. Repeating the process of randomly

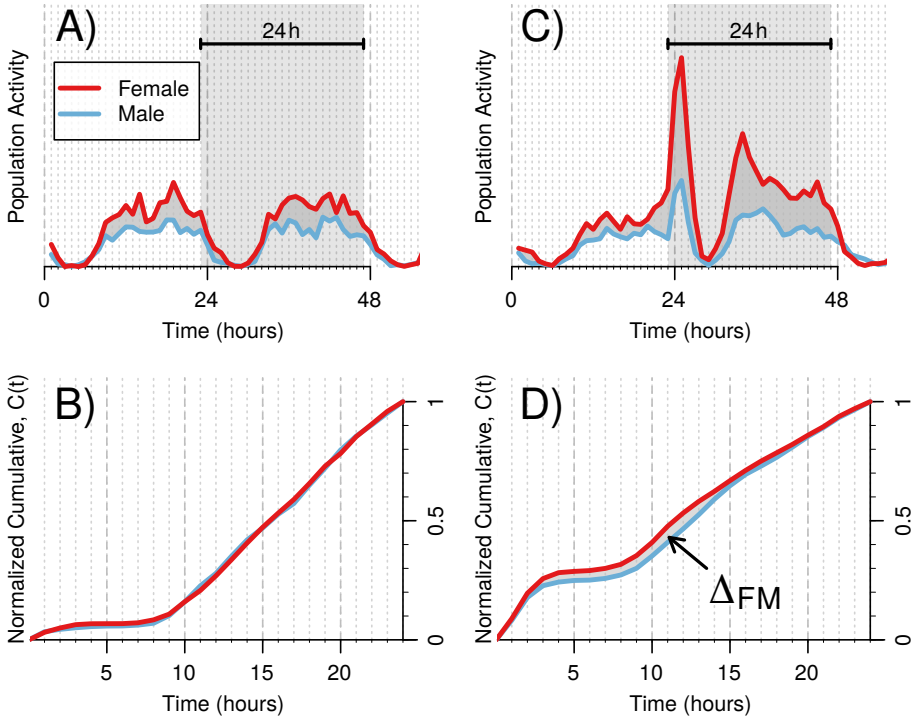

FIG. 2. **Comparison of gender activities following an attack and in a representative background week.** A) Example of activities on normal days and C) activity following a terror attack. For our analysis, we consider a $T_{max} = 24hrs$ window. B) To quantify behavior differences between two groups of people, we use the area between normalized cumulative diurnal curves of telecommunication. On normal days, our measure detects no difference in the relative gender activities, however, D) following an attack, we see a pronounced difference marked by the area $\Delta_{\alpha\beta}$. See Materials and Methods for technical details of how the measure can be computed from raw telecommunication data.

splitting our population 10^5 times, we estimate the null distribution of $\Delta_{\tilde{F}\tilde{M}}$.

We now test if the communication patterns of the female and male participants are significantly different on the day of the attack by computing the probability p to observe an equally or more extreme value than the empirically computed value Δ_{MF}, i.e. p =Prob($\Delta_{\tilde{F}\tilde{M}} \geq \Delta_{FM}$). Figure 3 shows the null distribution and corresponding values of p. Combining the measurements over all the cities (see Material and Methods) leaves that the gender-specific patterns are different with a combined p value of less than 10^{-5}.

Although the analysis above shows that the difference in behavior patterns is larger in the

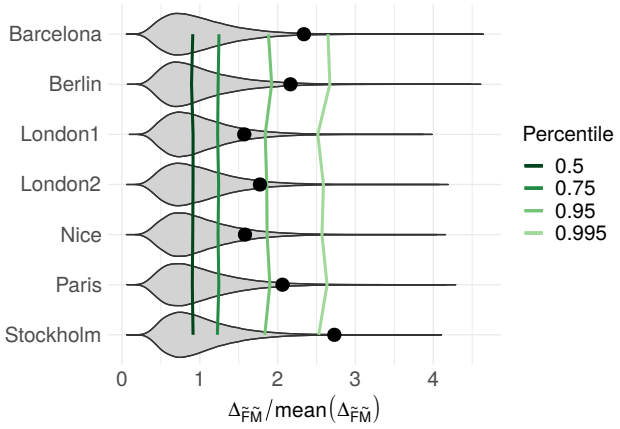

FIG. 3. **Gender differences in telecommunication on days of terror attacks.** Empirically observed gender difference in telecommunication following terror attacks (black circles) plotted relative to computed null distributions (violin plot) for all cities. The null-distributions were computed by randomly shuffling individuals between our two gender groups and measuring the difference in behavior of the new groups. Note that the true empirical values of the gender difference all lie beyond the 0.75 percentile of the null-distribution.

gender specific group than in randomly sampled groups, we cannot yet rule out that such a difference could be observed on ordinary days too. We therefore perform an additional test where we compare the behavior difference on the day of attack with the difference in the background weeks. Again, we quantify the behavior change by comparing Δ_{MF} to a null distribution of $\Delta_{\tilde{M}\tilde{F}}$. Instead of shuffling gender labels (within the day of the attack), we now randomly choose a recorded activity of the individuals from the 8 background weeks. Like above, we keep the sizes of the populations fixed, i.e. $|M| = |\tilde{M}|$ and $|F| = |\tilde{F}|$. We now compute a null distribution by replacing the 24 hour communication pattern of individuals with a randomly selected communication log (from a person of same gender) in one of the 8 background weeks. In this way, we keep the gender fixed, but the activity on the day of the terror is replaced by one from the background weeks. We finally quantify the difference in communication behavior by the area between the normalized cumulative diurnal telecommunication curves. We repeat this procedure 10^5 times to get a null distribution of differences between males and females communication activity on ordinary days.

We can now test if the differences between female and male communication patterns

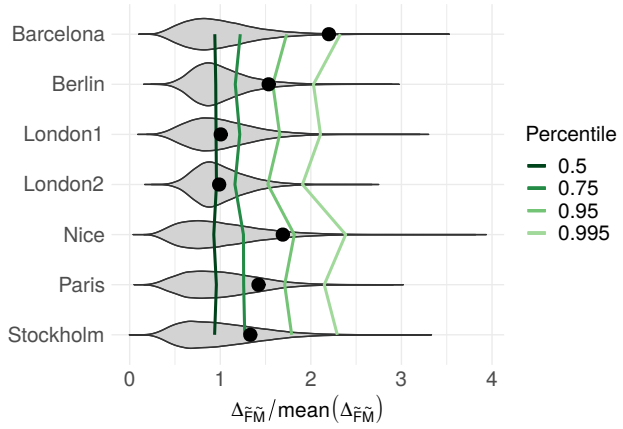

FIG. 4. **Amplified gender differences in behavior following terror attacks.** Empirically observed gender difference in telecommunication following terror attacks (black circles) plotted relative to computed null-distributions (violin plot) for all cities. The null-distributions were created by computing the difference in telecommunication between groups of randomly selected males and randomly selected females on days with no terror. The random population of males (females) consisted of telecommunication logs drawn uniformly-at-random from the activity of all males (females) during the 8 background weeks. Note that the true empirical values of the gender difference all lie beyond the median of the null-distribution. The probability of getting a set of empirical values this or more extreme on days with no terror is approximately two in a thousand.

are more extreme on the day of the attack compared to ordinary days. To this end we compute the probability to observe an equally or more extreme value than the empirical Δ_{MF}. Figure 4 shows our results. We find that, for all cities, this probability is smaller than 50%. Combining these probabilities yields a chance of getting a set of probabilities at least as extreme as these equal to $p \approx 0.002$.

III. DISCUSSION

Terror attacks take place around the world and it is important to understand how the general population reacts. Using real-time GPS and telecommunication data from $17,000$ people, we systematically studied behavior following 7 different terror attacks in Western European countries. In particular, we studied the behavioral change of the groups of females

and males in each city on the day of the attack as compared to ordinary days. We found that the telecommunication of both males and females spiked following all terror attacks. These spikes were significant deviations from normal telecommunication behavior.

One might expect that a sizable disturbance of a population, such as a terror attack, might cause the distribution of calls of females and males to become more similar than they would be otherwise. Juxtaposing the behavior of the two genders following terror attacks, we found significant differences in the behavioral change of the two genders compared to a group where gender labels are assigned randomly. The differences between the groups of males and females after the attacks, were large even when correcting for differences on ordinary background days. It is an open question what causes the observed gender differences in behavior following terror attacks. From a psychological perspective, differences in personality characteristics for males and females could be relevant. Previously reported differences between women and men in personality characteristics include scores in Emotionality and Honesty-Humility (for a recent meta-analysis, see for example [29]). In this light, it would be interesting to test whether the gender differences we observe can be attributed more directly to personality traits known to differ between genders. It is important to qualify the point that these results were obtained for the aggregated behavior of females and males. The uncovered gender differences on the aggregate level do not imply that every female and every male act significantly different from each other. The aggregated communication could be influenced by "extreme" individuals. If this is the case, such extremes seem to be present systematically in the different cities. Furthermore, systematic studies of the variance in behavior patterns inside each group would be worthwhile to conduct.

Finally, future research should examine whether there are any cultural or regional differences in the behavioral response to terror attacks. In our analysis, we found significant gender differences in behavioral change following terror attacks supported by the analysis presented in Figure 4. This figure also shows that although the difference in behavioral change is generally large, the empirical values for the two London attacks lie almost exactly at the null-distribution median. This begs the question whether London is different or if this is just random coincidence. If London is different, is this difference rooted in history, culture, geography, the nature of the attacks or some other variable? Knowledge on how terror attacks impact the general population is important in formulating a public response to such offenses, and we hope in this regard that our study will inspire further work on this

City	Time of attack	No. Fatalities/No. Injured	No. People in data
Paris (FR)	00:58, November 14, 2015	137/368 [30]	2523
Nice (FR)	10:30 pm, July 14 2016	86/201 [31]	237
Berlin (DE)	8:02 pm, December 19 2016	12/56 [31]	2295
London (UK)	2:40 pm, March 22 2017	6/50 [32]	5415
Stockholm (SE)	2:53 pm, April 7, 2017	5/14 [32]	741
London (UK)	10:06 pm, June 3 2017	11/48 [32]	5131
Barcelona (ES)	4:54 pm, August 17 2017	15/131 [32]	688

TABLE I. **Details about the terror attacks included in the study and the data concerning each attack.**

topic.

IV. MATERIALS AND METHODS

A. Experimental design

We analyse behavioral change following 7 terror attacks carried out in different European countries. Details of the different attacks are listed in Table I including city name, time of the attack, the number of casualties and injured, and the number of people included in our data set. We monitor the behavior difference using telecommunication data on the week of the attack and compare it with 8 background weeks leading up to the terror attacks. For each background week, we consider the same 24-hour interval as we do following a terror attack. The 8 weeks used as background for each attack are listed in Table II.

B. Data description

We used a dataset of phone-app usage and GPS records collected by a global mobile phone and electronic company between 2015 and 2017. We considered 7 terror attacks, and selected $\sim 17,000$ users who lived in the same city where an attack occurred at the time it happened. Specifically, we selected users whose most visited location in the period under study (see Table II) is within a bounding box around the city where the attack happened (see

City	First background week Monday	Last background week Sunday
Paris (FR)	September 14, 2015	November 22, 2015
Nice (FR)	May 19, 2016	July 17, 2016
Berlin (DE)	October 24, 2016	December 18, 2016
London (UK)	January 25, 2017	March 21, 2017
Stockholm (SE)	February 10, 2017	April 6, 2017
London (UK)	April 7, 2017	June 2, 2017
Barcelona (ES)	June 22, 2017	August 16, 2017

TABLE II. **Details about background weeks used in the analysis.**

Supplementary Table S1). We considered the usage of applications the company categorized as "Communication". About 60% of events in this category concern the usage of 5 Android apps: Phone, Messaging, WhatsApp Messenger, Facebook, Gmail and Facebook Messenger. Users are aged between 18 and 80 years old, with an average age of 36 years. About 42% of the users are female. Written consent in electronic form has been obtained for all study participants.

C. Statistical methods

1. Measure from telecommunication data

In the following we formally define the measure – the area between normalized cumulative diurnal curves of telecommunication – we are use in our analyses. In a given time interval, $[0, t_{\max}]$, individual participants, γ, initiate N_γ communication events at times $\{t_{i,\gamma}\}_{i=1}^{N_\gamma}$. We define the activity function $A^{(\gamma)}(t)$ of an individual in terms of the point process

$$A^{(\gamma)}(t) = \sum_{i=1}^{N_\gamma} \delta(t - t_{i,\gamma}), \tag{1}$$

where $\delta(x)$ is the Dirac delta function. The activity function of a population X is the sum of individual activity functions,

$$A_X(t) = \sum_{\gamma \in X} A^{(\gamma)}(t). \tag{2}$$

For each population activity function $A_X(t)$, we define the corresponding normalized cumulative activity function

$$C_X(t) = \frac{\int_0^t A_X(t')dt'}{\int_0^{t_{\max}} A_X(t')dt'}. \tag{3}$$

where the denominator is the total number of initiated communication events in our population, $N_X = \sum_{\gamma \in X} N_\gamma$, and thus $C_X(t)$ is equal to the fraction of communication events that were initiated before the time t. To assess the differences in communication patterns for two populations X and Y in a time interval $[0, t_{\max}]$, we compare how communication events are distributed over the time interval for the two populations. Specifically, we calculate the area between the cumulative activity functions for the two populations,

$$\Delta_{XY} = \int_0^{t_{\max}} |C_X(t) - C_Y(t)|\, dt. \tag{4}$$

In this study, the length of the time interval, $t_{\max}$, is fixed to be 24 hours. On a normal day, females, in our population, are on average 18% more active than males. Fig. 2A illustrates this; similar curves are shown for the all cities included in this study in Supplementary Figure 1. The measure, defined in Eq. (4), has a number of attractive features. It is not sensitive to the imbalance in gender activities and allows us to quantify changes to the diurnal rhythm. Moreover, our measure does not require any artificial binning of data and is not particularly sensitive to the chosen time interval.

Combining the results to probe for gender differences. In our analysis, we obtain probabilities for the random occurrence of gender differences of the same size as observed following the terror attacks. If the null hypothesis, that there are no enhanced gender differences, were true, these probabilities would be uniformly sampled on the interval $[0, 1]$. We test this as follows. If $X_1, X_2, \ldots, X_n$ are stochastic variables drawn from a uniform distribution, the random variables

$$Y_i = -2\ln(X_i), \tag{5}$$

are independent and identically distributed according to the chi-square distribution with 2 degrees of freedom. The sum of these variables

$$T = \sum_{i=1}^{n} Y_i, \tag{6}$$

is distributed according to the chi-square distribution with $2n$ degrees of freedom. To test whether our obtained probabilities support the hypothesis that the gender differences are

	Barcelona	Berlin	London1	London2	Nice	Paris	Stockholm
Fig 3	0.01312	0.02543	0.10505	0.06394	0.10809	0.03104	0.00233
Fig 4	0.00862	0.06071	0.44336	0.45604	0.07581	0.15288	0.21411

TABLE III. **Fraction of null distributions more or equally extreme as empirical values in Figs. 3 and 4**. The fraction of null distributions depicted in Figs. 3 and 4 that lie beyond the corresponding empirically observed values. We subtract each of these values from 1 and plug them into Eq. (5) and then (6) to calculate a combined probability using Eq. (7).

not larger than should be expected from ordinary days, we calculate this T value using Equations (5) and (6). We then calculate the area under the chi-square distribution with $2n$ degrees of freedom, at values larger than T,

$$p_{\text{combined}} = \int_T^\infty \chi^2_{2n}(x)dx. \tag{7}$$

This integral is equal to the chance of getting the set of probabilities if $X_1, X_2, \ldots, X_n$ were drawn from a uniform distribution.

2. p-values used in calculating probability of observing behavior differences randomly

The distributions depicted in Figures 4 and 3 give us two sets of p-values. In each case, we used the method described above to estimate the probability that the empirically observed measure values would be obtained if the values were results of statistical fluctuations. The p-values are shown in Tab. III. Combining these p-values give the combined probabilities listed in the main text.

[1] Martha Crenshaw. The causes of terrorism. *Comparative politics*, 13(4):379–399, 1981.

[2] Max Abrahms. Why terrorism does not work. *International Security*, 31(2):42–78, 2006.

[3] European Parliament and Council of European Union. Directive (eu) 2017/541 of the european parliament and of the council of 15 march 2017 on combating terrorism and replacing council framework decision 2002/475/jha and amending council decision 2005/671/jha, 2017. `http://data.europa.eu/eli/dir/2017/541/oj`.

[4] Roxane Cohen Silver, E Alison Holman, Daniel N McIntosh, Michael Poulin, and Virginia Gil-Rivas. Nationwide longitudinal study of psychological responses to september 11. *Jama*, 288(10):1235–1244, 2002.

[5] Liat Korn and Gil Zukerman. Affective and behavioral changes following exposure to traumatic events: the moderating effect of religiosity on avoidance behavior among students studying under a high level of terror event exposure. *Journal of religion and health*, 50(4):911–921, 2011.

[6] Sabrina Oppenheimer, Yael Villa, and Alan Apter. Effects of prolonged exposure to terrorism on israeli youth: Stress-related responses as a function of place of residence, news consumption, and gender. *Adolescent Psychiatry*, 1(2):152–162, 2011.

[7] Shani Shenhar-Tsarfaty, Nadav Yayon, Nir Waiskopf, Itzhak Shapira, Sharon Toker, David Zaltser, Shlomo Berliner, Ya'acov Ritov, and Hermona Soreq. Fear and c-reactive protein cosynergize annual pulse increases in healthy adults. *Proceedings of the National Academy of Sciences*, 112(5):E467–E471, 2015.

[8] William E Schlenger. Psychological impact of the september 11, 2001 terrorist attacks: Summary of empirical findings in adults. *Journal of aggression, maltreatment & trauma*, 9(1-2):97–108, 2005.

[9] Rafael Gabriel, Laura Ferrando, Enrique Sainz Cortón, Carlos Mingote, Eduardo García-Camba, Alberto Fernández Liria, and Sandro Galea. Psychopathological consequences after a terrorist attack: an epidemiological study among victims, the general population, and police officers. *European Psychiatry*, 22(6):339–346, 2007.

[10] Sandro Galea, Jennifer Ahern, Heidi Resnick, Dean Kilpatrick, Michael Bucuvalas, Joel Gold, and David Vlahov. Psychological sequelae of the september 11 terrorist attacks in new york city. *New England Journal of Medicine*, 346(13):982–987, 2002.

[11] Shaul Kimhi and Michal Shamai. Are women at higher risk than men? gender differences among teenagers and adults in their response to threat of war and terror. *Women & Health*, 43(3):1–19, 2006.

[12] Jose M Salguero, A Cano-Vindel, I Iruarrizaga, P Fernández-Berrocal, and S Galea. Trajectory and predictors of depression in a 12-month prospective study after the madrid march 11 terrorist attacks. *Journal of psychiatric research*, 45(10):1395–1403, 2011.

[13] Ruth Pat-Horenczyk, Osnat Peled, Tomer Miron, Daniel Brom, Yael Villa, and Claude M Chemtob. Risk-taking behaviors among israeli adolescents exposed to recurrent terrorism: provoking danger under continuous threat? *American Journal of Psychiatry*, 164(1):66–72, 2007.

[14] Zahava Solomon, Marc Gelkopf, and Avraham Bleich. Is terror gender-blind? gender differences in reaction to terror events. *Social Psychiatry and Psychiatric Epidemiology*, 40(12):947–954, 2005.

[15] Xin Lu, Linus Bengtsson, and Petter Holme. Predictability of population displacement after the 2010 haiti earthquake. *Proceedings of the National Academy of Sciences*, 109(29):11576–11581, 2012.

[16] Linus Bengtsson, Xin Lu, Anna Thorson, Richard Garfield, and Johan Von Schreeb. Improved response to disasters and outbreaks by tracking population movements with mobile phone network data: a post-earthquake geospatial study in haiti. *PLoS medicine*, 8(8):e1001083, 2011.

[17] James P Bagrow, Dashun Wang, and Albert-Laszlo Barabasi. Collective response of human populations to large-scale emergencies. *PloS one*, 6(3):e17680, 2011.

[18] Dirk Helbing, Anders Johansson, and Habib Zein Al-Abideen. Dynamics of crowd disasters: An empirical study. *Physical review E*, 75(4):046109, 2007.

[19] Anders Johansson, Dirk Helbing, Habib Z Al-Abideen, and Salim Al-Bosta. From crowd dynamics to crowd safety: a video-based analysis. *Advances in Complex Systems*, 11(04):497–527, 2008.

[20] Aaron Clauset, Maxwell Young, and Kristian Skrede Gleditsch. On the frequency of severe terrorist events. *Journal of Conflict Resolution*, 51(1):58–87, 2007.

[21] Aaron Clauset, Ryan Woodard, et al. Estimating the historical and future probabilities of large terrorist events. *The Annals of Applied Statistics*, 7(4):1838–1865, 2013.

[22] Aaron Clauset, Cristopher Moore, and Mark EJ Newman. Hierarchical structure and the prediction of missing links in networks. *Nature*, 453(7191):98, 2008.

[23] Pedro Manrique, Zhenfeng Cao, Andrew Gabriel, John Horgan, Paul Gill, Hong Qi, Elvira M Restrepo, Daniela Johnson, Stefan Wuchty, Chaoming Song, et al. Women's connectivity in extreme networks. *Science advances*, 2(6):e1501742, 2016.

[24] A Grimm, L Hulse, and Sarah Schmidt. Risk perception and psychological reactions in public crisis situations using the example of terror attacks. *Bundesgesundheitsblatt, Gesundheitsforschung, Gesundheitsschutz*, 52(12):1129–1140, 2009.

[25] Joshua Kenneth Montes. *The Effects of Changes in the National Terror Alert Level on Consumer Behavior*. PhD thesis, Miami University, 2006.

[26] Guy Stecklov and Joshua R Goldstein. Terror attacks influence driving behavior in israel. *Proceedings of the National Academy of Sciences of the United States of America*, 101(40):14551–14556, 2004.

[27] Dániel Kondor, Pierrick Thebault, Sebastian Grauwin, István Gódor, Simon Moritz, Stanislav Sobolevsky, and Carlo Ratti. Visualizing signatures of human activity in cities across the globe. *arXiv preprint arXiv:1509.00459*, 2015.

[28] Talayeh Aledavood, Sune Lehmann, and Jari Saramäki. Digital daily cycles of individuals. *Frontiers in Physics*, 3:73, 2015.

[29] Morten Moshagen, Isabel Thielmann, Benjamin E Hilbig, and Ingo Zettler. Meta-analytic investigations of the hexaco personality inventory (-revised). *Zeitschrift für Psychologie*, 2019.

[30] Europol. *TE-SAT 2016: EU Terrorism Situation and Trend Report*. Publications Office of the European Union, 2016.

[31] Europol. *TE-SAT 2017: EU Terrorism Situation and Trend Report*. Publications Office of the European Union, 2017.

[32] Europol. *TE-SAT 2018: EU Terrorism Situation and Trend Report*. Publications Office of the European Union, 2018.

Funding: J.S.J. J.D. I.Z. S.L. and J.M. received funding through the University of Copenhagen UCPH 2016 Excellence Programme for Interdisciplinary Research. **Author contributions:** All authors designed the research. J.S.J., L.A., S.L., and J.M. designed the statistical method. J.S.J and L.A. performed the data analysis. All authors wrote the paper. **Competing interests:** The authors declare that they have no competing interests. **Data and materials availability:** All data needed to evaluate the conclusions in the paper are present in the paper and/or the Supplementary Materials. Additional data related to this paper may be requested from the authors.

city	min lat	max lat	min lon	max lon
Berlin	52.369276	52.650018	13.091432	13.754525
Nice	43.646275	43.758400	7.178630	7.338724
Barcelona	41.310933	41.465339	2.058793	2.244023
London	51.325628	51.672014	-0.472381	0.268712
Stockholm	59.298186	59.371545	17.945337	18.154841
Copenhagen	55.5531	55.8175	12.2607	12.7043
Paris	48.7106	48.9991	2.0641	2.6463

TABLE S1. Bounding boxes used to select individuals living in the cities under study. The table reports the minimum and maximum values of the latitude and longitude.

SUPPLEMENTARY MATERIALS

SI. GEOGRAPHY OF THE CITIES UNDER STUDY.

We selected individuals whose most visited locations during the period under study (see Table II) is located within the city where the attack happened. The bounding boxes characterizing each city are described in Table S1.

SII. DIURNAL COMMUNICATION ON ORDINARY DAYS

The populations of males and females show distinct diurnal communication patterns in all of the cities we include in our analysis. Fig S1 shows these curves for all background weeks used in our study. The curves are almost identical for all background weeks, indicating that averaging over the weeks yields a good estimate of the diurnal activity. Females communicate on average 18% more than males but normalizing their activity yield indistinguishable curves. These normalized curves are shown in Fig. 1 of the main text.

SIII. SIGNIFICANCE OF PEAKS FOLLOWING TERROR ATTACKS

Figure 1 shows that a terror attack is followed by a spike in telecommunication activity for both genders for all cities in our study. In order to assess the significance of the spikes in

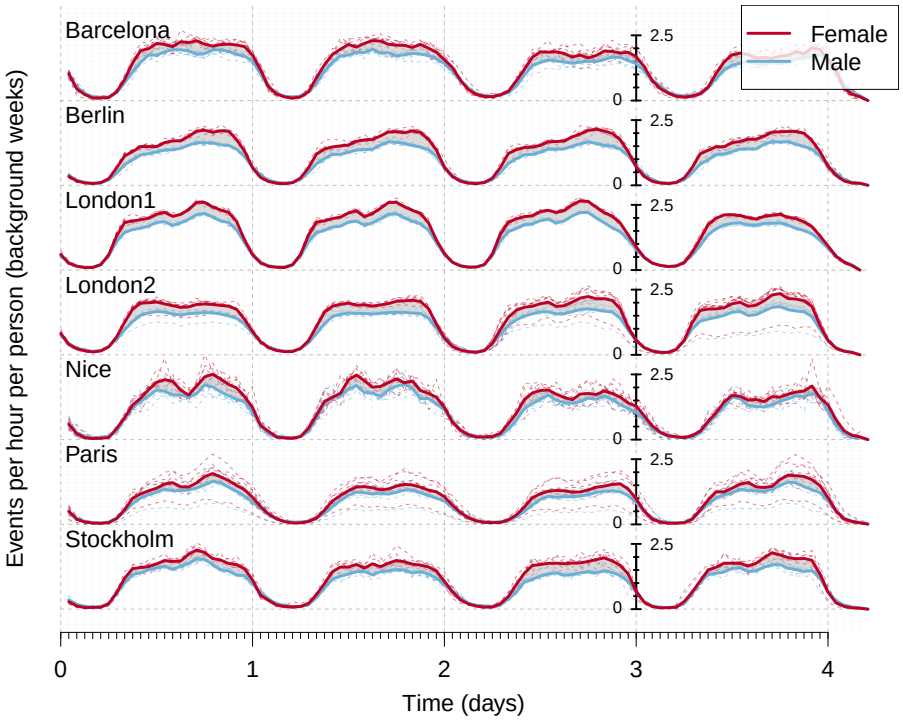

FIG. S1. Illustration of diurnal communication patterns during ordinary days. Data for all background week are plotted in dashed lines. The mean activity for each gender is plotted with full lines. On average, females communicate 18% more than men.

the communication, we compare with a null model in the following way. We first compute a null-distribution of the area between normalized cumulative diurnal telecommunication curves by bootstrapping. The null-distribution quantifies natural variation to the diurnal pattern. More specifically, in a population of for example n males, we create a set of individual activities on ordinary days $\{A^{(p)}\}_{p\in M}$ where M is the subset of males in our population and each element is a 24 hour sequence of communication events, see Eq. (2). This set has $8n$ elements, one for each person and for each of the 8 background weeks. We draw n random elements from $\{A^{(p)}\}_{p\in M}$ (allowing for repeated draws of the same element) corresponding to n activity functions, from which we get a single background cumulative activity function using Eqs. (2) and (3). We then choose one of the 8 ordinary days, i, and calculate the area between the cumulative activity functions for the male population at day i, and the cumulative activity function for the n randomly picked individuals. By repeating this procedure 10^5 times for each background week i, we obtain 8 null distributions of areas.

City	Gender	Combined
Nice	Male	$2.91 \cdot 10^{-19}$
London2	Female	$1.88 \cdot 10^{-5}$
London2	Male	$7.59 \cdot 10^{-6}$
London1	Female	$7.08 \cdot 10^{-20}$
London1	Male	$1.07 \cdot 10^{-36}$

TABLE S2. Combined p-values for peaks following terror attacks (peaks illustrated in Fig. 1). All combinations of attack and gender that are not listed had p-values indistinguishable from 0.

Then, we test the alternatives (a) and (b), by computing the probability to observe the empirical communication activity measured on the day of the attack during any of the background weeks. We obtain these empirical values by calculating the area between the cumulative activity function of the male population on the day of the attack, and the cumulative activity function of the male population on each of the ordinary days. The percentage of the measure-value null distribution of week i that is larger than or equal to the empirical value for week i represents the probability that the empirical value is a result of random noise. These 8 probabilities can be combined into a single p-value, expressing the likelihood of getting the 8 probabilities given that the telecommunication was unaffected compared to ordinary days (see Materials & Methods). For all cities and both genders, we find that the probability associated to alternative (a) is less than $1.88 \cdot 10^{-5}$, revealing that the telecommunication observed in the 24 hours following the terror attacks is unlikely to be observed on ordinary days (see Table S2).

The least significant peak is the one exhibited by females after the second London attack. For this population, we obtained the p-values 0.99988, 0.8216, 0.89666, 0.9994, and 0.99502. Combining these in the way described in "Materials & Methods" yields the single p-value $1.88 \cdot 10^{-5}$. Other than this population, only 4 populations did not have every p-value smaller than 10^{-5}. The combined p-values for these are all below 10^{-5} (best estimate is listed in Table S2).

8.4 Conclusions and perspectives for further research

In this third part of my dissertation, I have presented two manuscripts. In the first of these manuscripts, we examined the connection between narcissistic scores and behavior using telecommunication data of a population of undergraduate students. We found that narcissistic-admiration scores correlated with both in and out-degree in text-message and call networks where all links carried equal weights. Contrary to this, narcissistic-rivalry scores only correlated with out-degree in networks assigning the strongest interactions disproportionately large weights. We also found homophily in narcissistic admiration in networks of the strongest text-message and proximity interactions. These observations are in line with existing psychological hypotheses portraying narcissists as being attention-seeking, but only narcissists with high ADM to be successful in attracting attention from others.

In the second manuscript, we examined behavior patterns following terror attacks. We studied the behavior of females and males separately and found that the telecommunication of both populations spiked following the attacks. Although these spikes were significant deviations from the normal behavior, we also found the behavior patterns of the two populations to be significantly different from each other. The difference was even greater than would be expected based on ordinary-day behavior.

There are exciting directions to pursue in relation to both projects. The data set used in the narcissism study only included data for undergraduate students. It would be interesting and important to replicate our study using a more representative population sample. Another interesting point to raise concerning this project is the problem of missing links. We could only analyse communication that took place within the sample. However, we should expect a large fraction of the actual communication to occur between participants and people that are not part of the study. How this skews our results, we currently do not know. In the future, it would be essential to understand these skewing effects.

For the second project, understanding the presence of gender differences is imperative. Are the observed differences due to differences in personality between males and females in our population? If so, which personality traits can account for the behavioral differences? To examine this, large-scale experiments combining psychological profiling and collection of telecommunication data would be necessary to carry out.

A simpler research direction would be to investigate individual behavior patterns instead of the aggregated behavior of all females or all males. It is possible that the observed gender differences are largely due to extreme individuals dominating the aggregated behavior. If this is the case, these extreme individuals are systematically present in the different cities experiencing terror attacks. Alas, it would be interesting to examine whether gender could be reliably predicted using behavior patterns following terror attacks.

Lastly, investigating how the change of behavior following terror attacks depends on, e.g., the culture of participants, previous exposure to attacks, or the nature of terror attacks would be an exciting direction for future research. In our analysis, the change of behavior took different magnitudes in different cities. In particular, the citizens of London showed no gender differences in behavior change following terror attacks. Understanding whether this is a mere coincidence, or whether populations do react differently to such hostile strikes is important.

Bibliography

Acebrón, Juan A et al. (2005). "The Kuramoto model: A simple paradigm for synchronization phenomena". In: *Reviews of modern physics* 77.1, p. 137.

Acemoglu, Daron, Asuman Özdaglar, and Alireza Tahbaz-Salehi (2015). "Systemic risk and stability in financial networks". In: *American Economic Review* 105.2, pp. 564–608.

Adamic, Lada A (1999). "The small world web". In: *International Conference on Theory and Practice of Digital Libraries*. Springer, pp. 443–452.

Adamic, Lada A et al. (2016). "Information evolution in social networks". In: *Proceedings of the Ninth ACM International Conference on Web Search and Data Mining*. ACM, pp. 473–482.

Ahn, Yong-Yeol, James P Bagrow, and Sune Lehmann (2010). "Link communities reveal multiscale complexity in networks". In: *Nature* 466.7307, p. 761.

Ajzen, Icek (2005). *Attitudes, personality, and behavior*. McGraw-Hill Education (UK).

Allen, Franklin and Ana Babus (2009). "Networks in finance". In: *The network challenge: strategy, profit, and risk in an interlinked world* 367.

Alon, Uri (2007). "Network motifs: theory and experimental approaches". In: *Nature Reviews Genetics* 8.6, p. 450.

Amaral, Luıs A Nunes et al. (2000). "Classes of small-world networks". In: *Proceedings of the National Academy of Sciences* 97.21, pp. 11149–11152.

Amini, Hamed, Rama Cont, and Andreea Minca (2016). "Resilience to contagion in financial networks". In: *Mathematical Finance* 26.2, pp. 329–365.

Andersen, Hans Christian. *No doubt about it!* https://www.andersenstories.com/language.php?andersen=058&l=en&r=da. Accessed: 2019-12-03.

— (2004). *H.C. Andersen – en eventyrlig digter*. words2you.

Anderson, Ashton et al. (2015). "Global diffusion via cascading invitations: Structure, growth, and homophily". In: *Proceedings of the 24th International Conference on World Wide Web*. International World Wide Web Conferences Steering Committee, pp. 66–76.

Anderson, Nate (2012). "Confirmed: US and Israel created Stuxnet, lost control of it". In: *Ars technica* 1.

Anderson, Roy M and Robert M May (1992). *Infectious diseases of humans: dynamics and control*. Oxford University Press.

Andreasen, Viggo, Cécile Viboud, and Lone Simonsen (2008). "Epidemiologic characterization of the 1918 influenza pandemic summer wave in Copenhagen: implications for pandemic control strategies". In: *The Journal of infectious diseases* 197.2, pp. 270–278.

Aoyama, Hirohiko and Ken Asamoto (1988). "Determination of somite cells: independence of cell differentiation and morphogenesis". In: *Development* 104.1, pp. 15–28.

Aral, Sinan, Lev Muchnik, and Arun Sundararajan (2009). "Distinguishing influence-based contagion from homophily-driven diffusion in dynamic networks". In: *Proceedings of the National Academy of Sciences* 106.51, pp. 21544–21549.

Aral, Sinan, Lev Muchnik, and Arun Sundararajan (2013). "Engineering social contagions: Optimal network seeding in the presence of homophily". In: *Network Science* 1.2, pp. 125–153.

Aral, Sinan and Christos Nicolaides (2017). "Exercise contagion in a global social network". In: *Nature Communications* 8, p. 14753.

Aral, Sinan and Dylan Walker (2012). "Identifying influential and susceptible members of social networks". In: *Science* 337.6092, pp. 337–341.

Aschoff, Jürgen (1965). "Circadian rhythms in man". In: *Science* 148.3676, pp. 1427–1432.

Ash, Jeff and David Newth (2007). "Optimizing complex networks for resilience against cascading failure". In: *Physica A: Statistical Mechanics and its Applications* 380, pp. 673–683.

Aulehla, Alexander and Bernhard G Herrmann (2004). "Segmentation in vertebrates: clock and gradient finally joined". In: *Genes & Development* 18.17, pp. 2060–2067.

Aulehla, Alexander et al. (2003). "Wnt3a plays a major role in the segmentation clock controlling somitogenesis". In: *Developmental Cell* 4.3, pp. 395–406.

Aulehla, Alexander et al. (2008). "A β-catenin gradient links the clock and wavefront systems in mouse embryo segmentation". In: *Nature Cell Biology* 10.2, p. 186.

Back, Mitja D, Albrecht CP Küfner, and Marius Leckelt (2018). "Early impressions of grandiose narcissists: A dual-pathway perspective". In: *Handbook of trait narcissism*. Springer, pp. 309–316.

Back, Mitja D et al. (2013). "Narcissistic admiration and rivalry: Disentangling the bright and dark sides of narcissism." In: *Journal of Personality and Social Psychology* 105.6, p. 1013.

Backstrom, Lars et al. (2012). "Four degrees of separation". In: *Proceedings of the 4th Annual ACM Web Science Conference*. ACM, pp. 33–42.

Bagrow, James P, Dashun Wang, and Albert-László Barabási (2011). "Collective response of human populations to large-scale emergencies". In: *PLoS One* 6.3, e17680.

Bak, Per et al. (1984). "Josephson junctions and circle maps". In: *Solid State Communications* 51.4, pp. 231–234.

Baker, Ruth E, S Schnell, and PK Maini (2006a). "A mathematical investigation of a clock and wavefront model for somitogenesis". In: *Journal of Mathematical Biology* 52.4, pp. 458–482.

Baker, Ruth E, Santiago Schnell, and Philip K Maini (2006b). "A clock and wavefront mechanism for somite formation". In: *Developmental Biology* 293.1, pp. 116–126.

— (2008). "Mathematical models for somite formation". In: *Current Topics in Developmental Biology* 81, pp. 183–203.

Bandiera, Oriana and Imran Rasul (2006). "Social networks and technology adoption in northern Mozambique". In: *The Economic Journal* 116.514, pp. 869–902.

Banerjee, Abhijit et al. (2013). "The diffusion of microfinance". In: *Science* 341.6144, p. 1236498.

— (2014). *Gossip: Identifying central individuals in a social network*. Tech. rep. National Bureau of Economic Research.

— (2019). "Using gossips to spread information: Theory and evidence from two randomized controlled trials". In: *The Review of Economic Studies* 86.6, pp. 2453–2490.

Bar-Or, Ruth Lev et al. (2000). "Generation of oscillations by the p53-Mdm2 feedback loop: a theoretical and experimental study". In: *Proceedings of the National Academy of Sciences* 97.21, pp. 11250–11255.

Barabási, Albert-László and Réka Albert (1999). "Emergence of scaling in random networks". In: *Science* 286.5439, pp. 509–512.

Barabási, Albert-László and Zoltan N Oltvai (2004). "Network biology: understanding the cell's functional organization". In: *Nature Reviews Genetics* 5.2, p. 101.

Barahona, Mauricio and Louis M Pecora (2002). "Synchronization in small-world systems". In: *Physical Review Letters* 89.5, p. 054101.

Barber, Nigel (2016). "Does Trump suffer from narcissistic personality disorder". In: *Psychology Today Blogs*.

Bassett, Danielle S et al. (2011). "Dynamic reconfiguration of human brain networks during learning". In: *Proceedings of the National Academy of Sciences* 108.18, pp. 7641–7646.

Bassett, Danielle Smith and Edward Bullmore (2006). "Small-world brain networks". In: *The Neuroscientist* 12.6, pp. 512–523.

Battiston, Stefano et al. (2012). "Debtrank: Too central to fail? Financial networks, the fed and systemic risk". In: *Scientific Reports* 2, p. 541.

Bazzi, Marya et al. (2016). "Community detection in temporal multilayer networks, with an application to correlation networks". In: *Multiscale Modeling & Simulation* 14.1, pp. 1–41.

Beaupeux, Mathias and Paul François (2016). "Positional information from oscillatory phase shifts: insights from in silico evolution". In: *Physical Biology* 13.3, p. 036009.

Bengtsson, Linus et al. (2011). "Improved response to disasters and outbreaks by tracking population movements with mobile phone network data: a post-earthquake geospatial study in Haiti". In: *PLoS Medicine* 8.8, e1001083.

Bennett, Matthew et al. (2002). "Huygens's clocks". In: *Proceedings of the Royal Society of London. Series A: Mathematical, Physical and Engineering Sciences* 458.2019, pp. 563–579.

Benson, Austin R, David F Gleich, and Jure Leskovec (2016). "Higher-order organization of complex networks". In: *Science* 353.6295, pp. 163–166.

Benson, Austin R, David F Gleich, and Lek-Heng Lim (2017). "The spacey random walk: A stochastic process for higher-order data". In: *SIAM Review* 59.2, pp. 321–345.

Beretta, Edoardo and Yasuhiro Takeuchi (1995). "Global stability of an SIR epidemic model with time delays". In: *Journal of Mathematical Biology* 33.3, pp. 250–260.

Blondel, Vincent D et al. (2008). "Fast unfolding of communities in large networks". In: *Journal of Statistical Mechanics: Theory and Experiment* 2008.10, P10008.

Boccaletti, Stefano et al. (2006). "Complex networks: Structure and dynamics". In: *Physics Reports* 424.4-5, pp. 175–308.

Boguná, Marián, Romualdo Pastor-Satorras, and Alessandro Vespignani (2003). "Absence of epidemic threshold in scale-free networks with degree correlations". In: *Physical Review Letters* 90.2, p. 028701.

Bohr, Tomas, Per Bak, and Mogens H Jensen (1984). "Transition to chaos by interaction of resonances in dissipative systems. II. Josephson junctions, charge-density waves, and standard maps". In: *Physical Review A* 30.4, p. 1970.

Bollobás, Béla (1980). "A probabilistic proof of an asymptotic formula for the number of labelled regular graphs". In: *European Journal of Combinatorics* 1.4, pp. 311–316.

Bollobás, Béla and Oliver M Riordan (2003). "Mathematical results on scale-free random graphs". In: *Handbook of graphs and networks: from the genome to the internet*, pp. 1–34.

Bordyugov, Grigory et al. (2015). "Tuning the phase of circadian entrainment". In: *Journal of The Royal Society Interface* 12.108, p. 20150282.

Broder-Rodgers, David, Francisco J Pérez-Reche, and Sergei N Taraskin (2015). "Effects of local and global network connectivity on synergistic epidemics". In: *Physical Review E* 92.6, p. 062814.

Brown, Doris et al. (2006). "Loss of Aif function causes cell death in the mouse embryo, but the temporal progression of patterning is normal". In: *Proceedings of the National Academy of Sciences* 103.26, pp. 9918–9923.

Brummitt, Charles D, Raissa M D'Souza, and Elizabeth A Leicht (2012). "Suppressing cascades of load in interdependent networks". In: *Proceedings of the National Academy of Sciences* 109.12, E680–E689.

Buldyrev, Sergey V et al. (2010). "Catastrophic cascade of failures in interdependent networks". In: *Nature* 464.7291, p. 1025.

Bulusu, Vinay et al. (2017). "Spatiotemporal analysis of a glycolytic activity gradient linked to mouse embryo mesoderm development". In: *Developmental Cell* 40.4, pp. 331–341.

Caldarelli, Guido et al. (2002). "Scale-free networks from varying vertex intrinsic fitness". In: *Physical Review Letters* 89.25, p. 258702.

Callaway, Duncan S et al. (2000). "Network robustness and fragility: Percolation on random graphs". In: *Physical Review Letters* 85.25, p. 5468.

Callaway, Duncan S et al. (2001). "Are randomly grown graphs really random?" In: *Physical Review E* 64.4, p. 041902.

Carreras, Benjamin A et al. (2002). "Critical points and transitions in an electric power transmission model for cascading failure blackouts". In: *Chaos: An interdisciplinary journal of nonlinear science* 12.4, pp. 985–994.

Catania, JA et al. (1992). "The population-based AMEN (AIDS in Multi-Ethnic Neighborhoods) study". In: *Am. J. Public Health* 82, pp. 284–287.

Catanzaro, Michele, Marián Boguná, and Romualdo Pastor-Satorras (2005). "Generation of uncorrelated random scale-free networks". In: *Physical Review E* 71.2, p. 027103.

Centola, Damon (2010). "The spread of behavior in an online social network experiment". In: *Science* 329.5996, pp. 1194–1197.

Centola, Damon, Víctor M Eguíluz, and Michael W Macy (2007). "Cascade dynamics of complex propagation". In: *Physica A: Statistical Mechanics and its Applications* 374.1, pp. 449–456.

Centola, Damon and Michael Macy (2007). "Complex contagions and the weakness of long ties". In: *American Journal of Sociology* 113.3, pp. 702–734.

Cheng, Justin et al. (2014). "Can cascades be predicted?" In: *Proceedings of the 23rd International Conference on World Wide Web*. ACM, pp. 925–936.

Chierichetti, Flavio, David Liben-Nowell, and Jon M Kleinberg (2011). "Reconstructing patterns of information diffusion from incomplete observations". In: *Advances in Neural Information Processing Systems*, pp. 792–800.

Chin, Alex, Dean Eckles, and Johan Ugander (2018). "Evaluating stochastic seeding strategies in networks". In: *arXiv preprint arXiv:1809.09561*.

Chodrow, Philip S (2019). "Configuration Models of Random Hypergraphs and their Applications". In: *arXiv preprint arXiv:1902.09302*.

Clauset, Aaron, Mark EJ Newman, and Cristopher Moore (2004). "Finding community structure in very large networks". In: *Physical Review E* 70.6, p. 066111.

Cohen, Reuven et al. (2000). "Resilience of the internet to random breakdowns". In: *Physical Review Letters* 85.21, p. 4626.

Cont, Rama, Amal Moussa, and Edson Bastos e Santos (2010). "Network structure and systemic risk in banking systems". In: *Network Structure and Systemic Risk in Banking Systems*.

Cooke, John and Erik Christopher Zeeman (1976). "A clock and wavefront model for control of the number of repeated structures during animal morphogenesis". In: *Journal of Theoretical Biology* 58.2, pp. 455–476.

Cotterell, James, Alexandre Robert-Moreno, and James Sharpe (2015). "A local, self-organizing reaction-diffusion model can explain somite patterning in embryos". In: *Cell Systems* 1.4, pp. 257–269.

Crandall, Christian S (1988). "Social contagion of binge eating." In: *Journal of Personality and Social Psychology* 55.4, p. 588.

Cvitanovic, Predrag, Boris Shraiman, and Bo Söderberg (1985). "Scaling laws for mode lockings in circle maps". In: *Physica Scripta* 32.4, p. 263.

Czolczynski, Krzysztof et al. (2011). "Huygens' odd sympathy experiment revisited". In: *International Journal of Bifurcation and Chaos* 21.07, pp. 2047–2056.

De Domenico, Manlio et al. (2013). "Mathematical formulation of multilayer networks". In: *Physical Review X* 3.4, p. 041022.

De Domenico, Manlio et al. (2015a). "Ranking in interconnected multilayer networks reveals versatile nodes". In: *Nature Communications* 6, p. 6868.

De Domenico, Manlio et al. (2015b). "Structural reducibility of multilayer networks". In: *Nature Communications* 6, p. 6864.

De Domenico, Manlio et al. (2016). "The physics of spreading processes in multilayer networks". In: *Nature Physics* 12.10, pp. 901–906.

Del Vicario, Michela et al. (2016). "The spreading of misinformation online". In: *Proceedings of the National Academy of Sciences* 113.3, pp. 554–559.

Delaune, Emilie A et al. (2012). "Single-cell-resolution imaging of the impact of Notch signaling and mitosis on segmentation clock dynamics". In: *Developmental cell* 23.5, pp. 995–1005.

Dibner, Charna, Ueli Schibler, and Urs Albrecht (2010). "The mammalian circadian timing system: organization and coordination of central and peripheral clocks". In: *Annual Review of Physiology* 72, pp. 517–549.

Dodds, Peter Sheridan and Duncan J Watts (2004). "Universal behavior in a generalized model of contagion". In: *Physical Review Letters* 92.21, p. 218701.

— (2005). "A generalized model of social and biological contagion". In: *Journal of Theoretical Biology* 232.4, pp. 587–604.

Dubrulle, Julien, Michael J McGrew, and Olivier Pourquié (2001). "FGF signaling controls somite boundary position and regulates segmentation clock control of spatiotemporal Hox gene activation". In: *Cell* 106.2, pp. 219–232.

Dubrulle, Julien and Olivier Pourquié (2002). "From head to tail: links between the segmentation clock and antero-posterior patterning of the embryo". In: *Current Opinion in Genetics & Development* 12.5, pp. 519–523.

Dunty, William C et al. (2008). "Wnt3a/β-catenin signaling controls posterior body development by coordinating mesoderm formation and segmentation". In: *Development* 135.1, pp. 85–94.

Eguiluz, Victor M and Konstantin Klemm (2002). "Epidemic threshold in structured scale-free networks". In: *Physical Review Letters* 89.10, p. 108701.

Eilersen, Andreas and Kim Sneppen (2019). "Disease as an evolutionary weapon". In: *bioRxiv*, p. 721506.

Engene, Jan Oskar (2007). "Five decades of terrorism in Europe: The TWEED dataset". In: *Journal of Peace Research* 44.1, pp. 109–121.

Erdős, Paul and Alfréd Rényi (1960). "On the evolution of random graphs". In: *Publication of the Mathematical Institute of the Hungarian Academy of Sciences* 5.1, pp. 17–60.

Ergün, Güler and Geoff J Rodgers (2002). "Growing random networks with fitness". In: *Physica A: Statistical Mechanics and its Applications* 303.1-2, pp. 261–272.

Eriksen, Kasper Astrup et al. (2003). "Modularity and extreme edges of the Internet". In: *Physical Review Letters* 90.14, p. 148701.

Feigenbaum, Mitchell J, Leo P Kadanoff, and Scott J Shenker (1982). "Quasiperiodicity in dissipative systems: a renormalization group analysis". In: *Physica D: Nonlinear Phenomena* 5.2-3, pp. 370–386.

Fennell, Peter G and James P Gleeson (2019). "Multistate dynamical processes on networks: analysis through degree-based approximation frameworks". In: *SIAM Review* 61.1, pp. 92–118.

FiveThirtyEight 2016 final forecast. https://projects.fivethirtyeight.com/2016-election-forecast/. Accessed: 2019-11-29.

Fosdick, Bailey K et al. (2018). "Configuring random graph models with fixed degree sequences". In: *SIAM Review* 60.2, pp. 315–355.

Foster, Joshua D and W Keith Campbell (2007). "Are there such things as "narcissists" in social psychology? A taxometric analysis of the Narcissistic Personality Inventory". In: *Personality and Individual Differences* 43.6, pp. 1321–1332.

Galam, Serge (1986). "Majority rule, hierarchical structures, and democratic totalitarianism: A statistical approach". In: *Journal of Mathematical Psychology* 30.4, pp. 426–434.

— (2004). "Contrarian deterministic effects on opinion dynamics:"the hung elections scenario"". In: *Physica A: Statistical Mechanics and its Applications* 333, pp. 453–460.

— (2016). "Stubbornness as an unfortunate key to win a public debate: an illustration from sociophysics". In: *Mind & Society* 15.1, pp. 117–130.

Galam, Serge and Taksu Cheon (2019). "Tipping point dynamics: a universal formula". In: *arXiv preprint arXiv:1901.09622*.

Galam, Serge and Frans Jacobs (2007). "The role of inflexible minorities in the breaking of democratic opinion dynamics". In: *Physica A: Statistical Mechanics and its Applications* 381, pp. 366–376.

Geva-Zatorsky, Naama et al. (2006). "Oscillations and variability in the p53 system". In: *Molecular Systems Biology* 2.1.

Ghoshal, Gourab et al. (2009). "Random hypergraphs and their applications". In: *Physical Review E* 79.6, p. 066118.

Girvan, Michelle and Mark EJ Newman (2002). "Community structure in social and biological networks". In: *Proceedings of the National Academy of Sciences* 99.12, pp. 7821–7826.

Glazier, James A et al. (1986). "Structure of Arnol'd tongues and the $f(\alpha)$ spectrum for period doubling: Experimental results". In: *Physical Review A* 34.2, p. 1621.

Gleeson, James P (2008). "Cascades on correlated and modular random networks". In: *Physical Review E* 77.4, p. 046117.

— (2011). "High-accuracy approximation of binary-state dynamics on networks". In: *Physical Review Letters* 107.6, p. 068701.

Gleeson, James P and Diarmuid J Cahalane (2007). "Seed size strongly affects cascades on random networks". In: *Physical Review E* 75.5, p. 056103.

Goel, Sharad, Duncan J Watts, and Daniel G Goldstein (2012). "The structure of online diffusion networks". In: *Proceedings of the 13th ACM Conference on Electronic Commerce*. ACM, pp. 623–638.

Goel, Sharad et al. (2015). "The structural virality of online diffusion". In: *Management Science* 62.1, pp. 180–196.

Golub, Benjamin and Matthew O Jackson (2010). "Using selection bias to explain the observed structure of internet diffusions". In: *Proceedings of the National Academy of Sciences* 107.24, pp. 10833–10836.

Gomez, Céline et al. (2008). "Control of segment number in vertebrate embryos". In: *Nature* 454.7202, p. 335.

Granovetter, Mark (1978). "Threshold models of collective behavior". In: *American Journal of Sociology* 83.6, pp. 1420–1443.

Granovetter, Mark S (1977). "The strength of weak ties". In: *Social Networks*. Elsevier, pp. 347–367.

Gregor, Thomas et al. (2005). "Diffusion and scaling during early embryonic pattern formation". In: *Proceedings of the National Academy of Sciences* 102.51, pp. 18403–18407.

Grosz, Michael P et al. (2015). "Who is open to a narcissistic romantic partner? The roles of sensation seeking, trait anxiety, and similarity". In: *Journal of Research in Personality* 58, pp. 84–95.

Grover, Aditya and Jure Leskovec (2016). "node2vec: Scalable feature learning for networks". In: *Proceedings of the 22nd ACM SIGKDD International Conference on Knowledge Discovery and Data Mining*. ACM, pp. 855–864.

Guilbeault, Douglas, Joshua Becker, and Damon Centola (2018a). "Complex contagions: A decade in review". In: *Complex Spreading Phenomena in Social Systems*. Springer, pp. 3–25.

— (2018b). "Social learning and partisan bias in the interpretation of climate trends". In: *Proceedings of the National Academy of Sciences* 115.39, pp. 9714–9719.

Hackett, Adam, Sergey Melnik, and James P Gleeson (2011). "Cascades on a class of clustered random networks". In: *Physical Review E* 83.5, p. 056107.

Hagerstrand, Torsten (1968). *Innovation diffusion as a spatial process*. Chicago, USA: Univ. Chicago Press.

Haldane, Andrew G and Robert M May (2011). "Systemic risk in banking ecosystems". In: *Nature* 469.7330, p. 351.

Hardin, Paul E, Jeffrey C Hall, and Michael Rosbash (1990). "Feedback of the Drosophila period gene product on circadian cycling of its messenger RNA levels". In: *Nature* 343.6258, p. 536.

Harima, Yukiko et al. (2013). "Accelerating the tempo of the segmentation clock by reducing the number of introns in the Hes7 gene". In: *Cell Reports* 3.1, pp. 1–7.

Haydon, Daniel T et al. (2003). "The construction and analysis of epidemic trees with reference to the 2001 UK foot–and–mouth outbreak". In: *Proceedings of the Royal Society of London. Series B: Biological Sciences* 270.1511, pp. 121–127.

Helbing, Dirk, Anders Johansson, and Habib Zein Al-Abideen (2007). "Dynamics of crowd disasters: An empirical study". In: *Physical review E* 75.4, p. 046109.

Heltberg, Mathias et al. (2016). "Noise induces hopping between NF-κB entrainment modes". In: *Cell Systems* 3.6, pp. 532–539.

Heltberg, Mathias L, Sandeep Krishna, and Mogens H Jensen (2019). "On chaotic dynamics in transcription factors and the associated effects in differential gene regulation". In: *Nature Communications* 10.1, p. 71.

Hinz, Oliver et al. (2011). "Seeding strategies for viral marketing: An empirical comparison". In: *Journal of Marketing* 75.6, pp. 55–71.

Hobolt, Sara B (2016). "The Brexit vote: a divided nation, a divided continent". In: *Journal of European Public Policy* 23.9, pp. 1259–1277.

Holme, Petter (2004). "Efficient local strategies for vaccination and network attack". In: *Europhysics Letters* 68.6, p. 908.

Holme, Petter (2005). "Network reachability of real-world contact sequences". In: *Physical Review E* 71.4, p. 046119.

Holme, Petter and Jari Saramäki (2012). "Temporal networks". In: *Physics Reports* 519.3. Temporal Networks, pp. 97 –125.

Horikawa, Kazuki et al. (2006). "Noise-resistant and synchronized oscillation of the segmentation clock". In: *Nature* 441.7094, p. 719.

Hurd, Thomas R and James P Gleeson (2013). "On Watts' cascade model with random link weights". In: *Journal of Complex Networks* 1.1, pp. 25–43.

Iacopini, Iacopo et al. (2019). "Simplicial models of social contagion". In: *Nature Communications* 10.1, p. 2485.

Iyer, Shankar and Lada A Adamic (2018). "The Costs of Overambitious Seeding of Social Products". In: *International Conference on Complex Networks and their Applications*. Springer, pp. 273–286.

Jackson, Matthew O, Suraj Malladi, and David McAdams (2018). "Learning through the grapevine: the impact of message mutation, transmission failure, and deliberate bias". In: *Transmission Failure, and Deliberate Bias*.

Jacobs, Frans and Serge Galam (2019). "Two-Opinions-Dynamics Generated By Inflexibles And Non-Contrarian And Contrarian Floaters". In: *Advances in Complex Systems* 22.04, p. 1950008.

Jamieson, Kathleen Hall and Bruce W Hardy (2014). "Leveraging scientific credibility about Arctic sea ice trends in a polarized political environment". In: *Proceedings of the National Academy of Sciences* 111.Supplement 4, pp. 13598–13605.

Jang, S Mo et al. (2018). "A computational approach for examining the roots and spreading patterns of fake news: Evolution tree analysis". In: *Computers in Human Behavior* 84, pp. 103–113.

Jensen, Gorm Gruner, Florian Uekermann, and Kim Sneppen (2019). "Multi stability and global bifurcations in epidemic model with distributed delay SIRnS-model". In: *The European Physical Journal B* 92.2, p. 28.

Jensen, Gorm Gruner et al. (2019). "Could short-lasting non-specific immunity explain seasonal spacing of epidemic diseases?" In: *arXiv preprint arXiv:1908.00925*.

Jensen, Mogens H, Per Bak, and Tomas Bohr (1983). "Complete devil's staircase, fractal dimension, and universality of mode-locking structure in the circle map". In: *Physical Review Letters* 50.21, p. 1637.

— (1984). "Transition to chaos by interaction of resonances in dissipative systems. I. Circle maps". In: *Physical Review A* 30.4, p. 1960.

Jensen, Mogens H and Sandeep Krishna (2012). "Inducing phase-locking and chaos in cellular oscillators by modulating the driving stimuli". In: *FEBS Letters* 586.11, pp. 1664–1668.

Jensen, Peter B et al. (2010). "A Wnt oscillator model for somitogenesis". In: *Biophysical journal* 98.6, pp. 943–950.

Jeong, Hawoong et al. (2000). "The large-scale organization of metabolic networks". In: *Nature* 407.6804, p. 651.

Jesus, Rut, Martin Schwartz, and Sune Lehmann (2009). "Bipartite networks of Wikipedia's articles and authors: a meso-level approach". In: *Proceedings of the 5th international symposium on Wikis and open collaboration*. ACM, p. 5.

Johansson, Anders et al. (2008). "From crowd dynamics to crowd safety: a video-based analysis". In: *Advances in Complex Systems* 11.04, pp. 497–527.

Juul, Jonas S, Mogens H Jensen, and Sandeep Krishna (2019). "Constraints on somite formation in developing embryos". In: *Journal of the Royal Society Interface* 16.158.

Juul, Jonas S and Christopher H Joyner (2018). "Isospectral discrete and quantum graphs with the same flip counts and nodal counts". In: *Journal of Physics A: Mathematical and Theoretical* 51.24, p. 245101.

Juul, Jonas S, Sandeep Krishna, and Mogens H Jensen (2018). "Entrainment as a means of controlling phase waves in populations of coupled oscillators". In: *Physical Review E* 98.6, p. 062412.

Juul, Jonas S and Mason A Porter (2018). "Synergistic effects in threshold models on networks". In: *Chaos: An Interdisciplinary Journal of Nonlinear Science* 28.1, p. 013115.

— (2019). "Hipsters on networks: How a minority group of individuals can lead to an antiestablishment majority". In: *Physical Review E* 99.2, p. 022313.

Juul, Jonas S and Steven H Strogatz (2019). "Scaling law for the impact of mutant contagion". In: *arXiv preprint arXiv:1910.00655*.

Karimi, Fariba et al. (2018). "Homophily influences ranking of minorities in social networks". In: *Scientific Reports* 8.1, p. 11077.

Karnouskos, Stamatis (2011). "Stuxnet worm impact on industrial cyber-physical system security". In: *IECON 2011-37th Annual Conference of the IEEE Industrial Electronics Society*. IEEE, pp. 4490–4494.

Karsai, Márton et al. (2011). "Small but slow world: How network topology and burstiness slow down spreading". In: *Physical Review E* 83.2, p. 025102.

Karsai, Márton et al. (2014). "Complex contagion process in spreading of online innovation". In: *Journal of The Royal Society Interface* 11.101, p. 20140694.

Keeling, Matt J and Pejman Rohani (2011). *Modeling infectious diseases in humans and animals*. Princeton University Press.

Keizer, Gregg (2010). "Is Stuxnet the 'best'malware ever". In: *Computerworld, September* 16.

Kermack, William Ogilvy and Anderson G McKendrick (1927). "A contribution to the mathematical theory of epidemics". In: *Proceedings of the Royal Society of London. Series A, Containing papers of a mathematical and physical character* 115.772, pp. 700–721.

Khalil, Nagi and Raúl Toral (2019). "The noisy voter model under the influence of contrarians". In: *Physica A: Statistical Mechanics and its Applications* 515, pp. 81–92.

Kiss, István Z, Joel C Miller, Péter L Simon, et al. (2017). "Mathematics of epidemics on networks". In: *Cham: Springer* 598.

Kivelä, Mikko et al. (2014). "Multilayer networks". In: *Journal of Complex Networks* 2.3, pp. 203–271.

Klamser, Pascal P et al. (2017). "Zealotry effects on opinion dynamics in the adaptive voter model". In: *Physical Review E* 96.5, p. 052315.

Kleinberg, Jon M (2000). "Navigation in a small world". In: *Nature* 406.6798, p. 845.

Koonin, Eugene V, Yuri I Wolf, and Georgy P Karev (2002). "The structure of the protein universe and genome evolution". In: *Nature* 420.6912, p. 218.

Korn, Liat and Gil Zukerman (2011). "Affective and behavioral changes following exposure to traumatic events: the moderating effect of religiosity on avoidance behavior among students studying under a high level of terror event exposure". In: *Journal of Religion and Health* 50.4, pp. 911–921.

Kovanen, Lauri et al. (2011). "Temporal motifs in time-dependent networks". In: *Journal of Statistical Mechanics: Theory and Experiment* 2011.11, P11005.

Krapivsky, Paul L, Sidney Redner, and Daniel Volovik (2011). "Reinforcement-driven spread of innovations and fads". In: *Journal of Statistical Mechanics: Theory and Experiment* 2011.12, P12003.

Kuramoto, Yoshiki (2003). *Chemical oscillations, waves, and turbulence*. Courier Corporation.

Kureh, Yacoub H and Mason A Porter (2019). "Fitting In and Breaking Up: A Nonlinear Version of Coevolving Voter Models". In: *arXiv preprint arXiv:1907.11608*.

Lambiotte, Renaud, Martin Rosvall, and Ingo Scholtes (2019). "From networks to optimal higher-order models of complex systems". In: *Nature Physics* 15.4, pp. 313–320.

Lambiotte, Renaud, Lionel Tabourier, and Jean-Charles Delvenne (2013). "Burstiness and spreading on temporal networks". In: *The European Physical Journal B* 86.7, p. 320.

Latora, Vito and Massimo Marchiori (2001). "Efficient behavior of small-world networks". In: *Physical Review Letters* 87.19, p. 198701.

Lauschke, Volker M et al. (2013). "Scaling of embryonic patterning based on phase-gradient encoding". In: *Nature* 493.7430, p. 101.

Lavner, Justin A et al. (2016). "Narcissism and newlywed marriage: Partner characteristics and marital trajectories." In: *Personality Disorders: Theory, Research, and Treatment* 7.2, p. 169.

Lee, Eun et al. (2017). "Homophily explains perception biases in social networks". In: *arXiv preprint arXiv:1710.08601*.

Lehmann, Sune and Yong-Yeol Ahn (2018). *Complex spreading phenomena in social systems*. Springer.

Leskovec, Jure, Lada A Adamic, and Bernardo A Huberman (2007). "The dynamics of viral marketing". In: *ACM Transactions on the Web* 1.1, p. 5.

Leskovec, Jure and Christos Faloutsos (2006). "Sampling from large graphs". In: *Proceedings of the 12th ACM SIGKDD International Conference on Knowledge Discovery and Data Mining*. ACM, pp. 631–636.

Leskovec, Jure, Jon Kleinberg, and Christos Faloutsos (2007). "Graph evolution: Densification and shrinking diameters". In: *ACM Transactions on Knowledge Discovery from Data (TKDD)* 1.1, p. 2.

Levin, Sam et al. (2016). "Bernie Sanders: Donald Trump harnessed anti-establishment anger". In: *The Guardian*. URL: https://www.theguardian.com/us-news/2016/nov/10/bernie-sanders-donald-trump-harnessed-anti-establishment-anger (visited on 11/29/2019).

Lewis, Julian (2003). "Autoinhibition with transcriptional delay: a simple mechanism for the zebrafish somitogenesis oscillator". In: *Current Biology* 13.16, pp. 1398–1408.

Liben-Nowell, David and Jon Kleinberg (2007). "The link-prediction problem for social networks". In: *Journal of the American society for information science and technology* 58.7, pp. 1019–1031.

— (2008). "Tracing information flow on a global scale using Internet chain-letter data". In: *Proceedings of the National Academy of Sciences* 105.12, pp. 4633–4638.

Liu, Chuang et al. (2015). "How events determine spreading patterns: information transmission via internal and external influences on social networks". In: *New Journal of Physics* 17.11, p. 113045.

Lloyd-Smith, James O et al. (2009). "Epidemic dynamics at the human-animal interface". In: *Science* 326.5958, pp. 1362–1367.

Lü, Linyuan, Duan-Bing Chen, and Tao Zhou (2011). "The small world yields the most effective information spreading". In: *New Journal of Physics* 13.12, p. 123005.

Lu, Xin, Linus Bengtsson, and Petter Holme (2012). "Predictability of population displacement after the 2010 Haiti earthquake". In: *Proceedings of the National Academy of Sciences* 109.29, pp. 11576–11581.

Lynall, Mary-Ellen et al. (2010). "Functional connectivity and brain networks in schizophrenia". In: *Journal of Neuroscience* 30.28, pp. 9477–9487.

Maaß, Ulrike et al. (2016). "Narcissists of a feather flock together: Narcissism and the similarity of friends". In: *Personality and Social Psychology Bulletin* 42.3, pp. 366–384.

Mahajan, Vijay (2010). "Innovation diffusion". In: *Wiley International Encyclopedia of Marketing*.

Mandelbrot, Benoit (1974). "A population birth-and-mutation process, I: explicit distributions for the number of mutants in an old culture of bacteria". In: *Journal of Applied Probability* 11.3, pp. 437–444.

Martin, S and W Martienssen (1986). "Circle maps and mode locking in the driven electrical conductivity of barium sodium niobate crystals". In: *Physical Review Letters* 56.15, p. 1522.

Masamizu, Yoshito et al. (2006). "Real-time imaging of the somite segmentation clock: revelation of unstable oscillators in the individual presomitic mesoderm cells". In: *Proceedings of the National Academy of Sciences* 103.5, pp. 1313–1318.

Maslov, Sergei and Kim Sneppen (2002). "Specificity and stability in topology of protein networks". In: *Science* 296.5569, pp. 910–913.

Masuda, Naoki and Renaud Lambiotte (2016). *A guidance to temporal networks*. World Scientific.

McClintock, Martha K (1971). "Menstrual synchrony and suppression". In: *Nature* 229.5282, pp. 244–245.

Mellor, Andrew et al. (2015). "Influence of Luddism on innovation diffusion". In: *Physical Review E* 92.1, p. 012806.

Melnik, Sergey et al. (2011). "The unreasonable effectiveness of tree-based theory for networks with clustering". In: *Physical Review E* 83.3, p. 036112.

Melnik, Sergey et al. (2013). "Multi-stage complex contagions". In: *Chaos: An Interdisciplinary Journal of Nonlinear Science* 23.1, p. 013124.

Mengel, Benedicte et al. (2010). "Modeling oscillatory control in NF-κB, p53 and Wnt signaling". In: *Current Opinion in Genetics & Development* 20.6, pp. 656–664.

Meunier, David et al. (2009). "Hierarchical modularity in human brain functional networks". In: *Frontiers in Neuroinformatics* 3, p. 37.

Milgram, Stanley (1967). "The small world problem". In: *Psychology Today* 2.1, pp. 60–67.

Miller, Joel C (2009). "Spread of infectious disease through clustered populations". In: *Journal of the Royal Society Interface* 6.41, pp. 1121–1134.

Miller, Joel C and James M Hyman (2007). "Effective vaccination strategies for realistic social networks". In: *Physica A: Statistical Mechanics and its Applications* 386.2, pp. 780–785.

Milo, Ron et al. (2002). "Network motifs: simple building blocks of complex networks". In: *Science* 298.5594, pp. 824–827.

Mislove, Alan et al. (2008). "Growth of the flickr social network". In: *Proceedings of the First Workshop on Online Social Networks*. ACM, pp. 25–30.

Mollgaard, Anders et al. (2016). "Measure of node similarity in multilayer networks". In: *PLoS One* 11.6, e0157436.

Mollison, Denis and Mollison Denis (1995). *Epidemic models: their structure and relation to data*. Vol. 5. Cambridge University Press.

Molloy, Michael and Bruce Reed (1995). "A critical point for random graphs with a given degree sequence". In: *Random Structures & Algorithms* 6.2-3, pp. 161–180.

— (1998). "The size of the giant component of a random graph with a given degree sequence". In: *Combinatorics, Probability and Computing* 7.3, pp. 295–305.

Monk, Nicholas AM (2003). "Oscillatory expression of Hes1, p53, and NF-κB driven by transcriptional time delays". In: *Current Biology* 13.16, pp. 1409–1413.

Mønsted, Bjarke et al. (2017). "Evidence of complex contagion of information in social media: An experiment using Twitter bots". In: *PLoS One* 12.9, e0184148.

Montes, Joshua Kenneth (2006). "The Effects of Changes in the National Terror Alert Level on Consumer Behavior". PhD thesis. Miami University.

Morelli, Sylvia A et al. (2017). "Empathy and well-being correlate with centrality in different social networks". In: *Proceedings of the National Academy of Sciences* 114.37, pp. 9843–9847.

Moreno, Jacob L and Helen H Jennings (1938). "Statistics of social configurations". In: *Sociometry*, pp. 342–374.

Moreno, Jacob Levy, Ernest Stagg Whitin, and Helen Hall Jennings (1932). *Application of the group method to classification*. National Committee on Prisons and Prison Labor.

Murray, Philip J, Philip K Maini, and Ruth E Baker (2011). "The clock and wavefront model revisited". In: *Journal of Theoretical Biology* 283.1, pp. 227–238.

Myers, Seth A et al. (2014). "Information network or social network?: the structure of the twitter follow graph". In: *Proceedings of the 23rd International Conference on World Wide Web*. ACM, pp. 493–498.

Nakashima, Ellen and Joby Warrick (2012). "Stuxnet was work of US and Israeli experts, officials say". In: *Washington Post* 2, p. 13.

Neuhäuser, Leonie, Andrew Mellor, and Renaud Lambiotte (2019). "Multi-body Interactions and Non-Linear Consensus Dynamics on Networked Systems". In: *arXiv preprint arXiv:1910.09226*.

Newman, Mark (2018). *Networks*. Oxford university press.

Newman, Mark EJ (2001). "The structure of scientific collaboration networks". In: *Proceedings of the National Academy of Sciences* 98.2, pp. 404–409.

— (2002a). "Assortative mixing in networks". In: *Physical Review Letters* 89.20, p. 208701.

— (2002b). "Spread of epidemic disease on networks". In: *Physical review E* 66.1, p. 016128.

— (2003a). "Mixing patterns in networks". In: *Physical Review E* 67.2, p. 026126.

— (2003b). "The structure and function of complex networks". In: *SIAM Review* 45.2, pp. 167–256.

— (2006). "Modularity and community structure in networks". In: *Proceedings of the National Academy of Sciences* 103.23, pp. 8577–8582.

— (2009). "Random graphs with clustering". In: *Physical Review Letters* 103.5, p. 058701.

Newman, Mark EJ and Michelle Girvan (2003). "Mixing patterns and community structure in networks". In: *Statistical Mechanics of Complex Networks*. Springer, pp. 66–87.

— (2004). "Finding and evaluating community structure in networks". In: *Physical Review E* 69.2, p. 026113.

Newman, Mark EJ, Steven H Strogatz, and Duncan J Watts (2001). "Random graphs with arbitrary degree distributions and their applications". In: *Physical Review E* 64.2, p. 026118.

Newman, Mark EJ and Duncan J Watts (1999). "Renormalization group analysis of the small-world network model". In: *Physics Letters A* 263.4-6, pp. 341–346.

Nyczka, Piotr and Katarzyna Sznajd-Weron (2013). "Anticonformity or independence?—insights from statistical physics". In: *Journal of Statistical Physics* 151.1-2, pp. 174–202.

Nyczka, Piotr, Katarzyna Sznajd-Weron, and Jerzy Cisło (2012). "Phase transitions in the q-voter model with two types of stochastic driving". In: *Physical Review E* 86.1, p. 011105.

Oates, Andrew C, Luis G Morelli, and Saúl Ares (2012). "Patterning embryos with oscillations: structure, function and dynamics of the vertebrate segmentation clock". In: *Development* 139.4, pp. 625–639.

Ogura, Masaki, Wenjie Mei, and Kenji Sugimoto (2019). "Synergistic Effects in Networked Epidemic Spreading Dynamics". In: *IEEE Transactions on Circuits and Systems II: Express Briefs*.

Oh, Se-Wook and Mason A Porter (2018). "Complex contagions with timers". In: *Chaos: An Interdisciplinary Journal of Nonlinear Science* 28.3, p. 033101.

Oliver, J Eric and Wendy M Rahn (2016). "Rise of the Trumpenvolk: Populism in the 2016 Election". In: *The Annals of the American Academy of Political and Social Science* 667.1, pp. 189–206.

Oppenheimer, Sabrina, Yael Villa, and Alan Apter (2011). "Effects of prolonged exposure to terrorism on Israeli youth: Stress-related responses as a function of place of residence, news consumption, and gender". In: *Adolescent Psychiatry* 1.2, pp. 152–162.

Orford, Jim (1986). "The rules of interpersonal complementarity: Does hostility beget hostility and dominance, submission?" In: *Psychological Review* 93.3, pp. 365–377.

Osat, Saeed, Filippo Radicchi, and Fragkiskos Papadopoulos (2019). "k-core structure of real multiplex networks". In: *arXiv preprint arXiv:1911.10743*.

Oster, Emily and Rebecca Thornton (2012). "Determinants of technology adoption: Peer effects in menstrual cup take-up". In: *Journal of the European Economic Association* 10.6, pp. 1263–1293.

Overgoor, Jan, Austin Benson, and Johan Ugander (2019). "Choosing to grow a graph: modeling network formation as discrete choice". In: *The World Wide Web Conference*. ACM, pp. 1409–1420.

Özbudak, Ertuğrul M and Olivier Pourquié (2008). "The vertebrate segmentation clock: the tip of the iceberg". In: *Current Opinion in Genetics & Development* 18.4, pp. 317–323.

Ozik, Jonathan, Brian R Hunt, and Edward Ott (2004). "Growing networks with geographical attachment preference: Emergence of small worlds". In: *Physical Review E* 69.2, p. 026108.

Packard Jr, David S and Antone G Jacobson (1976). "The influence of axial structures on chick somite formation". In: *Developmental Biology* 53.1, pp. 36–48.

Palmeirim, Isabel et al. (1997). "Avian hairy gene expression identifies a molecular clock linked to vertebrate segmentation and somitogenesis". In: *Cell* 91.5, pp. 639–648.

Paranjape, Ashwin, Austin R Benson, and Jure Leskovec (2017). "Motifs in temporal networks". In: *Proceedings of the Tenth ACM International Conference on Web Search and Data Mining*. ACM, pp. 601–610.

Parliament, European and Council of European Union (2017). *Directive (EU) 2017/541 of the European Parliament and of the Council of 15 March 2017 on combating terrorism and replacing Council Framework Decision 2002/475/JHA and amending Council Decision 2005/671/JHA*. http://data.europa.eu/eli/dir/2017/541/oj. Accessed: 2019-12-21.

Pastor-Satorras, Romualdo and Alessandro Vespignani (2001a). "Epidemic dynamics and endemic states in complex networks". In: *Physical Review E* 63.6, p. 066117.

— (2001b). "Epidemic spreading in scale-free networks". In: *Physical Review Letters* 86.14, p. 3200.

Pastor-Satorras, Romualdo and Alessandro Vespignani (2002). "Epidemic dynamics in finite size scale-free networks". In: *Physical Review E* 65.3, p. 035108.

Pastor-Satorras, Romualdo et al. (2015). "Epidemic processes in complex networks". In: *Reviews of Modern Physics* 87.3, p. 925.

Pat-Horenczyk, Ruth et al. (2007). "Risk-taking behaviors among Israeli adolescents exposed to recurrent terrorism: provoking danger under continuous threat?" In: *American Journal of Psychiatry* 164.1, pp. 66–72.

Pedersen, Lykke, Mogens Høgh Jensen, and Sandeep Krishna (2011). "Dickkopf1-a new player in modelling the Wnt pathway". In: *PLoS One* 6.10, e25550.

Pérez-Reche, Francisco J et al. (2011). "Synergy in spreading processes: from exploitative to explorative foraging strategies". In: *Physical Review Letters* 106.21, p. 218701.

Petersen, Michael Bang, Mathias Osmundsen, and Kevin Arceneaux (2018). "A "Need for Chaos" and the Sharing of Hostile Political Rumors in Advanced Democracies". In: *PsyArXiv preprint*.

Pikovsky, Arkady, Michael Rosenblum, and Jürgen Kurths (2003). *Synchronization: a universal concept in nonlinear sciences*. Vol. 12. Cambridge University Press.

Pilosof, Shai et al. (2017). "The multilayer nature of ecological networks". In: *Nature Ecology & Evolution* 1.4, p. 0101.

Porter, Mason A and James P Gleeson (2016). "Dynamical systems on networks". In: *Frontiers in Applied Dynamical Systems: Reviews and Tutorials* 4.

Pourquié, Olivier (2004). "The chick embryo: a leading model in somitogenesis studies". In: *Mechanisms of Development* 121.9, pp. 1069–1079.

Price, Derek de Solla (1976). "A general theory of bibliometric and other cumulative advantage processes". In: *Journal of the American Society for Information Science* 27.5, pp. 292–306.

Qian, Jiang, Nicholas M Luscombe, and Mark Gerstein (2001). "Protein family and fold occurrence in genomes: power-law behaviour and evolutionary model". In: *Journal of Molecular Biology* 313.4, pp. 673–681.

RealClearPolitics 2016 final forecast. https://www.realclearpolitics.com/epolls/2016/president/va/virginia_trump_vs_clinton_vs_johnson_vs_stein-5966.html. Accessed: 2019-11-29.

Rocha, Luis EC, Fredrik Liljeros, and Petter Holme (2011). "Simulated epidemics in an empirical spatiotemporal network of 50,185 sexual contacts". In: *PLoS Computational Biology* 7.3, e1001109.

Rogers, Everett M (1976). "New product adoption and diffusion". In: *Journal of Consumer Research* 2.4, pp. 290–301.

— (2010). *Diffusion of innovations*. Simon and Schuster.

Ross, Robert JH, Charlotte Strandkvist, and Walter Fontana (2019a). "Compressibility of random walker trajectories on growing networks". In: *Physics Letters A* 383.17, pp. 2028–2032.

— (2019b). "Random walker's view of networks whose growth it shapes". In: *Physical Review E* 99.6, p. 062306.

Rosvall, Martin and Carl T Bergstrom (2008). "Maps of random walks on complex networks reveal community structure". In: *Proceedings of the National Academy of Sciences* 105.4, pp. 1118–1123.

Rosvall, Martin et al. (2014). "Memory in network flows and its effects on spreading dynamics and community detection". In: *Nature Communications* 5, p. 4630.

Rushmore, Julie et al. (2014). "Network-based vaccination improves prospects for disease control in wild chimpanzees". In: *Journal of the Royal Society Interface* 11.97, p. 20140349.

Sachs, Horst, Michael Stiebitz, and Robin J Wilson (1988). "An historical note: Euler's Königsberg letters". In: *Journal of Graph Theory* 12.1, pp. 133–139.

Saga, Yumiko and Hiroyuki Takeda (2001). "The making of the somite: molecular events in vertebrate segmentation". In: *Nature Reviews Genetics* 2.11, p. 835.

Salathé, Marcel et al. (2010). "A high-resolution human contact network for infectious disease transmission". In: *Proceedings of the National Academy of Sciences* 107.51, pp. 22020–22025.

Salehi, Mostafa et al. (2015). "Spreading processes in multilayer networks". In: *IEEE Transactions on Network Science and Engineering* 2.2, pp. 65–83.

Santos, Francisco C, João F Rodrigues, and Jorge M Pacheco (2005). "Epidemic spreading and cooperation dynamics on homogeneous small-world networks". In: *Physical Review E* 72.5, p. 056128.

Sanz, Joaquín et al. (2014). "Dynamics of interacting diseases". In: *Physical Review X* 4.4, p. 041005.

Saumell-Mendiola, Anna, M Ángeles Serrano, and Marián Boguná (2012). "Epidemic spreading on interconnected networks". In: *Physical Review E* 86.2, p. 026106.

Schaub, Michael T et al. (2017). "The many facets of community detection in complex networks". In: *Applied Network Science* 2.1, p. 4.

Schlenger, William E (2005). "Psychological impact of the September 11, 2001 terrorist attacks: Summary of empirical findings in adults". In: *Journal of Aggression, Maltreatment & Trauma* 9.1-2, pp. 97–108.

Schnell, Santiago and Philip K Maini (2000). "Clock and induction model for somitogenesis". In: *Developmental Dynamics: An Official Publication of the American Association of Anatomists* 217.4, pp. 415–420.

Scott, Jacob G et al. (2019). "Inferring tumour proliferative organisation from phylogenetic tree measures in a computational model". In: *Systematic Biology*, pp. 1–41.

Sekara, Vedran, Arkadiusz Stopczynski, and Sune Lehmann (2016). "Fundamental structures of dynamic social networks". In: *Proceedings of the National Academy of Sciences* 113.36, pp. 9977–9982.

Shah, Devavrat and Tauhid Zaman (2011). "Rumors in a network: Who's the culprit?" In: *IEEE Transactions on Information Theory* 57.8, pp. 5163–5181.

— (2012). "Finding rumor sources on random graphs". In: *Proceedings of the 12th ACM SIGMETRICS/PERFORMANCE joint international conference on Measurement and Modeling of Computer Systems*.

— (2016). "Finding rumor sources on random trees". In: *Operations Research* 64.3, pp. 736–755.

Shen-Orr, Shai S et al. (2002). "Network motifs in the transcriptional regulation network of Escherichia coli". In: *Nature Genetics* 31.1, p. 64.

Shulgin, Boris, Lewi Stone, and Zvia Agur (1998). "Pulse vaccination strategy in the SIR epidemic model". In: *Bulletin of Mathematical Biology* 60.6, pp. 1123–1148.

Silver, Roxane Cohen et al. (2002). "Nationwide longitudinal study of psychological responses to September 11". In: *Jama* 288.10, pp. 1235–1244.

Solomon, Zahava, Marc Gelkopf, and Avraham Bleich (2005). "Is terror gender-blind? Gender differences in reaction to terror events". In: *Social Psychiatry and Psychiatric Epidemiology* 40.12, pp. 947–954.

Sonnen, Katharina F and Alexander Aulehla (2014). "Dynamic signal encoding—From cells to organisms". In: *Seminars in Cell & Developmental Biology*. Vol. 34. Elsevier, pp. 91–98.

Sonnen, Katharina F et al. (2018). "Modulation of phase shift between Wnt and Notch signaling oscillations controls mesoderm segmentation". In: *Cell* 172.5, pp. 1079–1090.

Soroldoni, Daniele et al. (2014). "A Doppler effect in embryonic pattern formation". In: *Science* 345.6193, pp. 222–225.

Stecklov, Guy and Joshua R Goldstein (2004). "Terror attacks influence driving behavior in Israel". In: *Proceedings of the National Academy of Sciences* 101.40, pp. 14551–14556.

Steel, Mike and Andy McKenzie (2001). "Properties of phylogenetic trees generated by Yule-type speciation models". In: *Mathematical Biosciences* 170.1, pp. 91–112.

Stern, Claudio D et al. (1988). "A cell lineage analysis of segmentation in the chick embryo". In: *Development* 104.Supplement, pp. 231–244.

Stewart, Alexander J et al. (2019). "Information gerrymandering and undemocratic decisions". In: *Nature* 573.7772, pp. 117–121.

Stopczynski, Arkadiusz, Alex Sandy Pentland, and Sune Lehmann (2015). "Physical proximity and spreading in dynamic social networks". In: *arXiv preprint arXiv:1509.06530*.

Strogatz, Steven (2004). *Sync: The emerging science of spontaneous order*. Penguin UK.

Strogatz, Steven H (2018). *Nonlinear dynamics and chaos: with applications to physics, biology, chemistry, and engineering*. CRC Press.

Sznajd-Weron, Katarzyna and Rafal Weron (2003). "How effective is advertising in duopoly markets?" In: *Physica A: Statistical Mechanics and its Applications* 324.1-2, pp. 437–444.

Tam, PPL (1981). "The control of somitogenesis in mouse embryos". In: *Development* 65.Supplement, pp. 103–128.

Taraskin, Sergei N and Francisco J Pérez-Reche (2013). "Effects of variable-state neighborhoods for spreading synergystic processes on lattices". In: *Physical Review E* 88.6, p. 062815.

— (2019). "Bifurcations in synergistic epidemics on random regular graphs". In: *Journal of Physics A: Mathematical and Theoretical* 52.19, p. 195101.

Ternovski, John and Taha Yasseri (2019). "Social complex contagion in music listenership: A natural experiment with 1.3 million participants". In: *Social Networks*.

Theiler, Karl et al. (1972). *The house mouse. Development and normal stages from fertilization to 4 weeks of age.* Springer Verlag.

Touboul, Jonathan (2014). "The hipster effect: When anticonformists all look the same". In: *arXiv preprint arXiv:1410.8001v1*.

— (2019). "The hipster effect: When anticonformists all look the same". In: *arXiv preprint arXiv:1410.8001v2*.

Traud, Amanda L, Peter J Mucha, and Mason A Porter (2012). "Social structure of Facebook networks". In: *Physica A: Statistical Mechanics and its Applications* 391.16, pp. 4165–4180.

Travers, Jeffrey and Stanley Milgram (1977). "An experimental study of the small world problem". In: *Social Networks*. Elsevier, pp. 179–197.

Tsiairis, Charisios D and Alexander Aulehla (2016). "Self-organization of embryonic genetic oscillators into spatiotemporal wave patterns". In: *Cell* 164.4, pp. 656–667.

Ugander, Johan et al. (2011). "The anatomy of the facebook social graph". In: *arXiv preprint arXiv:1111.4503*.

Ugander, Johan et al. (2012). "Structural diversity in social contagion". In: *Proceedings of the National Academy of Sciences* 109.16, pp. 5962–5966.

Vassell, Gregory S (1990). "The northeast blackout of 1965". In: *Public Utilities Fortnightly;(United States)* 126.8.

Vázquez, Alex (2004). "Causal Tree of Disease Transmission and The Spreading of Infectious Diseases." In: *Discrete Methods in Epidemiology*, pp. 163–180.

Volkening, Alexandria et al. (2018). "Forecasting elections using compartmental models of infections". In: *arXiv preprint arXiv:1811.01831*.

Vosoughi, Soroush, Deb Roy, and Sinan Aral (2018). "The spread of true and false news online". In: *Science* 359.6380, pp. 1146–1151.

Wang, Dashun et al. (2011). "Information spreading in context". In: *Proceedings of the 20th International Conference on World Wide Web*. ACM, pp. 735–744.

Watts, Duncan J (1999). "Networks, dynamics, and the small-world phenomenon". In: *American Journal of Sociology* 105.2, pp. 493–527.

— (2002). "A simple model of global cascades on random networks". In: *Proceedings of the National Academy of Sciences* 99.9, pp. 5766–5771.

Watts, Duncan J and Steven H Strogatz (1998). "Collective dynamics of 'small-world'networks". In: *nature* 393.6684, p. 440.

Watts, Duncan J et al. (2005). "Multiscale, resurgent epidemics in a hierarchical metapopulation model". In: *Proceedings of the National Academy of Sciences* 102.32, pp. 11157–11162.

Watts, Joe (2018). "Brexit: Leave campaign no longer viewed as anti-establishment movement as Remainers turn to insurgent strategyt". In: *The Independent*. URL: https://www.independent.co.uk/news/uk/politics/brexit-leave-campaign-remainers-peoples-vote-final-say-yougov-survey-a8486626.html (visited on 11/29/2019).

Weitzman, Elliot D et al. (1982). "Chronobiology of aging: temperature, sleep-wake rhythms and entrainment". In: *Neurobiology of Aging* 3.4, pp. 299–309.

Weng, Lilian, Filippo Menczer, and Yong-Yeol Ahn (2013). "Virality prediction and community structure in social networks". In: *Scientific Reports* 3, p. 2522.

Woller, Aurore et al. (2016). "A mathematical model of the liver circadian clock linking feeding and fasting cycles to clock function". In: *Cell Reports* 17.4, pp. 1087–1097.

Xia, Yongxiang, Jin Fan, and David Hill (2010). "Cascading failure in Watts–Strogatz small-world networks". In: *Physica A: Statistical Mechanics and its Applications* 389.6, pp. 1281–1285.

Yin, Hao et al. (2017). "Local higher-order graph clustering". In: *Proceedings of the 23rd ACM SIGKDD International Conference on Knowledge Discovery and Data Mining*. ACM, pp. 555–564.

Young, Jean-Gabriel et al. (2017). "Construction of and efficient sampling from the simplicial configuration model". In: *Physical Review E* 96.3, p. 032312.

Yule, George Udny (1925). "II.—A mathematical theory of evolution, based on the conclusions of Dr. JC Willis, FR S". In: *Philosophical Transactions of the Royal Society of London. Series B, containing papers of a biological character* 213.402-410, pp. 21–87.

Zhang, Qian et al. (2017). "Spread of Zika virus in the Americas". In: *Proceedings of the National Academy of Sciences* 114.22, E4334–E4343.

Zhang, Zi-Ke et al. (2016). "Dynamics of information diffusion and its applications on complex networks". In: *Physics Reports* 651, pp. 1–34.